UNTERSUCHUNGEN ZU DEN MOLEKULAREN URSACHEN DER X-GEBUNDENEN JUVENILEN RETINOSCHISIS – VOM GENDEFEKT ZUM MAUSMODELL

Von der Krankheit

Dissertation zur Erlangung des
naturwissenschaftlichen
Doktorgrades
der Bayerischen Julius-Maximilians-
Universität Würzburg

vorgelegt
von Andrea Gehrig
aus Miltenberg

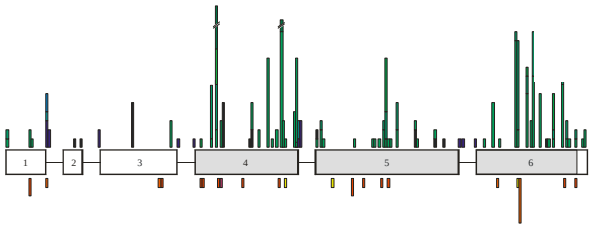

über das Gen

zum Mausmodell

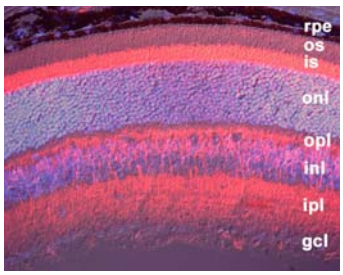

und zur Therapie

UNTERSUCHUNGEN ZU DEN MOLEKULAREN URSACHEN DER X-GEBUNDENEN JUVENILEN RETINOSCHISIS – VOM GENDEFEKT ZUM MAUSMODELL

Dissertation zur Erlangung des
naturwissenschaftlichen Doktorgrades
der Bayerischen Julius-Maximilians-Universität Würzburg

vorgelegt von

Andrea Gehrig

aus Miltenberg

Würzburg 2003

Eingereicht am:

bei der Fakultät für Biologie

Mitglieder der Promotionskommission
Vorsitzender:

Gutachter: Prof. Dr. Bernhard Weber

Gutachter: Prof. Dr. Jürgen Kreft

Tag des Promotionskolloquiums:

Doktorurkunde ausgehändigt am:

Erklärung

Die vorliegende Arbeit wurde von mir selbständig durchgeführt.
Andere als die angegebenen Hilfsmittel und Quellen wurden nicht verwendet.
Hiermit erkläre ich, daß ich diese Dissertation weder in gleicher, noch in ähnlicher Form in einem anderen Prüfungsverfahren bereits vorgelegt habe.
Es wurde zuvor kein anderer akademischer Grad erworben.

Würzburg, den

Die hier vorliegende Arbeit wurde am Institut für Humangenetik der Bayerischen Julius-Maximilians-Universität von Mai 1997 bis August 2003 unter der Leitung von Prof. Dr. Bernhard Weber angefertigt. Die Arbeit wurde im Rahmen der DFG-Projekte WE 1259/5-2, WE 1259/5-3, WE 1259/12-1 und WE 1259/12-2 finanziell gefördert.

Mein Dank gilt Herrn Prof. Dr. Bernhard Weber für die Überlassung des behandelten Themas und sein ständiges Interesse an dieser Arbeit. Insbesondere möchte ich ihm dafür danken, daß er es mir ermöglichte, neuste molekularbiologischen Methoden anzuwenden.

Herrn Prof. Dr. Jürgen Kreft danke ich für die Begutachtung dieser Arbeit.

Desweiteren möchte ich mich bei allen MitarbeiterInnen des Instituts für Humangenetik für die tatkräftige Unterstützung bedanken. Besonderer Dank gilt vor allem Sissi, Andrea R., Vladimir, Heidi St. und Birgit Halliger-Keller.

Meinen Eltern danke ich dafür, daß sie mir diese Ausbildung ermöglicht haben.

Bei Frank möchte ich mich dafür bedanken, daß er mich immer unterstützt hat.

MEINEN ELTERN

INHALTSVERZEICHNIS

I. Liste der vorgelegten Veröffentlichungen

Anlage 1 Felbor, U.; Gehrig, A.; Sauer, C.G.; Marquardt, A.; Köhler, M.; Schmid, M.; Weber, B.H.F.; (1998) Genomic organization and chromosomal localization of the interphotoreceptor matrix proteoglycan-1 (IMPG1) gene: a candidate for 6q-linked retinopathies. *Cytogenet. Cell. Genet.* 81: 12-17.

Anlage 2 Gehrig, A.; Felbor, U.; Kelsell, R.E.; Hunt, D.M.; Maumenee, I.H.; Weber, B.H.F.; (1998) Assessment of the interphotoreceptor matrix proteoglycan-1 (IMPG-1) gene localised to 6q13-q15 in autosomal dominant Stargardt-like disease (ADSTGD), progressive bifocal chorioretinal atrophy (PBCRA), and North Carolina macular dystrophy (MCDR1). *J. Med. Genet.* 35: 641-645.

Anlage 3 Stöhr, H.; Klein, J.; Gehrig, A.; Koehler, M.R.; Jurklies, B.; Kellner, U.; Leo-Kottler, B.; Schmid, M.; Weber, B.H.F.; (1999) Mapping and genomic characterization of the gene encoding diacylglycerol kinase γ (DAGK3): assessment of its role in dominant optic atrophy (OPA1). *Hum. Genet.* 104: 99-105.

Anlage 4 Warneke-Wittstock, R.; Marquardt, A.; Gehrig, A.; Sauer, C.G.; Gessler, M.; Weber, B.H.F.; (1998) Transcript Map of a 900-kb Genomic Region in Xp22.1-p22.2: Identification of 12 Novel Genes. *Genomics* 51: 59-67.

Anlage 5 Sauer, C.G.; Gehrig, A.; Warneke-Wittstock, R.; Marquardt, A.; Ewing, C.C.; Gibson, A.; Lorenz, B.; Jurklies, B.; Weber, B.H.F.; (1997) Positional cloning of the gene associated with X-linked juvenile retinoschisis. *Nat. Genet.* 17: 164-170.

Anlage 6 Gehrig, A.; Lorenz, B.; Andrassi, M.; Weber, B.H.F.; (1999) First molecular evidence for a de novo mutation in RS1 (XLRS) associated with X linked juvenile retinoschisis. *J. Med. Genet.* 36: 932-934.

Anlage 7 Gehrig, A.; White, K.; Lorenz, B.; Andrassi, M.; Clemens, S.; Weber, B.H.F.; (1999) Assessment of RS1 in X-linked juvenile retinoschisis and sporadic senile retinoschisis. *Clin. Genet.* 55: 461-465.

Anlage 8 Gehrig, A.; Warneke-Wittstock, R.; Sauer, C.G.; Weber, B.H.F.; (1999) Isolation and characterization of the murine X-linked juvenile retinoschisis (*Rs1h*) gene. *Mamm. Genome* 10: 303-307.

Anlage 9 Weber, B.H.F.; Schrewe, H.; Molday, L.L.; Gehrig, A.; White, K.L.; Seeliger, M.W.; Jaissle, G.B.; Friedburg, C.; Tamm, E.; Molday, R.S.; (2002) Inactivation of the murine X-linked juvenile retinoschisis gene, *Rs1h*, suggests a role of retinoschisin in retinal cell layer organization and synaptic structure. *Proc. Nat. Acad. Sci.* 99: 6222-6227.

II. Zusammenfassung

Hereditäre Netzhautdegenerationen betreffen weltweit etwa 15 Millionen Menschen. Sie sind klinisch und genetisch auffällig heterogen. Bisher wurden 139 verschiedene chromosomale Genorte mit Netzhautdystrophien assoziiert, wovon inzwischen 90 Gene identifiziert werden konnten. Mit Hilfe verschiedener Klonierungsstrategien konnte in der vorgelegten Arbeit ein Beitrag zur Aufklärung der genetischen Ursachen einiger ausgewählter Retinopathien geleistet werden. So konnte durch die Positionsklonierung das Gen, das mit der X-gebundenen juvenilen Retinoschisis (RS) assoziiert ist, identifiziert werden. Funktionelle Analysen des Genproduktes sowie die Generierung eines Mausmodells der RS geben einen Einblick in die Physiologie der Retina sowie den Pathomechanismus der Erkrankung.

Die genomische Organisation des Interphotorezeptor-Matrixproteoglykans-1 (*IMPG1*) wurde aufgeklärt und die chromosomale Lokalisation auf 6q13-15 bestimmt. Damit kartierte das Gen in eine Region, in die die Genorte für 7 Retinopathien des Menschen kartiert wurden. Durch Kopplungs- und Mutationsanalysen konnten unsere Arbeiten ausschließen, daß *IMPG1* mit North Carolina Makuladystrophie (MCDR1) oder der progressiven bifokalen chorioretinalen Atrophie (PBCRA) in Zusammenhang steht.

Die Diacylglycerin Kinase-3 (*DAGK3*) konnte nach der Bestimmung der genomischen Organisation in die Region 3q27-28 kartiert werden. Dieser chromosomale Abschnitt deckt sich mit der chromosomalen Lokalisation der autosomal dominanten Optikusatrophie (OPA1). Auch hier konnte mit Hilfe von Mutationsanalysen ein Ausschluß des Gens erfolgen.

Die X-gebundene juvenile Retinoschisis ist eine häufige Ursache juveniler Makula-degenerationen und betrifft etwa 300.000 junge Männer weltweit. Charakteristische Kennzeichen der Erkrankung sind Aufspaltungen in den inneren Netzhautschichten, die zu zystischen Veränderungen der zentralen Retina führen. Ungefähr 50 % der Patienten entwickeln auch periphere Manifestationen. Durch die Arbeit unserer und anderer Forschergruppen konnte der Krankheitslokus in einen etwa 900 kb großen Bereich auf dem kurzen Arm des X-Chromosoms (Xp22.2) kartiert werden. Durch einen Vergleich der genomischen DNA Sequenzen mit öffentlich zugänglichen ESTs (*expressed sequence tags*) konnte ein retinaspezifisches Transkript identifiziert werden. Es besteht aus 6 Exonen und kodiert für ein putatives 224 Aminosäuren großes Protein, das sekretiert wird und ein

hochkonserviertes Discoidindomänen-Motiv enthält. Discoidindomänen sind in Zelladhäsion oder in Zell-Zell Interaktionen involviert. Mutationsanalysen in RS-Patienten bestätigten, daß es sich bei diesem Transkript um *RS1*, d.h. um das krankheitsassoziierte Gen der X-gebundenen juvenilen Retinoschisis handelte. Das RS1-Protein (Retinoschisin) kommt in homo-oligomeren Komplexen, die über Disulfidbrücken miteinander verbunden sind, auf der Zelloberfläche der Photorezeptoren und der Bipolaren sowie in den synaptischen Regionen der äußeren (OPL) und innere plexiformen Schicht (IPL) vor.

Um die Funktion des normalen Retinoschisins zu untersuchen und um einen Einblick in die RS-Pathogenese zu bekommen, wurde nach der Charakterisierung des orthologen murinen Gens (*Rs1h*) eine Retinoschisin-defiziente knock-out Maus generiert. Ophthalmologische und histologische Untersuchungen der *Rs1h*$^{-/Y}$-Maus zeigen signifikante Parallelen zu dem RS-Erkrankungsbild des Menschen. Damit stellt die *Rs1h* knock-out Maus ein ideales Tiermodell für die Untersuchung des zugrundeliegenden Krankheitsmechanismusses dar. So konnten wir inzwischen zeigen, daß apoptotische Prozesse zur Degeneration der Photorezeptoren führen. Gegenwärtig werden mit diesem Tiermodell erste gentherapeutische Versuche durchgeführt. Diese Arbeiten sollen Aufschluß darüber geben, ob ein Adeno-assoziierter Virus (AAV)-Transfer des *RS1* Gens in die erkrankte Retina ein möglicher Therapieansatz für RS auch beim Menschen sein könnte.

III. Summary

The World Health Organization (WHO) estimates that worldwide approximately 15 million people are affected with hereditary retinal degenerations. Retinal dystrophies are clinically and genetically heterogeneous. To date, 90 retinal disease genes have been identified and of 139 retinal disease genes the chromosomal location is known. In this study, different strategies of disease gene cloning were utilized to elucidate the underlying genetic defects of selected retinopathies. This has led to the identification of the gene associated with X-linked juvenile retinoschisis (RS) by positional cloning. Both, functional analysis of the gene product, named retinoschisin (RS1), and the generation of a mouse model for RS provide novel insight into retinal physiology and the pathomechanism of the disease.

The genomic organization of the interphotoreceptor matrix proteoglycan-1 (*IMPG1*) was established and its chromosomal localization was identified (6q13-15). Seven different human retinal dystrophies have previously been mapped to this region on chromosome 6. A possible genetic association between *IMPG1* and two retinal dystrophies, North Carolina macular dystrophy (MCDR1) and progressive bifocal chorioretinal atrophy (PBCRA), was investigated. By means of linkage studies and mutation analysis in affected patients the involvement of *IMPG1* in these two different diseases was ruled out.

The genomic organization of diacylglycerol kinase-3 (*DAGK3*) was determined and the gene locus was mapped to chromosome 3q27-28. The autosomal dominant optic atrophy (OPA1) was independently localized to the same chromosomal region. This has prompted us to investigate the role of *DAGK3* in OPA1. By mutation analysis such a correlation could be excluded.

X-linked juvenile retinoschisis is a common cause of juvenile macular degeneration affecting approximately 300.000 young males worldwide. The disease is characterized by a slitting of the inner retinal layers resulting in cystic degeneration of the central retina. Half of the patients also develop peripheral manifestations. Our laboratory and others localized the RS gene to a 900 kb interval on the short arm of chromosome Xp22.2. Comparison of genomic DNA sequences with publicly available expressed sequence tags (ESTs) have identified a retina-specific transcript. This novel transcript is composed of six exons that encode a 224-amino acid protein including a 23 amino acid signal peptide. Bioinformatical analysis

revealed that the putative protein consists almost exclusively of a discoidin domain wich is highly conserved from slime mold to human. Discoidin domains are implicated in cell adhesion or cell-cell interactions. On the basis of mutation analysis in patients affected with RS, we confirmed that the gene indeed is responsible for RS pathology. The RS1 protein is found at the cell surfaces of photoreceptors and bipolar cells and within the synaptic regions of the outer (OPL) and the inner plexiform layers (IPL) most likely as a homo-oligomeric complex.

To clarify the function of the normal RS1 and to gain insight into RS pathogenesis a mouse model deficient of the endogenous RS1 protein was generated. For these purposes the genomic organization of the murine orthologous RS1 gene (*Rs1h*) was identified. Ophthalmologic and histologic analysis of *Rs1h*$^{-/Y}$ mice revealed significant parallels to the human RS phenotyp. Therefore, the knock-out mouse represents an ideal model to further study the underlying disease mechanism. Recently, we showed that apoptosis is the final pathway of photoreceptor degeneration in *Rs1h*$^{-/Y}$ mice. Most importantly this mouse model can serve as proof-of-concept for gene therapy. Towards this end we are testing adeno-associated virus (AAV)-based gene transfer of RS1 into the defect murine retina. This may pave the way for a gene based future intervention in humans affected with this condition.

IV. Einleitung

1. Aufbau und Funktion der menschlichen Netzhaut

Die Netzhaut (Retina) ist ein hochspezialisiertes Gewebe. Sie enthält 5 Hauptzelltypen, die in 3 Schichten angeordnet sind. Die äußere Schicht besteht aus Photorezeptorzellen, die Lichtreize in elektrische Signale umwandeln, die mittlere aus Bipolar-, Horizontal- und Amakrinzellen, die die Signale analog verarbeiten, und die innere Schicht aus Ganglienzellen, deren Ausgangssignale als Impulse durch den Sehnerv in die höheren Zentren der Signalverarbeitung weitergeleitet werden (Abb. 1).

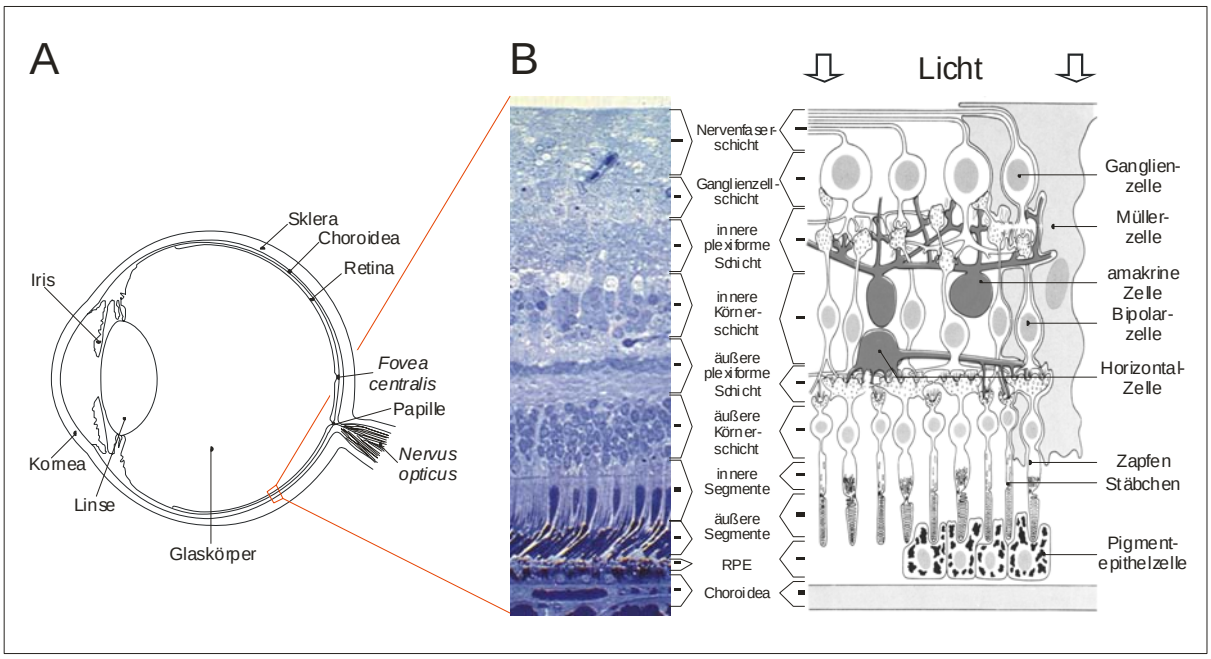

Abb. 1: Querschnitt durch das menschliche Auge und die Netzhaut
(**A**) Schematischer Querschnitt durch das menschliche Auge. (**B**) Histologischer und schematischer Querschnitt durch die menschliche Netzhaut (nach Spalton et al. 1993; Hollwich 1988). Erklärungen siehe Text.

Die Photorezeptoren liegen auf der dem Licht abgewandten Seite und setzen sich aus 6 Millionen Zapfen und 120 Millionen Stäbchen zusammen. Die Außensegmente dieser lichtempfindlichen Photorezeptoren tauchen in das dahinterliegende, einschichtige retinale Pigmentepithel (RPE) ein, das Nährstoffe wie z.B. Vitamin A aus der Aderhaut (Choroidea) zur Netzhaut und Stoffwechselabbauprodukte von der Netzhaut zu den Blutgefäßen transportiert. Die Melaningranula des RPEs dienen u.a. der Absorption von Streulicht. Zapfen und Stäbchen unterscheiden sich in Aufbau und Funktion. Die Stäbchen liegen in der Peripherie und sind für das Dämmerungs- und Bewegungssehen verantwortlich, während sich die Zapfen vorwiegend in der Netzhautmitte befinden und für das Tagsehen und die

Farbwahrnehmung zuständig sind. Die äußeren Segmente der Photorezeptoren sind aus gestapelten Membranscheibchen aufgebaut, an denen die Phototransduktion abläuft. Diese Membranscheibchen besitzen nur eine begrenzte Lebensdauer und werden kontinuierlich erneuert. Die inneren Segmente beinhalten vor allem Mitochondrien und Ribosomen und sind damit für die Energiebereitstellung und Proteinsynthese verantwortlich. Die Zellkerne der Photorezeptoren liegen in der äußeren Körnerschicht (ONL), während sich die Synapsen für die Verschaltung in der äußeren plexiformen Schicht (OPL) befinden.

Den Photorezeptoren nachgeschaltet sind in der inneren Körnerschicht (INL) die Bipolarzellen als zweites Neuron und in der Ganglienzellschicht (GCL) die Ganglienzellen als drittes Neuron. Sie bilden zusammen mit weiteren retinalen Neuronen, wie Horizontal- und Amakrinzellen, ein komplexes neuronales Netzwerk und ermöglichen eine visuelle Signalverarbeitung bereits auf retinaler Ebene. Die Axone der Ganglienzellen bilden den Sehnerv (*nervus opticus*). Dieser tritt an der Papille (*blinder Fleck*) aus und leitet die gesammelte Information an das Gehirn weiter.

Die Müller-Zellen der Netzhaut sind Gliazellen, die den gesamten neuronalen Bereich durchziehen. Sie dienen neben ihrer anatomischen Stützfunktion unter anderem der Versorgung der inneren Segmente.

Das Zentrum der Retina, die sogenannte Makula oder „gelber Fleck“, ist der funktionell wichtigste Teil der Netzhaut. Die Makula ist für das hohe Auflösungsvermögen und das Farbsehen verantwortlich. In ihrer Mitte befindet sich die stäbchenfreie Sehgrube, die *Fovea zentralis*, die aufgrund ihrer sehr hohen Zapfendichte und einer direkten eins zu eins Verschaltung zwischen Zapfen und nachfolgenden Neuronen die Stelle des schärfsten Sehens darstellt.

Zur Funktionsprüfung der Netzhaut sind verschiedene Untersuchungsverfahren wichtig. Die Sehschärfe (Visus) ist eine wesentliche Größe zur Beurteilung des Sehvermögens. Mit Hilfe des Augenspiegels wird der Augenhintergrund (Fundus) betrachtet. Die Perimetrie gibt Aufschluß über Gesichtsfeldausfälle. Zusätzlich wird die Blendempfindlichkeit und das Farbsehen überprüft. Die Ableitung eines Elektroretinogramms (ERG) ermöglicht eine Aussage über den physiologischen Zustand der Netzhaut. Beim ERG werden in folge einer Reizung der Netzhaut mit Licht Summenantworten der neuronalen Zellen der Netzhaut

abgeleitet. Durch Variation der Reizbedingungen (z.B. die Helligkeit des Reizes und die Dunkel- oder Helladaption der Netzhaut) ist es möglich, separate Informationen über die Stäbchen und Zapfen sowie die mittlere Netzhautschicht (Bipolarzellen) zu erhalten. Mit dem multifokalen ERG ist durch eine besondere Reizung der Makula eine detaillierte Untersuchung der Zapfen in der zentralen Netzhaut möglich. Die Messung der Autofluoreszenz des retinalen Pigmentepithels und die Fluoreszenzangiografie der Netzhaut ergänzen die morphologischen Untersuchungsmethoden.

2. Hereditäre Netzhautdystrophien

Hereditäre Netzhautdystrophien sind eine klinisch und genetisch heterogene Gruppe von Erkrankungen, die zu einem progressiven Verlust von Visus und Gesichtsfeld führen. Die Inzidenz beträgt ca. 20 pro 100.000 Einwohner in Deutschland (Krumpaszyk and Klauß 1996). Insgesamt werden 10 % aller Erblindungsfälle von hereditären Netzhautdystrophien verursacht. Grundsätzlich lassen sich generalisierte Netzhautdystrophien mit peripherem oder zentralem Beginn von regional begrenzten Makuladystrophien abgrenzen (Tab. 1).

Generalisierte Netzhautdystrophien mit peripherem Beginn wie z.B. die Retinitis pigmentosa sind durch anfängliche Nachtblindheit und peripher beginnende Gesichtsfeldausfälle gekennzeichnet. In den späteren Stadien kommt es zur Entstehung eines Tunnelblicks und zur Farbsinnstörung. Das ERG zeigt fehlende oder stark reduzierte Potenziale der Stäbchen und weniger ausgeprägte Veränderungen in den Zapfen.

Netzhautdystrophien mit zentralem Beginn hingegen, wie z.B. die Zapfen-Stäbchendystrophien oder Sorsby Fundusdystrophie führen früh zur Visusminderung und zum Verlust der Lesefähigkeit. Charakteristisch sind Farbsinnstörungen, Blendempfindlichkeit und zentrale Gesichtsfeldausfälle, während das periphere Gesichtsfeld und das Nachtsehen erst später beeinträchtigt werden. Hier zeigt das ERG stark reduzierte Potenziale der Zapfen und nur geringe Veränderungen in den Potenzialen der Stäbchen.

Die regional begrenzten Makuladystrophien wie z.B. Morbus Best oder Morbus Stargardt zeigen anfangs eine ähnliche Symptomatik wie die generalisierten Netzhautdystrophien mit zentralem Beginn. Auch hier treten Farbsinnstörung, Verlust der Lesefähigkeit und

Zentralskotome auf. Das periphere Gesichtsfeld bleibt jedoch erhalten, und auch die Blendungsempfindlichkeit ist weniger stark ausgeprägt. Das Ganzfeld-ERG ist in der Regel normal, während das multifokale ERG reduzierte zentrale Potenziale zeigt.

Tab. 1: Vererbung und Häufigkeit verschiedener Netzhautdystrophien (nach Kellner 1997)

Diagnose	**Erbgang***	**Häufig-keit****
Generalisierte Netzhaut-Aderhautdystrophien mit peripherem Beginn		
Retinitis pigmentosa	ad, ar, x	1
Usher Syndrom	ar	2
Leber's kongenitale Amaurose	ar	3
Wagner-Syndrom	ad	5
Stickler Syndrom	ad	4
Generalisierte Netzhaut-Aderhautdystrophien mit zentralem Beginn		
Zapfendystrophie	ad, ar, x	3
Zapfen-Stäbchendystrophie	ad, ar, x	2
Sorby Fundusdystrophie	ad	4
Makuladystrophien		
Morbus Stargardt (Fundus flavimaculatus)	ar, ad	1
Morbus Best	ad	2
X-gebundene juvenile Retinoschisis	x	2
North Carolina Makuladystrophie	ad	4
Dominante radiäre Drusen	ad	4

* ad, autosomal dominant; ar, autosomal rezessiv; x, X-chromosomal. ** Beurteilung der Häufigkeit: Ein Augenarzt wird von Patienten mit dieser Netzhautdystrophie (1) einen oder mehrere sehen, (2) wahrscheinlich einen sehen, (3) in spezialisierten Zentren einen oder mehrere sehen, (4) in spezialisierten Zentren wahrscheinlich einen sehen, (5) auch in spezialisierten Zentren nur selten einen sehen.

Ausgelöst werden diese Netzhautdystrophien in der Regel durch einen Defekt in einem der vielen hochspezialisierten Gene der Retina. Bisher wurden 139 verschiedene chromosomale Genorte mit Netzhautdystrophien assoziiert, wovon 90 Gene bereits kloniert werden konnten (Retnet, http://www.sph.uth.tmc.edu/Retnet/). Die Zahl sowohl der lokalisierten als auch der klonierten Gene ist in den letzten Jahren exponentiell angestiegen (Abb. 2).

Bei einigen Erkrankungen wie z.B. Morbus Best oder X-gebundene juvenile Retinoschisis gibt es eine eindeutige Korrelation zwischen dem klinischen Bild und der Mutation in einem

bestimmten Gen. Hier läßt sich in fast allen klinischen Verdachtsfällen eine Mutation in dem jeweiligen Gen (*VMD2*, *RS1*) nachweisen. Andere Erkrankungen zeigen dagegen eine starke Lokusheterogenität. Beispielweise sind für Retinitis pigmentosa (RP) mindestens 30 verschiedene Genorte bekannt. Im Gegensatz dazu gibt es auch Beispiele dafür, daß Defekte eines Gens unterschiedliche Krankheitsbilder hervorrufen können. Mutationen im Rhodopsingen können autosomal dominante oder rezessive RP, oder auch stationäre kongenitale Nachtblindheit verursachen. Eine solche unterschiedliche klinische Ausprägung ist nicht allein abhängig von der jeweiligen Mutation innerhalb eines Gens. Sie kann selbst bei derselben Mutation innerhalb einer Familie variieren. Es wurde z.B. eine Familie mit einer Mutation im RDS/Peripheringen beschrieben, deren Betroffene entweder an RP, an Musterdystrophie oder an *Fundus flavimaculatus* erkrankt sind (Weleber 1993). Diese intrafamiliäre Variation steht eventuell mit modifizierenden genetischen Faktoren in Zusammenhang. Möglicherweise spielen hier auch noch nicht identifizierte interagierende Proteine eine wichtige Rolle (Bessant 2001).

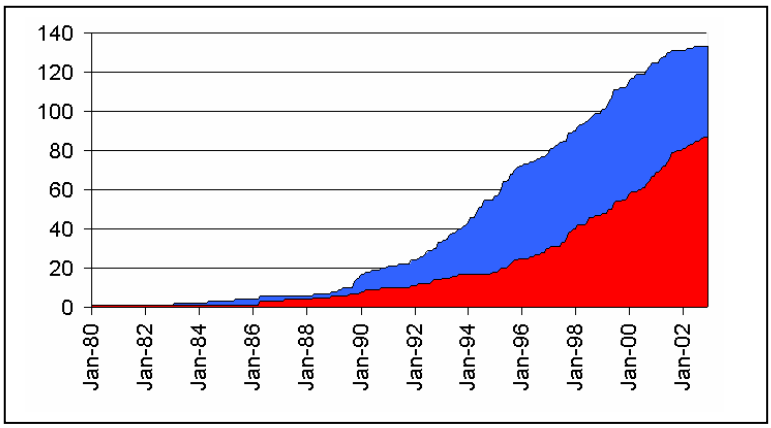

Abb. 2: Kartierte und klonierte retinale Krankheitsgene von 1980-2003
Kartierte Gene sind blau, klonierte Gene rot dargestellt (Retnet, Juni 2003).

Die meisten Netzhautdystrophien werden monogen vererbt. Es sind jedoch auch Familien mit digenischem Erbgang bekannt. Bei einer Familie mit Bardet-Biedl Syndrom (BBS) führt z.B. die Kombination von Mutationen im *BBS2*- und im *BBS6*-Gen zur Erkrankung (Katsanis et al. 2001). Des weiteren wurde eine Familie mit RP beschrieben, bei der das Zusammentreffen einer Mutation im Peripheringen und einer weiteren im *ROM1*-Gen für die Manifestation des Krankheitsbildes erforderlich ist (Kajiwara et al. 1994).

Von einigen dieser Gene, deren Mutationen Netzhautdystrophien auslösen, ist die physiologische Aufgabe des Genproduktes bekannt. Häufig handelt es sich um Strukturproteine der Retina z.B. Peripherin/RDS (Keen and Inglehearn 1996), Retinoschisin (eigene Anlage 5), um Proteine der Phototransduktionskaskade z.B. Rhodopsin (Dryja et al. 1990, Dryja et al. 1993),

Transducin (Dryja et al. 1996), Arrestin (Fuchs et al. 1995), um Proteine, die für den Transport von Substraten zwischen Netzhaut und RPE notwendig sind z.B. ABCR (Allikmets 1997) oder auch um retinaspezifische Transkriptionsfaktoren z.B. CRX (Freund et al. 1997). Daneben gibt es viele krankheitsassoziierte Gene, deren Funktion bisher noch unbekannt ist.

3. Strategien zur Identifizierung von Krankheitsgenen

In den letzten Jahren wurden zum Klonieren von Genen, die für eine monogene Erkrankung verantwortlich sind, verschiedene Strategien entwickelt.

Funktionelle Klonierung

Voraussetzung für die funktionelle Klonierung ist die Kenntnis des primären biochemischen Defekts. Ausgangspunkt ist z.B. ein gereinigtes Protein. Anhand der Aminosäuresequenz kann dann mit degenerierten Oligonucleotiden die cDNA des korrespondierenden Gens isoliert werden. Dieser Schritt wird heute oft durch das Durchsuchen von cDNA-Expressionsbanken mit spezifischen Antikörpern ersetzt. Anschließende Mutationsanalysen der Patienten-DNAs geben Aufschluß darüber, ob das korrespondierende Gen tatsächlich in die Krankheit involviert ist. Diese Strategie wurde z.B. zur Isolierung der Gene für Hämophilie A und Phenylketonurie erfolgreich angewandt (Gitschier et al. 1984, Robson et al. 1982).

Funktionelle Kandidatengen-Klonierung

Anhand der Krankheitssymptome läßt sich abschätzen, welche Art von Protein für den pathogenetischen Prozeß verantwortlich sein könnte. Dementsprechend wählt man aus bekannten Genen Kandidaten aus und untersucht sie mit Hilfe geeigneter Mutationsanalyseverfahren. Diese Strategie zeigt zum Teil geringe Effizienz und führt häufig nur zu einem Ausschluß eines Kandidatengens. Dies liegt neben der großen Anzahl an möglichen Kandidaten-Genen vor allem daran, daß nur wenige Gene funktionell gut charakterisiert sind.

Positionsklonierung

Eine sehr erfolgreiche Methode ist die 1986 erstmals angewandte Positionsklonierung (Abb. 3). Voraussetzung hierfür sind gut charakterisierte Familien mit mehreren betroffenen und nichtbetroffenen Mitgliedern. Isoliert wird das verantwortliche Gen ausschließlich aufgrund

seiner Position im Genom. Keinerlei Vorkenntnis über die Funktion des Genproduktes ist erforderlich. Mit Hilfe von genetischen Kopplungsanalysen wird zunächst die chromosomale Lokalisation des Genortes bestimmt. Dabei wird nach DNA-Markern gesucht, die mit der Erkrankung kosegregieren und daher nahe des Krankheitsgens liegen sollten. Die somit eingegrenzte Region, meistens noch einige tausend Kilobasen DNA, wird aus einer Genombibliothek (BAC (*bacterial artificial chromosome*) - oder PAC (*Phage P1-derived artificial chromosome*) - Banken) in Form überlappender Fragmente isoliert und sequenziert. Eine solche Gruppe von DNA-Klonen wird als contig (*contiguous DNA fragments*) bezeichnet.

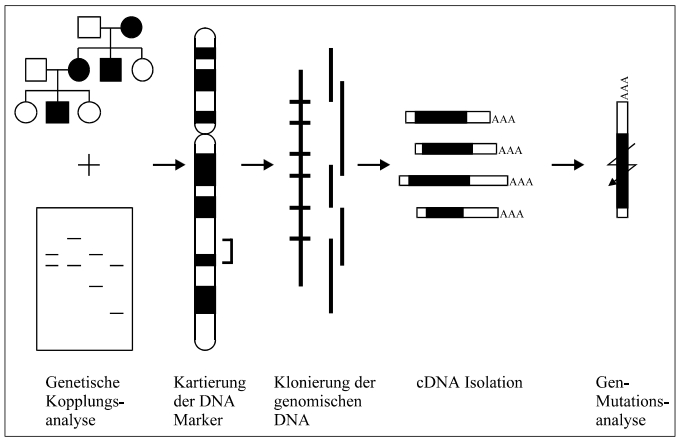

Abb. 3: Wesentliche Schritte der Positionsklonierungs-Strategie
Erklärungen siehe Text.

Zum anschließenden Erstellen der Transkriptkarte dieser Kandidatenregion kann man verschiedene Methoden wie z.B. das Hybridisieren von cDNA-Banken, cDNA-Selektion (Rommens et al.1993), EST-Datenbankanalysen, die Identifizierung von CpG-Inseln (Valdes et al. 1994) oder das Exon-*trapping* (Nehls et al. 1994) nutzen. Heute wird sehr häufig mit computergestützten Vorhersagen nach codierenden Bereichen gesucht (Claverie 1997). Fehlende 5'- oder 3'-Enden erhält man mit Hilfe der RACE (*rapid amplification of cDNA ends*)-Methode. Einen Hinweis darauf, ob es sich um ein mögliches Kandidatengen handelt, erhält man durch eine Expressionsanalyse in verschiedenen Geweben. Der Nachweis des tatsächlichen Krankheitsgens wird wieder durch Mutationsanalysen erbracht.

Positionelle Kandidatengen-Klonierung

Bei der positionellen Kandidatengen-Klonierung (Abb. 4) wird das Krankheitsgen mit unbekannter Funktion genomisch kartiert. Eine Transkriptkarte gibt Aufschluß darüber, welche Gene in dieser Region lokalisiert sind. Diese werden bei den betroffenen Patienten molekulargenetisch untersucht. Krankheitsverursachende Veränderungen zeigen an, daß es sich um das gesuchte Krankheitsgen handelt. Diese Strategie hat sich nach der vollständigen

Sequenzierung des Genoms und den damit zunehmend verfeinerten Transkriptkarten zur Standardmethode entwickelt.

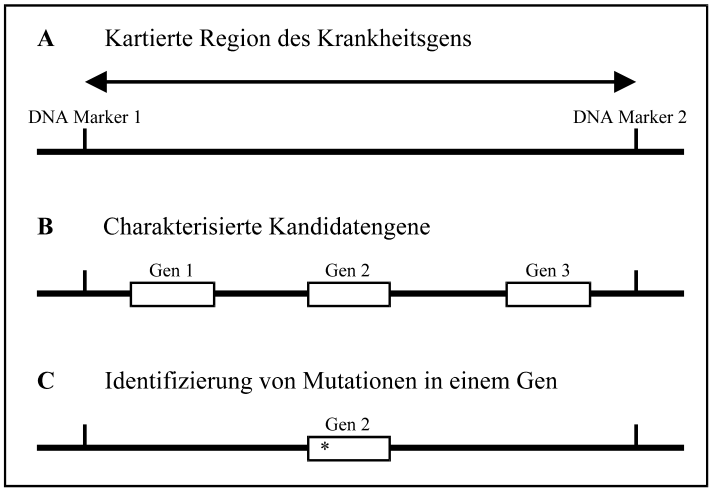

Abb. 4: Schritte der positionellen Kandidatengen-Klonierung
Die einzelnen Schritte der positionellen Kandidatengen-Klonierung beinhalten (**A**) die Kartierung des Krankheits-Genortes mittels der genetischen Kopplungsanalyse, (**B**) das Durchforsten einer Transkriptkarte nach möglichen Kandidatengenen und (**C**) die Untersuchung eines Kandidatengens auf Mutationen in den Patienten mit der jeweiligen Erkrankung (nach Weber 1997).

4. Zielsetzung

In der vorliegenden Arbeit sollten Gene identifiziert werden, die ursächlich mit hereditären Netzhautdystrophien des Menschen assoziiert sind. Des weiteren sollte ein Beitrag zur funktionellen Charakterisierung des *RS1* Gens geleistet werden. Mutationen im *RS1* Gen führen zum klinischen Bild der RS. Des weiteren sollte der Pathomechanismus der RS aufgeklärt werden. Dazu wurde ein Mausmodell generiert, das vergleichbare funktionelle Ausfallerscheinungen wie bei menschlichen RS-Patienten zeigt.

In der vorliegenden Arbeit sollten insgesamt 3 Krankheitsorte näher untersucht werden. Zunächst sollte die genomische Organisation und chromosomale Lokalisation des Gens *IMPG1* aufgeklärt werden, um dann anhand von Mutationsanalyseverfahren zu untersuchen, ob *IMPG1* das krankheitsassoziierte Gen für eine der in diesem Chromosomenabschnitt lokalisierten genetischen Netzhauterkrankungen darstellt.

Eine positionelle Kandidatengen-Klonierung sollte auch für *DAGK3* angewandt werden. Mutationsanalysen sollten Aufschluß darüber geben, ob bei OPA1-Patienten ein Defekt im *DAGK3*-Gen vorliegt.

Bei der X-gebundenen juvenilen Retinoschisis sollte das korrespondierende Gen mit Hilfe der Positionsklonierung gefunden werden. Krankheitsassoziierte Gene bzw. die Funktion ihrer

Genprodukte sollen Aufschluß über die Physiologie der Retina geben. Da die Netzhaut wesentliche Gehirnfunktionen in einem definierten System abbildet, könnte ihre Erforschung neben der Aufklärung des komplexen Sehvorganges auch einen Beitrag zum Verständnis der Funktion und Pathologie des Gehirns leisten.

Des weiteren sollte der Pathomechanismus der RS aufgeklärt werden. Zu diesem Zweck sollte ein Mausmodell generiert und charakterisiert werden.

Versuche an diesem Mausmodell sollen zeigen, ob ein gentherapeutischer Ersatz des RS1 Proteins eine Behandlungsmöglichkeit für Patienten mit X-gebundener juveniler Retinoschisis darstellen könnte.

V. Darstellung der vorgelegten Veröffentlichungen

1. Analyse eines Kandidatengens (*IMPG1*) in MCDR1, PBCRA und autosomal dominanter Stargardt-ähnlicher Makuladystrophie (STGD3)

Die Interphotorezeptor-Matrix (IPM) befindet sich als eine spezielle Form der extrazellulären Matrix zwischen den äußeren Segmenten der Photorezeptoren und dem RPE. Sie besteht aus einer Vielzahl von Proteinen, Glykoproteinen und Proteoglykanen. Die IPM ist für Interaktionen zwischen neuronaler Retina und RPE von großer Bedeutung. Bei diesen Interaktionen handelt es sich um den Austausch von Metaboliten und katabolen Nebenprodukten, die Regulation des Ionenmilieus, die Absonderung von Wachstumsfaktoren sowie die Aufrechterhaltung der Photorezeptoren in bezug auf Polarisierung, Orientierung, Umsatz und Lebensfähigkeit (Hewitt et al. 1990, Hageman and Johnson 1991). Die Glykokonjugate der IPM vermitteln die Adhäsion der neuronalen Retina an das RPE, besonders Chondroitinsulfate scheinen dabei eine wichtige Rolle zu spielen (Hageman et al. 1995).

1995 wurde die humane cDNA des *IMPG1* isoliert (Kuehn and Hageman 1995). Sie kodiert für ein 150 kDa Chondroitin 6-Sulfat Proteoglykan, das 4 Konsensussequenzen für Hyaluronanbindung, 3 N-Glykosylierungs- und mehrere potentielle O-Glykosylierungsstellen enthält. Kuehn and Hageman (1999) berichten, daß die cDNA in den Photorezeptoren der Retina, aber auch in Lunge, Leber, Niere, Thymus und Dünndarm exprimiert wird. Dies steht jedoch im Widerspruch zu unseren eigenen Ergebnissen, die ausschließlich Expression in der Retina, jedoch nicht in anderen Geweben, wie z.B. Lunge zeigen (Anlage 1).

Wir haben anschließend mit Hilfe der cDNA Sequenz die genomische Organisation des *IMPG1* Gens bestimmt. Es besteht aus 17 kodierenden Exonen und umspannt mindestens 50 kb genomische DNA. Die chromosomale Lokalisation wurde anhand von somatischen Zellhybriden und FISH (Fluoreszenz in situ Hybridisierung) auf den Lokus 6q13-15 festgelegt (Anlage 1). Dieses Intervall überlappt mit der chromosomalen Lokalisation mehrerer humaner Makuladystrophien, wie z.B. MCDR1 (Small et al. 1992), PBCRA (Kelsell et al. 1995) sowie STGD3 (Stone et al. 1994) (Abb. 5).

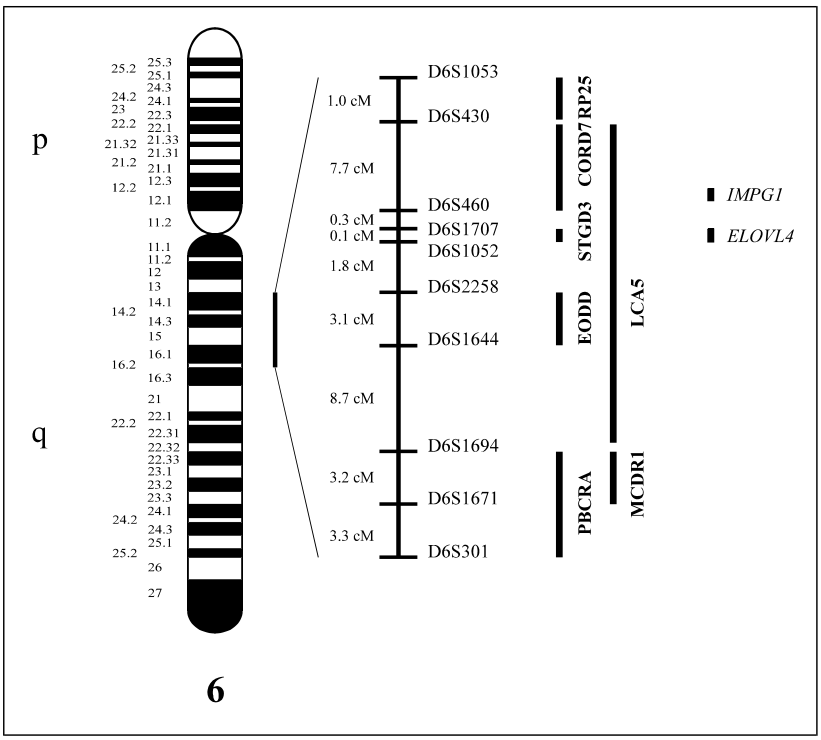

Abb. 5: Chromosomale Lokalisation und genetische Kartierung der Chromosom 6 Retinopathien
Die Region zwischen den Markern D6S1053 und D6S301 beinhaltet 7 Krankheitsloci für Retinopathien (Retinitis Pigmentosa (RP25), Zapfen-Stäbchen Dystrophie (CORD7), Lebers kongenitale Amaurose (LCA5), dominate Stargardt-ähnliche Makuladystrophie (STGD3), juvenile dominante Drusen (EODD), North Carolina Makuladystrophie (MCDR1) und progressive bifokale chorioretinale Atrophie (PBCRA). Die relative Lage von *ELOVL4* und *IMPG1* ist eingezeichnet (nach Donoso et al. 2001).

MCDR1 ist gekennzeichnet durch Drusen, Makulaläsionen mit zentralem Verlust von Photorezeptoren und Pigmentzellen, Pigmentverdichtungen und choriodaler Atrophie. Sie zeigt selten einen progressiven Verlauf. Bei PBCRA handelt es sich hingegen um eine progressive Erkrankung. Sie beginnt in der ersten Lebensdekade mit chorioretinaler Atrophie, in der zweiten Lebensdekade kommt ein nasaler Atrophieherd hinzu. In dem Bereich dazwischen bleiben Netz- und Aderhaut intakt. Weitere Symptome sind Nystagmus, Strabismus und ein stark reduzierter Visus, Netzhautablösungen sind möglich (Kellner 2003). Das charakteristische Merkmal von STGD3 sind die fleckförmigen Veränderungen im Bereich der Makula (*fundus flavimaculatus*). Später kommt es zu zentraler Atrophie mit Visusminderung und zu einem zentralen Verlust von Pigmentzellen und Photorezeptoren.

Das *IMPG1*-Gen stellte aufgrund seiner chromosomalen Lokalisation und der Tatsache, daß der Verlust von Chondroitin 6-Sulfat Proteoglykan zu lokal begrenzter Netzhautablösung und zur Degeneration der äußeren Segmente der Photorezeptoren führen kann (Lazarus and Hageman 1992), positionell und funktionell ein ausgezeichnetes Kandidatengen für jede der genannten Makuladystrophien dar.

Mutationsanalysen in drei MCDR1-Familien und einer PBCRA-Familie, deren Krankheitsloci alle auf 6q kartiert waren, und in einer autosomal dominanten STGD-Familie zeigten keine krankheitsverursachenden Veränderungen (Anlage 2). Die anschließende Kopplungsanalyse

mit einem intragenischen Polymorphismus ergab aufgrund einer Rekombination zwischen dem Marker und dem Krankheitslokus einen Ausschluß des *IMPG1*-Gens für die PBCRA-Familie, erwies sich in den MCDR1-Familien jedoch als nicht informativ (Anlage 2). Da drei nicht verwandte MCDR1-Familien untersucht wurden, kann trotz der SSCP (*single strand conformation polymorphism*)-Analysen, die lediglich eine Entdeckungsrate von 75-85 % aufweisen, das *IMPG1*-Gen als verantwortliches Gen für diese Erkrankung weitgehend ausgeschlossen werden. Die Möglichkeit, daß *IMPG1* das krankheitsassoziierte Gen für STGD3 ist, ist weiterhin gegeben, da unsere autosomal dominante STGD-Familie aufgrund der Familiengröße nicht kartiert werden konnte, und Stargardt-ähnliche Makuladystrophien genetisch heterogen sind. Inzwischen konnten jedoch in mehreren STGD3-Familien Mutationen in *ELOVL4 (elongation of very long chain fatty acids-4)*, einem retinaspezifischen Gen der Fettsäurebiosynthese, nachgewiesen werden (Zhang et al. 2001, Bernstein et al. 2001).

2. Analyse eines Kandidatengens (*DAGK3*) in OPA1

Diacylglycerin Kinasen (DAGK) spielen eine wichtige Rolle in der Phosphoinositidkaskade, die extrazelluläre in intrazelluläre Signale umwandelt. Phosphatidylinositol-4,5-biphosphat (PIP2), ein Phospholipid der Plasmamembran, wird dabei durch aktivierte Phospolipase C in die zweiten Messenger Inositol-1,4,5-triphosphat (IP3) und Diacylglycerin (DAG) hydrolysiert (Kanoh et al. 1990). DAG aktiviert die Protein Kinase C, die wiederum Serin- und Threoninreste vieler Zielproteine phosphoryliert (Bell 1986). Die Funktion der DAGKs besteht darin, DAG durch Phosphorylierung in Phosphatidsäure umzuwandeln, und somit die intrazelluläre DAG-Konzentration zu kontrollieren. Die Phosphoinositidkaskade vermittelt z.B. die Sehreizübertragung in Photorezeptoren von Wirbellosen, einen direkten Beweis für eine Intervention in die Phototransduktionskaskade bei Säugetieren gibt es allerdings nicht (Stryer 1991).

Interessant im Hinblick auf hereditäre Netzhauterkrankungen wurden die DAGKs, als 1994 die cDNA für DAGK3 (DAGKγ) kloniert wurde, die hauptsächlich in der Retina exprimiert wird (Kai et al. 1994). Des weiteren wiesen Mutationen in einer augenspezifischen Diacylglycerinkinase (*DAGK2*), die in *Drosophila melongaster* die retinale Degeneration A (*rdgA*) hervorrufen, auf eine mögliche Rolle der DAGKs in Augenerkrankungen hin (Masai et

al. 1993). Inzwischen kennt man insgesamt 9 DAGK-Isoformen, die in 5 Untergruppen unterteilt sind. DAGK3 bildet zusammen mit DAGKα und DAGKβ den ersten Subtyp, der sich durch zwei konservierte kalziumbindende EF-Hand Motive und zwei Zinkfingerdomänen auszeichnet.

Wir bestimmten zunächst die genomische Organisation von *DAGK3*. Das Gen besteht aus 24 kodierenden Exonen und umspannt etwa 30 kb genomische DNA (Anlage 3). Mit Hilfe von somatischen Zellhybriden und FISH wurde der Genlokus auf die Region 3q27-28 kartiert (Anlage 3). Diese Region überlappt mit der chromosomalen Lokalisation von OPA1, die mit Hilfe mehrerer Familien auf 3q28-29 kartiert worden war (Eiberg et al. 1994, Lunkes et al. 1995, Bonneau et al. 1995, Brown et al. 1997, Johnston et al. 1997, Votruba et al. 1997 und 1998a) (Abb. 6).

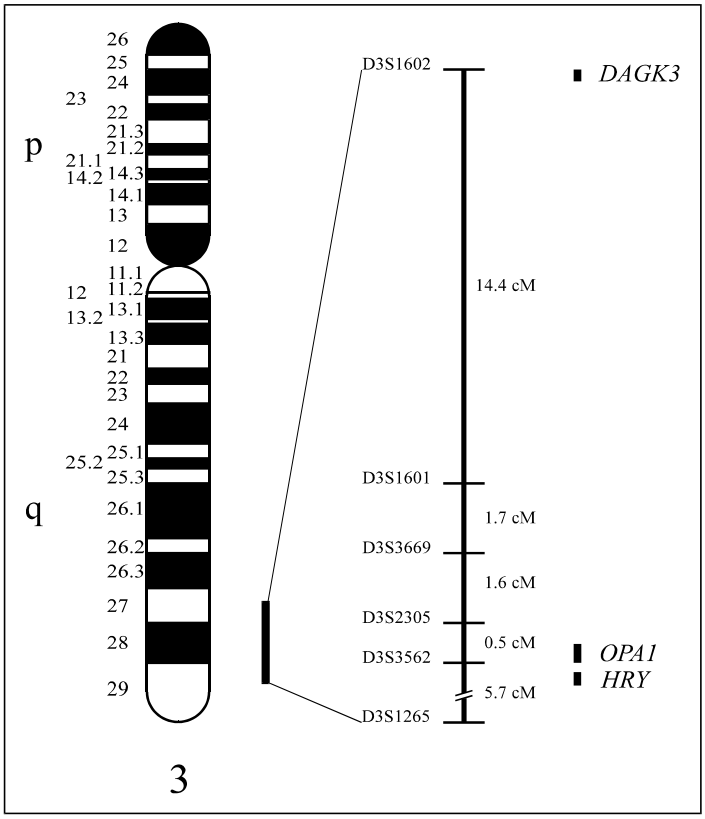

Abb. 6: Genetische Karte der Region 3q27-q29.
Die Region zwischen den Markern D3S1602 und D3S1265 beinhaltet insgesamt 25 STS-Marker und 28 Transkripte (OMIM Gene Map, http://www.ncbi.nlm.nih.gov:80/htbin-post/Omim/getmap, Stand Juli 2003). Es wurde nur eine Auswahl dargestellt. Die relative Lage von *DAGK3*, *OPA1* und *HRY* ist eingezeichnet.

Die autosomal dominante Optikusatrophie beginnt in der frühen Kindheit. Sie ist gekennzeichnet durch einen unterschiedlich starken Verlust der Sehschärfe, bitemporale Gesichtsfeldausfälle, Defekte im Farbsehen und einer bilateralen Atrophie des Sehnervs (Votruba et al. 1998). Der primäre Defekt könnte in der Degeneration von retinalen Ganglienzellen liegen (Johnston et al. 1979).

Da *DAGK3* ein gutes positionelles Kandidatengen für OPA1 war, untersuchten wir neunzehn OPA1-Patienten mit SSCP-Analysen auf Mutationen in diesem Gen. Die Mutationsanalysen ergaben keine krankheitsverursachenden Veränderungen (Anlage 3). Deshalb wurde das *DAGK3*-Gen als krankheitsassoziiertes Gen für OPA1 ausgeschlossen.

Zusätzlich wurden die Haplotypen der Marker D3S1601 und D3S1265, die die OPA1-Region flankieren, in drei OPA1-Multigenerations-Familien erstellt. Bei zwei dieser Familien (Fam. 1, Fam. 2) segregiert das Krankheitsallel mit den beiden Markern. Die Erkrankten der dritten Familie (Fam. 3) weisen am 3q28-q29 Lokus keinen gemeinsamen Haplotyp auf, was auf einen weiteren Genlokus in dieser Familie hinweist. Aus der Literatur sind noch zwei andere OPA-Loci auf Chromosom X und 18 bekannt (Assink et al. 1997, Kerrison et al. 1998).

1998 war bereits das *HRY* (*hairy homolog* (Drosophila))-Gen, das ebenfalls in dieser Region liegt, als Kandidatengen ausgeschlossen worden (Votruba et al.1998b). Inzwischen wurde jedoch auch für OPA1 das verantwortliche Gen, *OPA1*, eine Dynamin-verwandte GTPase, gefunden. Krankheitsverursachende Veränderungen konnten in vielen OPA1-Familien nachgewiesen werden. (Alexander 2000, Delettre 2000). Das Protein sitzt in der inneren Mitochondrienmembran und ist daher ubiquitär exprimiert. Da der Verlust des OPA1-Genprodukts direkt zur Apoptose führt, vermutet man, daß es evtentuell eine Rolle bei der Sequestration von Cytochrom c spielt. Diese Apoptose könnte der Grund für die Degeneration der Ganglienzellen in den OPA1-Patienten sein (Olichon et al. 2003).

3. X-gebundene juvenile Retinoschisis (RS) – Von der Krankheit über das Gen zur Therapie

3.1 Epidemiologie, Prevalenz und klinische Merkmale

Die X-gebundene juvenile Retinoschisis (RS, OMIM #312700) ist die häufigste Ursache für eine Makuladegeneration bei Jungen im Kindesalter. Weibliche Überträgerinnen dieser rezessiven Erkrankung sind klinisch nicht betroffen (George et al. 1995). Das erste Mal wurde RS bereits 1898 von dem deutschen Augenarzt Josef Haas beschrieben (Haas 1898). Das gemeinsame Merkmal aller Betroffenen ist eine bilaterale radspeichenartige Schisis in der Fovea (George et al. 1996). Die Ursache dieser Spaltung sind gelbliche Zysten, die sich im

inneren Bereich der Retina, zwischen Nervenfaserschicht und der restlichen Retina, bilden Buch). Bei 50 % der Patienten findet man diese Zysten auch in der peripheren Retina, meist temporal unten. Die von der Schisis betroffene retinale Schicht ist sehr dünn und reißt leicht ein (Abb. 1 Anlage 4). Werden dabei auch Blutgefäße der inneren Retina verletzt, kommt es zu einer vitreoretinalen Hämorrhagie. Eher selten bilden sich in der Schicht oberhalb der Schisis Risse, die dazu führen, daß Flüssigkeit unter das RPE eintreten kann und sich die Retina ablöst (de la Chapelle et al. 1994). Mit der Zeit kollabieren die Zysten im Bereich der Makula. Daher ist bei Erwachsenen oft keine zentrale Retinoschisis mehr erkennbar. In der Makula bleiben dann noch Pigmentveränderungen und große choroidale Gefäße vorhanden, die dem klinischen Bild einer altersabhängigen Makuladegeneration sehr ähnlich sind (de la Chapelle et al. 1994). Die Veränderungen in der inneren sensorischen Retina führen sekundär auch zu Funktionsstörungen der äußeren sensorischen Retina, z.B. durch die Degeneration von Photorezeptoren (Minato et al. 1991).

Erste Krankheitssymptome treten meist zwischen der ersten und zweiten Lebensdekade auf, können aber auch schon bei der Geburt vorhanden sein (Kawano et al. 1981). Die phänotypische Ausprägung ist selbst innerhalb einzelner Familien sehr variabel. Sie reicht von leichter Visusminderung, zumindest bis zum 40.-50. Lebensjahr, bis zur Erblindung bereits im frühen Kindesalter. Dies ist unter anderem davon abhängig, wie stark die Makula betroffen ist. In den seltenen Fällen früher Erblindung ist oft die ganze Retina und Aderhaut disorganisiert (de la Chapelle et al. 1994).

Die Penetranz der Erkrankung liegt bei 100 %. Die Inzidenz beträgt weltweit zwischen 1:15.000 und 1:30.000 (de la Chapelle et al. 1994). Wahrscheinlich ist die Krankheit aufgrund der leichteren Fälle und der teilweise schwierigen Diagnose, besonders in späteren Stadien der Patienten, die keine periphere Retinoschisis aufweisen, eher unterdiagnostiziert. Ein wichtiges diagnostisches Hilfsmittel ist das ERG. Im helladaptierten Auge des Patienten kommt es zu einer ausgeprägten B-Wellenreduktion, die auf eine reduzierte Aktivität der inneren Retina hinweist. Lange Zeit ging man davon aus, daß die B-Welle durch die Depolarisation der Müllerzellen entsteht. Inzwischen vermutet man jedoch, daß sie direkt mit den Interaktionen zwischen depolarisierten und hyperpolarisierten Bipolarzellen in Zusammenhang steht (Sieving et al. 1994). Die zapfenabhängigen Reizantworten können reduziert sein. Weibliche Konduktorinnen können leichte ERG-Veränderungen zeigen. Ein Zentralskotom kann bei den Erkrankten ganz unterschiedlich ausgeprägt sein, die peripheren Einschränkungen korrelieren

mit der peripheren Retinoschisis. Beim Farbsehen treten leichte unspezifische Störungen auf. Wichtig zur Abgrenzung von kongenitaler stationärer Nachtblindheit, die ebenfalls kongenitale Visusminderung und ein ähnliches ERG aufweist, ist die fehlende Nachtblindheit (Kellner 2003).

Bisher ist keine Therapie zur Heilung dieser degenerativen Prozesse bekannt. Prophylaktische Laserkoagulationen der peripheren Retinoschisis sind aufgrund des Ablatiorisikos kontraindiziert (Kellner 2003). Glaskörperblutungen resorbieren sich in der Regel spontan. Bei stärkeren Blutungen ist eine Vitrektomie angezeigt. Die seltenen Ablösungen der Retina müssen mit konventionellen chirurgischen Methoden behandelt werden (de la Chapelle et al. 1994).

3.2 Identifizierung des RS1-Gens

3.2.1 Kartierung des Krankheitsgens

Als Josef Haas die X-gebundene juvenile Retinoschisis 1898 erstmals beschrieb, vermutete er, daß die Veränderungen in der Netzhaut durch eine Entzündung verursacht werden (Haas 1898). 1913 publizierte Pagenstecher einen RS-Stammbaum mit X-gebundener Vererbung (Pagenstecher 1913). Erste Kartierungsversuche ergaben eine lose Kopplung von RS mit dem Blutgruppenlokus Xg (Eriksson et al. 1969, Ives et al. 1970, Race and Sanger 1975, Boman et al. 1976, Forsius and Eriksson 1980).

Mit Hilfe des Restriktionslängenpolymorphismus (RFLP) RC8 (DXS9) wurde RS in zwei Familien auf den distalen kurzen Arm des X-Chromosoms lokalisiert (Wieacker et al. 1983). Nachdem in dieser Region weitere RFLPs identifiziert worden waren, wurde der RS-Genlokus zwischen den Markern (DXS207, DXS43) und (DXS274, DXS41) kartiert (Alitalo et al. 1987, 1988, Dahl et al. 1988, Gellert et al. 1988, Alitalo et al. 1991). Die Distanz zwischen den flankierenden Markern wurde zu dem damaligen Zeitpunkt auf 7 cM geschätzt (de la Chapelle et al. 1994). Die Kopplung fast aller RS-Familien mit diesen Markern zeigte die genetische Homogenität dieser Erkrankung (de la Chapelle et al. 1994). Daher konnten diese Marker bereits für Überträgerinnen- und Pränataldiagnostik benutzt werden. Das Risiko eines Rekombinationsereignisses mußte allerdings berücksichtigt werden (Kaplan et al. 1991).

Als dann erste polymorphe Mikrosatelliten-Marker verfügbar wurden, gelang es, den Bereich immer weiter einzugrenzen (Bergen et al. 1994, Weber et al. 1995). Die engsten flankierenden Marker, bei denen noch Crossing-over nachgewiesen werden konnten, waren DXS418 und DXS999/DXS7161 (Dumur et al. 1995, Pawar et al. 1995, Trump et al. 1996, Van de Vosse et al. 1996). Sie umspannen eine ungefähr 900 Kilobasen große Region (Huopaniemi et al. 1997). Es wurden mehrere YAC- und PAC-contigs erstellt, die das Intervall abdecken (Alitalo et al. 1995, Ferrero et al. 1995, Van de Vosse et al. 1996, Huopaniemi et al. 1997). Diese Informationen lieferten einen exzellenten Ausgangspunkt für eine positionelle Klonierung des gesuchten RS-Gens.

3.2.2 Erstellen einer Transkriptkarte des RS-Genlokus

Zunächst wurde mit Hilfe verschiedener Methoden wie Exon-*trapping*, EST-Datenbankanalysen und computergestützter Exonvorhersage (GRAIL) eine Transkriptkarte der Kandidatenregion generiert (Anlage 4). Beschleunigt wurde dies dadurch, daß ca. 800 Kilobasen der genomischen DNA zwischen DXS418 und DXS999 bereits durch die Sequenzierarbeiten des Sanger Centers (http://www.sanger.ac.uk/) bekannt und verfügbar waren. Durch Exon-*trapping* Versuche konnten 46 Exone kloniert werden, von denen 30 einen offenen Leseraster (ORF) aufwiesen. Datenbankanalysen in diesem nicht vollständigen Bereich ergaben 162 ESTs, die zu 16 Sequenzen zusammengefaßt werden konnten. Expressionsanalysen dieser putativen kodierenden Bereiche bestätigten uns, daß wir insgesamt mindestens 13 neue Transkriptionseinheiten (TUs) identifiziert hatten. Des weiteren enthält die 900 kb großen Kandidatenregion das *PPEF*-Gen, eine Serin-Threonin Phosphatase (Montini et al. 1997) (Abb. 1, Anlage 4).

3.2.3 Klonierung des *RS1*-Gens

Eine der Transkriptionseinheiten bestand aus 4 ESTs, die alle der Soares Retina cDNA-Bank entstammten, und stellte damit ein besonders interessantes Kandidatengen dar. Mittels Durchsuchen einer Phagen-cDNA-Bank und 5'RACE-Experimenten konnte die vollständige cDNA-Sequenz identifiziert werden (Anlage 5). Sie enthält 6 kodierende Exone und einen offenen Leseraster von 687 bp. Die ersten 23 Aminosäuren des Proteins wurden als Signalpeptid vorhergesagt, das bei der Ausschleusung aus der Zelle abgespalten werden sollte. Das kalkulierte Molekulargewicht des sekretierten Proteins sollte somit etwa 23 kDa (201 Aminosäuren) betragen. Codon 101-203 des Proteins weisen eine hohe Ähnlichkeit zur

Discoidin-Domäne auf, einem hochkonservierten Motiv, das eine Rolle bei der Zelladhäsion spielt (Anlage 5). Auf die Funktion der Discoidindomäne wird in Folgenden noch genauer eingegangen (s. S. 26). Expressionsanalysen zeigen, daß das Transkript retinaspezifisch ist und eine Länge von 3,1 kb besitzt (Anlage 5). Die Exon/Intron-Grenzen konnten größtenteils anhand der veröffentlichten DNA-Sequenzen bestimmt werden. Zusätzlich mußte ein PAC-Subklon teilweise sequenziert werden.

Anschließende Mutationsanalysen in je einem Betroffenen von 9 unabhängigen RS-Familien ergaben eine Nonsense-, eine *frame shift*-, eine Spleiß- und sechs Missense-Mutationen, die alle mit dem RS-Phänotyp segregierten (Anlage 5). Damit war der Nachweis erbracht, daß es sich bei diesem Kandidatengen tatsächlich um das verantwortliche Gen, *RS1*, für die X-gebundene juvenile Retinoschisis handelte.

RS1 war nach *Peripherin/RDS*, *TIMP3* und *ABCR* das vierte Gen, das mit einer Makuladystrophie in Verbindung gebracht wurde (Keen et al. 1996, Weber et al. 1994, Allikmets et al. 1997). Darüber hinaus war *RS1* das erste Makuladystrophie-Gen, das durch einen reinen positionellen Klonierungsansatz gefunden worden war.

3.3 Bestätigung des *RS1*-Gens

3.3.1 Beschriebene Mutationen

Bis heute wurden insgesamt 376 Mutationen im *RS1*-Gen beschrieben (http://www.dmd.nl/rs/). Davon sind 75,5 % (284) Missense-, 5,6 % (21) Nonsense-Mutationen, 5,6 % (21) Basenaustausche, die Spleißstellen verändern, 10,1 % (38) Deletionen, 2,1 % (8) Duplikationen und 0,8 % (3) Insertionen. Die Mutationen sind nicht zufällig über das ganze Gen verteilt, sondern zeigen auffällige regionale Anhäufungen (Abb.7).

Die meisten Mutationen, vor allem die Missense-Mutationen, befinden sich in den Exonen 4 bis 6, dem Bereich, der eine Discoidindomäne kodiert. Homologievergleiche der Discoidindomäne mit denen verschiedener anderer Proteine unterschiedlicher Spezies ergaben, daß häufig hochkonservierte Aminosäuren betroffen sind (Anlage 5, Retinoschisis Consortium 1998). Auffällig ist, daß 20 % (56) der Missense-Mutationen Cysteinreste involvieren. Dies deutet auf die Wichtigkeit von Disulfidbrücken für die Proteinstruktur und

die Funktion des Proteins hin. Deletionen, Duplikationen und Insertionen kommen vor allem in den Exonen 1-3 gehäuft vor. Sie führen durch Verschiebungen des Leserahmens (*frameshifts*) oder durch veränderte Spleißstellen in der Regel zu einem frühzeitigen Abbruch der Proteintranslation. Die Tatsache, daß in den ersten 3 Exonen praktisch keine Missense-Mutationen gefunden wurden, läßt vermuten, daß dem unbekannten Bereich zwischen den Aminosäuren 24 bis 62 des nativen Proteins keine wichtig Funktion zukommen dürfte.

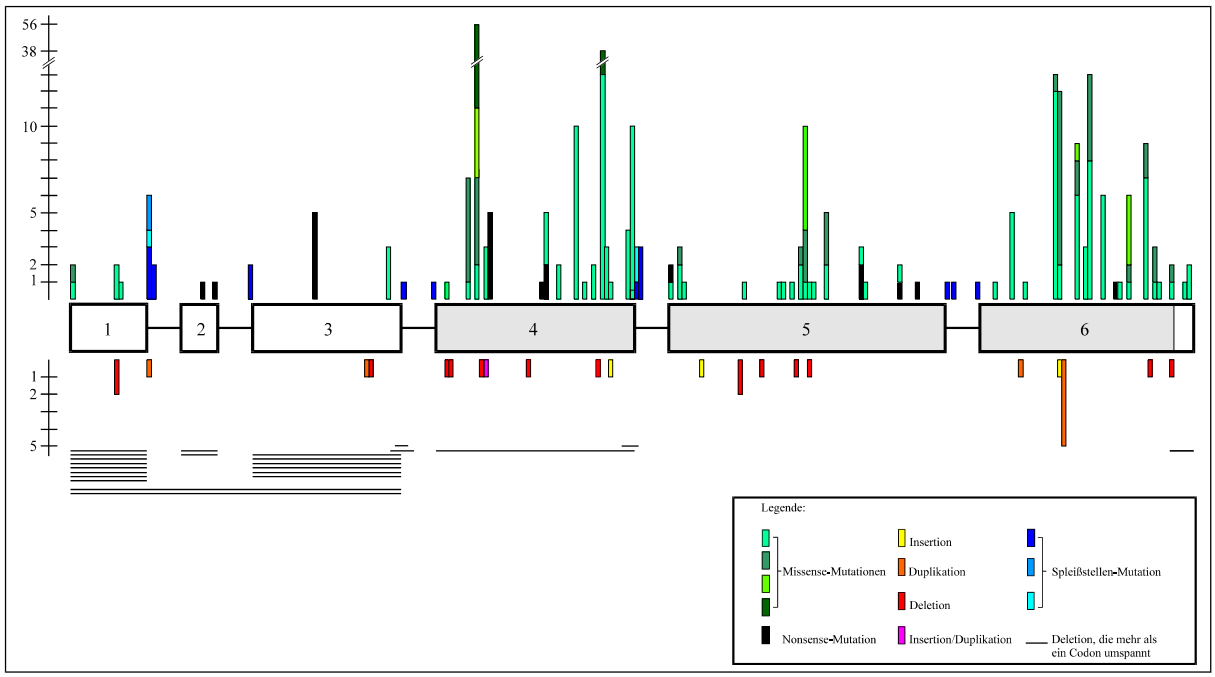

Abb. 7: Mutationen in *RS1*
Das *RS1*-Gen ist schematisch dargestellt. Die Discoidin-Domäne ist grau unterlegt. Die Lokalisierung der einzelnen Mutationen bezieht sich auf das jeweils betroffene Codon und ist maßstabsgetreu angegeben. Missense-, Nonsense- und Spleißstellen-Mutationen befinden sich oberhalb, Deletionen, Insertionen und Duplikationen unterhalb des Gens. Unterschiedliche Missense- bzw. Spleißstellen-Mutationen eines Codons sind farblich voneinander abgegrenzt. Der Maßstab zeigt an, wie viele Mutationen insgesamt das jeweilige Codon betreffen. Quelle der Mutationen: http://www.dmd.nl/rs/.

3.3.2 *De novo* Mutationen

1999 konnten wir eine erste *de novo* Mutation im *RS1*-Gen bestätigen (Anlage 6). Wir untersuchten eine griechische Familie, in der zwei 9 und 5 Jahre alte Brüder an X-gebundener juveniler Retinoschisis erkrankt waren. Alle anderen Familienmitglieder hatten einen normalen Fundus und auch keine Veränderungen im ERG. Beide Brüder zeigten mit Retinaablösung, peripherer Schisis und stark verminderter Sehschärfe bereits im Kindesalter schwerwiegende und eindeutige RS-Symptome.

Die Mutationsanalyse ergab bei beiden Brüdern und der Mutter einen Pro203Leu Austausch (Anlage 6). Die anschließende Testung der beiden mütterlichen Großeltern ergab, daß keiner der beiden diese Basenveränderung trug. Die Vaterschaft konnte bestätigt werden. Mit

mehreren *RS1*-flankierenden Markern wurde der krankheitsassoziierte Haplotyp in der Familie bestimmt (Anlage 6). Diese Analyse lieferte den Nachweis, daß die Mutation mit großer Wahrscheinlichkeit *de novo* auf dem großväterlichen X-Chromosom entstanden war.

Anhand dieses Einzelbefundes einer *de novo* Mutation kann keine Aussage über die Neumutationsrate in *RS1* getroffen werden. Die Tatsache jedoch, daß distinkte Mutationen (z.B. Glu72Lys, Arg141Cys) in mehreren Patienten unterschiedlicher ethnischer Herkunft gefunden werden, läßt auf eine signifikante Neumutationsrate schließen. Die Pro203Leu Mutation der griechischen Familie, die eine hochkonservierte Aminosäure der Discoidindomäne verändert, ist beispielsweise in 5 anderen Familien aus Frankreich, Japan, Finnland und den Niederlanden nachgewiesen worden (http://www.dmd.nl/rs/).

Die meisten dieser häufiger auftretenden Mutationen betreffen CpG Dinucleotide, die aufgrund der Instabilität des Cytosins besonders sensible Positionen (*hotspots*) darstellen (Retinoschisis Consortium 1998). Auch die Pro203Leu Mutation liegt in einem CpG Dinucleotid (Codon 203: C**C**G nach C**T**G). Wird das Cytosin eines solchen Dinucleotids methyliert, wird es häufig spontan desaminiert, so daß ein Thymin entsteht. Da die falsche T-G Basenpaarung von dem DNA-Reparatursystem nur schlecht erkannt wird, entsteht eine C→T Transition.

3.3.3 Die senile Retinoschisis

Neben der X-gebundenen juvenilen Retinoschisis gibt es noch weitere angeborene und erworbene Formen mit klinischen Manifestationen einer Retinoschisis (Gorlin and Knobloch 1972). Bei der sporadischen senilen Retinoschisis werden zwei Formen unterschieden. In der milderen peripheren Form befindet sich die Schisis in der äußeren plexiformen Schicht. Die bullöse Form ist schneller fortschreitend und führt unter Umständen zur Ablösung der Retina. In beiden Formen treten die Symptome erst im Erwachsenenalter auf. Des weiteren kann die senile Form durch die fehlende radspeichenartige Schisis der Fovea und einer negativen Familiengeschichte von der X-gebundenen juvenilen Retinoschisis abgegrenzt werden. Da die bullöse Form gewisse Ähnlichkeiten mit der RS aufweist, haben wir 7 Patienten mit seniler Retinoschisis nach Mutationen in dem *RS1*-Gen untersucht (Anlage 7). Wir konnten keine Veränderungen entdecken und schlossen daraus, daß dieses Gen nicht an der Pathogenese der senilen Retinoschisis beteiligt ist (Anlage 7).

3.4 Funktionelle Analyse

3.4.1 Immunohistochemische Lokalisation des Retinoschisins in der Retina

Um mehr über die Funktion von RS1 zu erfahren, wurde zunächst die immunohistochemische Lokalisation von RS1 in der Retina bestimmt. Dazu wurde ein Antikörper gegen ein 17 Aminosäuren großes Peptid (Aminosäure 22-39) hergestellt. Dieser Antikörper erkennt spezifisch sowohl das humane als auch das murine Retinoschisin. Molday et al. (2001) konnten nachweisen, daß *RS1* in den Photorezeptorzellen und den Bipolarzellen der Retina exprimiert wird. Das sekretierte Protein befindet sich in der Umgebung der Photorezeptoren, in der OPL und IPL und vermutlich im extrazellulären Bereich in enger Assoziation mit Zellmembranen der INL (Molday et al. 2001, Abb. 6b, Anlage 9). Zusätzlich wurde RS1 in den Endfüßen der Müllerzellen in der Nervenfaserschicht, der Region, in der bei RS-Patienten die Zysten entstehen, nachgewiesen (Reid et al. 2003). Westernblotanalysen retinaler Homogenate zeigen, daß sich RS1 in der Membranfraktion befindet. Das Protein scheint daher mit Zellmembranen assoziiert zu sein (Molday et al. 2001).

3.4.2 Funktion der Discoidindomäne

Das RS1-Protein besteht fast ausschließlich aus einer Discoidindomäne (Aminosäureposition 63-219). Die Anhäufung der *RS1*-Mutationen in dieser Domäne unterstreicht deren Bedeutung. Erstmals beschrieben wurde die Domäne im Discoidin I des Schleimpilzes *Dictyostelium discoideum* (Springer et al. 1984). Dieses Protein ist ein Lektin, das notwendig ist für die Erhaltung der Morphologie, der Organisation des Zytoskeletts und für die Zelladhäsion während der Zellaggregation (Alexander et al. 1992). Inzwischen sind bei Invertebraten und Säugetieren über 20 weitere Proteine mit Discoidindomänen bekannt, wie z.B. Neurexin IV, Neuropilin-1, Blutgerinnungsfaktor V und VIII, Milchfettprotein-E8 und das Endothelzell-spezifische Del-1 (Anlage 5, Baumgartner 1998). Sie kommen in membrangebundenen und in sekretierten Proteinen vor. Die meisten dieser Proteine enthalten zusätzlich zu den 1-2 Discoidindomänen noch weitere funktionelle Bereiche wie z.B. die Tyrosinkinase im Discoidindomänen-Rezeptor 1 (DDR-1). Häufig findet man zusätzliche EGF (*epidermal growth factor*)-Domänen, die mit ihrer RGD (Arg-Gly-Asp)-Sequenz an Integrine binden, wie z.B. in Del-1 und Neurexin IV (Baumgartner 1998).

Eine gemeinsame Funktion der Mitglieder der Discoidin-ähnlichen Familie scheint die Bindung an Proteine der extrazellulären Matrix (ECM) oder an Zelloberflächen zu sein. Die Discoidindomäne von DDR1 ist für die Collagen-Bindung und die Dimerisierung des Proteins verantwortlich (Curat et al. 2001). Von den Blutgerinnungsfaktoren V und VIII ist bekannt, daß die Discoidindomänen während der Blutgerinnung an Phospholipiden auf der Oberfläche der Blutplättchen binden (Kane and Davie 1988).

Kürzlich wurde die 3-dimensionale Kristallstruktur der C2 Discoidindomäne der beiden Blutgerinnungsfaktoren bestimmt (Pratt et al. 1999, Macedo-Ribeiro 1999). Es handelt sich um ein globuläres Protein mit β-Faltblattstruktur, das 5 parallele und 3 antiparallele Stränge enthält. Basierend auf dieser Struktur wurde ein Homologie-Modell der RS1-Discoidindomäne erstellt (Fraternali et al. 2003) (Abb. 8).

Abb. 8: Strukturmodell der Discoidindomäne des Retinoschisins
Das Strukturmodell wurde anhand der bekannten Kristallstruktur der C2 Discoidindomäne von Faktor V und VIII mit Hilfe von SWISS-MODEL (Guex and Peitsch 1997) erstellt. Es enthält die Aminosäurereste C63 bis C222 des nativen Retinoschisins. Die Position von fünf Cysteinresten (Cys63, Cys83, Cys110, Cys142 und Cys219) ist eingezeichnet.

Dieses Modell ermöglicht es, die Auswirkungen der Missense-Mutationen auf die Struktur des Proteins besser zu verstehen. Man kennt nun die putative Umgebung der veränderten Aminosäure und kann eher abschätzen, welche Konsequenzen ein bestimmter Aminosäureaustausch hat. Aminosäureaustausche im Inneren der Proteinstruktur führen häufig durch Ladungsänderungen und Änderung der hydrophoben Eigenschaften zur Destabilisierung der Proteinfaltung. Bestätigt wurde dies durch Expressionsexperimente mit mutiertem Retinoschisin. Bei vielen Missense-Mutationen kommt es durch Mißfaltung des

Proteins nicht zur Ausschleusung aus dem endoplasmatischen Retikulum (ER). Die mutanten Proteine werden bereits im ER abgebaut (Wang et al. 2002, Wu and Molday 2003). Diese intrazelluläre Degradierung erklärt teilweise die fehlende Korrelation zwischen Mutationstyp und Schwere der Erkrankung, da verschiedene Mutationen zu demselben Ergebnis führen, dem Nichtvorhandensein von RS1.

Aminosäureaustausche an der Oberfläche des Proteins beeinträchtigen direkt die Interaktion mit anderen Proteinen. Durch die Analyse der Oberfläche des RS1-Modells konnte ein exponierter hydrophober Bereich identifiziert werden. Möglicherweise ist das RS1 an dieser Stelle in der Zellmembran verankert, analog zu der Phosphatidylserinbindung der Blutgerinnungsfaktoren (Fraternali et al. 2003). Diese momentan nur theoretische Phospholipidinteraktion bedarf einer experimentellen Bestätigung.

3.4.3 Strukturelle Analyse - Disulfidbrücken und Oligomerisierung

Westernblotanalysen zeigen, daß Retinoschisin unter nicht-reduzierenden Bedingungen in Form eines großen Komplexes von ca. 160 kDa vorliegt (Molday 2001). Inzwischen weiß man, daß dieser Komplex ein Retinoschisin-Oligomer, wahrscheinlich ein Oktamer, darstellt (Wu and Molday 2003). Studien, in denen Cystein-Serin Mutanten von Retinoschisin in Zellkulturexperimenten untersucht wurden, brachten neue Erkenntnisse über die Funktion der Disulfidbrücken. Wu und Molday (2003) fanden heraus, daß 4 Cysteine der Discoidindomäne 2 intramolekulare Disulfidbrücken bilden (Abb. 9). Ist eines davon von einem Basenaustausch betroffen, kann sich das Protein im ER nicht richtig falten und wird abgebaut.

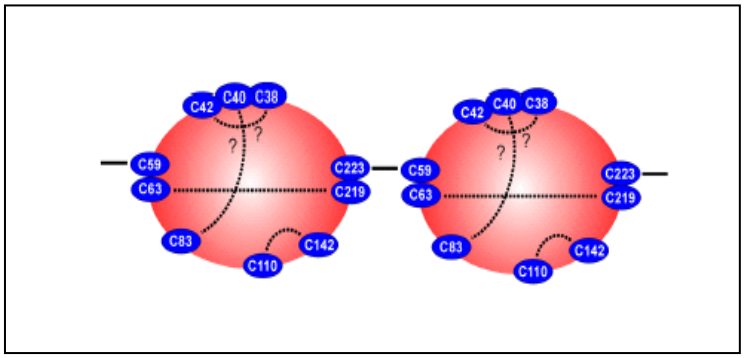

Abb. 9: Modell der Disulfidbrücken des Retinoschisins
Dargestellt ist das putative Muster der Disulfidbrücken in Retinoschisin. C59 und C223 bilden intermolekulare, C110/C142 und C63/C219 intramolekulare Disulfidbrücken. Eine mögliche Disulfidbrückenbildung der anderen vier Cysteine ist in Analogie zu den Vernetzungen in β-Integrinen dargestellt (nach Abb. 6B, Wu and Molday 2003).

Die 2 Cysteine, welche die Discoidindomäne flankieren, sind für die Disulfid-vernetzte Oligomerisierung verantwortlich. Mutanten in diesen Aminosäureresten (C59S, C223S) werden ausgeschleust, können aber keine Oligomere bilden (Wu and Molday 2003). Vermutlich findet eine Interaktion von Zellen der Retina unter anderem durch

Oligomerisierung membranassoziierter RS1-Moleküle statt. Eventuell sind in diese Komplexe weitere, bisher noch unbekannte Proteine involviert.

3.5 Ein Tiermodell für die X-gebundene juvenile Retinoschisis - die Retinoschisin-defiziente Maus

3.5.1 Mausmodelle

Tiermodelle menschlicher Erkrankungen leisten wichtige Beiträge zum Verständnis der molekularen Pathogenese und erlauben es, neue Therapieansätze zu erproben. Die Maus ist das am häufigsten verwendete Tiermodell. Sie ist das kleinste Säugetier und kann in ausreichend großer Zahl auf vergleichsweise wenig Raum artgerecht und kostengünstig gehalten werden. Mit einer Generationszeit von nur 3 Monaten und einer Wurfgröße von 6-10 Jungtieren läßt sich schnell eine relativ große Anzahl von Tieren züchten. Die Auswirkungen von pathogenen Mutationen können leicht über mehrere Generationen hinweg verfolgt werden. Die kurze Lebensdauer von ungefähr zwei Jahren bietet den Vorteil, auch die Krankheitssymptome, die erst in höherem Alter auftreten, in überschaubaren Zeiträumen untersuchen zu können.

Vor etwa 150 Jahren begann in Europa und Nordamerika die gezielte Zucht von Mausvarianten. Dabei wurden Mäuse mit natürlich vorkommenden, genetisch bedingten Krankheiten identifiziert, die wichtige Parallelen zu menschlichen Krankheitsbildern aufweisen (z.B *rds*-Maus, *retinal degeneration slow*, Travis et al. 1989).Heute werden mit chemischen Agenzien wie z.B. Ethylnitrososharnstoff (ENU) Mutationen induziert. Sind unter diesen mutanten Tiere welche, die zufällig den gesuchten Phänotyp zeigen, kann zunächst der Krankheitslokus und dann das dazugehörige Gen bestimmt werden.

Ende der 80er Jahre ist es gelungen, murine embryonale Stammzellen (ES-Zellen) zu kultivieren und mittels homologer Rekombination gezielt Mutationen in diese ES-Zellen einzuführen. Gelingt es, diese Zellen in die Keimbahn zu bringen, können genetisch veränderte Mäuse gezüchtet werden. Je nach Mutationstyp bezeichnet man die Tiere als knock-out (Funktionsverlust des Gens, *loss of function*) oder als knock-in (neue Funktion des Gens, *gain of function*) Mäuse. Grundsätzlich können knock-out oder knock-in Mäuse unterschiedliche Phänotypen entwickeln. Häufig sind homozygot mutante Tiere nicht

lebensfähig (Letalmutanten). Es gibt auch zahlreiche Beispiele dafür, daß sich die Mutation nicht ausprägt. Vermutlich spielen hier Phänomene wie Redundanz von Proteinfunktionen oder genetische Hintergründe bestimmter Mausstämme eine wichtige Rolle. Überdies kann der Phänotyp einer gezielten Mutation bei verschiedenen Mausstämmen variieren. Nur im günstigsten Fall spiegelt die mutante Maus das Krankheitsbild des Menschen wider. Im Falle der RS-Erkrankung kommt hinzu, daß es sich hierbei primär um eine Makuladegeneration handelt, die Maus jedoch als nachtaktives Tier keine Makula besitzt.

Rezessive Erkrankungen werden meist durch einen Funktionsverlust des Proteins ausgelöst. Deshalb haben wir uns entschlossen, eine *Rs1h* knock-out Maus herzustellen. Typischerweise wird zur Generierung einer knock-out Maus ein wichtiger Bestandteil des endogenen Gens durch ein Antibiotikaresistenzgen ersetzt. Dazu mußte zunächst erst das orthologe murine *RS1*-Gen identifiziert und charakterisiert werden.

3.5.2 Charakterisierung des murinen RS1 homologen Genortes (*Rs1h*)

Das orthologe *RS1*-Gen der Maus, *Rs1h*, konnte mit degenerierten Oligonukleotiden amplifiziert und anschließend kloniert werden. Auf Nukleotidebene beträgt die Homologie 89%, während die Sequenz des Translationsprodukts sogar zu 96 % identisch ist (Anlage 8). Analog zum Menschen ergibt die Expressionsanalyse zwei retinaspezifische Transkripte, die 5,6 bzw. 4,9 kb groß sind (Abb. 4 Anlage 8). 5'RACE-Produkte weisen sowohl bei Mensch als auch bei Maus auf multiple Transkriptionsstartpunkte hin. Die genomische Organisation wurde mit Hilfe einer genomischen Maus-Phagenbank aufgeklärt. Die Introngrößen wurden über PCRs mit flankierenden Oligonukleotiden bestimmt. Die Exon/Intron-Struktur ist hochkonserviert, die kodierende Sequenz ist an der selben Stelle wie beim Menschen von Introns unterbrochen, die sich allerdings in ihrer Größe unterscheiden. Wie in dem humanen Gen liegt jedoch auch bei der Maus das größte Intron zwischen Exon 1 und 2 (Abb. 10)

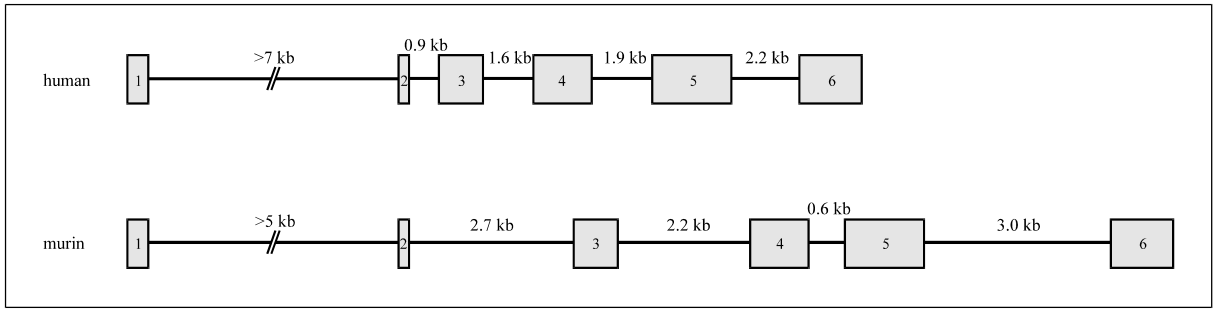

Abb. 10: Vergleich der genomischen Organisation des humanen und murinen *RS1*-Gens
Exone und Introne sind jeweils maßstabsgetreu dargestellt.

Zusätzlich wurden noch die 5'-untranslatierten Bereiche, d.h. die möglichen Promotor-regionen, von *RS1* und *Rs1h* auf konservierte Elemente untersucht. Ein Abschnitt von ungefähr 150 bp strangaufwärts vom Startcodon ATG weist sogar fast 82 % Identität auf. Auch dies ist ein Beweis, daß es sich tatsächlich um das orthologe Gen handelt.

Datenbankrecherchen ergeben mehrere mögliche Transkriptionsfaktor-Bindungsstellen in den konservierten Bereichen der beiden Species (Abb. 2 Anlage 8). Besonders interessant ist die Bindungsstelle für den trans-aktivierenden CRX-Faktor (*cone-rod homeobox*). Dieser CRX-Faktor scheint die Transkription vieler Photorezeptor-spezifischer Gene wie z.B. *cone opsin* und *arrestin*, zu regulieren (Furukawa et al. 1997). Microarrayanalysen mit mRNAs von Wildtyp und $CRX^{-/-}$ Retinae identifizierten 10 Photorezeptor-spezifische Gene, die in $CRX^{-/-}$ Mutanten herunterreguliert sind. Eines von ihnen ist *Rs1h* (Livesey et al. 2000).

Zusammenfassend läßt sich feststellen, daß das murine *Rs1h*-Gen sowohl strukturell als auch funktionell hoch konserviert ist und die Maus daher ein gutes Modellsystem für die Untersuchung der RS1-Funktion, besonders auch im Hinblick auf die Pathogenese bei RS, darstellen sollte. Mit der Kenntnis der genomischen Struktur des Mausgens konnte nun das Konstrukt für eine Rs1h knock-out Maus hergestellt werden.

3.5.3 Generierung der *Rs1h* knock-out Maus

Für das Konstrukt wurde ein *lacZ*-Reportergen mit PolyA-Signal in den Leseraster des Exon 3 kloniert. Damit wird das *Rs1h*-Gen bereits vor der Discoidindomäne, dem Hauptbestandteil des RS1-Proteins, unterbrochen. Als Antibiotikaresistenzgen wurde eine Neomycinkassette mit separatem Promotor eingebaut. Umgeben ist diese Kassette mit 129SV spezifischer DNA von 2,4 kb bzw. 3,5 kb, die für homologe Rekombinationen notwendig und im Prinzip ausreichend ist (Abb. 1 Anlage 9). Nach der Injektion mutierter ES-Zellen in C57BL/6 Blastozysten wurden zwei Chimären mit Keimbahntransmission erhalten. Aus der Verpaarung heterozygoter F1-Weibchen mit C57BL/6 WT-Männchen gingen die ersten Nachkommen hemizygot für die *Rs1h*-Mutation hervor. Der Genotyp wurde mittels PCR und Northern-Blot bestätigt. Westernblotanalysen mit dem gegen den N-Terminus gerichteten RS1-Antikörper ergeben bei $Rs1h^{-/Y}$ Mäusen kein Signal, was bedeutet, daß es sich bei dem unterbrochenen *Rs1h*-Locus tatsächlich um ein wahres Null-Allel handelt. Möglicherweise wird das Fusionsprotein bereits im endoplasmatischen Retikulum als „falsch" erkannt und entsprechend abgebaut. Ursprünglich wollten wir die Expression des *Rs1h*-Gens im Laufe der

Entwicklung des Auges bei der *Rs1h*$^{-/Y}$ Maus durch eine spezielle Färbung mit Hilfe des LacZ-Proteins untersuchen. Dies ist aufgrund des defizienten Fusionsproteins nicht möglich.

3.5.4 Phänotyp der *Rs1h*$^{-/Y}$ Maus

Äußerlich kann man die *Rs1h*$^{-/Y}$ Mäuse nicht von den WT-Mäusen desselben Wurfs unterscheiden. Die Untersuchung des Fundus ergab kleine zystenähnliche Strukturen in der inneren Retina, die manchmal bis in die Nervenfaserschicht reichen. Im Gegensatz zum Menschen, bei dem sich diese Zysten hauptsächlich auf die Makula beschränken, sind sie bei der Maus über die gesamte Retina verteilt. Größere Zysten befinden sich ähnlich wie beim Menschen in der Peripherie der Retina. Dunkeladaptierte ERGs zeigen bei den 3 Monate alten knock-out Tieren den für RS-Patienten typischen Verlust der positiven B-Welle, der auf funktionelle Störungen in der inneren Retina hindeutet. Die negative A-Welle, für die eine normale Funktion der inneren und äußeren Retinazellen verantwortlich ist, ist zwar etwas niedriger als normal, zeigt aber einen ähnlichen Verlauf. Helladaptierte ERGs sind stark reduziert, was für eine Dysfunktion im Zapfensystem spricht (Abb. 2, Abb. 3 Anlage 9). Obwohl die Maus also keine Makula besitzt, weist der Phänotyp der *Rs1h*$^{-/Y}$ Maus viele Parallelen zu dem RS-Erkrankungsbild des Menschen auf, und stellt damit durchaus ein geeignetes Modellsystem dar, um die molekulare Pathogenese bei RS im Detail zu studieren.

3.5.5 Histologie

Histologische Untersuchungen der Retina 2 Monate alter *Rs1h*$^{-/Y}$ Mäuse zeigen eine allgemeine Disorganisation der Zellen sowohl in der äußeren als auch in der inneren Retina (Abb. 11).

In der inneren Körnerschicht befinden sich teilweise große Schisis-artige Hohlräume. Elektronenmikroskopische Aufnahmen zeigen, daß sich dort zelluläre Abbauprodukte und Mikrogliazellen mit ihrem filamentösen Material ansammeln (Abb. 5 Anlage 9). Besonders auffällig ist jedoch die Reduktion der Photorezeptorzellen. Bei 2 Monate alten Tieren enthält die äußere Körnerschicht nur noch 4-5 statt 10 Reihen an Zellkernen. Anfangs scheinen die Zapfen deutlich stärker als die Stäbchen betroffen zu sein (Anlage 9).

Immunohistochemische Färbungen mit dem Antikörper gegen das Zapfen-spezifische Opsin markieren bei der *Rs1h*$^{-/Y}$ Maus nicht nur die äußeren Segmente, sondern zusätzlich auch die

inneren Segmente, Zellkörper und synaptische Regionen (Abb. 6 Anlage 9). Die Frage, ob diese Delokalisation direkt mit dem fehlenden RS1 zusammenhängt, kann momentan noch nicht beantwortet werden. Färbungen mit einem Antikörper gegen PSD-95, einem Synapsenprotein, zeigten, daß in der mutanten Maus statt OPL und IPL nun die inneren Segmente und die OPL markiert waren. Dies könnte auf eine direkte oder indirekte Involvierung von RS1 in die Synapsenbildung und ihre Stabilität hinweisen. Diese veränderte PSD-95 Lokalisation konnte allerdings mit zusätzlichen anti-PSD-95 Antikörpern, die gegen andere Epitope des PSD-95 gerichtet waren, nicht bestätigt werden, insbesondere aufgrund der Tatsache, daß sie weder bei der WT- noch bei der *Rs1h*$^{-/Y}$-Maus die IPL anfärben. Ob RS1 also tatsächlich auch im Bereich der eigentlichen Synapsenstruktur eine wichtige Rolle spielt, bleibt zunächst offen und muß im Detail weiterhin untersucht werden.

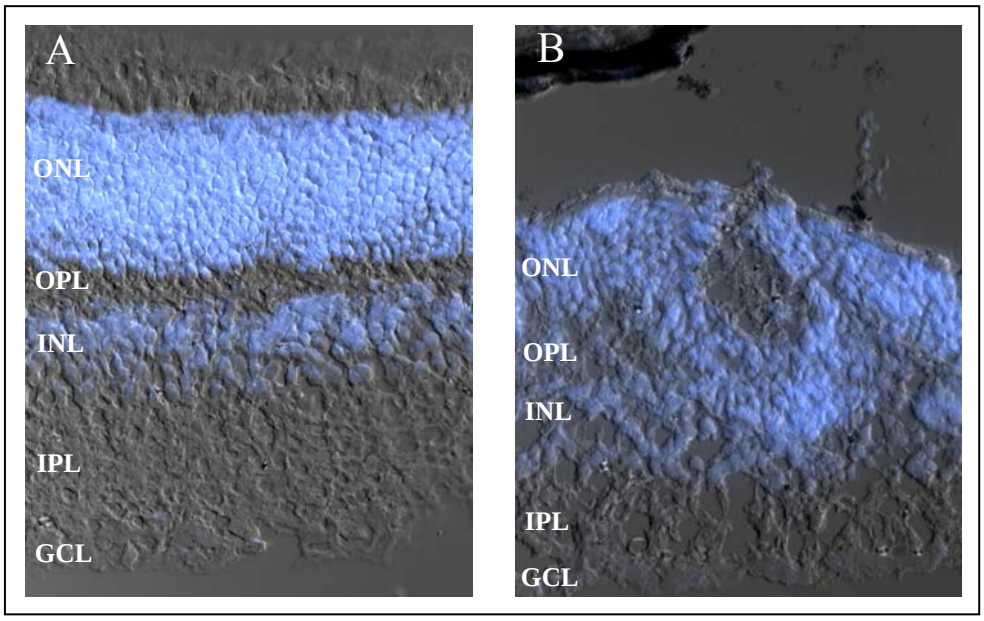

Abb. 11: Fluoreszenzmikroskopie von Retinaschnitten 21 Tage alter WT und Rs1h$^{-/Y}$-Mäuse
Fluoreszenzaufnahmen einer DAPI Kernfärbung (blau) und Aufnahmen mit differentiellem Interferenzkontrast (DIC) sind übereinandergelagert. (**A**) Ausschnitt einer WT-Retina und (**B**) einer Rs1h$^{-/Y}$-Retina. Die ONL der Rs1h$^{-/Y}$-Retina zeigt rosettenförmige Disorganisation, ONL und INL sind nicht mehr klar voneinander abgegrenzt. Abkürzungen: ONL, äußere Körnerschicht; OPL, äußere plexiforme Schicht; INL, innere Körnerschicht; IPL, innere plexiforme Schicht; GCL, Ganglienzellschicht.

Die beobachtete Disorganisation der verschiedenen Retinaschichten bei der *Rs1h*$^{-/Y}$-Maus läßt sich aufgrund des Verlusts des RS1-Proteins verstehen. Durch eine fehlende Zelladhäsion zwischen benachbarten Zellen bzw. gegenüber der Zellmatrix, die durch die Discoidindomäne des RS1-Proteins vermittelt werden könnte, kann die Zellarchitektur der Retinaschichten beeinträchtigt werden.

3.5.6 Apoptose in der Retina der *Rs1h*$^{-/Y}$-Maus

Bei einigen Tiermodellen verschiedener Netzhautdystrophien kommt es durch den Verlust der Photorezeptoren zur Degeneration der Retina. Dies scheint auch bei der *Rs1h*$^{-/Y}$-Maus der Fall zu sein (Manuskript in Vorbereitung). Von Mausmodellen mit Mutationen in Rhodopsin, in Untereinheiten der Phosphodiesterase, in Peripherin/RDS oder auch in *ROM-1* ist bekannt, daß trotz der unterschiedlichen Pathomechanismen apoptotische Prozesse zu dem Zelltod der Photorezeptoren führen (Chang et al. 1993).

Um zu untersuchen, ob auch bei der *Rs1h*$^{-/Y}$-Maus Apoptose für die Photorezeptorabnahme verantwortlich ist, benutzten wir den TUNEL (terminal dUTP nick end labeling)-Assay in Retinaschnitten von 5 Tage bis 9 Monate alten WT-, *Rs1h*$^{-/Y}$- und Swiss Webster (SW)-Mäusen (Tab. 2).

Tab. 2: TUNEL-Assay von Retinaschnitten verschiedener Mausstämme

Alter	Anzahl markierter Zellen								
	WT*			Rs1h$^{-/Y}$			SW		
	ONL**	INL	GCL	ONL	INL	GCL	ONL	INL	GCL
P 5	n.a.***	n.a.	n.a.	-	48,7	13	-	43,3	12
P 7	1,3****	84	8,3	5	89,3	7,7	6,7	125	6
P 9	8	66	4	6,7	75,7	5,3	25	74,7	2,3
P 12	9,7	29	0,7	10,3	24	1	n.a.	n.a.	n.a.
P 14	20,3	8,7	1	18,3	12	-	68,7	2	1
P 18	9	3,3	0,7	48,3	2,3	-	n.a.	n.a.	n.a.
P 21	3	-	-	39,7	4	0,7	4,7	0,3	0,3
P 24	4,7	-	-	24,3	-	-	n.a.	n.a.	n.a.
P 28	3,7	-	-	18	-	-	n.a.	n.a.	n.a.
P 35	5	-	-	14	0,3	-	n.a.	n.a.	n.a.
3 Mo	1	-	0,7	6,7	0,7	-	n.a.	n.a.	n.a.
6 Mo	0,7	-	-	3	-	-	n.a.	n.a.	n.a.
9 Mo	0,7	-	-	1,7	-	-	n.a.	n.a.	n.a.

* WT, Wild-Typ, Rs1h$^{-/Y}$, hemizygote *Rs1h* knock-out Maus, SW, Swiss-Webster; ** ONL, äußere Körnerschicht, INL innere Körnerschicht, GCL, Ganglienzellschicht; *** n.a., nicht analysiert; **** Die angegebenen Werte sind Mittelwerte dreier Meßwerte.

Während der Entwicklung der Retina (bis etwa postnataler Tag 12 (P12)) kann vor allem in der INL, aber auch in der GCL Apoptose nachgewiesen werden, die sich jedoch zwischen den Retinae der WT-, *Rs1h* knock-out- und SW-Maus nicht unterscheidet (Abb. 12). Die Apoptose ist für die Differenzierung der Retina notwendig (Young 1984). Zellen, die sich nach der Ausbildung der distinkten Retinaschichten nicht im richtigen Umfeld befinden, sterben ab.

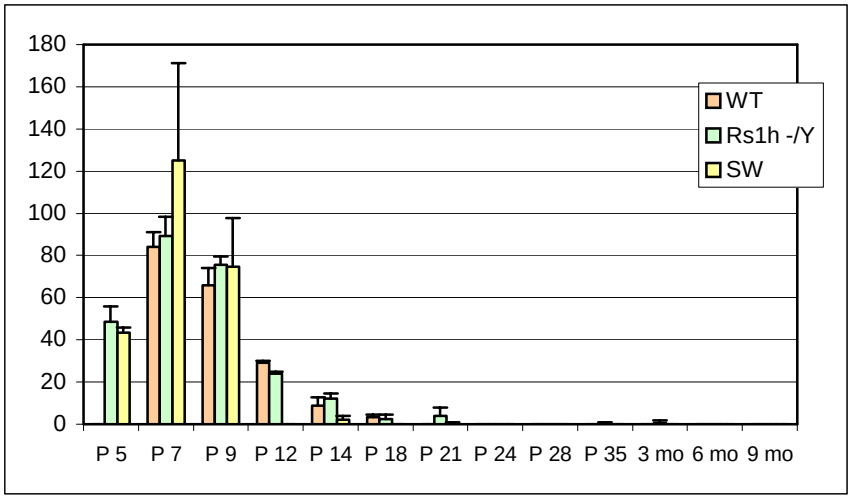

Abb. 12: Apoptose in der inneren Körnerschicht verschiedener Mausstämme
Graphische Darstellung der Anzahl der apoptotischen Kerne in der INL während der Entwicklung der Retina (P5 bis 9 Monate) in 3 Mausstämmen.
Abkürzungen: WT, Wild-Typ Maus; $Rs1h^{-/Y}$, RS1 defiziente Maus; SW, Swiss Webster Maus. Erklärungen s. Text.

Bei der SW-Maus enthält die ONL am Tag P14 besonders viele apoptotische Kerne. Die SW-Maus besitzt wie die *retinal degeneration* (*rd*) Maus ein Gendefekt in der β-Untereinheit der cGMP-Phosphodiesterase (Y347X). Die Photorezeptoren entwickeln sich während der ersten zwei Lebenswochen normal, dann beginnt ihre Degeneration, die sehr schnell fortschreitet (Abb. 13). Am Tag P17 sind bereits die meisten Photorezeptoren degeneriert.

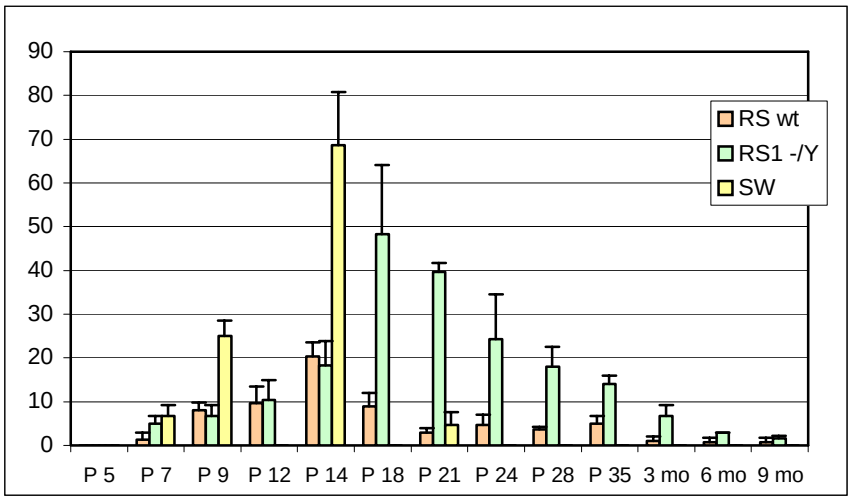

Abb. 13: Apoptose in der äußeren Körnerschicht verschiedener Mausstämme
Graphische Darstellung der Anzahl der apoptotischen Kerne in der ONL während der Entwicklung der Retina (P5 bis 9 Monate) in 3 Mausstämmen.
Abkürzungen: WT, Wild-Typ Maus; $Rs1h^{-/Y}$, RS1 defiziente Maus; SW, Swiss Webster Maus. Erklärungen s. Text.

Bei *Rs1h*$^{-/Y}$-Mäusen finden sich zwischen P16 und P24 vermehrt Signale von absterbenden Photorezeptorkernen, während bei den Kontrollmäusen zu diesem Zeitpunkt fast keine Apoptose mehr stattfindet, da die Retina im Wesentlichen ausdifferenziert ist (Abb. 13, Abb. 14).

In späteren Stadien, in denen der Verlust der Photorezeptoren morphologisch deutlicher wird, sind nur noch vereinzelt apoptotische Kerne in der ONL zu beobachten. Diese Diskrepanz läßt sich möglicherweise dadurch erklären, daß später Mikrogliazellen, die erst durch die absterbenden Photorezeptoren aktiviert werden, die apoptotischen Zellen sehr schnell

phagozytieren. Es bleibt noch im Detail zu klären, wie die Abwesenheit von RS1 die Apoptose der *Rs1h*$^{-/Y}$-Maus initiieren kann.

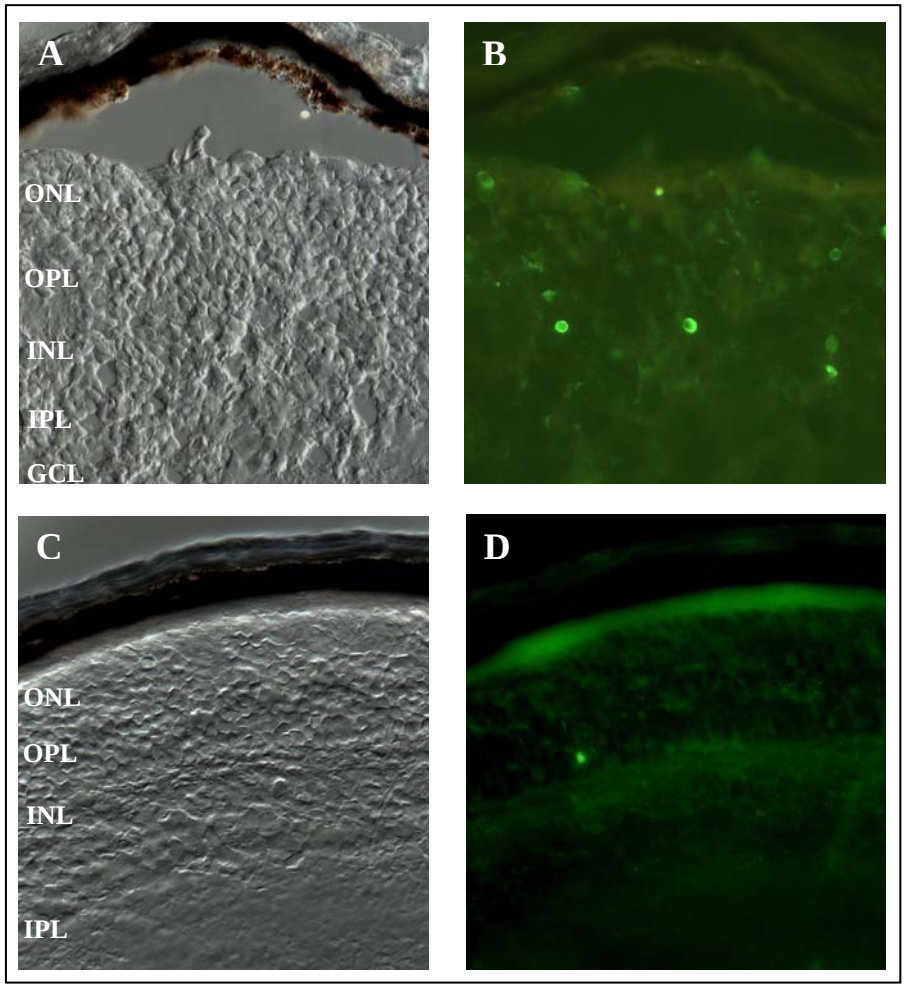

Abb. 14: Fluoreszenzmikroskopie TUNEL-markierter Retinaschnitte 21 Tage alter Rs1h$^{-/Y}$ und WT-Mäuse (**A**) DIC- und (**B**) Fluoreszenzaufnahme einer TUNEL-markierten Rs1h$^{-/Y}$-Retina. TUNEL-markierte, apoptotische Kerne zeigen grüne Fluoreszenz. Es sind vor allem Zellen der ONL, die in andere Zellschichten abgewandert sind. (**C**) DIC- und (**D**) Fluoreszenzaufnahme einer TUNEL-markierten WT-Retina. Die WT-Retina enthält nur einen apoptotischen Kern. Bei der Färbung am oberen Rand der ONL handelt es sich um ein Artefakt. Abkürzungen: ONL, äußere Körnerschicht; OPL, äußere plexiforme Schicht; INL, innere Körnerschicht; IPL, innere plexiforme Schicht; GCL, Ganglienzellschicht.

3.5.7 Untersuchungen zur Aufklärung der RS-Pathomechanismen

3.5.7.1 Microarrayanalysen

Mit Hilfe von Microarrays lassen sich die Expressionsprofile von Genen untersuchen. In Zusammenarbeit mit Dr. Barnstable von der Yale University haben wir die Transkriptome der Retinae der WT- und der *Rs1h*$^{-/Y}$ Maus miteinander verglichen. Dazu wurde RNA aus Mausaugen von 10, 14, 21 und 270 Tage alten WT- und *Rs1h*$^{-/Y}$ Tieren isoliert. Die RNA wurde im Labor von Dr. Barnstable amplifiziert, mit Cy3 bzw. Cy5 markiert und auf Microarrays hybridisiert. Die Microarrays enthalten Plasmid-DNA von 9.216 sequenzierten retinalen cDNAs (Schena et al. 1995). Es ist zu erwarten, daß in der Retina der Retinoschisin-defizienten Maus die Expression vieler Gene herunter- bzw. hochreguliert ist. Da wir besonders an Genen interessiert sind, die direkt in den Pathomechanismus involviert sind, haben wir unter anderem sehr junge Tiere (P10, P14) in die Untersuchungen einbezogen, bei

denen sich die Erkrankung gerade manifestiert. In späteren Stadien wird das Transkriptom durch den Verlust der Photorezeptoren vermutlich stark verändert sein. Zur Zeit werden die Untersuchungen und Ergebnisauswertungen der Analysen durchgeführt.

3.5.7.2 2 D-Gele

Um zu untersuchen, wie die Proteinnetzwerke in der Retina Retinoschisin-defizienter Mäuse im Laufe der Pathogenese beeinflußt werden, verwendeten wir die 2 D-Gelelektrophorese. Hierbei werden Proteingemische in 2 Dimensionen aufgetrennt, zuerst nach ihrem isoelektrischen Punkt und anschließend nach ihrem Molekulargewicht.

Wir isolierten die Retinae von WT- und *Rs1h*$^{-/Y}$ Mäusen verschiedener Altersstadien (4 Wochen, 8 Wochen, 9 Monate) und lösten ihre Proteine in einem Harnstoffpuffer. Nach der Gelelektrophorese wurden die Proteine mit Silber angefärbt und die Proteinmuster der WT- und *Rs1h*$^{-/Y}$ Mäuse der miteinander verglichen. Auffällige Proteinspots werden zur Zeit mittels Massenspektrometrie sequenziert (Abb.15). Mit diesem proteomorientierten Ansatz hoffen wir weitere Einblicke in den RS-Pathomechanismus zu gewinnen.

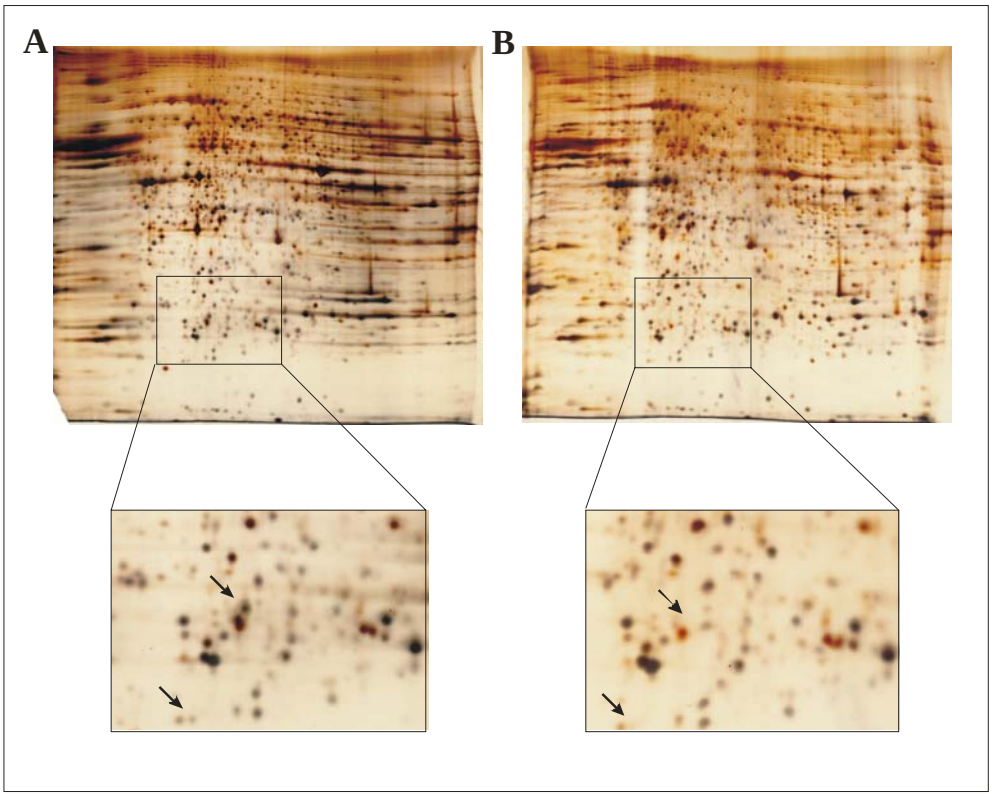

Abb. 15: 2-D Gelanalyse einer Rs1h$^{-/Y}$ Mausretina
Dargestellt sind 2-D Gele der Retinae (**A**) einer 9 Monate alten WT-Maus und (**B**) einer Rs1h$^{-/Y}$-Maus desselben Alters. Die isoelektrische Fokusierung erfolgte zwischen pH 5 und pH 8. Auffällige Proteinspots sind in den vergrößerten Ausschnitten mit Pfeilen markiert.

3.6 Ausblick - Gentherapie

3.6.1 Therapiemöglichkeiten hereditärer Netzhautdystrophien

Wie bereits erwähnt stellen hereditäre Netzhautdystrophien eine große Gruppe genetisch und phänotypisch heterogener Erkrankungen dar. Es wird geschätzt, daß weltweit über 15 Millionen Menschen davon betroffen sind. Voraussetzung für eine genetische Beratung, DNA Diagnostik oder therapeutische Ansätze ist eine genaue Klassifizierung der Erkrankung mit Hilfe des Genotyps (Bessant et al. 2001). Zur Zeit gibt es nur in beschränktem Umfang Möglichkeiten, retinale Degenerationen zu behandeln. Für viele Patienten wäre es bereits hilfreich, wenn die Progression der Erkrankung verlangsamt und somit der Zeitpunkt einer schweren Sehbehinderung hinausgezögert werden könnte. Nur bei einigen seltenen Netzhautdystrophien können Diäten das Krankheitsbild positiv beeinflussen. Beim Refsum-Syndrom ist z.B. ein Verzicht auf phytansäurehaltige Nahrung notwendig. Die A-Betalipoproteinämie erfordert eine Fettrestriktion und Supplementation von Vitamin A, E und K sowie essentieller Fettsäuren (Berson et al. 2000). Die fortschreitenden Erkenntnisse der Molekulargenetik und Molekularbiologie der Netzhautdystrophien könnte eine Grundlage für neue zukünftige Therapieverfahren sein.

3.6.2 Konventionelle Therapieformen

3.6.2.1 Medikamentöse Therapie

Ein detailliertes Wissen über physiologische Vorgänge in der Retina liefert erste Angriffspunkte für spezifische Medikation. So können durch tägliche Gabe von D-cis-Diltiazem, einem Kalziumkanal Blocker, bei *rd*-Mäusen die Photorezeptoren und damit die Sehfunktion erhalten werden (Frasson et al. 1999). Ein weiteres Beispiel ist die orale Verabreichung von 9-cis-Retinal bei *RPE65*$^{-/-}$-Mäusen, die dadurch in der Lage sind, Rhodopsin zu bilden (Van Hooser et al. 2000). Mit rekombinanten neurotrophen Faktoren, wie z.B. BDNF (*brain derived neurotrophic factor*) und CNTF (*ciliar neurothrophic factor*), und Caspaseinhibitoren wird zur Zeit versucht, regulatorisch in die Apoptose einzugreifen. Bei der *tubby*–Maus, einem Tiermodell für das Usher Syndrom Typ I, konnte durch die Injektion eines Inhibitors der Caspase 3 der Zelltod der Photorezeptoren reduziert werden (Bode and Wolfrum 2003).

3.6.2.2 Transplantation von Zellen

Die Transplantation von Pigmentepithelzellen ist in Einzelfällen schon bei Patienten mit altersabhängiger Makuladegeneration durchgeführt worden (Algvere et al. 1994). Die Transplantation von Photorezeptorzellen erwies sich als weitaus schwieriger (Kwan et al. 1999). Die Zellen müssen sich dauerhaft in das Gewebe integrieren, die äußeren Segmente erhalten und geeignete synaptische Verbindungen zu den bipolaren Zellen herstellen. Neuere Versuche mit retinalen Stammzellen ergaben, daß sie in der Zellkultur zu Photorezeptoren, Bipolaren und Müllerzellen differenzieren können (Tropepe et al. 2000). Möglicherweise sind sie für eine Rekonstruktion der degenerierten Retina geeignet. Diese Strategie hätte gegenüber der Gentherapie (s. unten) den Vorteil, daß bereits zerstörte Photorezeptoren ersetzt werden könnten.

3.6.3 Gentherapie

Bei der somatischen Gentherapie werden mit Hilfe viraler Vektoren Gene in Zellen eingeschleust. AAV-Vektoren integrieren sich an einer bestimmten Stelle im Genom. Dadurch wird ein entsprechendes Gen stabil über einen langen Zeitraum exprimiert. Bei Gentherapieversuchen mit rekombinanten AAV-Vektoren konnte die Expression noch nach einem Jahr nachgewiesen werden (Bennett et al. 1999, Guy et al. 1999). Schwierigkeiten gibt es unter anderem noch mit der Dosierung der Expression. Selbst wenn die Proteintranslation von dem nativen, oft zellspezifischen Promotor reguliert wird, kommt es häufig durch mehrere eingebaute Kopien zur Überexpression des Genprodukts. Die erhöhte Proteinmenge kann sich negativ auf die Zelle auswirken (Sarra et al. 2001). In seltenen Fällen kann sie über eine Immunantwort zu einer Entzündungsreaktion führen (Narfström et al. 2003).

Für eine Gentherapie zur Behandlung hereditärer Netzhautdegenerationen gibt es verschiedene Ansatzpunkte. Eine Möglichkeit besteht darin, mit dem Einschleusen von Genen bestimmter antiapoptotischer Faktoren die Apoptose zu beeinflussen. So konnte z.B. über AAV-vermittelten Transfer das Gen für CNTF in die Retina der *rd*-Maus eingebracht werden, was den typischen Verlust der Photorezeptoren um mindestens 3 Monate verzögerte (Cayouette and Gravel 1997). Auch *bcl-2* verzögert die Degeneration bei *rd*-Mäusen (Bennett et al. 1998). Der Vorteil der oben erwähnten Strategien liegt darin, daß sie für ein breites Spektrum von Netzhauterkrankungen angewandt werden können. Da der primäre Gendefekt jedoch nicht korrigiert wird, verspricht diese Behandlung keine Heilung. Bei vielen

Erkrankungen könnte man jedoch bereits durch den Erhalt der Photorezeptoren die starke Visusminderung bzw. die Erblindung positiv beeinflussen.

Während bei dominant vererbten Erkrankungen das mutierte Genprodukt z.B. durch Ribozyme zerstört werden muß (Lewin et al. 1998), kann man bei autosomal und X-chromosomal rezessiv vererbten Erkrankungen direkt das fehlende Genprodukt den Zellen ersetzen. Die von uns generierte *Rs1h* knock-out Maus stellt ein ideales Tiermodell für eine solche Gentherapie dar. Wir wollen in der nahen Zukunft das intakte *Rs1h*-Gen mittels AAV-Transfer in die Retina einbringen. Da ein auf diesem Wege eingeschleustes Gen erst nach etwa 14 Tagen exprimiert wird (Ali et al. 1998), sollte das Einschleusen des *Rs1h*-Gens sehr früh erfolgen, wenn die Retina noch nicht geschädigt ist. Der rekombinante AAV Vektor wird einen Maus *opsin* Promotor (Mops) enthalten, um eine starke, photorezeptor-spezifische Expression des *Rs1h*-Gens zu garantieren.

Lösliche Faktoren, die von sterbenden Zellen bzw. aktivierten Mikrogliazellen sekretiert werden, können umliegende gesunde Zellen zur Apoptose führen („Bystander Effekt“). Deshalb sollte man darüber nachdenken, die *Rs1h*-Gentherapie mit einer Methode zur Unterbrechung der Apoptose zu kombinieren.

Die gentherapeutisch behandelten Tiere sollen zu verschiedenen Zeitpunkten sowohl mit SLO (*scanning laser ophthalmology*) und ERG, als auch durch histologische und immunohisto-chemische Färbungen von Retinaschnitten untersucht werden. Wenn die Ergebnisse es zulassen, sollen daran anschließend vorklinische und klinische Versuche durchgeführt werden, um zu prüfen, ob diese Therapieform eine Behandlungsmöglichkeit für RS-Patienten darstellt.

VI. Referenzen

Alexander, S.; Sydow, L.M.; Wessels, D.; Soll, D.R.; (1992) Discoidin proteins of Dictyostelium are necessary for normal cytoskeletal organization and cellular morphology during aggregation. *Differentiation* 51: 149-161.

Alexander, C.; Votruba, M.; Pesch, U.E.A.; Thiselton, D.L.; Mayer, S.; Moore, A.; Rodriguez, M.; Kellner, U.; Leo-Kottler, B.; Auburger, G.; Bhattacharya, S.S.; Wissinger, B.; (2000) OPA1, encoding a dynamin-related GTPase, is mutated in autosomal dominant optic atrophy linked to chromosome 3q28. *Nat. Genet.* 26: 211-215.

Algvere, P.V.; Berglin, L.; Gouras, P.; Sheng, Y.; (1994) Transplantation of fetal retinal pigment epithelium in age-related macular degeneration with subfoveal neovascularization. *Graefes Arch. Clin. Exp. Ophthalmol.* 232: 707-716.

Ali, R.R.; Reichel, M.B.; de Alwis, M.; Kanuga, N.; Kinnon, C.; Levinsky, R.J.; Hunt, D.M.; Bhattacharya, S.S.; Thrasher, A.J.; (1998) Adeno-associated virus gene transfer to mouse retina. *Hum. Gene Ther.* 9: 81-86.

Alitalo, T.; Forsius, H.; Karna, J.; Frants, R.R.; Eriksson, A.W.; Wood. S.; Kruse, T.A.; de la Chapelle, A.; (1988) Linkage relationships and gene order around the locus for X-linked retinoschisis. *Am. J. Hum. Genet.* 43: 476-483.

Alitalo, T.; Francis, F.; Kere, J.; Lehrach, H.; Schlessinger, D.; Willard, HF.; (1995) A 6 Mb YAC contig in Xp22.1-Xp22.2 spanning the DXS69E, XE59, GLRA2; PIGA, GRPR, CALB3 and PHKA2 genes. *Genomics* 25: 691-700.

Alitalo, T.; Karna, J.; Forsius, H.; de la Chapelle, A.; (1987) X-linked retinoschisis is closely linked to DXS41 and DXS16 but not DXS85. *Clin. Genet.* 32: 192-195.

Alitalo, T.; Kruse, T.A.; de la Chapelle A.; (1991) Refined Localization of the Gene Causing X-Linked Juvenile Retinoschisis. *Genomics* 9: 505-510.

Allikmets, R.; Singh, N.; Sun, H.; Shroyer, N.F.; Hutchinson, A.; Chidambaram, A.; Gerrard, B.; Baird, L.; Stauffer, D.; Peiffer, A.; Rattner, A.; Smallwood, P.; Li, Y.; Anderson, K.L.; Lewis, R.A.; Nathans, J.; Leppert, M.; Dean, M.; Lupski, J.R.; (1997) A photoreceptor cell specific ATP binding transporter gene (ABCR) is mutated in recessive Stargardt macular dystrophy. *Nat. Genet.* 15: 236-246.

Assink, J.J.; Tijmes, N.T.; ten Brink, J.B.; Oostra, R.J.; Riemslag, F.C.; deJong, P.T.; Bergen, A.A.; (1997) A gene for X-linked optic atrophy is closely linked to the Xp11.4-Xp11.2 region of the X chromosome. *Am. J. Hum. Genet.* 61: 934-939.

Baumgartner, S.; Hofmann, K.; Chiquet-Ehrismann, R.; Bucher, P.; (1998) The discoidin domain family revisited: new members from procaryotes and a homology-based fold prediction. *Protein Sci.* 7: 1626-1631.

Bell, R.M.; (1986) Protein Kinase C Activation by Diacylglycerol Second Messengers. *Cell* 45: 631-632.

Bennett, J.; Maguire, A.M.; Cideciyan, A.V.; et al.; (1999) Stable transgene expression in rod photoreceptors after recombinant adeno-associated virus-mediated gene transfer to monkey retina. *Proc. Natl. Acad. Sci. USA* 96: 9920-9925.

Bennett, J.; Zeng, Y.; Bajwa, R.; et al.; (1998) Adenovirus-mediated delivery of rhodopsin-promoted bcl-2 results in a delay in photoreceptor cell death in the rd/rd mouse. *Gene Ther.* 5: 1156-1164.

Bergen, A.A.B.; ten Brink, J.B.; Bleeker-Wagemakers, L.M.; van Schooneveld, M.J.; (1994) Refinement of the chromosomal position of the X linked juvenile retinoschisis gene. *J. Med. Genet.* 31: 972-975.

Bernstein, P.S.; Tammur, J.; Singh, N.; Hutchinson, A.; Dixon, M.; Pappas, C.M.; Zabriskie, N.A.; Zhang, K.; Petrukhin, K.; Leppert, M.; Allikmets, R.; (2001) Diverse macular dystrophy phenotype caused by a novel complex mutation in the ELOVL4 gene. *Invest. Ophthal. Vis. Sci.* 42: 3331-3336.

Berson, E.L.; (2000) Nutrition and retinal degenerations. *Int. Ophthalmol. Clin.* 40: 93-111.

Bessant, D.A.R.; Ali, R.R.; Bhattacharya, S.S.; (2001) Molecular genetics and prospects for therapy of the inherited retinal dystrophies. *Curr. Opin. Genet. Dev.* 11: 307-316.

Bode, C.; Wolfrum, U.; (2003) Caspase-3 inhibitor reduces apoptotic photoreceptor cell death during inherited retinal degeneration in *tubby* mice. *Mol. Vis.* 9: 144-150.

Boman, H.; Heilig, P.; Kolder, H.E.; Giblett, E.R.; Fialkow, P.J.; (1976) Hereditary retinoschisis. Linkage studies in a family and considerations in genetic counselling. *Can. J. Ophthalmol.* 10: 11-16.

Bonneau, D.; Souied, E.; Gerber, S.; Rozet, J.-M.; D'Haens, E.; Journel, H.; Plessis, G.; Weissenbach, J.; Munnich, A.; Kaplan, J.; (1995) No evidence of genetic heterogeneity in dominant optic atrophy. *J. Clin. Genet.* 32: 951-953.

Brown, J., Jr.; Fingert, J.H.; Taylor, C.M.; Lake, M.; Sheffield, V.C.; Stone, E.M.; (1997) Clinical and genetic analysis of a family affected with dominant optic atrophy (OPA1) *Arch. Ophthalmol.* 115: 95-99.

Cayouette, M.; Gravel, C.; (1997) Adenovirus-Mediated Gene Transfer of Ciliary Neurotrophic Factor Can Prevent Photoreceptor Degeneration in the Retinal Degeneration (*rd*) Mouse. *Hum. Gene Ther.* 8: 423-430.

Chang, G.-Q.; Hao, Y.; Wong, F.; (1993) Apoptosis: Final Common Pathway of Photoreceptor Death in *rd*, *rds*, and Rhodopsin Mutant Mice. *Neuron* 11: 595-605.

Claverie, J.M.; (1997) Computational methods for the identification of genes in vertebrate genomic sequences. *Hum. Mol. Genet.* 6: 1735-1744.

Curat, C.A.; Eck, M.; Dervillez, X.; Vogel, W.F.; (2001) Mapping of Epitopes in Discoidin Domain Receptor 1 Critical for Collagen Binding. *J. Biol. Chem.* 276: 45952-45958.

Dahl, N.; Goonewardena, P.; Chotai, J.; Anvret, M.; Pettersson, U.; (1988) DNA linkage of X-linked retinoschisis. *Hum. Genet.* 78: 228-232.

de la Chapelle, A.; Alitalo, T.; Forsius, H.; (1994) X-linked juvenile retinoschisis. In: Wright, A.; Jay, B. (eds.) : *Molecular Genetics of Inherited Eye Disorders*. Chur: Harwood Academic Publ. (1st ed.), 339-357.

Delettre, C.; Lenaers, G.; Griffoin, J.-M.; Gigarel, N.; Lorenzo, C.; Belenguer, P.; Pelloquin, L.; Grosgeorge, J.; Turc-Carel, C.; Perret, E.; Astarie-Dequeker, C.; Lasquellec, L.; Arnaud, B.; Ducommun, B.; Kaplan, J.; Hamel, C.P.; (2000) Nuclear gene OPA1, encoding a mitochondrial dynamin-related protein, is mutated in dominant optic atrophy. *Nat. Genet.* 26: 207-210.

Donoso, L.A.; Edwards, A.O.; Frost, A.; Vrabec, T.; Stone, E.M.; Hageman, G.S.; Perski, T.; (2001) Autosomal dominant Stargardt-like macular dystrophy. *Surv. Ophthalmol.* 46: 149-163.

Dryja, T.P.; Berson, E.L.; Rao, V.R.; Oprian, D.D. (1993) Heterozygous missense mutation in the rhodopsin gene as a cause of congenital stationary night blindness. *Nat. Genet.* 4: 280-283.

Dryja, T.P.; Hahn, L.B.; Reboul, T.; Arnaud, B. (1996) Missense mutation in the gene encoding the alpha subunit of rod transducin in the Nougaret form of congenital stationary night blindness. *Nat. Genet.* 13: 358-365.

Dryja, T.P.; McGee, T.L.; Hahn, L.B.; Cowley, G.S.; Olsson, J.E.; Reichel, E.; Sandberg, M.A.; Berson, E.L. (1990) Mutations within the rhodopsin gene in patients with autosomal dominant retinitis pigmentosa. *New Eng. J. Med.* 323: 1302-1307.

Dumur, V.; Trivier, E.; Puech, B.; Peugnet, F.; Zanlonghi, X.; Hache, J.C.; Hanauer, A.; (1995) Genetic analysis of new French X-linked juvenile retinoschisis kindreds using microsatellite markers closely linked to the RS locus: further narrowing of the RS candidate region. *Hum. Genet.* 96: 79-82.

Eiberg, H.; Kjer, B.; Kjer, P.; Rosenberg, T.; (1994) Dominant optic atrophy (OPA1) mapped to chromosome 3q region. I. Linkage analysis. *Hum. Mol. Genet.* 3: 977-980.

Eriksson, A.W.; Fellman, J.; Vainio-Mattila, B.; Forsius, H.; (1969) X-chromosomal retinoschisis (retinal detachment) in Finland. *Bulletin of the European Society of Human Genetics* 3: 67-76.

Ferrero, G.B.; Franco, B.; Roth, E.J.; Firulli, BA.; Borsani, G.; Delmas-Mata, J.; Weissenbach, J.; et al. (1995) An integrated physical and genetic map of a 35 Mb region on chromosome Xp22.3-Xp21.3. *Hum. Mol. Genet.* 4: 1821-1827.

Forsius, H.R.; Eriksson, A.W.; (1980) Retinoschisis X-chromosomalis. In *Population structure and genetic disorders* pp. 673-676. Eds.: Eriksson, A.W.; Forsius, H.; Nevanlinna, H.R.; Workman, P.L. & Norio, R.K.; Academic Press, London.

Frasson, M.; Sahel, J.A.; Fabre, M.; Simonutti, M.; Dreyfus, H.; Picaud, S.; (1999) Retinitis pigmentosa: rod photoreceptor rescue by a calcium-channel blocker in the *rd* mouse. *Nat. Med.* 5: 1183-1187.

Fraternali, F.; Cavallo, L.; Musco, G.; (2003) Effects of patholgical mutations on the stability of a conserved amino acid triad in retinoschisin. *FEBS Lett.* 544: 21-26.

Freund, C.L.; Gregory-Evans, C.Y.; Furukawa, T.; Papaioannou, M.; Looser, J.; Ploder, L.; Bellingham, J.; Ng, D.; Herbrick, J.A.; Duncan, A. et al. (1997) Cone-rod dystrophy due to mutations in a novel photoreceptor-specific homeobox gene (CRX) essential for maintenace of the photoreceptor. *Cell* 91: 543-553.

Fuchs, S.; Nakazawa, M.; Maw, M.; Tamai, M.; Oguchi, Y.; Gal, A. (1995) A homozygous 1-base pair deletion in the arrestin gene is a frequent cause of Oguchi disease in Japanese. *Nat. Genet.* 10: 360-362.

Furukawa, T.; Morrow, E.M.; Cepko, C.L.; (1997) *Crx*, a novel *otx*-like homeobox gene, shows photoreceptor-specific expression and regulates photoreceptor differentiation. *Cell* 91: 531-541.

Gellert, G.; Petersen, J.; Krawczak, M.; Zoll, B.; (1988) Linkage relationship between retino-schisis and four marker loci. *Hum. Genet.* 79: 382-384.

George, N.D.L.; Yates, J.R.W.; Moore, A.T.; (1995) X linked retinoschisis. *Brit. J. Ophthal.* 79: 697-702.

George, N.D.; Yates, J.R.; Moore, A.T.; (1996) Clinical features in affected males with X-linked retinoschisis. *Arch. Ophthalmol.* 114: 274-280.

Gitschier, J.; Wood, W.I.; Goralka, T.M.; et al.; (1984) Characterization of the human factor VIII gene. *Nature* 312: 326-330.

Gorlin, R.J.; Knobloch, W.H.; (1972) Syndromes of genetic juvenile retinal detachment. *Zeit-schrift für Kinderheilkunde* 113: 81-92.

Guex, N.; Peitsch, M.C.; (1997) SWISS-MODEL and the Swiss-PdbViewer: an environment for comparative protein modelling. *Electrophoresis* 18: 2714-2723.

Guy, J.; Qi, X.; Muzyczka, N.; (1999) Reporter expression persists 1 year after adeno-associated virus-mediated gene transfer to the optic nerve. *Arch. Ophthalmol.* 117: 929-937.

Haas, J.; (1898) Ueber das Zusammenvorkommen von Veränderungen der Retina und Choroidea. *Arch. Augenheilk.* 37: 343-348.

Hageman, G.S.; Johnson, L.V.; (1991) Structure, composition and function of the retinal interphotoreceptor matrix. *Prog. Retinal Res.* 10: 207-249.

Hageman, G.S.; Marmor, M.F.; Yao, X.Y.; Johnson, L.V.; (1995) The interphotoreceptor matrix mediates primate retinal adhesion. *Arch. Ophthalmol.* 113: 655-660.

Hewitt, A.T.; Lindsey, J.D.; Carbott, D.; Adler, R.; (1990) Photoreceptor survival-promoting activity in interphotoreceptor matrix preparations: characterization and partial purifycation. *Exp. Eye Res.* 50: 79-88.

Hollwich, F.; (1988) Augenheilkunde 11. neubearb. Auflage, Georg Thieme Verlag, Stuttgart.

Huopaniemi, L.; Rantala, A.; Tahvanainen, E.; de la Chapelle, A. ; Alitalo, T. ; (1997) Linkage disequilibrium and physical mapping of X-linked juvenile retinoschisis. *Am. J. Hum. Genet*. 60: 1139-1149.

Ives, E.J.; Ewing, C.C.; Innes, R.; (1970) X-linked juvenile retinoschisis and Xg linkage in five families.(Abstract) *Am. J. Hum. Genet.* 22: 17A-18A.

Johnston, P.B.; Gaster, R.N.; Smith, V.C.; Tripathi, R.C.; (1979) A clinicopathologic study of autosomal dominant optic atrophy. *Am. J. Ophthal.* 88: 868-875.

Johnston, R.L.; Burdon, M.A.; Spalton, D.J.; Bryant, S.P.; Behnam, J.T.; Seller, M.J.; (1997) Dominant optic atrophy, Kjer type: linkage analysis and clinical features in a large British pedigree. *Arch. Ophthalmol.* 115: 100-103.

Kane, W.H.; Davie, E.W.; (1988) Blood coagulation factors V and VIII: structural and functional similarities and their relationship to hemorrhagic and thrombotic disorders. *Blood* 71: 539-555.

Kai, M.; Sakane, F.; Imai, S.; Wada, I.; Kanoh, H.; (1994) Molecular cloning of a diacylglycerol kinase isozyme predominantly expressed in human retina with a truncated and inactive enzyme expression in most other human cells. *J. Biol. Chem.* 269: 18492-18498.

Kajiwara, K.; Berson, E.L.; Dryja, T.P.; (1994) Digenic retinitis pigmentosa due to mutations at the unlinked peripherin/RDS and ROM1 loci. *Science* 264: 1604-1608.

Kanoh, H.; Yamada, K.; Sakane, F.; (1990) Diacylglycerol kinase: a key modulator of signal transduction? *Trends Biochem. Sci.* 15: 47-50.

Kaplan, J.; Pelet, A.; Hentati, H.; Jeanpierre, M.; Briard, M.L.; Journel, H.; Munnich, A.; Dufier, J.L.; (1991) Contribution to carrier detection and genetic counselling in X linked retinoschisis. *J. Med. Genet.* 28: 383-388.

Katsanis, N.; Ansley, S.J.; Badano, J.L.; Eichers, E.R.; Lewis, R.A.; Hoskins, B.E.; Scambler, P.J.; Davidson, W.S.; Beales, P.L.; Lupski, J.R.; (2001) Triallelic inheritance in Bardet-Biedl syndrome, a mendelian recessive disorder. *Science* 293: 2256-2259.

Kawano, K.; Tanaka, K.; Murakami, F.; Ohba, N.; (1981) Congenital hereditary retinoschisis: evolution at the initial stage. *Albrecht von Graefes Archiv für Klinische und Experimentelle Ophthalmologie* 217: 315-323.

Keen, T.J.; Inglehearn, C.F.; (1996) Mutations and polymorphisms in the human peripherin-RDS gene and their involvement in inherited retinal degeneration. *Hum. Mutat*. 8: 297-303.

Kellner, U.; (1997) Hereditäre Netzhautdystrophien. Teil 2: Differentialdiagnose. *Ophthalmologe* 94: 450-465.

Kellner, U.; (2003) Vererbbare Netzhaut- und Sehbahnerkrankungen und klinische Elektrophysiologie. http://retinadiagnostic.de.

Kelsell, R.E.; Godley, B.F.; Evans, K.; Tiffin, P.A.C.; Gregory, C.Y.; Plant, C.; Moore, A.T.; Bird, A.C.; Hunt, D.M.; (1995) Localization of the gene for progressive bifocal chorioretinal atrophy (PBCRA) to chromosome 6q. *Hum. Mol. Genet.* 4: 1653-1656.

Kerrison, J.B.; Arnould, V.; Barmada, M.M.; Sallum, J.; Li, Y.Y.; Zhu, D.; Vagefi, M.R.; Mitchell, T.; Maumenee, I.H.; (1998) Autosomal dominant optic atrophy pedigree linked to chromosome 18q12.2-q12.3. *Invest. Ophthal. Vis. Sci.* 39: S511.

Krumpaszyk, H.G.; Klauß, V.; (1996) Epidemiology of blindness and eye disease. *Ophthalmologica* 210: 1-84.

Kuehn, M.H.; Hageman, G.S.; (1995) Characterization of a cDNA encoding IPM 150, a novel human interphotoreceptor matrix chondroitin 6-sulfate proteoglycan. *Invest. Ophthal. Vis. Sci.* 36: S510.

Kuehn, M.H.; Hageman, G.S.; (1999) Expression and characterization of the IPM 150 gene (IPMG1) product, a novel human photoreceptor cell-associated chondroitin-sulfate proteoglycan. *Matrix Biology* 18: 509-518.

Kwan, A.S.; Wang, S.; Lund, R.D.; (1999) Photoreceptor layer reconstruction in a rodent model of retinal degeneration. *Exp. Neurol.* 159: 21-33.

Lazarus, H.S.; Hageman, G.S.; (1992) Xyloside-induced disruption of interphotoreceptor matrix proteoglycans in retinal detachment. *Invest. Ophthal. Vis. Sci.* 33: 364-376.

Lewin, A.S.; Drenser, K.A.; Hauswirth, W.W.; Nishikawa, S.; Yasumura, D.; Flannery, J.G.; LaVail, M.M.; (1998) Ribozyme rescue of photoreceotor cells in a transgenic rat model of autosomal dominant retinitis pigmentosa. *Nat. Med.* 4: 967-971.

Livesey, F.J.; Furukawa, T.; Steffen, M.A.; Church, G.M.; Cepko, C.L.; (2000) Microarray analysis of the transcriptional network controlled by the photoreceptor homeobox gene *Crx*. *Curr. Biol.* 10: 301-310.

Lunkes, A.; Hartung, U.; Magarino, C.; Rodriguez, M.; Palmero, A.; Rodriguez, L.; Heredero, L.; Weissenbach, J.; Weber, J.; Auburger, G.; (1995) Refinement of the OPA1 gene locus on chromosome 3q28-q29 to a region of 2-8 cM, in one Cuban pedigree with autosomal dominant optic atrophy type Kjer. (Letter) *Am. J. Hum. Genet.* 57: 968-970.

Macedo-Ribeiro, S.; Bode, W.; Huber, R.; Quinn-Allen, M.A.; Kim, S.W.; Ortel, T.L.; Bourenkov, G.P.; Bartunik, H.D.; Stubbs, M.T.; Kane, W.H.; Fuentes-Prior, P.; (1999) Crystal structures of the membrane-binding C2 domain of human coagulation factor V. *Nature* 402: 434-439.

Masai, I.; Okazaki, A.; Hosoya, T.; Hotta, Y.; (1993) Drosophila retinal degeneration A gene encodes an eye-specific diacylglycerol kinase with cysteine-rich zinc-finger motifs and ankyrin repeats. *Proc. Nat. Acad. Sci.* 90: 11157-11161.

Minato, H.; (1991) Color vision defects of macular diseases. *Nippon Ganka Gakkai Zasshi* 95: 354-362.

Montini, E.; Rugarli, E.I.; Van de Vosse, E.; Andolfi, G.; Mariani, M.; Puca, A.A.; Consalez, G.G.; et al.; (1997) A novel human serine threonine phosphatase related to the Drosophila retinal degeneration C (*rdgC*) gene is selectively expressed in sensory neurons of neural crest origin. *Hum. Mol. Genet.* 6: 1137-1145.

Molday, L.L.; Hicks, D.; Sauer, C.G.; Weber, B.H.F.; Molday, R.S.; (2001) Expression of X-linked Retinoschisis Protein RS1 in Photoreceptor and Bipolar Cells. *Invest. Ophthal. Vis. Sci.* 42: 816-825.

Narfström, K.; Katz, M.L.; Bragadottir, R.; Seeliger, M.; Boulanger, A.; Redmond, T.M.; Caro, L.; Lai, C.-M.; Rakoczy, P.E.; (2003) Functional and Structural Recovery of the Retina after Gene Therapy in the RPE65 Null mutation Dog. *Invest. Ophthal. Vis. Sci.* 44: 1663-1672.

Nehls, M.; Pfeifer, D.; Boehm, T.; (1994) Exon amplification from complete libraries of genomic DNA using a novel phage vector with automatic plasmid excision facility: application to the mouse neurofibromatosis-1 locus. *Oncogene* 9: 2169-2175.

Olichon, A.; Baricault, L.; Gas, N.; Guillou, E.; Valette, A.; Belenguer, P.; Lenaers, G.;(2003) Loss of OPA1 perturbates the mitochondrial inner membrane structure and integrity, leading to cytochrome c release and apoptosis. *J. Biol. Chem.* 278: 7743-7746.

Pagenstecher, H.E.; (1913) Ueber eine unter dem Bilde der Netzhautablösung verlaufende, erbliche Erkrankung der Retina. *Graefes Arch. Ophthal.* 86: 457-462.

Pawar, H.; Bingham, E.L.; Lunetta, K.L.; Segal, M.; Richards, J.E.; Boehnke, M.; Sieving, P.A.; (1995) Refined genetic mapping of juvenile X-linked retinoschisis. *Hum. Hered.* 45: 206-210.

Pratt, K.P.; Shen, B.W.; Takeshima, K.; Davie, E.W.; Fujikawa, K.; Stoddard, B.L.; (1999) Structure of the C2 domain of human factor VIII at 1.5 A resolution. *Nature* 402: 439-442.

Race, R.R.; Sanger, R.; (1975) *Blood groups in man,* 6th ed. Blackwell Scientific Publications, Oxford.

Reid, S.N.M.; Yamashita, C.; Farber, D.B.; (2003) Retinoschisin, a Photoreceptor-secreted Protein, and Its Interaction with Bipolar and Müller Cells. *J. Neurosc.* 23(14): 6030-6040.

Retinoschisis Consortium; (1998) Functional implications of the spectrum of mutations found in 234 cases with X-linked juvenile retinoschisis (XLRS). *Hum. Mol. Genet.* 7: 1185-1192.

Robson, K.J.H.; Chandra, T.; Mac Gillivray, R.T.A.; Woo, S.L.C.; (1982) Polysome immuno-precipitation of phenylalanine hydroxylase mRNA from rat liver and cloning of its cDNA. *Proc. Natl. Acad. Sci. USA* 79: 4701-4705.

Rommens, J.M.; Lin, B.; Hutchinson, G.B.; Andrew, S.E.; Goldberg, Y.P.; Glaves, M.L.; Lai, V.; McArthur, J.; Nasir, J.; Theilmann, J.; McDonald, H.; Kalchman, M.; Clarke, L.A.; Schappert, K.; Hayden, M.R.; (1993) A transcription map of the region containing the Huntington disease gene. *Hum. Mol. Genet.* 2: 901-907.

Sarra, G.-M.; Stephens, C.; de Alwis, M.; Bainbridge, J.W.B.; Smith, A.J.; Thrasher, A.J.; Ali, R. R.; (2001) Gene replacement therapy in the retinal degeneration slow (*rds*) mouse: the effect on retinal degeneration following partial transduction of the retina. *Hum. Mol. Gen*. 10: 2353-2361.

Schena, M.; Shalon, D.; Davis, R.W.; Brown, P.O.; (1995) Quantitative monitoring of gene expression patterns with a complementary DNA microarray. *Science* 270: 467-470.

Sieving, P.A.; Murayama, K.; Naarendorp, F.; (1994) Push-pull model of the primate photopic electroretinogram: a role for hyperpolarizing neurons in shaping the b-wave. *Vis. Neurosci.* 11: 519-532.

Small, K.W.; Weber, J.L.; Roses, A.; Lennon, F.; Vance, J.M.; Pericak-Vance, M.A.; (1992) North Carolina macular dystrophy is assigned to chrosmosome 6. *Genomics* 13: 681-685.

Spalton, D.J.; Hitchings, R.A.; Holder, G.E.; (1993) Methods of ocular examination. In *Atlas of clinical Ophthalmology*, 2nd edition (Hrsg. Spalton, D.J.; Hitchings, R.A.; Hunter, P.A.;) Mosby-Year Book Europe Limited, London, 1-30.

Springer, W.R.; Cooper, D.N.; Barondes, S.H.; (1984) Discoidin I is implicated in cell-substratum attachment and ordered cell migration of *Dictyostelium discoideum* and resembles fibronectin. *Cell* 39: 557-564.

Stone, E.M.; Nichols, B.E.; Kimura, A.E.; Weingeist, T.A.; Drack, A.; Sheffield, V.C.; (1994) Clinical features of a Stargardt-like dominant progressive macular dystrophy with genetic linkage to chromosome 6q. *Arch. Ophthalmol.* 112: 765-772.

Stryer, L.; (1991) Visual excitation and recovery. *J. Biol. Chem.* 266: 10711-10714.

Travis, G.H.; Brennan, M.B.; Danielson, P.E.; Kozak, C.; Sutcliffe, J.G.; (1989) Identificationof a photoreceptor specific mRNA encoded by the gene responsible for retinal degeneration slow (*rds*). *Nature* 338: 70-73.

Tropepe, V.; Coles, B.L.; Chiasson, B.J.; Horsford, D.J.; Elia, A.J.; McInnes; R.R.; van der Kooy, D.; (2000) Retinal stem cells in the adult mammalian eye. *Science* 17: 2032-2036.

Trump, D.; George, N.D.L.; Walpole, S.M.; Bill, R.M.; Moore; A.T.; Yates, J.R.W.; (1996) Further genetic and physical mapping of X-linked retinoschisis. *Eur. J. Hum. Genet.* 4: 62.

Valdes, J.M.; Tagle, D.A.; Collins, F.S.; (1994) Island rescue PCR: a rapid and efficient method for isolating transcribed sequences from yeast artificial chromosomes and cosmids. *Proc. Natl. Acad. Sci.* USA 91: 5377-5381.

Van de Vosse, E.; Bergen, A.A.B.; Meershoek, E.J.; Oosterwijk, J.C.; Gregory, S.; Bakker, B.; Weissenbach, J.; Coffey, A.J.; van Ommen, G.-J.B.; Den Dunnen, J.T.; (1996) An Xp22.1-p22.2 YAC contig encompassing the disease loci for RS, KFSD, CLS, HYP and RP15: refined localization of RS. *Europ. J. Hum. Genet.* 4: 101-104.

Van Hooser, J.P.; Aleman, T.S.; He, Y.G.; Cideciyan, A.V.; Kuksa, V.; Pittler, S.J.; Stone, E. M.; Jacobson, S.G.; Placzewski, K.; (2000) Rapid restoration of visual pigment and function with oral retinoid in a mouse model of childhood blindness. *Proc. Natl. Acad. Sci. USA* 97: 8623-8628.

Votruba, M.; Fitzke, F.W.; Holder, G.E.; Carter, A.; Bhattacharya, S.S.; Moore, A.T.; (1998) Clinical features in affected individuals from 21 pedigrees with dominant optic atrophy. *Arch. Ophthalmol.* 116: 351-358.

Votruba, M.; Moore, A.T.; Bhattacharya, S.S.; (1997) Genetic refinement of dominant optic atrophy (OPA1) locus to within a 2 cM interval of chromosome 3q. *J. Med. Genet.* 34: 117-121.

Votruba, M.; Moore, A.T.; Bhattacharya, S.S.; (1998a) Demonstration of a founder effect and fine mapping of dominant optic atrophy locus on 3q28-qter by linkage disequilibrium method: a study of 38 British Isles pedigrees. *Hum. Genet.* 102: 79-86.

Votruba, M.; Payne, A.; Moore, A.T.; Bhattacharya, S.S.; (1998b) Dominant optic atrophy: exclusion and fine genetic mapping of the candidate gene, HRY. *Mamm. Genome* 9: 784-787.

Wang, T.; Waters, C.T.; Rozhman, A.M.K.; Jakins, T.J.; Römisch, K.; Trump, D.; (2002) Intracellular retention of mutant retinoschisin is the pathological mechanism underlying X-linked retinoschisis. *Hum. Mol. Genet.* 11: 3097-3105.

Weber, B.H.F.; (1997) Die Genetik der Makuladegenerationen. *Klin. Monatsbl. Augenheilkd.* 210: aA9-aA17.

Weber, B.H.F.; Janocha, S.; Vogt, G.; Sander, S.; Ewing, C.C.; Roesch, M.; Gibson, A.; (1995) X-linked juvenile retinoschisis (RS) maps between DXS987 and DXS443. *Cytogenet. Cell. Genet.* 69: 35-37.

Weber, B.H.F.; Vogt, G.; Pruett, R.C.; Stöhr, H.; Felbor, U.; (1994) Mutations in the tissue inhibitor metalloproteinases-3 (TIMP3) in patients with Sorsby's fundus dystrophy. *Nat. Genet*. 8: 352-356.

Weleber, R.G.; Carr, R.E.; Murphey, W.H.; Sheffield, V.C.; Stone, E.M.;(1993) Phenotypic variation including retinitis pigmentosa, pattern dystrophy, and fundus flavimaculatus in a single family with a deletion of codon 153 or 154 of the peripherin/RDS gene. *Arch. Ophthalmol.* 111: 1531-1542.

Wieacker, P.; Wienker, T.F.; Dallapiccola, B.; Bender, K.; Davies, K.E.; Ropers, H.H.; (1983) Linkage relationships between retinoschisis, Xg, and a cloned DNA sequence from the distal short arm of the X chromosome. *Hum. Genet.* 64: 143-145.

Wu, W.W.H.; Molday, R.S.; (2003) Defective Discoidin Domain Structure, Subunit Assembly, and Endoplasmatic Reticulum Processing of Retinoschisin are Primary Mechanisms Responsible for X-linked Retinoschisis. *J. Biol. Chem.* 278: 28139-28146.

Young, R.W.; (1984) Cell Death During Differentiation of the Retina in the Mouse. *J. Com. Neurol.* 229: 362-373.

Zhang, K.; Kniazeva, M.; Han, M.; Li, W.; Yu, Z.; Yang, Z.; Li, Y.; Metzker, M.L.; Allikmets, R.; Zack, D.J.; Kakuk, L.E.; Lagali, P.S.; Wong, P.W.; MacDonald, I.M.; Sieving, P.A.; Figueroa, D.J.; Austin, C.P.; Gould, R.J.; Ayyagari, R.; Petrukhin, K.; (2001) A 5-bp deletion in ELOVL4 is associated with two related forms of autosomal dominant macular dystrophy. *Nat. Genet.* 27: 89-93.

VII. Anhang

Verwendete Abkürzungen

AAV	Adeno-assoziierter Virus
ABCR	ATP-*binding cassette receptor*
BAC	*bacterial artificial chromosome*
BBS	Bardet-Biedl-Syndrom
bcl-2	*B-cell leukaemia/lymphoma-2*
BDNF	*brain derived neurotrophic factor*
bp	Basenpaare
bzw.	beziehungsweise
cDNA	*complementary* DNA
cGMP	zyklisches Guanosinmono-phosphat
cM	Centimorgan
CNTF	*ciliar neurotrophic factor*
contig	*contiguous DNA fragments*
CRX	*cone-rod homeobox*
Cy3	CYBR3
Cy5	CYBR5
2-D	zweidimensional
DAG	Diacylglycerin
DAGK	Diacylglycerin-Kinase
DAPI	4, 6-Diamidin-2-Phenylindol-Dihydrochlorid
DDR-1	Discoidin Domänen Rezeptor-1
Del-1	*Degenerin like*
DNA	Desoxyribonukleinsäure
ECM	Extrazelluläre Matrix
EGF	*epidermal growth factor*
ELOVL4	*elongation of very long chain fatty acids-4*
ER	endoplasmatisches Retikulum
ERG	Elektroretinogramm
EST	*expressed sequence tag*
ES-Zellen	embryonale Stammzellen
FISH	Fluoreszenz *in-situ* Hybridisierung
GCL	Ganglienzellschicht
HRY	hairy homolog (Drosophila)
IPL	innere plexiforme Schicht
IPM	Interphotorezeptor-Matrix
IMPG1	Interphotorezeptor-Matrix Proteoglykan-1
INL	innere Körnerschicht
kb	Kilobasen
lacZ	β-Galaktosidase
MCDR1	North Carolina Makuladystrophie
OMIM	*Online Mendelian Inheritance in Man*
ONL	äußere Körnerschicht
OPA1	autosomal dominante Optikusatrophie
OPL	äußere plexiforme Schicht
P	postnatal
PAC	*P1-derived artificial chromosome*
PBCRA	progressive bifokale chorioretinale Atrophie
PCR	Polymerase-Kettenreaktion
PSD-95	*postsynaptic density protein-95*
RACE	*rapid amplification of cDNA ends*
rd	*retinal degeneration*
rds	*retinal degeneration slow*
RFLP	Restriktionsfragmentlängen-polymorphismus
RNA	Ribonukleinsäure
ROM1	*rod outer segment-1*
RP	Retinitis pigmentosa
RPE	retinales Pigmentepithel
RS	X-gebundene juvenile Retinoschisis
RS1	Retinoschisin
RS1	Retinoschisis assoziiertes Gen
Rs1h	murines *RS1* Ortholog
$Rs1h^{-/Y}$	hemizygote *Rs1h* knock-out Maus
PPEF	*protein phpsphatase, EF-hand calcium-binding domain*
s.	siehe
SSCP	*single stranded conformation polymorphism*
STGD3	autosomal dominante Stargardt-ähnliche Makuladystrophie
STS	*sequenced tag site*
SW	Swiss-Webster
TIMP3	*tissue inhibitor of metalloproteinase-3*
TU	*transcription unit*
TUNEL	*terminal dUTP nick end labeling*
VMD2	Vitelliforme Makuladystrophie 2
WHO	World Health Organization
WT	Wild-Typ
z.B.	zum Beispiel

VIII. Sonderdrucke der vorgelegten Veröffentlichungen

1. Anlage 1

Genomic organization and chromosomal localization
of the interphotoreceptor matrix proteoglycan-1 (IMPG1) gene:
a candidate for 6q-linked retinopathies

Cytogenet. Cell. Genet. 81: 12-17

Cytogenet Cell Genet 81:12–17 (1998)

Cytogenetics and Cell Genetics

Genomic organization and chromosomal localization of the interphotoreceptor matrix proteoglycan-1 (IMPG1) gene: a candidate for 6q-linked retinopathies

U. Felbor, A. Gehrig, C.G. Sauer, A. Marquardt, M. Köhler, M. Schmid, and B.H.F. Weber

Institut für Humangenetik, Biozentrum, Universität Würzburg, Würzburg (Germany)

Abstract. The interphotoreceptor matrix is a unique extracellular matrix occupying the space between the photoreceptors and the retinal pigment epithelium. Due to its putative function in the maintenance and integrity of the photoreceptor cells, it is conceivable that it is involved in retinal degeneration processes. More recently, a novel gene encoding a 150-kDa interphotoreceptor matrix proteoglycan, designated IMPG1, was cloned and shown to be expressed in both rod and cone photoreceptor cells. To assess this gene in human retinal dystrophies, we have now determined the genomic organization and chromosome location of IMPG1. It is composed of 17 exons ranging from 21 to 533 bp, including an alternatively spliced exon 2. Using somatic cell hybrid mapping and FISH analysis, we have assigned the IMPG1 locus to 6q13→q15. As this interval overlaps with the chromosomal loci of several human retinopathies, including autosomal dominant Stargardt-like macular dystrophy (STGD3), progressive bifocal chorioretinal atrophy (PBCRA), and North Carolina macular dystrophy (MCDR1), IMPG1 represents an attractive candidate for these 6q-linked disorders.

The interphotoreceptor matrix (IPM) is a unique extracellular matrix located in the subretinal space between the neural retina and the retinal pigment epithelium (RPE). It has been implicated in photoreceptor cell-supportive functions by mediating interactions between the photoreceptors, the RPE, and Müller cells (Hewitt and Adler, 1989; Hageman and Johnson, 1991). In addition, IPM proteoglycans are thought to participate in the maintenance of normal retina-RPE adhesion and the integrity of cone photoreceptor cell outer segments (Yao et al., 1990; Lazarus and Hageman, 1992).

Several studies of retinal degeneration in animal models have addressed the possibility of disturbed cell-IPM interactions in photoreceptor degeneration (LaVail et al., 1993; Lazarus et al., 1993; Mieziewska et al., 1993a, b). In the progressive rod-cone degeneration miniature poodle (Mieziewska et al., 1993b), the murine autosomal recessive nervous mutation (LaVail et al., 1993), and the rod-cone dysplasia 1 Irish setter (Mieziewska et al., 1993a), progressive photoreceptor degeneration occurs slowly, with rods being affected earlier and more severely than cones. As compartmentalization of the IPM is most obvious in the so-called cone matrix sheaths (Johnson et al., 1986), a correlation between the degenerative processes in these animals and the integrity of specific IPM domains has been suggested, although the nature of this relationship remains unclear (Mieziewska et al., 1993a, b; LaVail et al., 1993). Furthermore, prior to photoreceptor loss in mice affected with mucopolysaccharidosis type VII, an altered distribution of IPM chondroitin 6-sulfate containing proteoglycan has been observed (Lazarus et al., 1993). It is noteworthy that retinal degeneration is also known to occur in humans affected with mucopolysaccharidoses, a heterogeneous group of lysosomal storage diseases caused by a deficiency of one of the key enzymes required for glycosaminoglycan degradation (Gills et al., 1965; Goldberg and Duke, 1967).

Chondroitin 6-sulfate containing glycoconjugates constitute a major component of the cone matrix sheaths (Hageman and

Supported by grants (We1259/2-3 and We1259/5-2) from the Deutsche Forschungsgemeinschaft (DFG). C.G.S. is supported by a PhD studentship from the Deutsche Retinitis Pigmentosa Vereinigung (DRPV). U.F. was a DFG postdoctoral fellow (Fe432/1-1).

GenBank Accession Nos. AF017760–AF017776.

Received 9 January 1998; revision accepted 11 March 1998.

Request reprints from Dr. Bernhard H.F. Weber, Institut für Humangenetik, Biozentrum, Am Hubland, D-97074 Würzburg (Germany);
telephone: +49-931-888-4062 or +49-931-888-4065;
fax: +49-931-888-4069; e-mail: bweb@biozentrum.uni-wuerzburg.de.

KARGER

E-mail karger@karger.ch
Fax + 41 61 306 12 34
http://www.karger.com

0301–0171/98/0811–0012$15.00/0

Accessible online at:
http://BioMedNet.com/karger

Johnson, 1987). More recently, the full length cDNA of IMPG1 encoding a 150-kDa chondroitin 6-sulfate proteoglycan was cloned (Kuehn and Hageman, 1995) and shown to be expressed in rod and cone photoreceptor cells (Kuehn et al., 1997). As part of our search for genes involved in human retinal disorders, we have determined the expression profile, genomic organization, and chromosomal localization of IMPG1 as a prerequisite for its mutational analysis in human retinopathies.

Materials and methods

Northern blot analysis

Total RNA was isolated from human lung, cerebellum, and retina and the human RPE cell line ARPE19 (Dunn et al., 1996), using the RNA-Clean-LS system (Angewandte Gentechnologie Systeme). The Northern blot contained 12 µg of total RNA in each lane. Hybridization with a radiolabeled 1,166-bp cDNA fragment was performed at 65 °C in 0.5 M $NaPO_4$ (pH 7.2), 7% SDS, and 1 mM EDTA (pH 8.0) (Church and Gilbert, 1984). The 1,166-bp cDNA fragment was PCR amplified from first stranded retinal cDNA using a Superscript Kit (GIBCO BRL) and oligonucleotide primers IPM5′F/IPM1399 designed according to the full-length IMPG1 cDNA sequence (Kuehn and Hageman, 1995).

Genomic and cDNA library

A human genomic PAC library (RPCI1) gridded in 321 individual 384-well microtiter plates was generously provided by Dr. Pieter de Jong (Roswell Park Cancer Institute, Buffalo, NY). For library screenings, the 1,166-bp cDNA PCR product was double-digested with *Hin*cII and *Eco*RI, resulting in a 515-bp fragment corresponding to the 5′ region of the gene. In addition, a 580-bp PCR probe was amplified from the 3′ end of IMPG1 with the primers C6SP-a/C6SP-m. PAC clone DNAs were obtained by the conventional alkaline lysis procedure. To establish overlaps between the isolated PAC clones DOP end-fragment-vector PCR was performed as described in Wu et al. (1996). A retinal cDNA library was kindly provided by Dr. J. Nathans, Johns Hopkins University, Baltimore, MD.

PAC subcloning

PAC clones dJ47C10 and dJ38F21 were digested with *Hin*dIII, *Eco*RI, and *Sau*3AI and subcloned into pBluescript II KS (+) phagemid vector (Stratagene). Exon-containing subclones were identified by colony filter hybridization with a 2,975-bp PCR fragment (1F/C6SP-m) and partially sequenced using the dideoxy chain termination method (Sequenas Version 2.0 DNA sequencing kit; US Biochemical) and internal oligonucleotides as given below. Exon/intron boundaries were identified by alignment of the genomic sequences with the published IMPG1 cDNA sequence (Kuehn and Hageman, 1995) using MacVector sequence analysis software (release 4.0).

Data analysis and oligonucleotide primers

To search for expressed sequence tags (ESTs) in the available databases, the BLASTN program of the GCG Package was utilized (Genetics Computer Group, 1996). The following oligonucleotide primers were used in this study: IPM5′F: 5′-TAG ACA ATC CCC AAG AAA TG-3′ (cDNA nucleotide [nt] position: +107 to +127); 1F: 5′-AGA TTT GAG GTT GTT CTG TG-3′ (nt −55 to −36); IPM605: 5′-AGA GAA GTT TCC CTG ACA G-3′ (nt +479 to +497); IPM789: 5′-TGT AGG CAT CTT GGT GTC G-3′ (nt +645 to +663); IPM947: 5′-TTA AGA AAC TTC CAG GAT TC-3′ (nt +821 to +840); IPM1328: 5′-CAG CAA AAG ATG TGG GCA G-3′ (nt +1,183 to +1,201); IPM1399: 5′-CTC CGT CCA CTG TCT CAA GC-3′ (nt +1,254 to +1,273); C6SP-a: 5′-ATT ACT GAC CGT AGA ATA TG-3′ (nt +2,340 to +2,359); C6SP-m: 5′-GAG GTT TGT GTT TAT CAG AC-3′ (nt +2,901 to + 2,920); M13f5: 5′-CGC CAG GGT TTT CCC AGT CAC GAC-3′; and M13r6: 5′-AGC GGA TAA CAA TTT CAC ACA GGA-3′.

Hybrid panel PCR

PCR was performed with a commercially available panel of 25 human × hamster hybrid cell line DNAs (BIOS Corporation) and oligonucleotide primers C6SP-a/C6SP-m. Giemsa banding was used to verify the presence of the correct human chromosomes.

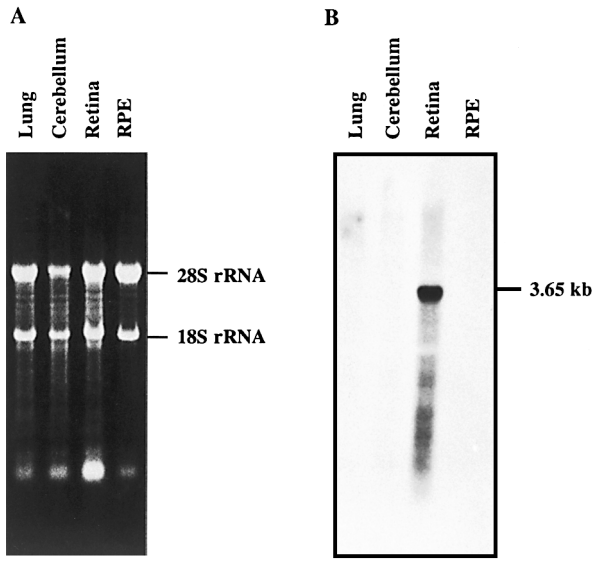

Fig. 1. Northern blot analysis of IMPG1. (**A**) Ethidium bromide-stained agarose gel showing the approximate amount of total human RNA loaded onto each lane. (**B**) Northern blot hybridization of the 1,166-bp IMPG1 cDNA fragment. An abundant 3.65-kb transcript is observed in retina. There are no signals in lung, cerebellum, or retinal pigment epithelium (RPE) total RNA.

Fluorescence in situ hybridization (FISH)

Metaphase chromosomes from peripheral blood lymphocytes were prepared using a standard 1:3 *(v/v)* acetic acid:methanol fixation protocol. Procedures for removal of interfering remnants of cellular RNA and cytoplasm, as well as standard methods for biotinylation of PAC dJ38F21 and FISH, were described elsewhere (Köhler and Vogt, 1994). To determine the cytogenetic band position of the IMPG1 gene, faint Q-bands observed after DAPI staining (Schweizer, 1976) of more than 25 metaphases were related to the position of hybridization signals on propidium-iodide counterstained chromosomes. In addition, the distance from centromere to signals was measured relative to the overall chromosome arm length. The ideogram established by Francke (1994) was used as a reference.

Results

Database analysis and expression profile of IMPG1

Alignment of IMPG1 cDNA sequences to the GenBank and dbEST databases revealed significant identity to ESTs yp48c06 (H38839, H38594), yp48e04.r1 (H38604), and 16h10 (W26960). These cDNA clones have been isolated exclusively from human retinal cDNA libraries (Soares et al. 1994). To analyze the expression pattern of IMPG1 in various adult human tissues, Northern blot analyses were performed with total human RNA isolated from retinal pigment epithelium, retina, lung, and cerebellum. Filter hybridization with probe IPM5′F/IPM1399 corresponding to nt 107 to 1,273 of the full-length cDNA revealed a 3.65-kb transcript in total retinal RNA (Fig. 1). No hybridization signals were detected in RNA from retinal pigment epithelium, lung, or cerebellum even after overexposure of the autoradiogram.

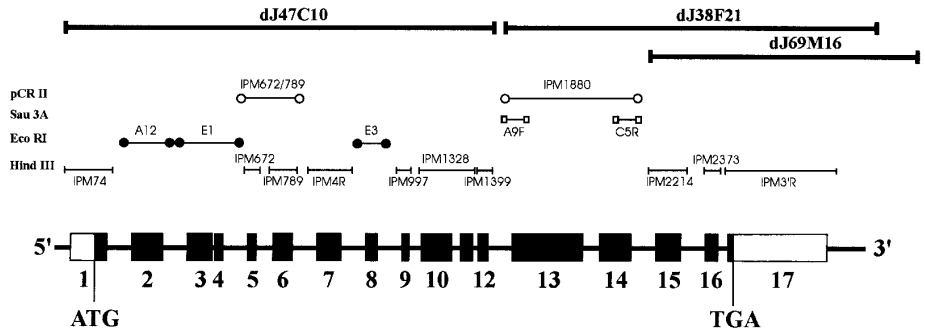

Fig. 2. Genomic organization of the IMPG1 gene. The top portion of the figure shows three PAC clones (dJ47C10, dJ38F21, and dJ69M16) together containing the entire coding sequence of the gene. The horizontal bars below depict PAC-derived plasmid subclones used in the sequencing analysis. Boxes represent exons 1 to 17; 5′- and 3′-flanking regions are shown as open boxes. Intron sizes are drawn to scale with the same size line for those that are over 4 kb in length.

Table 1. Exon/intron boundaries of the human IMPG1 gene

Splice acceptor	Score[a]	Exon No.	Coding sequence (bp)	Splice donor	Score	Intron (kb)	Intron phase[b]
–	–	1	67	AAGGTAAGT	0.2	> 4	I
AATCTTTCTTTTACAGA	3.9	2	234	GAGGTAAGG	1.7	> 4	I
TGACTCTGTATTACAGT	7.8	3	167	CAGGTGAGC	1.8	0.3	0
CTTTATCTTTTTGCAGA	3.4	4	29	CAGGCAAGT	5.4	> 4	II
TCTATTGTACTAATAGA	9.3	5	65	CAGGTAAGC	0.9	2.7	I
TTTAAAATTTTCACAGA	8.9	6	104	ACAGTAAGA	4.7	> 4	0
CCTTTTTTAAACTCAGG	5.5	7	141	CAGGTGAGT	0.1	> 4	0
TTCTTTCTCTCTGCAGA	1.4	8	59	TAGGTAAGT	1.3	4	II
GCATGATGAAATGAAGA	28.2	9	21	TGGGTAATT	5.5	2	II
CCTCTGCTATCTACAGC	4.6	10	248	ATGGTCAGT	4.8	1.3	I
GATTTTTTACCCATAGA	6.1	11	77	GAGGTAAGT	0.9	0.8	0
AAAATTCATTCTTCAGG	9	12	79	CTGGTAAGT	1.5	> 4	I
TGTACTTCCTCCACAGA	4.2	13	533	CTGGTGAGT	1.6	2.7	0
ATCTTTTATTTTGCAGC	4.7	14	220	CAGGTAAAA	3.6	> 4	I
GCCCCATTTCTTACAGC	5.7	15	199	CAGGTGGGT	2.0	> 4	II
TTGCTTTCTTTTGTAGG	3.2	16	73	AAGGTAAAA	3.8	1.6	0
ACTATTTCTCTTTCAGG	3.3	17	78	–	–		

[a] Score of perfect consensus = 0; worst score for acceptors = 42.5, for donors = 30.1.
[b] Phase 0 = position of introns between codons; phase I = interruption after first nucleotide; phase II = interruption after second nucleotide.

Genomic organization of the human IMPG1 gene

As a prerequisite for mutational analyses in human retinopathies, we determined the complete exon/intron organization of the full-length IMPG1 cDNA. Retinal cDNA probes corresponding to nt 164 to 679 and nt 2,340 to 2920 were used to screen a genomic human PAC library, RPCI1. Three independent PAC clones were isolated (dJ47C10, dJ38F21, and dJ69M16). By STS content and restriction enzyme mapping, PAC clones dJ38F21 and dJ69M16 were found to overlap (Fig. 2). By DOP-vector PCR, the T7- and SP6-endclone fragments of PAC dJ38F21 were amplified and used for Southern blot hybridization to *Eco*RI-restricted clones dJ47C10, dJ38F21, and dJ69M16 (data not shown). The 900-bp T7-end-fragment of dJ38F21 specifically hybridized to a 7-kb *Hin*cII and a 1.6-kb *Eco*RI fragment of clone dJ69M16, whereas the 800-bp SP6-endfragment of dJ38F21 did not reveal any hybridization signals, indicating that dJ38F21 does not overlap with PAC clone dJ47C10 (Fig. 2).

To identify restriction fragments containing exonic sequences, the full-length IMPG1 cDNA was colony filter hybridized to *Hin*dIII-, *Eco*R I-, and *Sau*3AI-restricted PAC plasmid sublibraries. Positive clones were purified and partially sequenced using the M13 forward and reverse primers, as well as cDNA-derived oligonucleotide primers. Alignment of the genomic and the cDNA sequences revealed the exon/intron boundaries of the human IMPG1 gene. A total of 17 coding exons were identified, ranging in length from 21 to 533 bp and spanning a genomic region of at least 50 kb (Fig. 2 and Table 1). Exon 1 contains the putative translation initiation start codon ATG, conforming to the Kozak consensus sequence (Kozak, 1996), and an additional 151 bp of upstream sequence, corresponding to the most 5′-extending cDNA clone isolated (Kuehn and Hageman, 1995). The start codon is preceded by two in frame termination codons at nt −57 and −60. A 6-kb *Hin*dIII fragment, IPM3′R, isolated from PAC clone dJ38F21, contains exon 17 with the translation stop codon TAA and an additional 745 bp of 3′-untranslated region.

With the exception of exon 4, all acceptor and donor splice sites strictly follow the GT/AG rule (Table 1). The donor splice junction of exon 4 contains a nonconforming "GC" rather than the universal "GT" at this position. Despite this anomaly, the donor splice sequence of exon 4 has a discrimination energy score of 5.4, well within the range expected for true splice junctions (average acceptor score, 5.1; donor score, 3.16) (Table 1).

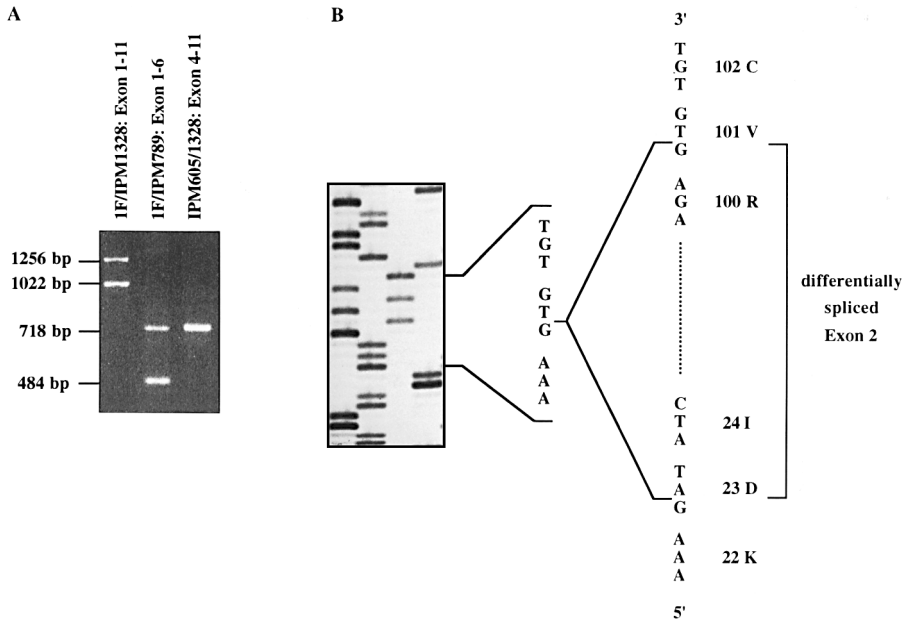

Fig. 3. Alternative splicing of exon 2 in the IMPG1 gene. (**A**) PCR amplification of a human retina cDNA library using primer pairs 1F/IPM1328 and 1F/IPM789 resulted in two distinct bands. The smaller transcript is 234 bp shorter than the expected size. (**B**) Sequencing of the subcloned PCR product 1F/IPM789 revealed splicing of the entire exon 2. As introns 1 and 2 both interrupt a codon after the first nucleotide, skipping of exon 2 does not lead to a frameshift.

(Berg and von Hippel, 1988; Penotti, 1991). The high score of the 3′-splice acceptor sequence of exon 9 has led us to resequence the cDNA and the genomic clone at this position. The cDNA fragment was obtained by PCR amplification from a human λgt10 retinal cDNA library using primers IPM947/IPM1399. This has verified the acceptor splice sequence as shown (Table 1). The approximate sizes of introns 3, 5, 8, 9, 10, 11, 13, and 17 were estimated by PCR amplification using intronic forward and reverse oligonucleotide primers (Table 1). No PCR amplification was observed for the remaining introns, suggesting the presence of introns larger than 4-5 kb.

Alternative splicing of the IMPG1 gene

PCR amplification of the human retinal λgt10 library using primer pairs 1F/IPM1328 (corresponding to exon 1 to 11) and 1F/IPM789 (corresponding to exon 1 to 6) resulted in two different size products (Fig. 3A). Conversely, only a single fragment using primers IPM605/IPM1328 (corresponding to exons 4 to 11) was obtained, suggesting an alternative splice within the first three exons. To test this possibility, the PCR products obtained with 1F/IPM789 were cloned into the pCRII vector, and 40 independent clones were analyzed. Fragments of both 718 bp and 484 bp in size were identified and sequenced (data not shown). Whereas the 718-bp fragment was identical to the known cDNA, the sequencing and comparison of the 484-bp fragment to the known cDNA confirmed an alternative splice event removing the entire exon 2 from the mature RNA (Fig. 3B). Since intron 1 and intron 2 both interrupt the respective codon after the first nucleotide at phase I (Table 1), skipping of exon 2 does not lead to a frameshift (Fig. 3B). Thus, the removal of exon 2 should result in a mature IMPG1 isoform that is missing 78 amino acids.

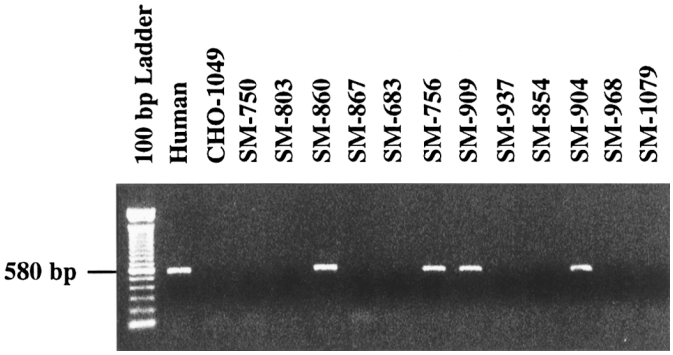

Fig. 4. PCR mapping of the IMPG1 gene using a commercial panel of human × hamster hybrid cell lines. The expected 580-bp PCR fragment was detected in cell hybrids containing human chromosome 6, but not in those lacking this chromosome.

Mapping of IMPG1 to chromosome 6q13→q15

To ascertain the chromosomal location of IMPG1, two independent methods were used. First, genomic DNA from a panel of somatic cell hybrids that retained different sets of human chromosomes was screened using PCR primers C6SP-a/C6SP-m, corresponding to sequences in the 3′-untranslated region of the IMPG1 gene. The PCR product yielded an expected 580-bp fragment in total human genomic DNA and somatic cell hybrids containing human chromosome 6 (SM-756, SM-860, SM-904, and SM-909). In contrast, no PCR product was obtained using DNAs from hybrid cell lines lacking chromosome 6 (GHO-1049, SM-683, SM-750, SM-803, SM-854, SM-867, SM-937, SM-968, and SM-1079) (Fig. 4). The PCR amplification results are consistent with a location of the IMPG1 gene on chromosome 6.

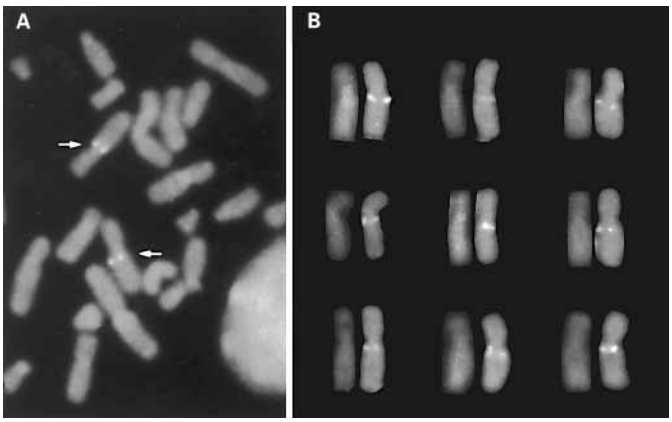

Fig. 5. FISH localization of IMPG1 to chromosome 6q13→q15. (**A**) Partial human metaphase plate after FISH with PAC dJ38F21. Hybridization signals on propidium iodide (PI)-counterstained chromosomes are marked by arrows. (**B**) Examples of hybridization signals observed on selected PI-counterstained human chromosomes 6. The corresponding DAPI-stained chromosomes are shown on the left, respectively.

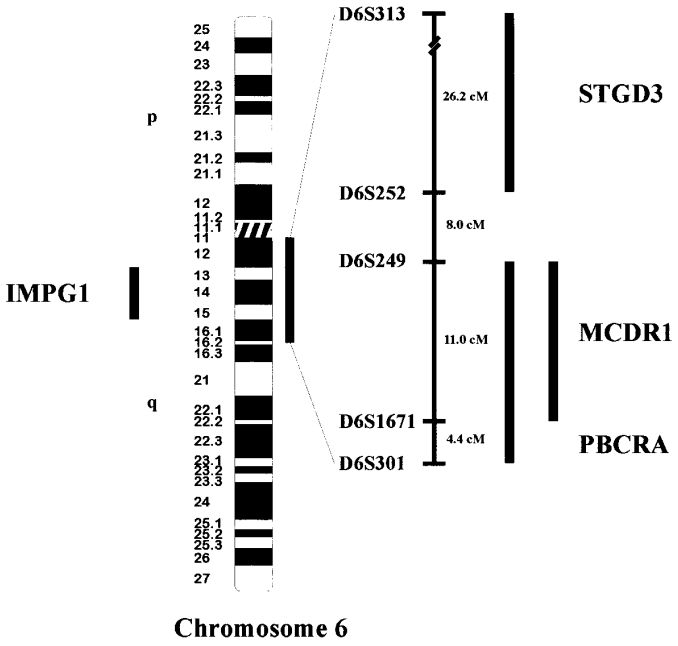

Fig. 6. Diagrammatic representation of the co-localization of IMPG1 and the loci for three maculopathies, STGD3, MCDR1, and PBCRA, on chromosome 6q. FISH hybridization results of IMPG1 are indicated on the left; the genetic locations of the three disorders are shown on the right and have been published previously (STGD3: Stone et al., 1994; MCDR1: Small et al., 1992; PBCRA: Kelsell et al., 1995).

To confirm this assignment and to determine further the subchromosomal location of IMPG1, FISH mapping was performed using a biotin-labeled PAC, dJ38F21. Signals on both chromatids of chromosome 6q13→q15 were repeatedly produced, whereas background signals were distributed randomly (Fig. 5).

Discussion

We report the expression, genomic organization, and chromosome location of a novel interphotoreceptor matrix gene, IMPG1. The selective expression in retinal tissue and the chromosomal mapping of IMPG1 to 6q13-q15 have identified this gene as an attractive candidate for several human macular dystrophies that have previously been localized to 6q11→q16.2 by genetic linkage analysis, viz., autosomal dominant Stargardt-like macular dystrophy (STGD3) (Stone et al., 1994), North Carolina macular dystrophy (MCDR1) (Small et al., 1992), and progressive bifocal chorioretinal atrophy (PBCRA) (Kelsell et al., 1995) (Fig. 6). These three maculopathies are rare hereditary disorders characterized by their mode of inheritance and loss of central vision. In particular, PBCRA is invariantly characterized by subretinal deposits nasal to the optic disc which appear soon after birth and atrophic macular lesions which lead to a progressive reduction in visual acuity and color vision. The expansion of both macular and nasal atrophic lesions toward the optic disc finally leaves only a narrow retinal bridge of relatively intact retina (Godley et al., 1996). In contrast, MCDR1 lesions are highly variable and rarely progress (Small et al., 1993). STGD3 presents with white-yellow macular flecks early in the disease course. Central atrophy develops later and is associated with a progressive loss of central vision in the second or third decade of life (Stone et al., 1994).

The characterization of the exon/intron boundaries of the IMPG1 gene provides the basis for mutational analysis of genomic DNA of affected individuals from the chromosome 6q-linked families. In addition, as STGD3, MCDR1, and PBCRA share some clinical features with other human maculopathies, particularly with age-related macular degeneration, an important cause of visual impairment in elderly patients (Ferris et al., 1984; Young, 1987), it is of importance to test other, as yet unlinked, retinopathies for a possible involvement of IMPG1 in their pathogeneses. The candidate gene approach is most relevant in retinopathies where genetic heterogeneity is a major problem in the identification of the genetic defect (reviewed by Sullivan and Daiger, 1996).

In conclusion, the chromosome mapping and genomic characterization of IMPG1, a novel proteoglycan of the interphotoreceptor matrix, has identified a candidate gene for retinal dystrophies. As the coding sequence of the gene is interrupted by only 16 intervening sequences, the number of exons appears reasonably small in order to enable the mutational analysis of many patients affected with various retinopathies. It is anticipated that the further characterization of function and dysfunction of IMPG1 will shed new light on IPM proteoglycans and their functional involvement in the human eye.

Acknowledgements

The authors wish to thank M. Kuehn and G.S. Hageman (University of Iowa, Iowa City, IA) for sharing IMPG1 cDNA sequence data.

References

Berg OG, von Hippel PH: Selection of DNA binding sites by regulatory proteins. II. The binding specificity of cyclic AMP receptor protein to recognition sites. J molec Biol 200:709–723 (1988).

Church GM, Gilbert W: Genomic sequencing. Proc natl Acad Sci, USA 81:1991–1995 (1984).

Dunn KC, Aotaki-Keen AE, Putkey FR, Hjelmeland LM: ARPE-19, a human retinal pigment epithelial cell line with differentiated properties. Expl Eye Res 62:155–169 (1996).

Ferris FL, Fine SL, Hyman L: Age-related macular degeneration and blindness due to neovascular maculopathy. Archs Ophthalmol 102:1640–1642 (1984).

Francke U: Digitized and differentially shaded human chromosome ideograms for genomic applications. Cytogenet Cell Genet 65:206–219 (1994).

Genetics Computer Group: Program Manual for Wisconsin Package, Version 9, Madison, WI (1996).

Gills JP, Hobson R, Hanley WB, McKusick VA: Electroretinography and fundus oculi findings in Hurler's disease and allied mucopolysaccharidoses. Archs Ophthalmol 74:596–603 (1965).

Godley BF, Tiffin PAC, Evans K, Kelsell RE, Hunt DM, Bird AC: Clinical features of progressive bifocal chorioretinal atrophy: a retinal dystrophy linked to chromosome 6q. Ophthalmology 103:893–898 (1996).

Goldberg MF, Duke JR: Ocular histopathology in Hunter's syndrome: systemic mucopolysaccharidosis type II. Archs Ophthalmol 77:503–512 (1967).

Hageman GS, Johnson, LV: Chondroitin 6-sulfate glycosaminoglycan is a major constituent of primate cone photoreceptor matrix sheaths. Curr Eye Res 6:639–646 (1987).

Hageman GS, Johnson LV: Structure, composition and function of the retinal interphotoreceptor matrix. Prog retinal Res 10:207–249 (1991).

Hewitt AT, Adler R: The retinal pigment epithelium and interphotoreceptor matrix: structure and specialized functions, in Ryan SJ (ed): Retina, Vol 1, pp 57–64 (CV Mosby, St Louis 1989).

Johnson LV, Hageman GS, Blanks JC: Interphotoreceptor matrix domains ensheath vertebrate cone photoreceptor cells. Invest Ophthalmol vis Sci 27: 129–135 (1986).

Kelsell RE, Godley BF, Evans K, Tiffin PAC, Gregory CY, Plant C, Moore AT, Bird AC, Hunt DM: Localization of the gene for progressive bifocal chorioretinal atrophy (PBCRA) to chromosome 6q. Hum molec Genet 4:1653–1656 (1995).

Köhler MR, Vogt PH: Interstitial deletions of repetitive DNA blocks in dicentric human Y chromosomes. Chromosoma 103:324–330 (1994).

Kozak M: Interpreting cDNA sequences: some insights from studies on translation. Mammal Genome 7:563–574 (1996).

Kuehn MH, Hageman GS: Characterization of a cDNA encoding IPM150, a novel human interphotoreceptor matrix chondroitin 6-sulfate proteoglycan. Invest Ophthalmol vis Sci 36:S510 (1995).

Kuehn MH, Stone EM, Hageman GS: Molecular analyses of IPM150, a photoreceptor cell-specific proteoglycan. Invest Ophthalmol vis Sci 38(Suppl): S599 (1997).

LaVail MM, White MP, Gorrin GM, Yasumura D, Porrello KV, Mullen RJ: Retinal degeneration in the nervous mutant mouse. I. Light microscopic cytopathology and changes in the interphotoreceptor matrix. J comp Neurol 333:168–181 (1993).

Lazarus HS, Hageman GS: Xyloside-induced disruption of interphotoreceptor matrix proteoglycans results in retinal detachment. Invest Ophthalmol vis Sci 33:364–376 (1992).

Lazarus HS, Sly WS, Kyle JW, Hageman GS: Photoreceptor degeneration and altered distribution of interphotoreceptor matrix proteoglycans in the mucopolysaccharidosis VII mouse. Expl Eye Res 56:531–541 (1993).

Mieziewska K, van Veen T, Aguirre GD: Development and fate of interphotoreceptor matrix components during dysplastic photoreceptor differentiation: a lectin cytochemical study of rod-cone dysplasia 1. Expl Eye Res 56:429–441 (1993a).

Mieziewska K, van Veen T, Aguirre GD: Structural changes of the interphotoreceptor matrix in an inherited retinal degeneration: a lectin cytochemical study of progressive rod-cone degeneration. Invest Ophthalmol vis Sci 34:3056–3067 (1993b).

Penotti FE: Human pre-mRNA splicing signals. J theor Biol 150:385–420 (1991).

Schweizer D: Reverse fluorescent chromosome banding with chromomycin and DAPI. Chromosoma 58:307–324 (1976).

Small KW, Weber JL, Roses A, Lennon F, Vance JM, Pericak-Vance MA: North Carolina macular dystrophy is assigned to chromosome 6. Genomics 13:681–685 (1992).

Small KW, Weber J, Roses A, Pericak-Vance P: North Carolina macular dystrophy (MCDR1): a review and refined mapping to 6q14-q16.2. Ophthal paediatr Genet 14:143–150 (1993).

Soares MB, Bonaldo MF, Jelene P, Su L, Lawton L, Efstratiadis A: Construction and characterization of a normalized cDNA library. Proc natl Acad Sci, USA 91:9228–9232 (1994).

Stone EM, Nichols BE, Kimura AE, Weingeist TA, Drack A, Sheffield VC: Clinical features of a Stargardt-like dominant progressive macular dystrophy with genetic linkage to chromosome 6q. Archs Ophthalmol 112:765–772 (1994).

Sullivan LS, Daiger SP: Inherited retinal degeneration: exceptional genetic and clinical heterogeneity. Mol Med Today 2:380–386 (1995).

Wu C, Zhu S, Simpson S, de Jong PJ: DOP-vector PCR: a method for rapid isolation and sequencing of insert termini from PAC clones. Nucl Acids Res 24:2614–2615 (1996).

Yao X-Y, Hageman GS, Marmor MF: Retinal adhesiveness is weakened by enzymatic modification of the interphotoreceptor matrix in vivo. Invest Ophthalmol vis Sci 31:2051–2058 (1990).

Young RW: Pathophysiology of age-related macular degeneration. Surv Ophthalmol 31:291–306 (1987).

2. Anlage 2

Assessment of the interphotoreceptor matrix proteoglycan-1 (IMPG-1) gene localised to 6q13-q15 in autosomal dominant Stargardt-like disease (ADSTGD), progressive bifocal chorioretinal atrophy (PBCRA), and North Carolina macular dystrophy (MCDR1)

J. Med. Genet. 35: 641-645

Reprinted from JOURNAL OF MEDICAL GENETICS, August 1998, Vol 35, No 8, p 641-645

Assessment of the interphotoreceptor matrix proteoglycan-1 (IMPG1) gene localised to 6q13-q15 in autosomal dominant Stargardt-like disease (ADSTGD), progressive bifocal chorioretinal atrophy (PBCRA), and North Carolina macular dystrophy (MCDR1)

Andrea Gehrig, Ute Felbor, Rosemary E Kelsell, David M Hunt, Irene H Maumenee, Bernhard H F Weber

Abstract

We have recently characterised the genomic organisation of a novel interphotoreceptor matrix proteoglycan, IMPG1, and have mapped the gene locus to chromosome 6q13-q15 by fluorescence in situ hybridisation. As the interphotoreceptor matrix (IPM) is thought to play a critical role in retinal adhesion and the maintenance of photoreceptor cells, it is conceivable that a defect in one of the IPM components may cause degenerative lesions in retinal structures and thus may be associated with human retinopathies. By genetic linkage analysis, several retinal dystrophies including one form of autosomal dominant Stargardt-like macular dystrophy (STGD3), progressive bifocal chorioretinal atrophy (PBCRA), and North Carolina macular dystrophy (MCDR1) have previously been localised to a region on proximal 6q that overlaps the IMPG1 locus. We have therefore assessed the entire coding region of IMPG1 by exon amplification and subsequent single stranded conformational analysis in patients from 6q linked multigeneration families diagnosed with PBCRA and MCDR1, as well as a single patient from an autosomal dominant STGD pedigree unlinked to either of the two known STGD2 and STGD3 loci on chromosomes 13q and 6q, respectively. No disease associated mutations were identified. In addition, using an intragenic polymorphism, IMPG1 was excluded by genetic recombination from both the PBCRA and the MCDR1 loci. However, as the autosomal dominant Stargardt-like macular dystrophies are genetically heterogeneous, other forms of this disorder, in particular STGD3 previously linked to 6q, may be caused by mutations in IMPG1.

(*J Med Genet* 1998;35:641–645)

Keywords: Stargardt-like macular dystrophy; MCDR1; PBCRA; interphotoreceptor matrix proteoglycan-1

Institut für Humangenetik, Biozentrum, Universität Würzburg, Am Hubland, D-97074, Germany
A Gehrig
U Felbor
B H F Weber

Augenklinik, Universität Würzburg, D-97074 Würzburg, Germany
U Felbor

Institute of Ophthalmology, University College London, London EC1V 9EL, UK
R E Kelsell
D M Hunt

The Wilmer Eye Institute, The Johns Hopkins Center for Hereditary Eye Diseases, Baltimore, MD 21287-9237, USA
I H Maumenee

Correspondence to:
Dr Weber.

Received 14 October 1997
Revised version accepted for publication 12 January 1997

The positional candidate approach relies on the mapping of a disease locus and a candidate gene to a common chromosomal region and the assessment of the functional properties of the gene product with regard to the disease pathology. Several criteria, such as tissue specificity of gene expression, cellular localisation of the transcript, immunohistochemical data, possibly in combination with interspecies nucleotide/protein sequence comparison or protein pattern database searches, may provide helpful information on the probable function of a candidate gene. With an increasing number of mapped genes and expressed sequence tags (ESTs) available through the international efforts of the Human Genome Project, the positional candidate strategy has become the method of choice for the identification of disease genes.[1]

Recently, a novel gene, IMPG1, encoding a major proteoglycan of the interphotoreceptor matrix (IPM), was identified and shown to be preferentially expressed in retina by both rod and cone photoreceptor cells.[2 3] The IPM occupies the space between the neurosensory retina and the retinal pigment epithelium (RPE) and is largely composed of insoluble glycoconjugates that appear to form specific structures around the rod and cone photoreceptor cells, commonly referred to as cone matrix sheaths and rod matrix domains.[4–7] The IPM glycoconjugates, which are primarily chondroitin sulphate proteoglycans, have been proposed to mediate interactions among various cell types, including the RPE, the photoreceptors, the glial Müller cells, and the choriocapillaris[8 9] and may be vital for retinal adhesion and maintenance of photoreceptor cells.[10 11]

More recently, we have determined the genomic organisation of IMPG1 and have mapped the gene locus to chromosomal region 6q13-q15[12] (fig 1). Interestingly, several retinal dystrophies including autosomal dominant Stargardt-like macular dystrophy (STGD3),[13] progressive bifocal chorioretinal atrophy (PBCRA),[14] and North Carolina macular dystrophy (MCDR1)[15] have been localised to an overlapping region on the proximal long arm of chromosome 6 by genetic linkage analysis (fig 1). In order to assess whether mutations in IMPG1 may be associated with one of these macular dystrophies, we have now analysed the 17 coding exons of the gene for disease causing mutations in a family with autosomal dominant Stargardt-like macular dystrophy (ADSTGD),

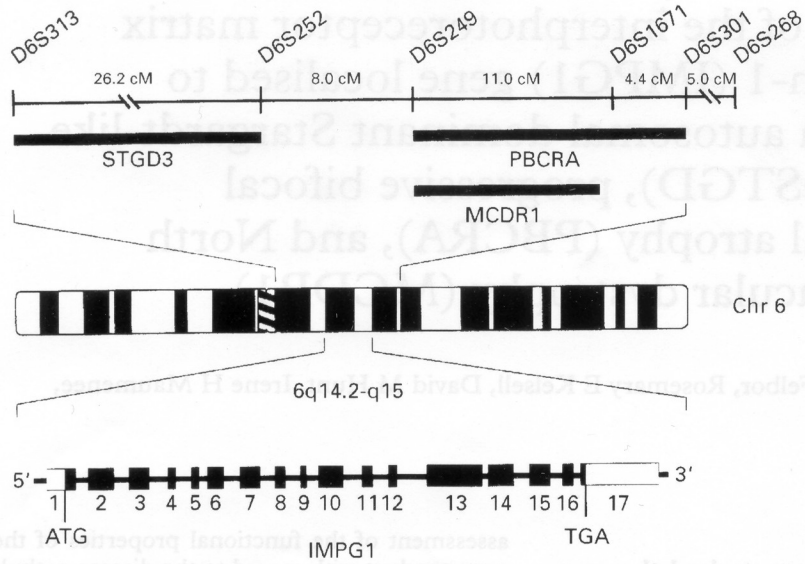

Figure 1 Idiogram of chromosome 6 and genetic map of proximal 6q illustrating the relative locations and flanking DNA markers of gene loci for autosomal dominant Stargardt-like macular dystrophy (STGD3),[13] North Carolina macular dystrophy (MCDR1),[15] and progressive bifocal chorioretinal atrophy (PBCRA).[14] Below, the genomic organisation of the gene encoding the interphotoreceptor matrix proteoglycan-1 (IMPG1) and its chromosomal localisation is shown.[12]

so far unlinked to STGD2 or STGD3,[16] in three MCDR1 pedigrees of German descent recently linked to proximal 6q[17 18] and in a five generation British PBCRA pedigree previously mapped to proximal 6q.[14] Our results definitively exclude IMPG1 as a candidate gene for MCDR1 and PBCRA on the basis of SSCA and the analysis of recombinant chromosomes. Furthermore, direct sequencing has not shown any disease associated mutations in our patient with ADSTGD. However, as autosomal dominant Stargardt-like macular dystrophies are known to be genetically heterogeneous,[13 16 19] an involvement of IMPG1 in one form of ADSTGD cannot be ruled out at present and must await the mutational analyses of the IMPG1 gene in STDG3 previously linked to proximal 6q.[13] The availability of the exon/intron structure will allow the further assessment of the potential role of IMPG1 in various retinopathies of unknown aetiology.

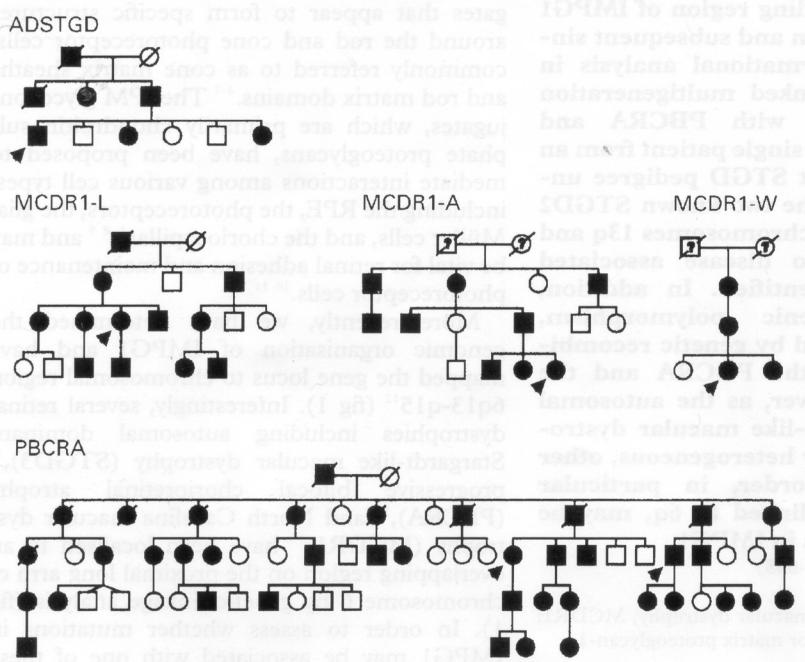

Figure 2 Pedigrees segregating autosomal dominant Stargardt-like macular dystrophy (ADSTGD),[16] North Carolina macular dystrophy (MCDR1),[15] and progressive bifocal chorioretinal atrophy (PBCRA).[14] The closed symbols indicate affected status, while open symbols indicate subjects who were examined and found to be clinically normal. Affected subjects analysed for mutations in the IMPG1 gene are marked by an arrow.

Materials and methods

PATIENTS AND FAMILIES

The clinical, histopathological, and ultrastructural phenotype of a three generation pedigree with autosomal dominant Stargardt-like macular dystrophy (also known as fundus flavimaculatus-like macular dystrophy) and late onset atrophic macular degeneration has been described in detail elsewhere.[16] In brief, mild blurring of central vision was first noted by the index patient at the age of 38. A paracentric scotoma was present in both eyes. Ophthalmoscopy showed a reddish foveal appearance surrounded by small yellowish-white, atrophic subretinal flecks and a reticular pattern of subretinal pigmentation in the midperiphery of both eyes. Multiple focal and confluent areas of choroidal hyperfluorescence were detected by fluorescein angiography. Bilateral retinal pigment epithelium (RPE) window defects were present in the fovea. There were areas of silent or dark choroid. The photopic electroretinogram (ERG) was subnormal in both eyes whereas scotopic ERG and electro-oculogram (EOG) were within the normal range. Inspection of the pedigree indicates autosomal dominant inheritance (fig 2). For mutational analysis, a DNA sample from a single affected subject was available (arrowed in fig 2).

In a recent study, the North Carolina macular dystrophy (MCDR1) phenotype was linked in three multigeneration families of German descent to DNA markers derived from chromosome 6q14-q16.2,[17 18] a region known to harbour the MCDR1 gene.[15] The family members underwent comprehensive ophthalmological examination. The affected subjects in families L, A, and W presented with fundus abnormalities consistent with MCDR1 and are described in detail elsewhere.[17 18] The DNA from one affected subject per family was used for the mutational analyses (arrowed in fig 2).

Genetic linkage analysis on a five generation British pedigree expressing the progressive bifocal chorioretinal atrophy (PBCRA) phenotype has mapped the gene locus by two point linkage to an interval between D6S249 and D6S301 on proximal chromosome 6q.[14] Detailed descriptions of ophthalmological findings in individual members of the PBCRA family are given in Douglas *et al*[20] and Godley *et al*.[21] Briefly, PBCRA is a progressive disease characterised by two distinct foci of atrophy, a temporal focus which is present at birth and a nasal focus which appears in the second decade of life. In addition, it is associated with nystagmus, myopia, and a significant reduction in visual acuity and colour vision. Photopsia and retinal detachment are complications of the disease.

MUTATIONAL ANALYSIS

DNA was isolated from leucocyte nuclei by standard extraction methods. Based on the genomic exon/intron sequences of IMPG1,[12]

Table 1 Exon/intron oligonucleotide primers for IMPG1

Exon No	*Exon size (bp)*	*Forward primer*	*Reverse primer*	*Fragment size (bp)*	*Annealing (°C)*
1	67	74: 5'-AGATTTGAGGTTGTTCTGTG-3'	74R:5'-TCGGTAGATTTTATAGATAAGC-3'	173	54
2	234	Ex2F: 5'-TATTCACCAGGATATCAATC-3'	5'R: 5'-ATAACACAAGGCTAAACGG-3'	303	51
3	167	429F: 5'- GACCCTCTTAGGCATGGCC-3'	429R: 5'-AACTGTTCGTGCAGTGTTCC-3'	254	58
4	29	605F: 5'-TCTTCGGTTGGCATTATCTC-3'	605R: 5'-GAATAGCTTAGTTTCACTCC-3'	165	53
5	65	672F: 5'-TCTCTTTCACCACCTCTTCC-3'	672R: 5'-TTGAATGAAAGTTGAGAAGC-3'	150	51
6	104	789F: 5'-CTCCATTCTCATTTTTGTGTC-3'	789R: 5'-ATGAAGAGCTAGATCAACTC-3'	182	53
7	141	4F: 5'-GTTTAGGTTAACAGAAGTCC-3'	4RII: 5'-CACCTCTCAGTCACAGCTTG-3'	235*	54
8	59	947F: 5'-AGCAGAACCAAAGAGTATT-3'	947R: 5'-AATTGAGAAGAGTTTGATTC-3'	132	49
9	21	993-1113F: 5'-TTGAATGTCTCAATAAATGTC-3'	993-1113R: 5'-ATATAAATTTGGGGGAGACG-3'	151	51
10	248	Ex8F: 5'-TTTGGGTGGGGAATGTGTC-3'	Ex8R: 5'-TAAACTCAGAACTAAGCAATC-3'	313	53
11	77	1328F: 5'-AGGAAAGATACATTCAAATC-3'	1328R: 5'-GGTTTTGAGACTTTGTTCC-3'	167	49
12	79	1399F: 5'-ACATCCTTTCTCAACATCTG-3'	1399R: 5'-CATAGACTTTGTGAGGGGAA-3'	146	53
13	533	1F: 5'-TTGGGGAATACTTGGACATA-3'	1880R: 5'-GAATTGTGAGCAGTGCCC-3'	600†	54
14	220	ExBF: 5'-AACACAGTTAAGAGGAAACC-3'	2R: 5'-CACTTTCTGGGTTGGATTCT-3'	280	53
15	199	2214F: 5'-GCTATTCATACATGCGTTAA-3'	3R: 5'-AATGAGTTCTTGAGTCTGTG-3'	281	51
16	73	2373F: 5'-AAGCCCAAGAAACAAGATAC-3'	2373R: 5'-TGCAACCAACTTAGAAAGTA-3'	145	51
17	78	3'F: 5'-CCTTGGGTGGCATTTCTTA-3'	2779R: 5'-AGAATTTACTGGTTGCCAAG-3'	295	54

*For SSCA: digestion with *Hin*fI results in two fragments of 100 and 135 bp.
†For SSCA: digestion with *Nla*IV results in three fragments of 250, 210, and 140 bp.

oligonucleotide primer pairs were designed to amplify the 17 coding exons of the gene using the polymerase chain reaction (PCR) (table 1). Reaction mixtures contained approximately 50 ng template DNA, 15 pmol of each primer, 100 µmol/l dNTPs, 0.1 µl [α-^{32}P]dCTP (3000 Ci/mmol), 1 × PCR buffer supplemented with 1-2 mmol/l $MgCl_2$, and 0.5 units of *Taq* DNA polymerase. The reaction mixture was denatured once at 94°C for five minutes and was subsequently subjected to 32 cycles of 30 seconds at 94°C, 30 seconds at an annealing temperature optimised for each primer pair (55-60°C), and 30 seconds at 72°C, followed by a final extension at 72°C for five minutes. Five microlitres of the 1:9 diluted PCR samples were subsequently added to 95% formamide, 5 mmol/l NaOH, 0.1% xylene cyanol, and 0.1% bromophenol blue. The samples were heat denatured for three minutes, immediately placed on ice, and electrophoretically separated at 4°C in 6% non-denaturing polyacrylamide gels which were run once with and once without 5% glycerol. The forward and reverse strands of PCR products corresponding to polymorphic mobility shifts were directly sequenced using the Thermo Sequenase radiolabelled terminator cycle sequencing kit (Amersham).

For the segregation analysis of the exon 13 polymorphism in the PBCRA and MCDR1 families, SSCP was carried out using the CleanGel-System (Pharmacia).[22] To increase the sensitivity of the SSCP analysis, the exon 13 PCR fragment was digested with restriction enzyme *Nla*IV (New England Biolabs) before loading on a 15% non-denaturing polyacrylamide gel. This resulted in three fragments of 250, 210, and 140 bp in size. Electrophoresis was done at 150 V, 6 W for 30 minutes followed by 550 V, 12 W for 60 minutes. The DNA was detected by silver staining as previously described.[23]

Results

MUTATIONAL ANALYSIS

For mutational analyses, DNA samples from one patient with late onset autosomal dominant Stargardt-like macular dystrophy,[16] three patients diagnosed with North Carolina macular dystrophy,[17 18] and two patients with progressive bifocal chorioretinal atrophy from a single family[14] were used (fig 2). The 17 exons of the IMPG1 gene were amplified using the

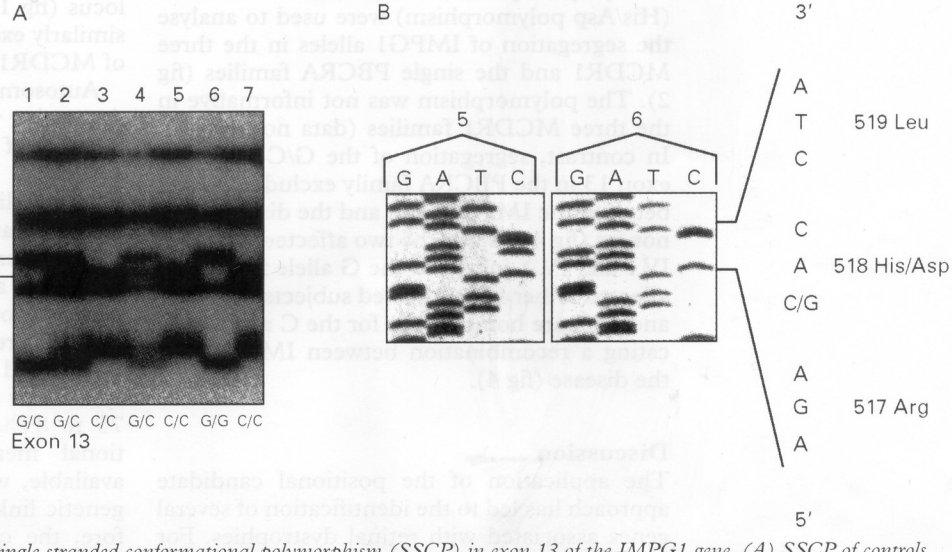

Figure 3 Single stranded conformational polymorphism (SSCP) in exon 13 of the IMPG1 gene. (A) SSCP of controls shows the polymorphic mobility shifts. (B) Sequencing of homozygous mobility shift as seen in controls 5 and 6 shows a C to G transversion at the first nucleotide of codon 518 resulting in a His/Asp protein polymorphism.

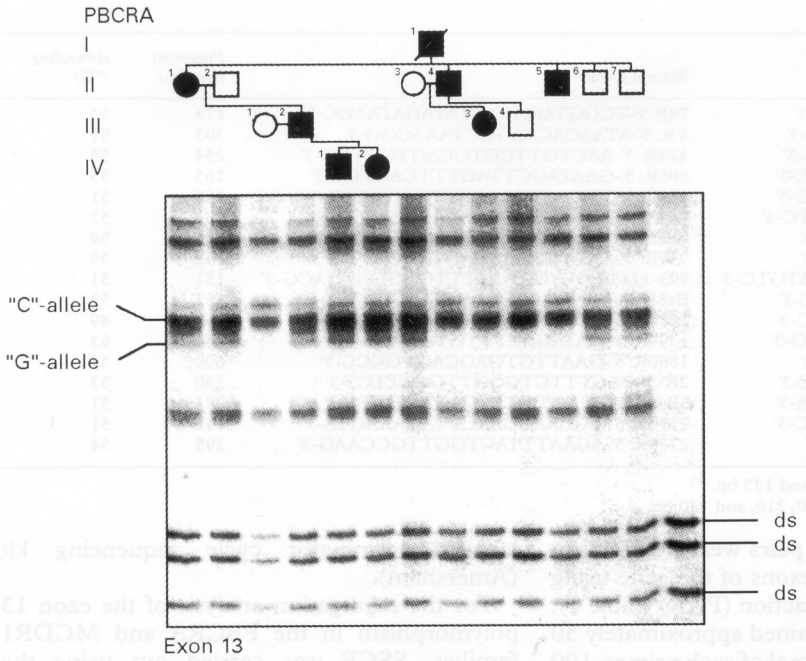

Figure 4 Segragation of C/G polymorphism in a branch of the PBCRA family. Affected subjects II.1, III.2, IV.1, and IV.2 are heterozygous for the "C" and "G" allele, respectively. Affected subjects IV.1 and IV.2 have inherited the "G" allele from their affected father III.2. In contrast, affected subjects II.4, II.5, and III.3 are homozygous for the "C" allele. This analysis shows a recombination event between PBCRA and IMPG1 in this pedigree. ds=double strand.

polymerase chain reaction (PCR) and intronic primers flanking the respective exons including the splice consensus acceptor and donor sequences (table 1). Subsequently, the PCR fragments were subjected to single stranded conformational analysis (SSCA) by using two gel running conditions to increase the sensitivity of mutation detection. Except for polymorphic mobility shifts in exon 13 (fig 3A), no altered migration patterns were identified in the remaining exons. Sequencing of exon 13 showed a G to C transversion in the first nucleotide of codon 518 changing the amino acid histidine (His) to aspartic acid (Asp) (fig 3B).

SEGREGATION ANALYSIS OF INTRAGENIC POLYMORPHISMS IN THE MCDR1 AND PBCRA FAMILIES

The polymorphic mobility shifts in exon 13 (His/Asp polymorphism) were used to analyse the segregation of IMPG1 alleles in the three MCDR1 and the single PBCRA families (fig 2). The polymorphism was not informative in the three MCDR1 families (data not shown). In contrast, segregation of the G/C alleles in exon 13 in the PBCRA family excludes linkage between the IMPG1 gene and the disease phenotype (fig 4). While the two affected children, IV.1 and IV.2, inherited the G allele from their affected father III.2, affected subjects II.4, II.5, and III.3 are homozygous for the C allele indicating a recombination between IMPG1 and the disease (fig 4).

Discussion

The application of the positional candidate approach has led to the identification of several genes associated with retinal dystrophies. For example, mutations in the rhodopsin gene have been shown to cause chromosome 3q linked autosomal dominant retinitis pigmentosa.[24] Similarly, the peripherin/RDS gene was found to be mutated in autosomal dominant retinitis pigmentosa linked to chromosome 6p.[25] Also, one form of Leber's congenital amaurosis was shown to be caused by mutations in the retinal specific guanylate cyclase on chromosome 17p.[26] Colocalisation of Sorsby's fundus dystrophy (SFD) and the tissue inhibitor of metalloproteinases-3 (TIMP3) on chromosome 22q13-qter has led to the identification of TIMP3 as the gene underlying SFD pathology.[27] Finally, functional aspects and chromosomal localisation to 1p has identified the rod photoreceptor cell specific ABC transporter as the gene causing autosomal recessive Stargardt's disease.[28]

Based on the chromosomal localisation of the interphotoreceptor matrix (IPM) proteoglycan gene, IMPG1, to 6q13-q15[12] and the potential role of IPM molecules in mediating interactions between retinal cells, the RPE and the choriocapillaris,[8 9] we reasoned that IMPG1 represents an excellent candidate for chromosome 6q linked retinopathies, including autosomal dominant Stargardt-like macular dystrophy (STGD3),[13] North Carolina macular dystrophy (MCDR1),[15 17 18] and progressive bifocal chorioretinal atrophy (PBCRA)[14] (fig 1). However, SSCP analysis has not shown any aberrant mobility shifts in the affected subjects. Furthermore, using an intragenic IMPG1 polymorphism in exon 13 we have identified a recombination event between the IMPG1 gene and the PBCRA locus.

Extended haplotype analysis has previously been performed in the PBCRA family using DNA markers spanning a genetic distance of approximately 50 cM and has excluded a location of the PBCRA locus centromeric to D6S249 and telomeric to D6S268 in recombinant subject II.1[14] (fig 2). The present IMPG1 allelotyping in the PBCRA family in combination with the previous findings in recombinant subject II.1 excludes the IMPG1 gene from an interval flanked by markers D6S249 and D6S268. As this genetic interval contains the region harbouring the MCDR1 locus (fig 1), the PBCRA recombination data similarly exclude the IMPG1 gene as the cause of MCDR1 as well as PBCRA.

Autosomal dominant Stargardt-like macular dystrophy was analysed in a single affected member of a three generation family with clear autosomal dominant transmission of the Stargardt-like phenotype.[16] Similarly to MCDR1 and PBCRA, SSCP analysis of the IMPG1 gene in the ADSTGD patient has not identified a disease causing mutation. However, it should be noted that such a mutation may have remained undetected owing to a well established detection sensitivity of the SSCP system for single base changes in the order of 75 to 85%. Since DNA samples from additional members of the family were not available, we have not been able to perform genetic linkage analysis on this family. Therefore, the chromosomal position of the gene locus in this family is still unknown. However, it is well established that the autosomal

dominant Stargardt-like macular dystrophies are genetically heterogeneous with at least two independent gene loci on chromosome 6q[13] and chromosome 13q.[19] Thus, our results cannot rule out that mutations in the IMPG1 gene are involved in one form of autosomal dominant Stargardt-like macular dystrophy. To resolve this issue additional patients diagnosed with autosomal dominant Stargardt-like macular dystrophy need to be analysed. In particular, the mutational testing of IMPG1 in affected members of an autosomal dominant Stargardt-like macular dystrophy family previously mapped to proximal chromosome 6q (designated STGD3)[13] will be useful.

This work was supported by grants from the Deutsche Forschungsgemeinschaft (DFG).

1 Collins FS. Positional cloning moves from perditional to traditional. *Nat Genet* 1995;**9**:347-50.
2 Kuehn MH, Hageman GS. Characterization of a cDNA encoding IPM150, a novel human interphotoreceptor matrix chondroitin 6-sulfate proteoglycan. *Invest Ophthalmol Vis Sci* 1995;**36**:S510.
3 Kuehn MH, Stone EM, Hageman GS. Molecular analyses of IPM150, a photoreceptor cell-specific proteoglycan. *Invest Ophthalmol Vis Sci* 1997;**38**:S599.
4 Johnson LV, Hageman GS, Blanks JC. Interphotoreceptor matrix domains ensheath vertebrate cone photoreceptor cells. *Invest Ophthalmol Vis Sci* 1986;**27**:129-35.
5 Hollyfield JG, Rayborn ME, Landers RA, Myers KM. Insoluble interphotoreceptor matrix domains surround rod photoreceptors in the human retina. *Exp Eye Res* 1990;**51**: 107-10.
6 Fariss RN, Anderson DH, Fisher SK. Comparison of photoreceptor-specific matrix domains in the cat and monkey retinas. *Exp Eye Res* 1990;**51**:473-85.
7 Mieziewska KE, van Veen T, Murray JM, Aguirre GD. Rod and cone specific domains in the interphotoreceptor matrix. *J Comp Neurol* 1991;**308**:371-80.
8 Hewitt AT. Extracellular matrix molecules: their importance in the structure and function of the retina. In: Adler R, Farber D, eds. *The retina: a model for cell biology studies*. Part II. London: Academic Press, 1986:170-201.
9 Hageman GS, Johnson LV. Structure, composition and function of the retinal interphotoreceptor matrix. In: Osborne N, Chader J, eds. *Progress in retinal research*. Vol 10. Oxford: Pergamon Press, 1991:207-49.
10 Lazarus HS, Hageman GS. Xyloside-induced disruption of interphotoreceptor matrix proteoglycans results in retinal detachment. *Invest Ophthalmol Vis Sci* 1992;**33**:364-76.
11 Hageman GS, Marmor MF, Yao XY, Johnson LV. The interphotoreceptor matrix mediates primate retinal adhesion. *Arch Ophthalmol* 1995;**113**:655-60.
12 Felbor U, Gehrig A, Sauer CG, *et al*. Genomic organization and chromosomal localization of the interphotoreceptor matrix proteoglycan-1 (IMPG1) gene: a candidate for 6q linked retinopathies. *Cytogenet Cell Genet* (in press).
13 Stone EM, Nichols BE, Kimura AE, Weingeist TA, Drack A, Sheffield VC. Clinical features of a Stargardt-like dominant progressive macular dystrophy with genetic linkage to chromosome 6q. *Arch Ophthalmol* 1994;**112**:765-72.
14 Kelsell RE, Godley BF, Evans K, *et al*. Localization of the gene for progressive bifocal chorioretinal atrophy (*PBCRA*) to chromosome 6q. *Hum Mol Genet* 1995;**4**:1653-6.
15 Small KW, Weber JL, Roses A, Lennon F, Vance JM, Pericak-Vance MA. North Carolina macular dystrophy is assigned to chromosome 6. *Genomics* 1992;**13**:681-5.
16 Lopez PF, Maumenee IH, de la Cruz Z, Green WR. Autosomal-dominant fundus flavimaculatus. Clinicopathologic correlation. *Ophthalmology* 1990;**97**:798-809.
17 Pauleikhoff D, Sauer CG, Müller CR, Radermacher M, Merz A, Weber BHF. Clinical and genetic evidence for autosomal dominant North Carolina macular dystrophy in a German family. *Am J Ophthalmol* 1997;**124**:412–15.
18 Sauer CG, Schworm HD, Ulbig M, *et al*. An ancestral core haplotype defines the critical region harbouring the North Carolina macular dystrophy gene (MCDR1). *J Med Genet* 1997;**34**:961-6.
19 Zhang K, Bither PP, Park R, Donoso LA, Seidman JG, Seidman CE. A dominant Stargardt's macular dystrophy locus maps to chromosome 13q34. *Arch Ophthalmol* 1994;**112**: 759-64.
20 Douglas AA, Waheed I, Wyse CT. Progressive bifocal chorio-retinal atrophy. A rare familial disease of the eyes. *Br J Ophthalmol* 1968;**52**:742-51.
21 Godley BF, Tiffin PA, Evans K, Kelsell RE, Hunt DM, Bird AC. Clinical features of progressive bifocal chorioretinal atrophy: a retinal dystrophy linked to chromosome 6q. *Ophthalmology* 1996;**103**:893-8.
22 Ainsworth PJ, Surh LC, Coulter-Mackie MB. Diagnostic single strand conformational polymorphism, (SSCP): a simplified non-radioisotopic method as applied to a Tay-Sachs B1 variant. *Nucleic Acids Res* 1991;**19**:405-6.
23 Bassam BJ, Caetano-Anolles G, Gresshoff PM. Fast and sensitive silver staining of DNA in polyacrylamide gels. *Anal Biochem* 1991;**196**:80-3.
24 Dryja TP, McGee TL, Reichel E, *et al*. A point mutation of the rhodopsin gene in one form of retinitis pigmentosa. *Nature* 1990;**343**:364-6.
25 Farrar GJ, Kenna P, Jordan-Fajendra KS, *et al*. A three-base-pair deletion in the peripherin-RDS gene in one form of retinitis pigmentosa. *Nature* 1991;**354**:478-80.
26 Perrault I, Rozet JM, Calvas P, *et al*. Retinal-specific guanylate cyclase gene mutations in Leber's congenital amaurosis. *Nat Genet* 1996;**14**:461-4.
27 Weber BHF, Vogt G, Pruett RC, Stöhr H, Felbor U. Mutations in the tissue inhibitor of metalloproteinases-3 (TIMP-3) in patients with Sorsby's fundus dystrophy. *Nat Genet* 1994;**8**:352-6.
28 Allikmets R, Singh N, Sun H, *et al*. A photoreceptor cell specific ATP binding transporter gene (ABCR) is mutated in recessive Stargardt macular dystrophy. *Nat Genet* 1997;**15**:236-46.

3. Anlage 3

Mapping and genomic characterization of the gene encoding diacylglycerol kinase γ (DAGK3): assessment of its role in dominant optic atrophy (OPA1)

Hum. Genet. 104: 99-105

Hum Genet (1999) 104:99–105

ORIGINAL INVESTIGATION

Heidi Stöhr · Jörg Klein · Andrea Gehrig
Michael R. Koehler · Bernhard Jurklies
Ulrich Kellner · Beate Leo-Kottler · Michael Schmid
Bernhard H. F. Weber

Mapping and genomic characterization of the gene encoding diacylglycerol kinase γ (*DAGK3*): assessment of its role in dominant optic atrophy (*OPA1*)

Received: 24 August 1998 / Accepted: 13 October 1998

Abstract The family of diacylglycerol kinases (DAGKs) is known to play an important role in signal transduction linked to phospholipid turnover. In the fruitfly *Drosophila melanogaster*, a human DAGK ortholog, *DGK2*, was shown to underlie the phenotype of the visual mutant retinal degeneration A (*rdgA*). Previously, the gene encoding a novel member of the human DAGK family, termed *DAGK3*, was cloned and demonstrated to be abundantly expressed in the human retina. Based on these findings we reasoned that *DAGK3* might be an excellent candidate gene for a human eye disease. In the present study, we report the genomic organization of the human *DAGK3* gene, which spans over 30 kb of genomic DNA interrupted by 23 introns. In addition, we have mapped the gene locus by fluorescence in situ hybridization to 3q27–28, overlapping the chromosomal region known to contain the gene underlying dominant optic atrophy (OPA1), the most common form of hereditary atrophy of the optic nerve. Mutational analysis of the entire coding region of *DAGK3* in 19 unrelated German OPA1 patients has not revealed any disease-causing mutations, therefore excluding *DAGK3* as a major cause underlying OPA1.

H. Stöhr · J. Klein · A. Gehrig · M. R. Koehler · M. Schmid
B. H. F. Weber (✉)
Institut für Humangenetik, Biozentrum, Universität Würzburg,
Am Hubland, D-97074 Würzburg, Germany
e-mail: bweb@biozentrum.uni-wuerzburg.de,
Tel.: +49-931-888-4062, Fax: +49-931-888-4069

B. Jurklies
Universitäts-Augenklinik Essen, Germany

U. Kellner
Universitäts-Klinikum Benjamin Franklin, Berlin, Germany

B. Leo-Kottler
Eberhard-Karls-Universität, Augenklinik, Tübingen, Germany

Introduction

Diacylglycerol kinase (DAGK) plays an important role in the regulation of cellular signal transduction. It initiates the regeneration of phosphatidylinositols by phosphorylation of diacylglycerol (DAG) to generate phosphatidic acid (PA) (Kanoh et al. 1990) thus controlling the intracellular concentration of the second messengers DAG and PA. While DAG is the physiological activator of protein kinase C (Nishizuka 1984), PA has been shown to modulate several enzymes in vitro, including phospholipase C-γ1 (Jones and Carpenter 1993), polyphosphoinositide kinase (Moritz et al. 1992) and *ras* GTPase-activating protein (Tsai et al. 1990).

To date, eight mammalian DAGK isozymes have been identified that differ from each other by characteristic molecular masses, enzymologic properties, substrate specificities and cell-specific expression profiles (reviewed in Sakane and Kanoh 1997). All DAGKs share a conserved putative catalytic domain at the C-terminus and two cysteine-rich zinc-finger motifs, but can be further divided into subgroups according to unique structural features, including EF-hand motifs, pleckstrin homology domains and ankyrin-like repeats.

In our search for genes involved in hereditary human eye disorders we considered one member of the DAGK family, *DAGK3*, to be an attractive candidate for human retinopathies for two reasons. First, *DAGK3* has been shown to be predominantly expressed in the human retina (Kai et al. 1994). Moreover, mutations in the gene encoding an eye-specific diacylglycerol kinase *(DGK2)* are known to cause defective phospholipid turnover in the *Drosophila melanogaster* visual mutant retinal degeneration A (*rdgA*) (Masai et al. 1993). Although there is no direct evidence for an involvement of the phosphoinositide cycle in mammalian phototransduction (Stryer 1991), the abundant presence of retinal phosphatidylinositol-related enzymes such as phospholipase C and DAGK strongly supports a functional role of these molecules in the visual system (Ferreira et al. 1993).

To assess further the involvement of *DAGK3* in human retinal diseases we first mapped the gene locus to

3q27–q28, the chromosomal region that has previously been demonstrated by genetic linkage analysis to harbor the disease gene associated with dominant optic atrophy (OPA1) (Eiberg et al. 1994). OPA1 is the most frequent form within the group of hereditary optic atrophies and has an estimated incidence of 1:50.000 (Lyle 1990). It is inherited as an autosomal dominant trait with almost complete penetrance (Kivlin et al. 1983) but highly variable expressivity. The disease is typically characterized by an insidious onset of clinical symptoms in early childhood, reduction of visual acuity, central, paracentral or cecocentral scotomas, colour vision defects and bilateral atrophy of the optic nerve, which can be seen as a pallor of the optic disc (Jaeger 1966; Kline and Glaser 1979). There is usually a slow progression of visual dysfunction throughout life (Eliott et al. 1993). Histopathologic examination of donor eyes of affected OPA1 patients suggests a primary dystrophic process in the retinal ganglion cell layer followed by ascending atrophy of the optic nerves (Johnston et al. 1979; Kjer et al. 1983).

Here, we report the complete genomic organization of *DAGK3* and the mutational analysis of the entire coding region of the gene in the genomic DNA of 19 individuals affected with dominant optic atrophy. No disease-associated mutations were identified, suggesting that *DAGK3* is not a major factor underlying OPA1 aetiology.

Materials and methods

Isolation of genomic clones containing *DAGK3*

The RPCI-1 human P1 bacterial artificial chromosome (PAC) library (Ioannou et al. 1994) was kindly provided by P. deJong (Roswell Park Cancer Institute, Buffalo, N.Y.) and was screened with a full-length *DAGK3* cDNA probe obtained by reverse transcription-polymerase chain reaction (RT-PCR) amplification of total human retinal RNA using oligonucleotide primers 5′-DAGK3 (CCAAGTAAGGGAATAAACCG) and 3′-DAGK3 (TGCTTTCTCTCTTGGTTTAG), designed according to published cDNA sequences (GenBank Accession No. D26135; Kai et al. 1994). Hybridization was performed at 65°C as described by Church and Gilbert (1984). Final washing conditions were at a stringency of 0.2×SSPE, 0.1% SDS.

Positive clones were isolated and DNAs were prepared from overnight cultures by standard alkaline lysis techniques. Purified DNA was *Eco*RI digested, electrophoresed on 0.8% agarose, blotted onto Hybond N^+ nylon membranes (Amersham) and hybridized to seven overlapping RT-PCR products together covering the entire coding sequence of the *DAGK3* gene. The nucleotide positions of the seven fragments (1A, 1B, 2A–C, 3A, 3B) with respect to the published cDNA and the sequences of the primers used for RT-PCR are as follows: 1A (–103 to +508, 611 bp): 5′-DAGK3b (ATCGCAAACCTGCAATGAGC) and DAGK-6 (AGGGACAGGTAGCACACAACA); 1B (+464 to +796, 333 bp): DAGK-5 (ATCCCCAGTGGTGTACCTG) and DAGK-2 (GAGCCAGAGTCATCCATCC); 2A (+756 to +1265, 509 bp): DAGK-1 (TCCCATTGCTGGTGCTCC) and DAGK-8 (CATGACAAGTTCGCCCTTG); 2B (+1212 to +1472, 260 bp): DAGK-7 (GGCCAGGTGAGAAGTCTGA) and DAGK-10 (ACCACAGGCCAAAACACGG); 2C (+1229 to +1667, 239 bp): DAGK-9 (ACTTTTTCCGTGATACTCCAG) and DAGK-4 (GTCCAGCATCACCAAGGGG); 3A (+1626 to +1926, 301 bp): DAGK-3 (ATCCTGAAAGACATTGAGCA) and DAGK-12 (CCCCATCACACTCCAACTCA); 3B (+1886 to +2414, 529 bp): DAGK-11 (CAAGAAACTCCACGACCAC) and 3′-DAGK3.

Characterization of exon/intron junctions and structure of *DAGK3*

*Hin*cII, *Hin*dIII and *Pst*I restriction fragments of overlapping PAC clones dJ207E13 and dJ131A16, containing the entire coding region of *DAGK3*, were separately subcloned into the plasmid vector pBluescript SK(–) (Stratagene). Exon-containing fragments were identified by colony hybridization of the seven cDNA fragments described above. Positive clones were sequenced using the Thermo Sequenase radiolabelled terminator cycle sequencing kit (Amersham) with vector- and exon-specific primers. The exon/intron boundaries were identified by alignment of the genomic sequence with the published *DAGK3* cDNA (Kai et al. 1994) using the MacVector sequence analysis software (release 4.0).

Chromosomal localization

Radiation hybrid mapping was performed by PCR using a commercially available panel of 25 human×hamster hybrid cell line DNAs (BIOS Corporation, New Haven, Conn.) and oligonucleotide primers DAGK-F (AAACCAAGAGAGAAAGCAAG) and DAGK-R (AATTCCCAGTTTCTCCGCTC) designed from the 3′ untranslated region (UTR) of the *DAGK3* cDNA (Kai et al. 1994). Fluorescence in situ hybridization (FISH) mapping was performed using PAC clone dJ131A16 as previously described (Köhler and Vogt 1994).

Patients

Twenty affected subjects of German origin who are unrelated on the basis of genealogy were ascertained from the University Eye Hospitals in Berlin, Essen and Tübingen. Diagnosis of dominant optic atrophy was based on the presence of typical clinical features, including reduced visual acuity, colour vision deficits, abnormal visual-evoked potentials, optic disc pallor and family history of the disease (Table 1). In three cases (patients 1–3), blood samples from additional affected and unaffected family members were available for DNA and haplotype analysis.

Haplotyping and single-strand conformation analysis (SSCA)

Genomic DNAs were extracted from blood lymphocytes and were used as templates for PCR amplification. For haplotype analysis, microsatellite markers at *D3S1601* and *D3S1265*, closely flanking the *OPA1* locus, were used (Bonneau et al. 1995; Johnston et al. 1997). Primer sequences and PCR conditions were taken from the literature. For SSCA, PCR primer pairs flanking the 24 exons of the *DAGK3* gene are listed in Table 2. PCR conditions were an initial denaturation of 1 min at 94°C, 30 cycles of 30 s at 94°C, 30 s at the exon-specific annealing temperature (Table 2) and 30 s at 72°C followed by a final extension of 5 min at 72°C. For SSCA, DNA was amplified in the presence of [^{32}P]dCTP (3000 Ci/mmol) and electrophoretically separated in a 6% non-denaturing polyacrylamide gel with or without 5% glycerol at 4°C, 25 W constant power for 2–11 h. PCR products with an aberrant mobility shift were cycle-sequenced as described above.

Results and discussion

Characterization of the genomic organization of *DAGK3*

Screening of the human RPCI-1 PAC library with the full-length *DAGK3* cDNA probe resulted in the isolation of six PAC clones: dJ91H22, dJ91L22, dJ115B1, dJ115H3, dJ131A16 and dJ207E13. Southern blots of *Eco*RI-digested PAC clones were probed with seven overlapping cDNA frag-

Table 1 Clinical data of OPA1 patients. (*VEP* visual evoked potential, *n.k.* not known)

Patient		Age onset/ age[a] (years)	Progression	Visual acuity (OD/OS)	Colour vision defect	VEP (Amplitude/latency)	Disc appearance	Family history
No.	ID							
1	3884-OAK	7/31	Slow	0.4/0.5	Non-specific	Diminished/ normal	Temporal pallor	Yes
2	250568996-DION	23/29	No	1.0/1.0	Non-specific	Normal	Normal	Yes
3	31XDION-12261	n.k.	n.k.	0.9/0.9	n.k.	n.k.	Temporal pallor	Yes
4	4917-OAK	20–30/51	Slow	0.2/0.4	Tritan defect	Diminished/ normal	Temporal pallor	Yes
5	5675-OAK	n.k.	n.k.	n.k.	n.k.	n.k.	Pallor diffuse	Yes
6	5579-OAK	6/13	No	0.3/0.2	Non-specific	Diminished/ prolonged	Temporal pallor	n.k.
7	4410-OAK	43/54	Rapid	0.1/0.1	Tritan defect	Diminished/ prolonged	Diffuse pallor	Yes
9	4195-OAK	13/16	No	1.0/0.8	Non-specific	Diminished/ normal	Temporal pallor	No
10	4999-OAK	12/24	No	0.4/0.4	Non-specific	n.k.	Temporal pallor	Yes
11	1331-OAK	35/38	Slow	0.4/0.5	Non-specific	n.k.	Diffuse pallor	No
12	4518-OAK	3/7	No	0.3/0.4	Non-specific	n.k.	Temporal pallor	Yes
13	555-OAK	6/19	No	0.3/0.3	Deutan defect	n.k.	Temporal pallor	Yes
14	542-OAK	8/23	No	0.4/0.4	Protan defect	n.k.	Temporal pallor	Yes
15	4049-OAK	12/22	No	0.4/0.3	Tritan defect	n.k.	Temporal pallor	Yes
16	1338-OAK	49/57	Slow	0.4/0.2	Deutan defect	n.k.	Temporal pallor	n.k.
18	3050-OAK	54/56	Slow	0.2/0.2	Tritan defect	n.k.	Temporal pallor	Yes
19	3288-OAK	Childhood/43	No	0.1/0.1	Deutan defect	n.k.	Temporal pallor	n.k.
20	53/931296 DHON	6/10	Slow	0.3/0.3	Tritan defect	Diminished/ normal	Temporal pallor	Yes
21	57/926096 DHON	Childhood/71	Slow	0.03/0.04	Tritan defect	Diminished/ prolonged	Diffuse pallor	Yes
22	63/X-DION	Childhood/56	Slow	0.05/0.05	n.k.	n.k.	Temporal pallor	Yes

[a]Age at final examination

ments (1A, 1B, 2A–C, 3A, 3B) covering the entire coding sequence of the *DAGK3* gene. A single PAC clone, dJ207E13, contains the most 5′ end of *DAGK3*, including fragments 1A, 1B, 2A–C and 3A, whereas the remaining PAC clones all hybridized to cDNA probes 2A–C, 3A and 3B and thus contain the 3′ end of the gene (data not shown). Overlapping PAC clones dJ207E13 and dJ131A16 were selected for further characterization of the *DAGK3* locus (Fig. 1).

Based on sequential hybridizations of overlapping cDNA fragments to high-density colony filters of subcloned PAC restriction fragments, exon-containing plasmids were identified and sequenced. This allowed us to deduce the genomic organization of the *DAGK3* gene, which consists of 24 exons spanning more than 30 kb of genomic DNA (Fig. 1). As shown in Table 3, the sizes of the exons range from 50 to 191 bp, while those of the introns vary from 100 bp to over 5 kb. Intron sizes were determined by restriction mapping or PCR analysis with primers flanking the respective introns. All acceptor and donor splice site junctions contain the invariant dinucleotides AG and GT, respectively, and boundary sequences that are in excellent agreement with 5′ and 3′ consensus splice sequences (Shapio and Senapathy 1987; Table 3).

Several functional domains have been defined in *DAGK3*, including two Ca^{2+}-coordinating EF-hand sequences, two zinc finger-like sequences and a putative ATP-binding motif (Kai et al. 1994). A comparison with the genomic exon/intron structure shows that the various protein domains are not strictly correlated with single exon boundaries, e.g. the second zinc finger-like motif is encoded in part by exon 11 (36 amino acids) and exon 12 (11 amino acids).

Several human tissues, including liver, kidney, spleen and testis, as well as hepatoma cell line HepG2 were found to express a catalytically inactive DAGK3 carrying an internal deletion of 25 amino acid residues (Kai et al. 1994). Our data demonstrate that the 25 amino acid residues are entirely encoded by exon 15, suggesting that the truncated DAGK3 isoform is the result of a skipping of exon 15. Both, the 3′ acceptor and the 5′ donor sequences of exon 15 have excellent splice site discrimination scores, 2.5 and 5.3, respectively, and therefore should represent strong splicing

Table 2 Oligonucleotide primers used for single-strand conformation analysis of *DAGK3*

Exon	Primer	Sequence (5′→3′)	Fragment size (bp)	T_A (°C)
1	5′ DAGK3	CCAAGTAAGGGAATAAACCG	210	62
	DAGK-13R	AGAAGAAATCCCGTCCCAG		
2	DAGK-53F	ATTTACTTGGCCCAGCTTC	194	60
	DAGK-22R	AAAGGCTAAAAAACACAGGG		
3	DAGK-67F	CCCTTTGCTTCTCTCCACTG	245	61
	DAGK-54R	GCGCAAGGTCTTCCCATC		
4	DAGK-24F	CAAGAAGCTAGAGGGCCT	155	60
	DAGK-55R	ATTCCCTACTTTTCCCACAA		
5	DAGK-40F	CTAAACAGAAAATGTCCTTGG	287	58
	DAGK-41R	GGAATAATGGATAGAACCCC		
6	DAGK-56F	CATCAAAACTTCAGCCATCC	189	60
	DAGK-35R	ATTCTTCCTCTGCTTGCC		
7	DAGK-42F	CTCTGGTTGTCTCCTTTTGAT	151	60
	DAGK-15R	ACTCCAAAGCCACCCCATC		
8	DAGK-57F	GAGGCAGAAGGCAGGTAGAC	234	60
	DAGK-66R	TTCCTGAATGGCAAGAGATC		
9	DAGK-68F	ATCTCAGGGCAGCCAGCT	197	61
	DAGK-26R	TGGGGGAAGAGGTTTGAAG		
10	DAGK-58F	TACGTGGCTATTCACAAGC	165	58
	DAGK-36R	CAGTAGAACAAGGCAGTAGATG		
11	DAGK-69F	GGTTCTGCCATTTTCCCTG	189	58
	DAGK-59R	GTTGAAAAGGAAGCAGGGC		
12	DAGK-28F	TTGCTCACTTTCACTCACTC	183	58
	DAGK-60R	AACCCGGAGAAGCTACAG		
13	DAGK-43F	TTGTGTTAGGCTTCTTTTTCC	145	58
	DAGK-44R	GTGCAATCGGATTTAGAGC		
14	DAGK-61F	CCTATTGGATGAAGCAGAGC	177	57
	DAGK-38R	CTGAGTCGTGTCGCCCTA		
15	DAGK-30F	GAACCCTCATCCCTGCCT	208	55
	DAGK-62R	AAGGGAGGGGGAGAAATAAG		
16	DAGK-45F	TAACAAGCCCATTTTGGCC	158	53
	DAGK-46R	TAAATAAGCAGAAAACGCCC		
17	DAGK-63F	CTCAAACATTCTACAGTCCCAT	174	59
	DAGK-39R	CCCAGGGTACCACCATTAG		
18	DAGK-47F	TGCTGTGGTGGCAAATGCA	273	64
	DAGK-48R	CCAGAGGGACAACAGAAGGC		
19	DAGK-70F	GGACCCTGAGATAGATAGCG	225	57
	DAGK-64R	AGAGAGCAGGTGAAAGGC		
20	DAGK-49F	CATGAGCATTTCAAGTATGGA	194	59
	DAGK-33R	CCAGGAGCAGAACCAAGATC		
21	DAGK-34F	TGAGGACACTAACAGATGGCC	274	59
	DAGK-65R	CTACTGGGCATTGACCTAAAAC		
22	DAGK-50F	CTGAGACCAAATGTGTATGCA	207	56
	DAGK-51R	TGGGTGACAAAGAGGCATAC		
23	DAGK-71FN	AAAAAGCTCACTGTGTTCTC	135	52
	DAGK-73R	GCTTCTCATCCCCATCTC		
24	DAGK-52F	GCGACTCACTCTCCCTTAG	205	56
	DAGK-R	AATCCCAGTTTCTCCGCTC		

signals (Penotti 1991). Thus far, the functional significance underlying the aberrant splicing event in some human tissues is unclear and needs further elucidation.

Mapping of the human *DAGK3* gene to chromosome 3q27–q28

To determine the chromosomal location of *DAGK3*, we applied a combination of two independent methods. We initially sublocalized *DAGK3* by PCR hybrid mapping using oligonucleotide primers that were designed from the locus-specific 3′-UTR of the gene. On the basis of the presence of the expected 778-bp PCR product in human genomic DNA and hybrid cell lines containing human chromosome 3 (SM-423, SM-507, SM-860, SM-861, SM-1079), and the absence of this fragment in the remaining 20 hybrids lacking chromosome 3 as well as the parental hamster ovary cell line CHO-104, we assigned the *DAGK3* locus to chromosome 3.

In addition, biotin-labelled PAC clone dJ131A16, containing exons 9 to 24 of *DAGK3* (Fig. 1), was used as a probe in FISH experiments on human metaphase spreads. Hybridization signals were repeatedly produced on both chromatids of chromosome 3q27–q28, whereas background signals were distributed randomly (Fig. 2). These results allowed us to refine further the subchromosomal position of the *DAGK3* locus to the 3q27–q28 region, confirming previous reports of *DAGK3* mapping performed by Fitzgibbon et al. (1995).

Mutational analysis of *DAGK3* in OPA1 patients

In several studies the autosomal dominant *OPA1* gene has been mapped to 3q28–q29 (Eiberg et al. 1994; Bonneau et al. 1995; Lunkes et al. 1995; Jonasdottir et al. 1997; Seller et al. 1997; Votruba et al. 1997, 1998), a chromosomal region overlapping the *DAGK3* location. We therefore decided to perform a mutational screen of the 24 exons of *DAGK3* in 19 OPA1 patients by SSCA (patient 3 was excluded from this analysis; see below).

Analysis of exon 4 revealed a complex pattern of band shifts as the result of a combination of three different variations in introns 3 and 4. Sequence changes IVS3–31T→C and IVS3–11T→C appear to be common polymorphisms with observed frequencies of the T alleles in control chromosomes of 37.0% and 53.2%, respectively (Table 4). The third alteration, IVS4+11G→A, was found once in patient 12 as well as in 4 out of 94 control alleles. An additional heterozygous sequence change, IVS5+12C→A, was observed in patient 11 but not in any other of the remaining 37 *OPA1* alleles nor in 188 unaffected control chromosomes (Table 4). This sequence alteration as well as the rare intronic base change IVS4+11G→A do not appear to influence the strength of the respective 5′ donor splice site signals. However, a possible functional effect on the correct splicing mechanism still needs to be assessed. In addition, the lack of available DNA samples from crucial family members of patients 11 and 12 has not allowed us to test for segregation of the rare variations with the disease. Finally, in exon 10 an A to G transition at nucleotide 947 results in a change of a lysine to an arginine residue at codon 316. This alteration was found in patients 4, 5 and 21 but also in

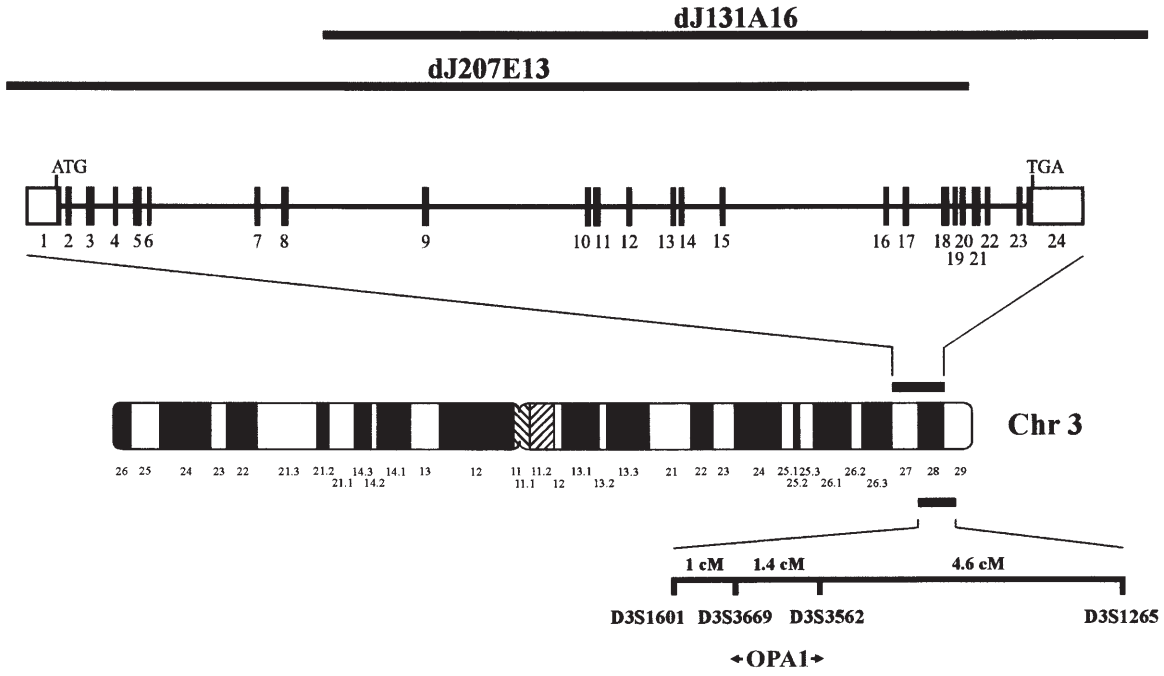

Fig. 1 Location and genomic organization of human *DAGK3*. *Top* PAC clones dJ207E113 and dJ131A16 containing the entire *DAGK3* gene are indicated by *horizontal bars*. The 24 exons of the gene are represented by *filled boxes*, the 3′ and 5′ untranslated regions by *open boxes*. *DAGK3* (Fitzgibbon et al. 1995; present study) and *OPA1* (Jonasdottir et al. 1997) have been mapped to overlapping genomic regions on 3q indicated by *solid bars* on each side of the idiogram of chromosome 3

Table 3 Exon/intron boundaries of the human *DAGK3* gene. Intronic and exonic sequences are given in lower and upper case letters, respectively

Intron	Exon		Intron	
3′ Splice acceptor	No.	Size (bp)	5′ Splice donor	Size (kb)
	1	67[a]	...AAT gtgagt	0.23
aattgtgtctcttcag A...	2	77	...GAG gtaaga	0.55
ttttgccccttctcag C...	3	166	...CAG gtacac	0.68
tctttttttttcctcag A...	4	63	...CTG gtaagt	0.56
cttttgttcatcgcag A...	5	171	...AGT gtaagt	0.27
ctgtgttttcttacag T...	6	50	...GCG gtaagt	3.30
ctttgctattttctag G...	7	75	...CCT gtgagt	0.75
tctttggattccacag A...	8	123	...TCT gtaagt	0.43
cctattacccctgcag G...	9	118	...CTC gtgagt	>5.0
ctttttttctttttcag A...	10	89	...GAG gttcgt	0.10
cgcttccctcccgcag G...	11	117	...ACG gtgggt	0.90
tcatttctccccccag T...	12	93	...CGG gtaagt	1.30
tcctttcttgtcacag G...	13	60	...CAG gtacct	0.20
tcttttacctttcaag T...	14	80	...AAG gtacgt	1.20
ctttttttttccatag A...	15	75	...AGG gtatgg	>5.0
tcttcttcttccccag G...	16	86	...TTG gtaagc	0.51
tctgtgtgtcttgcag A...	17	90	...GAG gtgagt	1.10
gtgctgtcctccacag G...	18	162	...GTG gtgagt	0.20
cacgttaccttcgcag G...	19	65	...CAG gtaagc	0.15
ctgctttgtggtccag G...	20	91	...GAG gtaagt	0.30
tctctccgtcctccag T...	21	191	...AAG gtaagc	0.25
gctgtctcctctgcag A...	22	121	...CCA gtgcgc	3.60
gtgttctgggttccag G...	23	61	...ACG gtgagt	0.10
gcctctttgcttttag A...	24	99[a]		

[a]Sizes correspond to the coding regions of these exons

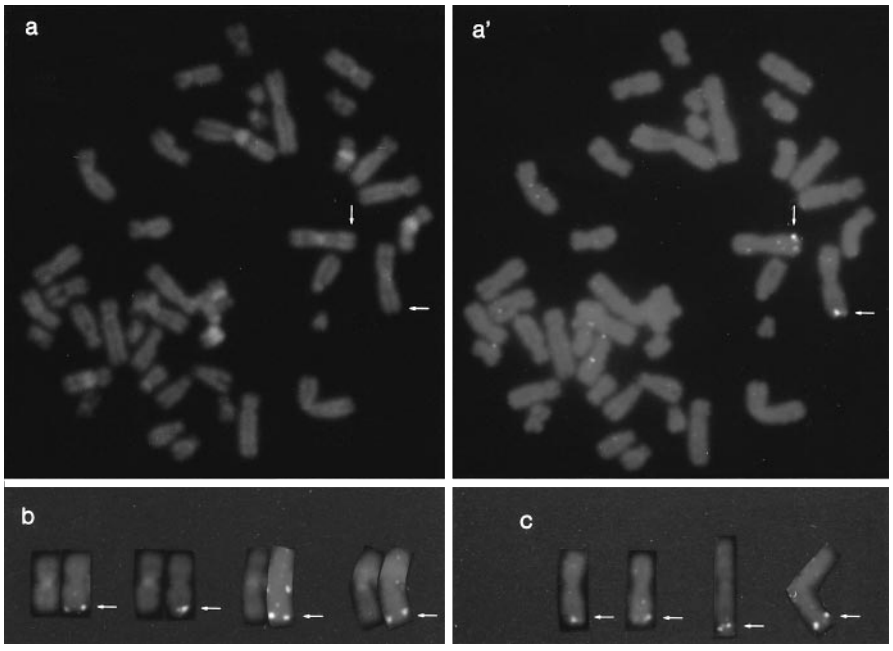

Fig. 2a–c Fluorescence in situ hybridization and 4′-6′-diamidino-2-phenylindole counterstaining (*blue*) on a human metaphase spread (**a**, **a′**) and on chromosomes 3 (**b**, **c**). Hybridization with PAC clone dJ131A16 as probe results in specific signals on 3q27–q28

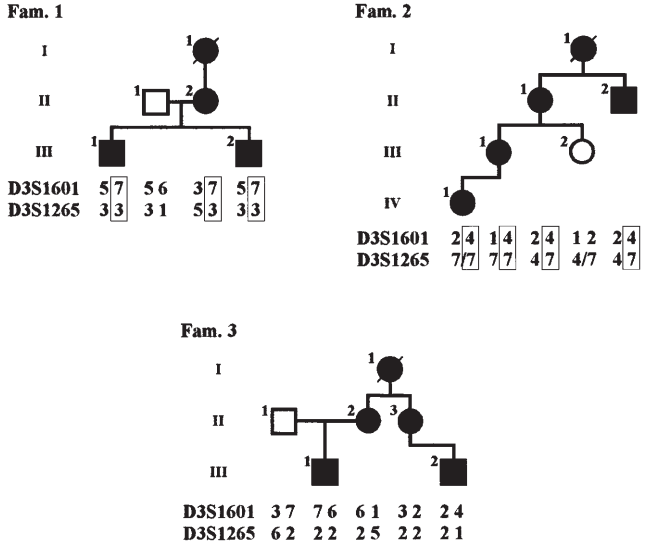

Fig. 3 Pedigrees and genotyping data of three multigeneration OPA1 families. Note that affected individuals in family 3 do not share a common allele at *D3S1601*, suggesting locus heterogeneity of OPA1 in this pedigree

20 out of 47 control individuals, suggesting that this amino acid change represents a neutral polymorphism. Taken together, of the five sequence variations identified in the OPA1 patients, three appear to be common polymorphisms while the biochemical significance of two nucleotide alterations is presently unknown.

While our mutational analyses were in progress, the Human Transcript Map reported a refined localization of the *DAGK3* gene approximately 20–25 cM centromeric to the *OPA1* minimal candidate region (http://www.ncbi.nlm.nih.gov/cgi-bin/SCIENCE96) thus physically excluding this gene from the *OPA1* locus. This is in full agreement with the results of our mutational analysis, which does not support a role of *DAGK3* in OPA1.

Table 4 Sequence alterations identified in the *DAGK3* gene and their frequencies

Sequence alteration (functional consequences)	Frequencies (no. of alleles)	
	OPA1 patients	Controls
IVS3–31T→C (polymorphism)	T=16; C=22	T=35; C=59
IVS3–11T→C (polymorphism)	T=17; C=21	T=50; C=44
IVS4+11G→A (unknown)	G=37; A=1	G=90; A=4
IVS5+12C→A (unknown)	C=37; A=1	C=188; A=0
A947G (K316R)	A=35; G=3	A=74; G=20

Genetic heterogeneity in OPA1

In more than 50 families from different ethnic populations, genetic linkage studies have mapped the dominant optic atrophy locus to the distal long arm of chromosome 3 (e.g. Eiberg et al. 1994; Bonneau et al. 1995; Lunkes et al. 1995; Jonasdottir et al. 1997; Seller et al. 1997; Votruba et al. 1997, 1998). However, there is recent evidence of genetic heterogeneity in this condition (Seller et al. 1997) with at least two additional OPA loci on Xp11.4–p11.2 and on 18q12.2–q12.3 (Assink et al. 1997; Kerrison et al. 1998).

Three of our patients (nos. 1, 2 and 3) are part of multigeneration pedigrees of whom blood samples of several affected and unaffected members were available for genetic linkage analysis. We genotyped all individuals at polymorphic DNA markers at *D3S1601* and *D3S1265* known to flank the *OPA1* candidate region (Bonneau et al. 1995; Johnston et al. 1997; Fig. 1, Fig. 3). In families 1 and 2 seg-

regation of marker alleles at both loci are consistent with linkage of *OPA1* in these families to distal 3q (Fig. 3). Moreover, haplotyping revealed two distinct haplotypes, suggesting that independent mutations underlie the OPA1 condition in the two families. Genotyping of members of family 3 demonstrates that the four affected individuals do not share a common disease allele at the highly informative locus *D3S1601*, located approximately 1–2 cM distal to the *OPA1* region (Votruba et al. 1998). These findings suggest locus heterogeneity in our OPA1 pedigree. Currently, additional affected and unaffected members are being recruited to pursue further the genetic localization of the disease locus in this family.

The present study represents the first characterization of the genomic organization of a member of the DAGK family. This work will greatly contribute to the future study of the evolution of the DAGK family in higher animals. Moreover, the knowledge of the detailed gene structure of *DAGK3* will facilitate the assessment of the gene in other human eye diseases and finally will allow further analysis of the biological properties and functional relevance of *DAGK3* in ocular tissues.

Acknowledgements The authors wish to thank the OPA1 patients and their families for their kind cooperation. This work was supported by grants from the Deutsche Forschungsgemeinschaft.

References

Assink JJ, Tijmes NT, Brink JB ten, Oostra RJ, Riemslag FC, deJong PT, Bergen AA (1997) A gene for X-linked optic atrophy is closely linked to the Xp11.4–Xp11.2 region of the X chromosome. Am J Hum Genet 61:934–939

Bonneau D, Souied E, Gerber S, Rozet J-M, D'Haens E, Journel H, Plessis G, Weissenbach J, Munnich A, Kaplan J (1995) No evidence of genetic heterogeneity in dominant optic atrophy. J Med Genet 32:951–953

Church GM, Gilbert W (1984) Genomic sequencing. Proc Natl Acad Sci USA 81:1991–1995

Eiberg H, Kjer B, Kjer P, Rosenberg T (1994) Dominant optic atrophy (OPA1) mapped to chromosome 3q region. I. Linkage analysis. Hum Mol Genet 3:977–980

Eliott D, Traboulsi E, Maumenee J (1993) Visual prognosis in autosomal dominant optic atrophy. Am J Ophthalmol 115:360–367

Ferreira PA, Shortridge RD, Pak WL (1993) Distinctive subtypes of bovine phospholipase C that have preferential expression in the retina and high homology to the norpA gene product of Drosophila. Proc Natl Acad Sci USA 90:6042–6046

Fitzgibbon J, Wells D, Pilz A, Delhanty J, Kai M, Kanoh H, Hunt D (1995) Localisation of the gene encoding diacylglycerol kinase 3 (DAGK3) to human chromosome 3q27–28 and mouse chromosome 16. Curr Eye Res 14:1041–1043

Ioannou PA, Amemiya CT, Garnes J, Kroisel PM, Shizuya H, Chen C, deJong PJ (1994) A new P1 derived vector for the propagation of large human DNA fragments. Nat Genet 6:84–89

Jaeger W (1966) Hereditary optic atrophies in childhood. J Genet Hum 15:312–321

Johnston PB, Gaster RN, Smith VC, Tripathi RC (1979) A clinicopathologic study of autosomal dominant atrophy. Am J Ophthalmol 88:868–875

Johnston RL, Burdon MA, Spalton DJ, Bryant SP, Behnam JT, Seller MJ (1997) Dominant optic atrophy, Kier type. Arch Ophthalmol 115:100–103

Jonasdottir A, Eiberg H, Kjer B, Kjer P, Rosenberg T (1997) Refinement of the dominant optic atrophy locus (OPA1) to a 1.4 cM interval on chromosome 3q28–3q29, within a 3-Mb YAC contig. Hum Genet 99:115–120

Jones GA, Carpenter G (1993) The regulation of phospholipase C-gamma 1 by phosphatidic acid. Assessment of kinetic parameters. J Biol Chem 268:20845–20850

Kai M, Sakane F, Imai S, Wasa I, Kanoh H (1994) Molecular cloning of a diacylglycerol kinase isozyme predominantly expressed in human retina with a truncated and inactive enzyme expression in most other human cells. J Biol Chem 269:18492–18498

Kanoh H, Yamada K, Sakane F (1990) Diacylglycerol kinase: a key modulator of signal transduction? Trends Biochem Sci 15:47–50

Kerrison JB, Arnould V, Barmada MM, Sallum J, Li YY, Zhu D, Vagefi MR, Mitchell T, Maumenee IH (1998) Autosomal dominant optic atrophy pedigree linked to chromosome 18q12.2–q12.3. Invest Ophthalmol Vis Sci 39:S511

Kivlin JD, Lovrien EW, Bishop T, Maumenee IH (1983) Linkage analysis in dominant optic atrophy. Am J Hum Genet 35:1190–1195

Kjer P, Jensen OA, Klinken L (1983) Histopathology of eye, optic nerve and brain in a case dominant optic atrophy. Acta Ophthalmol 61:300–312

Kline LB, Glaser JS (1979) Dominant optic atrophy. The clinical profile. Arch Ophthalmol 97:1680–1686

Köhler MR, Vogt PH (1994) Interstitial deletions of repetitive DNA blocks in dicentric human Y chromosomes. Chromosoma 103:324–330

Lunkes A, Hartung U, Magarino C, Rodriguez M, Palmero A, Rodriguez L, Heredero L, Weissenbach J, Weber J, Auburger G (1995) Refinement of the OPA1 gene locus on chromosome 3q28–q29 to a region of 2–8 cM, in one Cuban pedigree with autosomal dominant optic atrophy type Kjer. Am J Hum Genet 57:968–970

Lyle WM (1990) Genetic risks. University of Waterloo Press, Waterloo, Ontario

Masai I, Okazaki A, Hosoya T, Hotta Y (1993) Drosophila retinal degeneration A gene encodes an eye-specific diacylglycerol kinase with cysteine-rich zinc-finger motifs and ankyrin repeats. Proc Natl Acad Sci USA 90:11157–11161

Moritz A, Graan PNE De, Gispen WH, Wirtz KWA (1992) Phosphatidic acid is a specific activator of phosphatidylinositol-4-phosphate kinase. J Biol Chem 267:7207–7210

Nishizuka Y (1984) The role of protein kinase C in cell surface signal transduction and tumour promotion. Nature 308:693–698

Penotti FE (1991) Human pre-mRNA splicing signals. J Theor Biol 150:385–420

Sakane F, Kanoh H (1997) Diacylglycerol kinase. Int J Biochem Cell Biol 29:1139–1143

Seller MJ, Behnam JT, Lewis CM, Johnston RL, Burdon MA, Spalton DJ (1997) Linkage studies in dominant optic atrophy, Kjer type: possible evidence for heterogeneity. J Med Genet 34:967–972

Shapio M, Senapathy P (1987) RNA splice junction of different class of eukaryotes: sequence statistics and function implications in gene expression. Nucleic Acids Res 17:7155–7175

Stryer L (1991) Visual excitation and recovery. J Biol Chem 266:10711–10714

Tsai MH, Yu CL, Stacey DW (1990) A cytoplasmic protein inhibits the GTPase activity of H-Ras in a phospholipid-dependent manner. Science 250:982–985

Votruba M, Moore AT, Bhattacharya SS (1997) Genetic refinement of dominant optic atrophy (OPA1) locus to within a 2 cM interval of chromosome 3q. J Med Genet 34:117–121

Votruba M, Moore AT, Bhattacharya SS (1998) Demonstration of a founder effect and fine mapping of dominant optic atrophy locus on 3q28–qter by linkage disequilibrium method: a study of 38 British Isles pedigrees. Hum Genet 102:79–86

Anlage 4

Transcript Map of a 900-kb Genomic Region
in Xp22.1-p22.2:
Identification of 12 Novel Genes

Genomics 51: 59-67

GENOMICS 51, 59–67 (1998)
ARTICLE NO. GE985382

Transcript Map of a 900-kb Genomic Region in Xp22.1–p22.2: Identification of 12 Novel Genes

Regina Warneke-Wittstock,* Andreas Marquardt,* Andrea Gehrig,* Christian G. Sauer,* Manfred Gessler,† and Bernhard H. F. Weber*,[1]

*Institut für Humangenetik and †Physiologische Chemie I, Biozentrum, Universität Würzburg, 97074 Würzburg, Germany

Received February 25, 1998; accepted May 12, 1998

The Xp22.1–p22.2 interval is a focus of interest as a number of hereditary disease loci have been mapped to this region, including X-linked nonsyndromic sensorineural deafness (DFN6), X-linked juvenile retinoschisis (RS), and several X-linked mental retardation syndromes. In the course of cloning the RS gene we have assembled YAC and PAC contigs of the 900-kb candidate region delimited by DXS418 and DXS999. In this study, we now report the construction of a first transcript map of this chromosomal interval by combining exon trapping, EST mapping, and computational gene identification methods. Overall, this strategy has led to the assembly of at least 12 novel transcripts positioned within the DXS418–DXS999 region, one of these encoding a putative protein kinase motif with significant homology to the rat p58/GTA protein kinase domain and another a putative neuronal protein with strong homology to a *Drosophila* transcriptional repressor. © 1998 Academic Press

INTRODUCTION

The human Xp22.1–p22.2 region has been implicated in several hereditary disorders, such as X-linked juvenile retinoschisis (RS), X-linked liver glycogenosis (XLG1 and XLG2), pyruvate dehydrogenase (PDH) deficiency, keratosis follicularis spinulosa decalvans, X-linked hypophosphatemic rickets (HYP), nonsyndromic sensorineural deafness (DFN6), Nance–Horan syndrome, and a number of X-linked mental retardation syndromes like Coffin–Lowry syndrome (CLS), oral-facial-digital syndrome type 1, Snyder–Robinson syndrome, and several types of nonspecific X-linked mental retardation (Ferrero *et al.,* 1995; Lubs *et al.,* 1996; OMIM [http://www3.ncbi.nlm.nih.gov:80/htbin-post/Omim/getmap?chromosome=X]). To date, the causative genes for five of these disorders have been identified, namely, mutations in *RS1* (alias *XLRS1*) were shown to cause RS (Sauer *et al.,* 1997), the gene for the liver α-subunit of phosphorylase kinase (*PHKA2*) was associated with XLG1 and XLG2 (Hendrickx *et al.,* 1993, 1996), defects in the pyruvate dehydrogenase E1-α gene (*PDHA1*) were demonstrated to be responsible for PDH deficiency (Dahl *et al.,* 1990), mutations in the *PEX* (phosphate regulating gene with homologies to endopeptidases on the X chromosome) gene were associated with HYP (The HYP Consortium, 1995), and *RSK2* (ribosomal S6 kinase 2 gene) was shown to underlie CLS (Trivier *et al.,* 1996).

As part of our efforts to identify candidate genes for X-linked retinoschisis we generated a transcript map of the 900-kb candidate region between DXS418 and DXS999 in Xp22.1–p22.2. Our approach combined the methods of exon trapping, EST mapping, and computational gene identification. Over the past few years, exon trapping has become a method of choice for the isolation of novel genes, e.g., the Huntington disease gene (The HD Collaborative Research Group, 1993), the human homologue (*HES1*) of the zebrafish ES1 protein (Scott *et al.,* 1997), or the neural cell adhesion molecule gene, *NCAM2* (Paoloni-Giacobino *et al.,* 1997). In almost all of these studies, the plasmid vector pSPL3 (Church *et al.,* 1994) or one of its derivatives was used. However, in recent years the limited cloning capacity of this vector system has led to the development of new phage- (Nehls *et al.,* 1994) and, more recently, cosmid-based vectors (Datson *et al.,* 1996). In particular, the λGET vector utilized in the present study combines features of convenient plasmid subcloning with the high cloning efficiency of the λ phage vector and a cloning capacity that accommodates inserts from 6 to 19 kb of genomic DNA (Nehls *et al.,* 1994).

Almost 800 kb of genomic sequences of the DXS418–DXS999 interval were available through the Sanger Centre, Cambridge (http://www.sanger.ac.uk/). This facilitated comprehensive dbEST and nonredundant

Sequence data for this article have been deposited with the EMBL/GenBank Data Libraries under Accession Nos. AF045731–AF045738 and AF046127–AF046156.

[1] To whom correspondence should be addressed at Institut für Humangenetik, Biozentrum, Am Hubland, D-97074 Würzburg, Germany. Telephone: (+)49-931-888-4062. Fax: (+)49-931-888-4069. E-mail: BWEB@BIOZENTRUM.uni-wuerzburg.de.

0888-7543/98 $25.00

GenBank/protein database searches as well as GRAIL genomic exon prediction analyses. This has allowed us to assemble 16 independent EST contigs. In addition, sequence alignments identified three cDNA fragments of which two represent known genes within the interval, namely *RS1* (Sauer *et al.,* 1997) and *PPEF* (Montini *et al.,* 1997). Finally, computational GRAIL2 exon predictions yielded 71 exons with excellent or good potential of being true coding sequences.

Overall, our approach has identified at least 12 novel transcripts within the DXS418–DXS999 region, thus increasing the minimal number of genes in this chromosomal interval to 14. Two of the novel transcripts show significant homology to known amino acid sequences, namely to the rat galactosyltransferase p58/GTA protein kinase domain and to a *Drosophila* transcriptional repressor protein. One transcript represents a partially characterized gene expressed in macrophages. Further analyses will be needed to determine whether these transcripts may be involved in one of the numerous Xp22-linked disorders.

MATERIALS AND METHODS

YAC and PAC contigs. YAC and PAC contigs of the DXS418–DXS999 interval were assembled. Briefly, YAC clones positive for DXS999 were isolated from the CEPH megaYAC library (UK HGMP Resource Centre, Hinxton) (Fig. 1A). PAC clones were isolated by repeated screenings of P1-derived artificial chromosome libraries RPCI 1–5 (kindly provided by P. de Jong, RPCI, Buffalo, NY) with various STSs or end-clone probes derived from YAC clone 931E8. Published PAC clones mapped to the region (http://www.sanger.ac.uk) were included in the contig assembly (Fig. 1B).

Exon trapping. PAC DNA was isolated using standard alkaline lysis techniques. The DNA was partially digested with *Sau*3AI and agarose gel size selected for fragments ranging from 16 to 20 kb. The λGET vector (kindly provided by T. Boehm, DKFZ, Heidelberg) was prepared by *Xho*I and *Bam*HI digestion. Subsequently, the vector arms were purified as described (Nehls *et al.,* 1994). The genomic *Sau*3AI fragments were ligated to the vector arms, packaged using the Gigapack Gold packaging kit (Stratagene), and plated on *Escherichia coli* Y1090r$^-$. An aliquot of the phage library of each PAC containing approximately 1000 phage clones (99.9% probability of DNA sequence representation; Clarke and Carbon, 1976) was then converted into a plasmid library by infecting *E. coli* strain BNN132 (Nehls *et al.,* 1994). Plasmid DNA of each library was isolated from approximately 5000 clones pooled from LB plates using Qiagen tip 100 columns according to the manufacturer's recommendations (Qiagen).

Subconfluent COS cells were transfected with approximately 5 μg of plasmid library DNA by electroporation at 250 V and 960 μF. RNA was isolated after 48 h and reverse transcribed using primer extr-RT (5′-GAT CCA CGA TGC-3′). Subsequently, RT-PCR was performed with vector-specific exon primers extr1a (5′-GAG CGT GGA TTC TTC TAC ACA CCC-3′) and extr1b (5′-GCC GGG CCA CCT CCA GTG CC-3′). The products were size selected on agarose gels to exclude the vector-only splice product from further analyses. Using primers extr2a (5′-GCG AAG TGG AGG AGC CAC AAG-3′) and extr2b (5′-CAC CCA GCT CCA GTT GTG CCA-3′) a nested PCR was performed and products were cloned into the pCRII vector (Invitrogen). Inserts were isolated by PCR with primers M13-5f (5′-CGC CAG GGT TTT CCC AGT CAC GAC-3′) and M13-6r (5′-AGC GGA TAA CAA TTT CAC ACA GGA-3′) and nonredundant PCR products were directly sequenced using the Thermo Sequenase radiolabeled terminator cycle sequencing kit (Amersham).

Genomic mapping of trapped sequences. To confirm their genomic origin the trapped exons either were hybridized to PAC DNA dot blots using the ECL nonradioactive direct nucleic acid labeling and detection kit (Amersham) or were aligned to genomic PAC DNA sequences using the BLASTN search function available at the Sanger Centre, Cambridge (http://www.sanger.ac.uk/HGP/blast_server.shtml).

Database analysis. To search for similarities with known DNA or protein sequences the BLAST program of the GCG9 package was used (Genetics Computer Group, 1996). Exon predictions were performed using XGRAIL1.3 (Xu *et al.,* 1994). Protein motif searches were carried out with ProDom database release 34.1 (http://protein.toulouse.inra.fr/prodom/prodom.html).

Northern blot analysis. Total RNA was isolated from human lung, cerebellum, cortex, heart, retinal pigment epithelium (RPE), retina, and peripheral blood lymphocytes using the RNA-Clean-LS system (Angewandte Gentechnologie Systeme, AGS). In each lane 12 μg of total RNA was electrophoretically separated in a 1.2% agarose gel in the presence of formaldehyde and blotted onto a nylon membrane. The multiple tissue Northern blot purchased from Clontech Laboratories (Palo Alto, CA) was prepared with poly(A)$^+$ RNA isolated from human heart, brain, placenta, lung, liver, skeletal muscle, kidney, and pancreas. Hybridizations were carried out in 0.5 mM sodium phosphate buffer, pH 7.2; 7% SDS, 1 mM EDTA at 65°C (Church and Gilbert, 1984).

RESULTS

Analysis of Exon-Trapped cDNA Clones

Exon trapping was performed with genomic DNA from PAC clones dJ272E8, dJ410B11, dJ863K19, dJ958B3, dJ234C1, and dJ7D16 (Fig. 1B). For each PAC 40 to 60 clones containing exon-trapping products from cDNAs of transfected COS cells were analyzed for insert content and size. Redundant cDNA inserts were recognized by Southern blot hybridizations of selected clones to PCR-amplified exon-trapped products and excluded from further analyses. The remaining inserts were sequenced.

The genomic origin of trapped exons was verified by hybridization to PAC contig DNAs or alignment to available genomic PAC sequences. After removal of six repeat-containing trapping products, this strategy led to the isolation of 6 to 12 exons per PAC clone tested, resulting in a total of 51 trapped exons (Table 1). Of these, 27 were derived from splice products of 2 or more adjacent exons. In addition, 9 of these 27 exons were independently trapped as single exons. Moreover, in five cases identical exons were trapped from independent but overlapping PAC clones (e.g., dJ234C1 and dJ7D16). Taken together, the exon-trapping experiments yielded a total of 46 unique exons of which 30 were found to have an open reading frame (Table 1). Considering the size of the contig interval extending from dJ272E8 to dJ7D16 to be approximately 600 kb, we identified 1 trapped exon per 13 kb of genomic DNA (Fig. 1C; Table 1).

Computational Analysis of Trapped Exons

Alignment of trapped exons to the originating PAC sequences revealed their genomic context, including

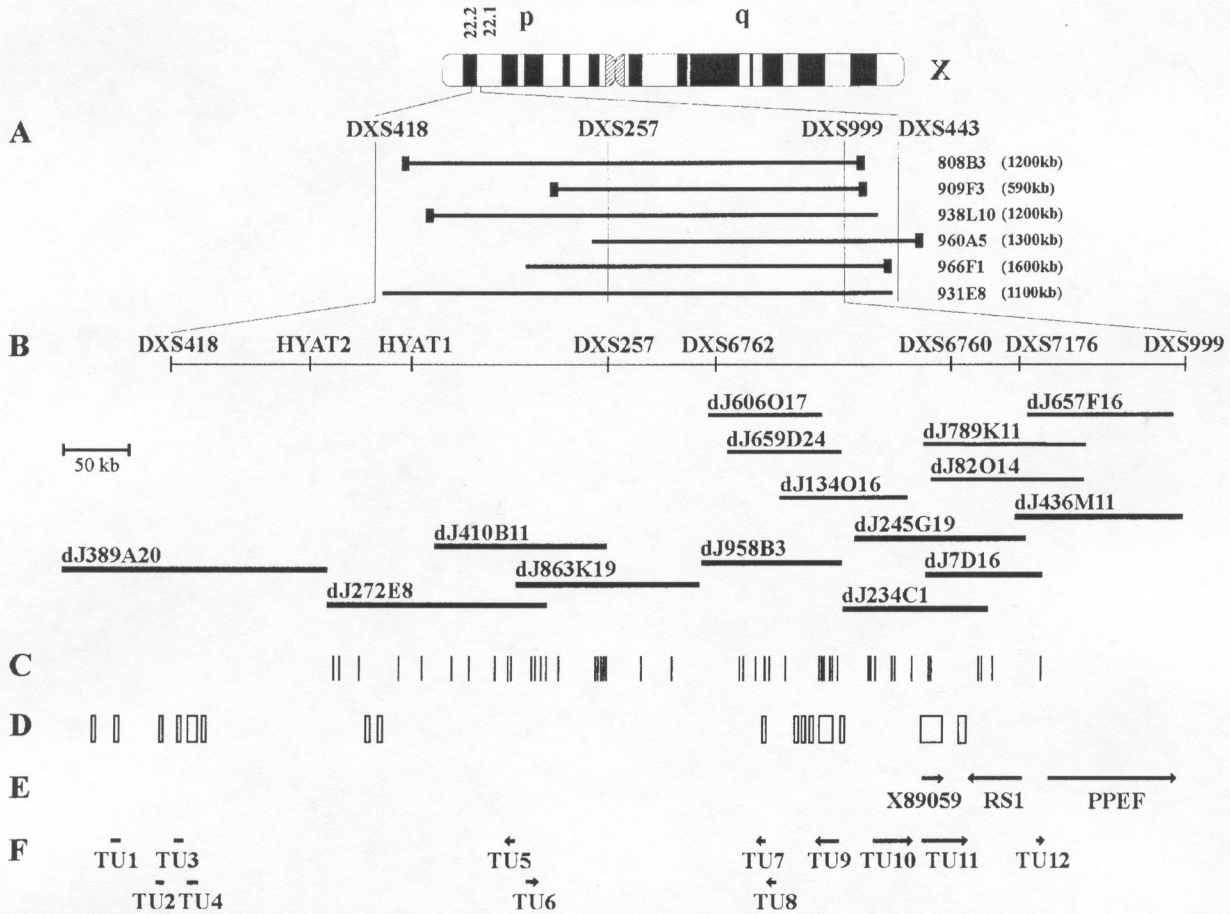

FIG. 1. Detailed physical map of the DXS418–DXS999 interval in Xp22.1–p22.2. (**A**) YAC clones identified with DXS999. The filled boxes at the end of the YAC clones indicate the presence of chimeric end fragments. (**B**) PAC contig of the region. Thick bars denote PACs analyzed in the present study. *Note.* The order and position of PAC clones dJ389A20, dJ272E8, dJ410B11, and dJ863K19 were taken from http://www.sanger.ac.uk/. Note that there may be two small gaps (**C**) Locations of 46 unique trapped exons. (**D**) Locations of 16 EST contigs assembled from BLAST searches using all available genomic PAC sequences. (**E**) Locations of 3 genes, including a serine–threonine phosphatase (PPEF), the gene associated with X-linked juvenile retinoschisis (RS1), and a macrophage transcript (X89059) coding for a protein of unknown function. (**F**) Locations of putative transcription units. If known, the orientation of transcription in (E) and (F) is indicated by arrows.

acceptor and donor splice junctions. The discrimination energy score of the identified splice acceptor and donor sequences was calculated, indicating the strength of conformity of our assigned splice junctions with previously published sequences (Berg and von Hippel, 1988; Penotti, 1991). The calculations for the 30 unique exons with open reading frames resulted in a mean value of 3.7 for the donor splice sites versus a mean value of 3.2 ± 1.8 for published sequences. Similarly, the mean discrimination energy score of the acceptor splice was 5.1 for the trapped exons compared to the empiric mean value of 5.1 ± 2.4. The mean values for acceptor and donor splice sites of the 16 trapped exons without ORFs did not significantly differ from those with an ORF. To verify the exon potential of the trapped exons further GRAIL2 analyses were performed with approximately 250 bp of flanking genomic DNA on either side of the trapped sequences. Excellent or good GRAIL2 exon predictions coincided with 16 of 46 trapped exons (Table 1).

Searches with the 46 unique trapped exons in the dbEST database identified three significant EST matches, namely AA227320, W07749, and W07775 (Table 1). Moreover, BLASTP protein database searches revealed two significant matches including a transcriptional repressor protein of *Drosophila melanogaster* (U49793) and the protein kinase p56 KKIAMRE (U35146) (see below).

Identification of EST and cDNA Clones from Genomic Sequence

At the time of analysis sequencing of PAC clones dJ389A20 (200 kb), dJ272E8 (160 kb), dJ410B11 (125 kb), dJ863K19 (140 kb), dJ958B3 (115 kb), dJ245G19 (130 kb), and dJ436M11 (130 kb) covering the 900-kb interval between DXS418 and DXS999 was approximately 85% completed at the Sanger Centre (Cambridge, UK) (Fig. 1B). From partially sequenced PAC clones (e.g., dJ272E8) only assembled sequences of more than 5 kb in size were included in the present study. dbEST and DNA database searches were per-

TABLE 1

Exons Trapped from the DXS418–DXS999 Region

PAC clone	Size[a] (kb)	Total No. of trapped exons	Trapped exons with ORF	Trapped exons with overlapping GRAIL exon prediction	Trapped exons detecting ESTs/ Acc.No. (TU No.)	Trapped exons detecting transcripts on Northern blots (TU No.)	Transcript size/tissue
dJ272E8	160	9	5	1	—	—	—
dJ410B11	125	11	5	2	—	410-34 (TU5)	1.2 kb/retina
dJ863K19	140	5	3	—	—	863-2/1 and 2/2 (TU6)	2.0 kb/liver
dJ958B3	115	12	9	5	5/AA227320 (TU9)/ W07749 (TU7)	958-14 (TU8)	1.4 kb/lung, cerebellum, retina, RPE, cortex
dJ234C1	110	8	6	5	2/W07775 (TU11)	—	—
dJ7D16	80	6	6	5	2/W07775 (TU11)	7D16-1 (TU12)	1.9 kb/retina, RPE
In total	740	51	34	18	9	5	4
Unique trapped exons	600[b]	46[c] (1/13 kb)	30 (1/20 kb)	16	7	5	

Note. RPE, retinal pigment epithelium.

[a] PAC sizes are taken from Walpole *et al.,* 1997.

[b] Nonoverlapping total size.

[c] Sequences have been deposited in GenBank under Accession Nos. AF045731–AF045738 and AF046127–AF046156.

formed using the GCG9 Wisconsin software package with stringency set to 90% sequence identity or higher at a window size of at least 50 bp. Using these parameters, a total of 163 ESTs and 9 cDNA clones were identified. Further computational alignments were performed to assemble the various sequences into 16 ESTs (Fig. 1D, Table 2) and 3 cDNA contigs (Table 2). Two cDNA contigs correspond to the known genes *RS1* and *PPEF*. Thus far, no functional information is available on cDNA clone X89059 (Krause *et al.,* 1996) (Fig. 1E, Table 2).

Northern Blot Analysis

To determine the expression profiles of trapped exons and EST clones, Northern blot analyses were performed. Five of the 46 unique trapped exons revealed hybridization signals (Fig. 2, Table 1). Of the 16 EST contigs mapped to the interval 11 were tested on Northern blots. Of these, 6 representative EST clones detected hybridization signals (Fig. 2, Table 2). Nonoverlapping EST clones AA376231 and W07775 both detected a single 7.5-kb transcript in retinal tissue, suggesting that they belong to a single transcription unit, designated TU11 (Table 2).

Assembly of Putative Transcription Units

The data obtained from exon trapping, computational analyses, and Northern blot hybridizations were combined to assemble individual putative transcription units (TUs). To meet the definition of a putative TU at least two of three criteria have to be fulfilled: (1) the presence of at least one trapped exon flanked by consensus splice site sequences in its genomic context, (2) significant sequence identity of genomic DNA with dbEST and/or protein database sequences, and (3) the presence of hybridization signals in Northern blot analyses. In addition, whenever possible the orientation of transcription was deduced from the exon/intron structure, thus facilitating in some instances the identification of two neighboring transcription units as distinct transcripts.

Six EST contigs were assigned to PAC clone dJ389A20 (Table 2). Northern blot hybridization of clone AA128046 detected a transcript of 2.2 kb in size in heart, RPE, and retina (Fig. 2, Table 2) representing TU1. TU2 was assigned to clone AA377701, which hybridized to a 1.7-kb transcript in retina and lymphocytes (Fig. 2, Table 2). Clone W69459 detected a 2.8-kb transcript in retina and revealed a minor signal in heart (TU3) (Fig. 2, Table 2). Finally, clone N68481 revealed an abundant transcript of approximately 1.0 kb in all tissues tested (TU4) (Fig. 2, Table 2).

A single 111-bp exon, 410-34, trapped from dJ410B11 detected a transcript of 1.2 kb in retinal tissue (TU5) (Fig. 2, Table 1). This exon was independently trapped from dJ272E8 (272-46B/2) together with 272-46B/1 (33 bp) in a single splice product which, on the genomic level, was interrupted by 340 bp of intervening sequences (data not shown). The orientation of donor and acceptor splice sites suggests an orientation of transcription of TU5 from centromere to telomere (Fig. 1). Northern blot analysis of exon-trapping product 863-2 revealed a 2.0-kb transcript in liver (TU6) (Fig. 2, Table 1). Clone 863-2 consists of two spliced exons, 863-2/1 and 863-2/2, which were also trapped independently as single exons in PAC clones dJ410B11 and dJ863K19. The orientation of transcription of TU6 was determined to be from telomere to centromere.

Three putative transcription units were assigned to PAC dJ958B3 (Fig. 1F). Exon-trapping clone 958-31 (133 bp) identified four EST sequences including W07749, AA435668, AA523922, and AA723822 and consequently

TABLE 2

EST and cDNA Clones Localized to the DXS418–DXS999 Region

PAC clone	Acc. Nos. of ESTs or cDNAs	Redundance of ESTs or cDNAs[a]	Expression profile in cDNA libraries or corresponding gene	Transcripts on Northern blots/ tissue[b] (TU No.)
dJ389A20	R74589	1	Placenta	—
	AA128046	25	Pregnant uterus, fetal heart, fetal brain, gall bladder	2.2 kb/heart, RPE, retina (TU1)
	AA377701	20	Synovial membrane, pregnant uterus, placenta, multiple sclerosis lesions	1.7 kb/retina, lymphocytes (TU2)
	W69459	7	Fetal heart, fetal cochlea, ovary	2.8 kb/retina, heart (TU3)
	N68481	5	Fetal liver/spleen, fetal lung, prostate	1.0 kb/heart, RPE, retina, lymphocytes (TU4)
	R13849	4	Infant brain	ntd
dJ272E8	D82460	24	Pancreatic islets, (fetal) heart, brain, mouse brain and plants	nd
	T57848	—	Lung	nd
dJ410B11	—	—	—	—
dJ863K19	—	—	—	—
dJ958B3	N74417	2	Fetal liver/spleen	ntd
	N83809	—	Fetal heart	ntd
	AA420669	20	Prostate, thyroid, fibroblasts, fetal lung, colon	nd
	AA227320	—	Neuroepithelial cells	nd
	H78265	—	Fetal liver/spleen	ntd
	W07749	1	Fetal lung, neuroepithelial cells	nd
dJ245G19	W07775	8	Fetal lung, testis, prostate, fetal liver/spleen	7.5 kb/retina (TU11)
	AA376231	30	Fibroblasts, infant brain, fetal heart, colon, placenta, retina; mixed: melanocytes, pregnant uterus, fetal heart	7.5 kb/retina (TU11)
	AF014459	5	RS1 (alias XLRS1)	3.1 and 1.1 kb/retina[c]
	X89059	—	Macrophages	nd
dJ436M11	X97867	1	PPEF	2.7 and 4.3 kb/brain[d]
Total	16/3	163/9		

Note. Expression information was retrieved from GenBank entries. nd, not determined; ntd, no transcript detectable on Northern blot.

[a] Contigs assembled from overlapping EST or cDNA clones are represented by one clone revealing highest homology; the number of additional clones in the contig is indicated.

[b] Northern blots contained total RNA from heart, retinal pigment epithelium (RPE), retina, and lymphocytes.

[c] Taken from Sauer *et al.,* 1997.

[d] Taken from Montini *et al.,* 1997.

was designated TU7. Furthermore, trapped exon 958-14 hybridized to a 1.4-kb transcript in lung, cerebellum, retina, RPE, and cortex (TU8) (Fig. 2, Table 1). The orientation of transcription of both transcripts, TU7 and TU8, is from centromere to telomere (Fig. 1F). Finally, TU9 is represented by two trapped clones representing splice products of two (958-8/1, -8/2) and three (958-3/1, -3/2, and -3/3) exons, respectively. The exons are 46, 69, 71, 235, and 89 bp in size, spanning a genomic distance of 13.8 kb in PAC clone dJ958B3. dbEST database alignments identified a single neuroepithelial cell line EST, AA227320, verifying the order of the trapped exons (Tables 1 and 2). The conceptual translation product of AA227320 revealed 58% sequence identity to a transcriptional repressor protein of *D. melanogaster* (U49793) and 40% identity to a *Caenorhabditis elegans* protein (Z71266). No transcript was detected on Northern blot analysis.

TU10 consists of three exons (234-1 and 234-14/1 and -14/2) trapped from PAC clone dJ234C1. The conceptual translation product of 234-14/1 and -14/2 revealed 49% sequence identity to the epidermal growth factor-stimulated protein kinase p56 KKIAMRE (U35146) and 39% identity to two serine–threonine protein kinases (S23383 and S22745) in their respective C-termini. In contrast, the 234-1 translation product (15 amino acids) shows homology to the N-terminus of S23383 and S22745, respectively. ProDom searches yielded significant homology to protein domain 17240 represented by a galactosyltransferase-associated protein kinase p58/GTA (Fig. 3).

TU11 is defined by two trapped exons originating from a single splice product that were independently isolated from PAC clones dJ234C1 and dJ7D16 (234-9/1, -9/2 and 7D16-2/1, -2/2) (Table 1). Database searches revealed a significant match to macrophage cDNA clone X89059. In addition, three significant EST matches were found including W07775, AA398911, and

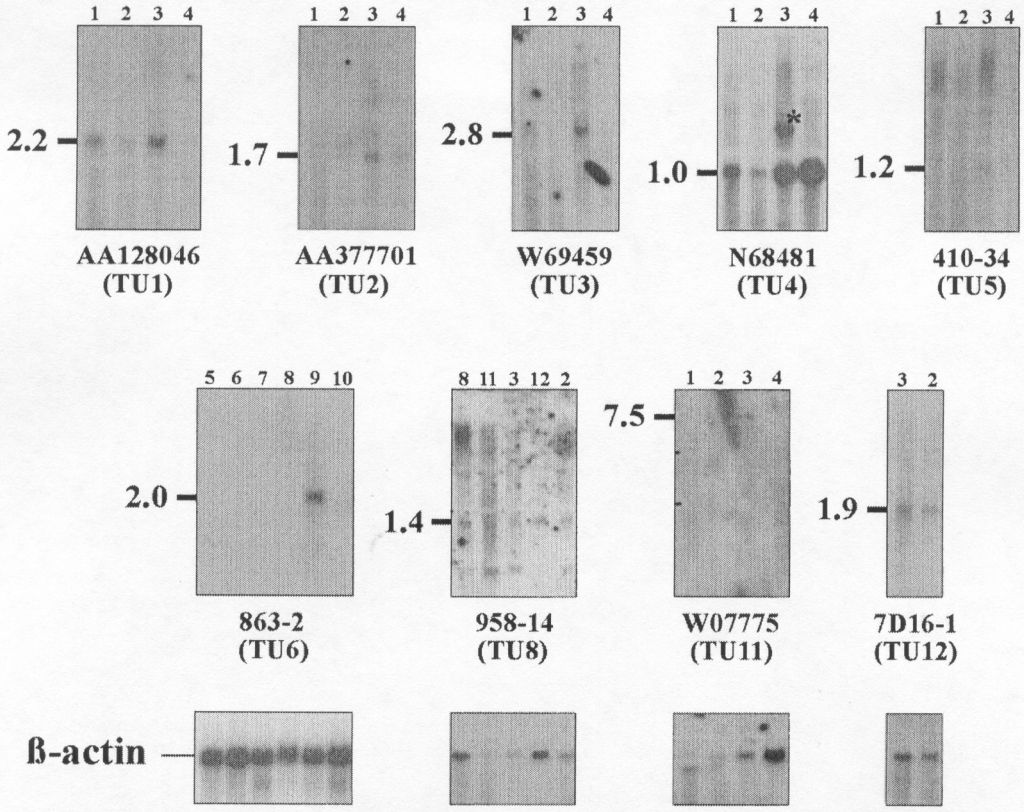

FIG. 2. Examples of Northern blot hybridizations of selected EST clones and trapped exons. Total RNA from (**1**) heart, (**2**) retinal pigment epithelium, (**3**) retina, (**4**) lymphocytes, (**8**) lung, (**11**) cerebellum, and (**12**) cortex as well as poly(A)$^+$ RNA from (**5**) heart, (**6**) brain, (**7**) placenta, (**8**) lung, (**9**) liver, and (**10**) skeletal muscle was used for Northern blot analysis. The poly(A)$^+$ RNA blot was purchased from Clontech, Inc. (lanes 5 to 10). To test for equal loading and RNA integrity the individual Northern blots were hybridized with a human β-actin probe. TU, transcription unit. The asterisk at TU4 indicates a 3.1-kb leftover signal in retina from a previous hybridization with a 214-bp RS1 cDNA probe (Sauer *et al.*, 1997).

N80713. On the genomic level clone X89059 is organized in five exons with the second and third of these corresponding to trapped exons 234-9/1 and -9/2. On Northern blot hybridizations, the trapped exons did not reveal a signal. In contrast, EST clone W07775 hybridized to a 7.5-kb transcript in retina (Fig. 2, Table 2). Similarly, EST clone AA376231, residing at a genomic distance of 12 kb from W07775, identified a transcript of identical size in retina (Table 2), suggesting that both EST clones should be part of a single transcript. Finally, TU12 represents a 1.9-kb transcript in retina and RPE as determined by Northern blot analysis of trapped exon 7D16-1 (Fig. 2, Table 1).

DISCUSSION

Combining phage-based exon trapping and in-depth computational analyses, we have established a transcript map of a 900-kb region in Xp22.1–p22.2. Overall, this has added at least 12 novel putative transcripts to

```
P46892     256 YSTACDMWSVGCIFGELLTQKPLFPGKSDIDQINKIFKDIGTPSEKIWPG
P21127     256 YSTAVDMWSVGCIFGELLTQKPLFPGKSEIDQINKVFKDLGTPSEKIWPG
Q09437     537 YSTPVDMWSVGCIMAEFILLKPLFPGRGELEQIKKIFMEMGTPTESIWPG
Q92241     187 YCTLIDIWSCGCILAEMIMGKPLFPGSNDEEQLKLIFDTMGTPVEQTWPQ
234_14p      3 YGKSVDMWSVGCILGELSDGQPLFPGESEIDQLFTIQKVLGPLPSEQMKL

P46892     306 YSELPAVKKMTFSELPYN.NLRKRF..GALLSDQGFDLM   341
P21127     306 YSELPAVKKMTFSEHPYN.NLRKRF..GALLSEQGFDLM   341
Q09437     587 VTELDGWKALTFEKYPYN.QLRKRFLAGRLLNDTGFKLL   624
Q92241     236 VTQLAKYNPLLPPHMPRDLKQLLQNNTEEVLDDNVVDLL   274
234_14p     53 FYSNPRFHGLRFPAVNHPQSLERRYLG..ILNSVLLDLM    89
```

FIG. 3. Alignment of translation product of exon-trapping clone 234C1-14 to serine–threonine protein kinases from yeast (Q92241), *C. elegans* (Q09437), rat (P46892), and human (P21127), demonstrating the presence of a conserved domain in 234-14. Alignment was done with the PileUp program of the GCG9 Wisconsin package. Black and gray shadings indicate sequence identity and sequence similarity, respectively.

the two known genes of this region that include a serine–threonine phosphatase, *PPEF* (Montini *et al.,* 1997), and *RS1* associated with X-linked juvenile retinoschisis (Sauer *et al.,* 1997).

Exon trapping using the λGET phage system (Nehls *et al.,* 1994) appears to have several advantages over conventional plasmid vector systems such as pSPL3 (Church *et al.,* 1994). Since the λGET vector has a cloning capacity for genomic inserts of up to 19 kb, large genomic regions of several hundred kilobases of DNA can readily be analyzed. In addition, large insert fragments provide a genomic context that is more favorable for an accurate splicing procedure of exonic sequences (Datson *et al.,* 1996). In support of the latter notion is our finding that shows 53% of trapped exons being isolated from splice products of two or three separate exons. In all cases in which a comparison to EST or cDNA sequences was possible the correct splice event in our phage exon trapping system could be verified. Finally, the percentage of false-positive trapping products appears to be relatively low in the λGET system. These include vector-only derived and repeat-containing sequences, which amounted to approximately 4 and 10%, respectively, in our experiments. Vector-only-derived false-positive trapping products due to cryptic splice sites have been a major problem in many plasmid-based trapping systems and have only recently been reduced to background level by construction of improved plasmid vectors (Burn *et al.,* 1995). Independent studies report similar levels of repeat sequences (Chen *et al.,* 1996), whereas other methods for isolation of transcribed sequences, e.g., direct cDNA selection, are known to enrich for repetitive sequences (Heiss *et al.,* 1996).

A well-known disadvantage of the exon-trapping method is the recurrent difficulty in verifying trapped exons as representing truly expressed sequences. In general, trapped exons appear to rarely detect database homologies. In our experiments we found significant matches in only 22% of trapped exons compared to, e.g., 32% in a study conducted by Chen *et al.* (1996). In addition, trapped exons may be part of a rare transcript or may be too small to be used successfully in Northern blot hybridization experiments (e.g., Kalachikov *et al.,* 1997). For example, in our experiments the trapped exon clone 234-9, which is 200 bp in size (TU 11), repeatedly did not reveal a hybridization signal on Northern blots. In contrast, overlapping EST clone W07775 (750 bp) readily hybridized to a 7.5-kb transcript in retinal tissue (Table 2). Furthermore, the lack of an open reading frame within a trapped exon per se is not sufficient to reject it as a potential exon. There are reports suggesting that even up to 30% of exons trapped from a genuine cDNA represent noncoding portions of the gene (Ruddy *et al.,* 1997). In our series of trapped exons we identified 16 of 46 (35%) unique exons without an open reading frame. Most of those have not been characterized further, but still may represent true transcripts of the DXS418–DXS999 interval.

In the present study, we analyzed a total of 11 assembled EST contigs by Northern blot hybridization of representative EST clones. Transcripts were identified for 6 of the 11 EST clones tested. It is of note that all clones revealing a positive hybridization signal belonged to EST contigs assembled from up to 30 independent ESTs, while the Northern blot-negative ESTs either were unique clones or were represented only a few times in the dbEST database. Although redundancy of EST clones in sequence databases may reflect the level of expression in a given tissue, rare ESTs need further confirmation to be regarded as truly expressed sequences, in particular since up to 30% of dbEST entries may represent noncoding genomic DNA (Ruddy *et al.,* 1997). As demonstrated for AA227320 (TU 9), a good indication of an EST sequence being genuine is the identification of exon/intron boundaries in its genomic context. GRAIL exon prediction may provide additional information to confirm the coding potential of exonic sequences. In our study, of 17 trapped exons assembled into transcription units, 10 (59%) were also predicted by GRAIL. Other reports have found a similar sensitivity of the GRAIL2 predictions ranging from 50 (Elkahloun *et al.,* 1997) to 70% (Claverie, 1997).

In contrast to the high density of putative transcription units in the 5′ and 3′ regions of the DXS418–DXS999 interval, an obvious paucity of transcripts between TU4 and TU5 as well as between TU6 and TU7 becomes evident from our analysis but may not reflect the true gene density in this region. This possible discrepancy may be due to several factors. First, for some of the PAC clones only incomplete genomic sequences were available. Thus, dbEST database analyses were not feasible for these clones, e.g., dJ272E8. Second, some genes may be expressed in very low copy numbers per cell and therefore may not be represented in current dbEST database releases nor be detectable in Northern blot hybridizations. Similarly, some transcripts may be tissue-specific for human tissues not included in our Northern blot analyses. It is of note that unlike EST clones trapped exons were identified evenly across the PAC contig analyzed. In addition, several neighboring trapped exons not yet integrated into an individual TU could be grouped with respect to their orientation of acceptor and donor splice site sequences, suggesting that they may be part of a common transcript. In fact, some of these exons were indeed identified in a single trapping product. Therefore, the identified trapped exons may provide a valuable resource for cloning additional and, in particular, rare or tissue-specific genes of the region. Due to the nature of such transcripts this may require alternative approaches such as exon connection or 5′ or 3′ RACE experiments.

Of the 12 putative transcription units assembled in this study, TU9 and TU10 may be of special interest with

respect to two disease loci mapped to this region. First, one form of nonsyndromic sensorineural deafness was reported in a five-generation Spanish family, and the disease locus, DFN6, was subsequently mapped to Xp22 flanked by markers at DXS7108 and DXS7105 (del Castillo, 1996). Based on high-resolution genetic maps (http://www.marshmed.org/genetics/), the 900-kb DXS418–DXS999 interval is entirely positioned within the DFN6 locus. More recently, the DFN6 gene has been suggested to be involved in inner ear defects that are found in some patients with HYP (Meisler, 1997). In these patients the inner ear defects are characterized by neuroepithelial abnormalities, namely degeneration of hair cells in the vestibular apparatus and cochlea. Interestingly, in another type of nonsyndromic deafness, DFN3, with stapes fixation and perilymphatic gusher upon stapes surgery, the disease gene, POU3F4, encodes a transcriptional regulator (Douville *et al.,* 1994). Our computational analysis has demonstrated that EST clone AA227320 (TU9), originating from a neuroepithelial cell cDNA library, likewise exhibits strong homology to a transcriptional repressor protein. Taken together, these considerations render TU9 a strong candidate for DFN6.

Second, Coffin–Lowry syndrome, an X-linked mental retardation syndrome, has been reported to be caused by mutations in RSK2, a growth-factor-regulated serine–threonine kinase (Trivier *et al.,* 1996). We have shown that TU10 exhibits strong homologies to serine–threonine protein kinases and shares a conserved domain with rat galactosyltransferase-associated p58/GTA protein kinase (Kerr *et al.,* 1994). Thus, TU10 appears to represent an excellent candidate for one of the mental retardation genes mapped to the distal short arm of the X chromosome (Lubs *et al.,* 1996).

In conclusion, our study provides the first gene map of the DXS418–DXS999 interval in Xp22.1–p22.2. Using stringent criteria we have identified at least 12 novel transcripts, most of which have been further verified by Northern blot hybridization. Together with the two known genes of the region, this increases the gene density in the 900-kb region to one gene per 64 kb of DNA. Further studies are required to obtain additional insight into the structure and possible metabolic functions of these genes and their gene products. However, preliminary analyses have already identified 2 transcripts, namely TU9 and TU10, that may represent excellent candidates for one form of X-linked hearing impairment as well as for some form of X-linked mental retardation. This study adds novel information to the overall efforts to construct a high-density gene map of the X chromosome.

ACKNOWLEDGMENTS

The authors thank T. Boehm (DKFZ, Heidelberg) for providing the λGET vector system and P. Cooper (Roswell Park Cancer Institute, Buffalo, NY) for PAC clones dJ436M11, dJ657F16, 789K11, dJ606O17, and dJ659D24. This work was supported by the Deutsche Forschungsgemeinschaft We1259/5-2 and the Retinitis Pigmentosa Foundation Germany.

REFERENCES

Berg, O. G., and von Hippel, P. H. (1988). Selection of DNA binding sites by regulatory proteins. *Trends Biochem. Sci.* **13:** 207–211.

Burn, T. C., Connors, T. D., Klinger, K. W., and Landes, G. M. (1995). Increased exon-trapping efficiency through modifications to the pSPL3 splicing vector. *Gene* **161:** 183–187.

Chen, H., Chrast, R., Rossier, C., Morris, M. A., Lalioti, M. D., and Antonarakis, S. E. (1996). Cloning of 559 potential exons of genes of human chromosome 21 by exon trapping. *Genome Res.* **6:** 747–760.

Church, C. M., and Gilbert, W. (1984). Genomic sequencing. *Proc. Natl. Acad. Sci. USA* **81:** 1991–1995.

Church, D. M., Stotler, C. J., Rutter, J. L., Murrell, J. R., Trofatter, J. A., and Buckler, A. J. (1994). Isolation of genes from complex sources of mammalian genomic DNA using exon amplification. *Nature Genet.* **6:** 98–105.

Clarke, L., and Carbon, J. (1976). A colony bank containing synthetic Col El hybrid plasmids representative of the entire *E. coli* genome. *Cell* **9:** 91–99.

Claverie, J.-M. (1997). Computational methods for the identification of genes in vertebrate genomic sequences. *Hum. Mol. Genet.* **6:** 1735–1744.

Dahl. H.-H. M., Maragos, C., Brown, R. M., Hansen, L. L., and Brown, G. K. (1990). Pyruvate dehydrogenase deficiency caused by deletion of a 7-bp repeat sequence in the E1-alpha gene. *Am. J. Hum. Genet.* **47:** 286–293.

Datson, N. A., Van de Vosse, E., Dauwerse, H. G., Bout, M., Van Ommen, G.-J. B., and Den Dunnen, J. T. (1996). Scanning for genes in large genomic regions: Cosmid-based exon trapping of multiple exons in a single product. *Nucleic Acids Res.* **24:** 1105–1111.

Del Castillo, I., Villamar, M., Sarduy, M., Romero, L., Herraiz, C., Hernandez, F. J., Rodriguez, M., Borras, I., Montero, A., Bellon, J., Cruz Tapia, M., and Moreno, F. (1996). A novel locus for nonsyndromic sensorineural deafness (DFN6) maps to chromosome Xp22. *Hum. Mol. Genet.* **5:** 1383–1387.

Douville, P. J., Atanasoski, S., Tobler, A., Fontana, A., and Schwab, M. E. (1994). The brain-specific POU-box gene Brn4 is a sex-linked transcription factor located on the human and mouse X chromosomes. *Mamm. Genome* **5:** 180–182.

Elkahloun, A. G., Krizman, D. B., Wang, Z., Hofmann, T. A., Roe, B., and Meltzer, P. S. (1997). Transcript mapping in a 46-kb sequenced region at the core of 12q13.3 amplification in human cancers. *Genomics* **42:** 295–301.

Ferrero, G. B., Franco, B., Roth, E. J., Firulli, B. A., Borsani, G., Delmas-Mata, J., Weissenbach, J., *et al.* (1995). An integrated physical and genetic map of a 35 Mb region on chromosome Xp22.3–Xp21.3. *Hum. Mol. Genet.* **4:** 1821–1827.

Genetics Computer Group (1996). "Program Manual for Wisconsin Package," Version 9, Madison, WI.

Heiss, N. S., Rogner, U. C., Kioschis, P., Korn, B., and Poustka, A. (1996). Transcriptional mapping in a 700-kb region around the DXS52 locus in Xq28: Isolation of six novel transcripts and a novel ATPase isoform (hPMCA5). *Genome Res.* **6:** 478–491.

Hendrickx, J., Coucke, P., Bossuyt, P., Wauters, J., Raeymaekers, P., Marchau, F., Smit, G. P. A., *et al.* (1993) X-linked liver glycogenosis: Localization and isolation of a candidate gene. *Hum. Mol. Genet.* **2:** 583–589.

Hendrickx, J., Dams, E., Coucke, P., Lee, P., Fernandes, J., and Willems, P. J. (1996). X-linked liver glycogenosis type II (XLG II) is caused by mutations in PHKA2 the gene encoding the liver alpha subunit of phosphorylase kinase. *Hum. Mol. Genet.* **5:** 649–652.

The Huntington's Disease Collaborative Research Group (1993). A novel gene containing a trinucleotide repeat that is expanded and unstable on Huntington's disease chromosomes. *Cell* **72:** 971–983.

The HYP Consortium (1995). A gene (PEX) with homologies to endopeptidases is mutated in patients with X-linked hypophosphatemic rickets. *Nat. Genet.* **11:** 130–136.

Kalachikov, S., Migliazza, A., Cayanis, E., Fracchiolla, N. S., Bonaldo, M. F., Lawton, L., Jelenc, P., *et al.* (1997). Cloning and gene mapping of the chromosome 13q14 region deleted in chronic lymphocytic leukemia. *Genomics* **42:** 369–377.

Kerr, M., Fischer, J. E., Purushotham, K. R., Gao, D., Nakagawa, Y., Maeda, N., Ghanta, V., *et al.* (1994). Characterization of the synthesis and expression of the GTA-kinase from transformed and normal rodent cells. *Biochim. Biophys. Acta* **1218:** 375–387.

Krause, S. W., Rehli, M., Kreutz, M., Schwarzfischer, L., Paulauskis, J. D., and Andreesen, R. (1996). Differential screening identifies genetic markers of monocyte to macrophage maturation. *J. Leukocyte Biol.* **60:** 540–545.

Lubs, H. A., Chiurazzi, P., Arena, J. F., Schwartz, C., Tranebjaerg, L., and Neri, G. (1996). XLMR genes: Update 1996. *Am. J. Med. Genet.* **64:** 147–157.

Meisler, M. (1997). Mutation watch: PEX PLUS? Gene(s) for X-linked hypophosphatemia and deafness. *Mamm. Genome* **8:** 543–544.

Montini, E., Rugarli, E. I., Van de Vosse, E., Andolfi, G., Mariani, M., Puca, A. A., Consalez, G. G., *et al.* (1997). A novel human serine–threonine phosphatase related to the *Drosophila* retinal degeneration C (rdgC) gene is selectively expressed in sensory neurons of neural crest origin. *Hum. Mol. Genet.* **6:** 1137–1145.

Nehls, M., Pfeifer, D., and Boehm, T. (1994). Exon amplification from complete libraries of genomic DNA using a novel phage vector with automatic plasmid excision facility: Application to the mouse neurofibromatosis-1 locus. *Oncogene* **9:** 2169–2175.

Paoloni Giacobino, A., Chen, H., and Antonarakis, S. E. (1997). Cloning of a novel human neural cell adhesion molecule gene (NCAM2) that maps to chromosome region 21q21 and is potentially involved in Down syndrome. *Genomics* **43:** 43–51.

Penotti, F. E. (1991). Human pre-mRNA splicing signals. *J. Theor. Biol.* **150:** 385–420.

Ruddy, D. A., Kronmal, G. S., Lee, V. K., Mintier, G. A., Quintana, L., Domingo, R., Meyer, N. C., *et al.* (1997). A 1.1-Mb transcript map of the hereditary hemochromatosis locus. *Genome Res.* **7:** 441–456.

Sauer, C. G., Gehrig, A., Warneke-Wittstock, R., Marquardt, A., Ewing, C. C., Gibson, A., Lorenz, B., Jurklies, B., and Weber, B. H. F. (1997). Positional cloning of the gene associated with X-linked juvenile retinoschisis. *Nat. Genet.* **17:** 164–170.

Scott, H. S., Chen, H., Rossier, C., Lalioti, M. D., and Antonarakis, S. E. (1997). Isolation of a human gene (HES1) with homology to an *Escherichia coli* and a zebrafish protein that maps to chromosome 21q22.3. *Hum. Genet.* **99:** 616–623.

Trivier, E., De Cesare, D., Jacquot, S., Pannetier, S., Zackai, E., Young, I., Mandel, J.-L., Sassone-Corsi, P., and Hanauer, A. (1996). Mutations in the kinase Rsk-2 associated with Coffin–Lowry syndrome. *Nature* **384:** 567–570.

Walpole, S. M., Nicolaou, A., Howell, G. R., Whittaker, A., Bentley, D. R., Ross, M. T., Yates, J. R. W., and Trump, D. (1997). High-resolution physical map of the X-linked retinoschisis interval in Xp22. *Genomics* **44:** 300–308.

Xu, Y., Mural, R., Shah, M., and Uberbacher, E. C. (1994). Recognizing exons in genomic sequence using GRAIL II. *Genet. Eng.* **16:** 241–253.

5. Anlage 5

Positional cloning of the gene

associated with

X-linked juvenile retinoschisis

Nat. Genet. 17: 164-170

Positional cloning of the gene associated with X-linked juvenile retinoschisis

Christian G. Sauer[1], Andrea Gehrig[1], Regina Warneke-Wittstock[1], Andreas Marquardt[1], Cecil C. Ewing[2], Alice Gibson[2], Birgit Lorenz[3], Bernhard Jurklies[4] & Bernhard H.F. Weber[1]

X-linked juvenile retinoschisis (RS) is a recessively inherited vitreo-retinal degeneration characterized by macular pathology and intraretinal splitting of the retina. The RS gene has been localized to Xp22.2 to an approximately 1 Mb interval between *DXS418* and *DXS999/DXS7161*. Mapping and expression analysis of expressed sequence tags have identified a novel transcript, designated *XLRS1*, within the centromeric RS locus that is exclusively expressed in retina. The predicted XLRS1 protein contains a highly conserved motif implicated in cell–cell interaction and thus may be active in cell adhesion processes during retinal development. Mutational analyses of *XLRS1* in affected individuals from nine unrelated RS families revealed one nonsense, one frameshift, one splice acceptor and six missense mutations segregating with the disease phenotype in the respective families. These data provide strong evidence that the *XLRS1* gene, when mutated, causes RS.

X-linked juvenile retinoschisis (RS: OMIM#312700) is a rare macular dystrophy first described in 1898 by the German ophthalmologist Josef Haas[1]. The disorder, which affects only males, has been reported in patients as young as three months and may already be present at or before birth[2,3]. Although foveal retinoschisis occurs in virtually all affected individuals, there is wide phenotypic variability: approximately 50% of the patients have bilateral schisis cavities in the peripheral retina (Fig. 1). Typically, in the early stages of the disease, perifoveal radial microcysts form in the deep nerve fibre layer in a cartwheel-like pattern. Other findings observed in the affected area are dentritic, opacified retinal vessels, chorioretinal abnormalities and changes related to the vitreous fluid. The major complications in RS include vitreal haemorrhage, retinal detachment and neovascular glaucoma[2–5]. Loss of visual acuity begins early in life and ranges from mild to severe, with some patients approaching legal blindness by the fifth or sixth decade[5,6].

Although little is known about RS pathogenesis, the lesions are thought to be related to a defect in retinal Müller cells. As the principal glia of the retina, Müller cells serve a variety of functions, such as mechanical stability, provision of nutrients to neurons and photoreceptor cells, synthesis and renewal of visual pigment, recycling of neurotransmitters, phagocytosis, neuronal signalling and clearance of K^+ ions from the extracellular space[7]. In particular, a defect in the last-mentioned function of the Müller cells is believed to contribute to a characteristic electrophysiological abnormality in RS patients, demonstrated by an absent or near-absent electroretinographic b wave in the light-adapted eye[2,8]. In addition, an abnormal suppressive rod–cone interaction—probably resulting from a postsynaptic feedback mechanism involving the rods, cones and horizontal cells of the retina—is typically present in RS patients and may be the only diagnostic sign of otherwise healthy female carriers[9]. As Müller cells have been shown to aid neurite outgrowth and neuronal connections[10,11], failure to establish the proper neuronal interaction may be the indirect result of a Müller-cell defect[9]. Consequently, it has been suggested that RS may be considered as a disorder of retinal development rather than a dystrophic process[9].

A large number of genetic linkage analyses have mapped the RS locus to the distal short arm of the X chromosome, indicating genetic homogeneity of this condition[12–15]. The closest DNA markers flanking the disease gene are at loci *DXS418* on the distal side and *DXS999/DXS7161* on the proximal side, encompassing approximately 1 Mb of DNA[16,17] (Fig. 2). Several YAC contigs were constructed spanning the minimal candidate region[16–19]. More recently, the Sanger Centre (Wellcome Trust Genome Campus, Hinxton, Cambridge, UK), in collaboration with the group of D. Trump (Addenbrooke's Hospital, Cambridge, UK), has undertaken the complete sequencing of the RS locus.

The availability of genomic sequences, together with a detailed characterization of transcripts within the RS locus, has led to the identification of a new 224-amino-acid precursor protein including a 23 residue leader sequence that would be predicted to mediate protein export. The mature protein shares a C-terminal discoidin domain with other peptide sequences that has been shown to mediate cell–cell interactions such as cell adhesion or intercellular signalling. Mutations in this gene, provisionally designated *XLRS1* (X-linked retinoschisis–1), cause X-linked juvenile retinoschisis in male patients.

Identification of the *XLRS1* gene

To search for transcripts within the RS locus, we used several approaches, including exon trapping[20], cDNA selection[21], database searches and Grail exon prediction[22], using the available genomic sequences from the RS locus. Overall, we identified 20 putative exons and 33 distinct expressed sequence tags (ESTs) (R.W.-W. *et al.*, manuscript in preparation). One of the EST sequences was represented by four independent clones in the dbEST database, all of which were isolated from a retinal cDNA library. Contig assembly of the 5′ and 3′ sequences of the four ESTs and alignment to the genomic sequence of PAC clone dJ245G19

[1]*Institut für Humangenetik, Universität Würzburg, 97074 Würzburg, Germany.* [2]*University of Saskatchewan, Saskatoon, Saskatchewan S7K 0M7, Canada.* [3]*Augenklinik der Universität, 93042 Regensburg, Germany.* [4]*Universitäts-Augenklinik, 45147 Essen, Germany. C.G.S., A.G. and R.W.-W. contributed equally to this work. Correspondence should be addressed to B.H.F.W. e-mail: bweb@biozentrum.uni-wuerzburg.de*

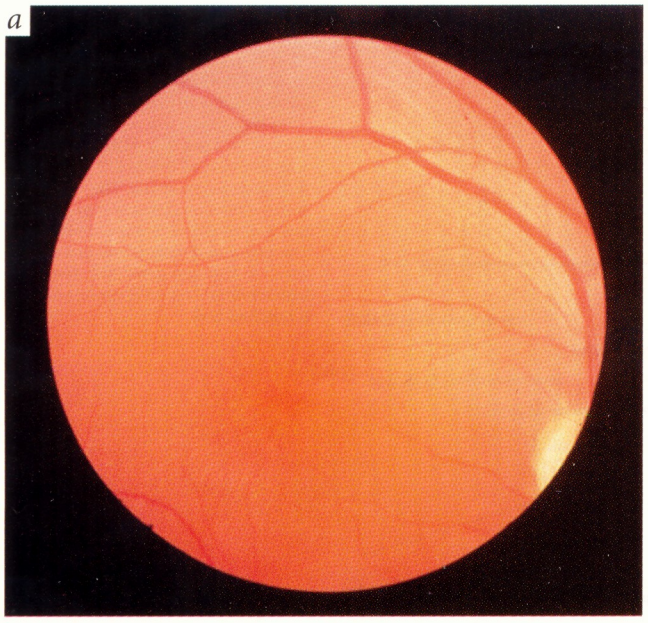

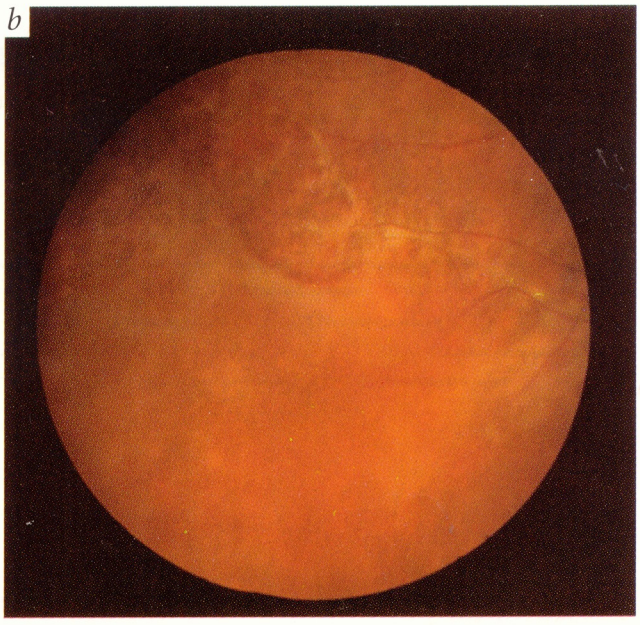

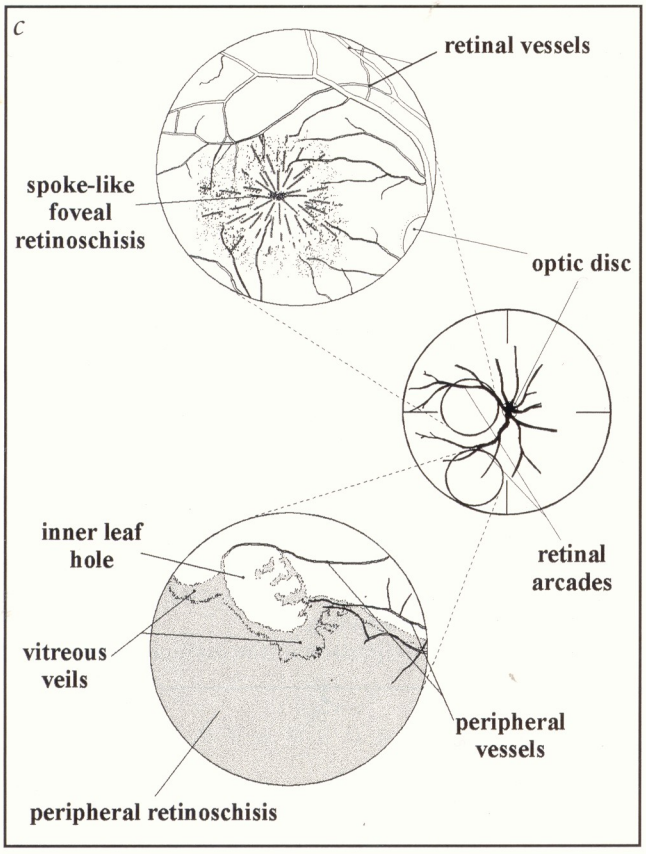

Fig. 1 Fundus photographs of the right eye of an 11-year-old RS patient. ***a***, Foveal retinoschisis producing a characteristic spoke-like appearance of the macula. ***b***, Extensive peripheral retinoschisis in the infero-temporal quadrant with a large inner leaf hole and vitreous veils. ***c***, Schematic drawing of the fundus illustrating the anatomic locations and the detailed clinical lesions shown in *a* and *b* (magnifications).

showed that the cDNA contig comprised approximately 1.8 kb of uninterrupted sequence containing a LINE/L1 repeat of almost 1.5 kb at the 3′ end (Fig. 2). To further expand the cDNA fragment in the 5′ direction, a repeat-free sequence corresponding to the first 214 bp (nucleotides +2287 to +2500) of EST clone ys86e07.r1 (H92424) was PCR amplified and used for a λgt10 retinal cDNA library screening. Several cDNA clones were identified. Sequencing of the 2.5-kb cDNA clone 12/9 revealed a 426-bp open reading frame (ORF). Re-screening of the retinal cDNA library with a 200-bp *Cla*I/*Eco*RI fragment from the 5′ end of clone 12/9 led to the isolation of another six cDNA fragments, yielding a further 261 bp of ORF. Additional library screenings and 5′-RACE experiments have not extended the cDNA towards the 5′ end. Preliminary results from primer extension experiments, however, indicate that a single transcription start site is approximately at cDNA nucleotide position –360 (data not shown). Together, the assembled cDNA fragments contain an ORF of 687 bp, with a first potential in-frame translation initiation codon, ATG, starting fifteen nucleotides downstream. The extent of the 3′-UTR remains elusive, as none of the EST or cDNA clones contained a polyA tail. Two putative polyA signal sequences are predicted at nucleotide positions +847 to +852 and +4020 to +4025, respectively. Whereas the former polyA signal may give rise to a 1.1-kb transcript, the latter appears inconsistent with a transcript size of 3.1 kb as determined by northern-blot analysis (see below).

Expression analysis of *XLRS1*

We investigated the expression of *XLRS1* by northern-blot analysis using two probes, namely cDNA clone 6/4 corresponding to nucleotides –15 to +940 and a 214-bp PCR-derived fragment corresponding to nucleotides +2287 to +2500 of the 3′-UTR. A multiple-tissue northern blot of polyA$^+$ RNA from various human tissues (including heart, brain, placenta, lung, liver, skeletal muscle, kidney and pancreas) and total RNA northern blots from lung, lymphocyte, cerebellum, retina and retinal pigment epithelium were used. Hybridization signals were detected exclusively in total RNA from human retina (Fig. 4). However, while cDNA clone 6/4 revealed two signals in retinal RNA corresponding to transcript sizes of 1.1 kb and 3.1 kb, respectively, the 214-bp PCR fragment detected only the 3.1 kb *XLRS1* transcript (Fig. 4). These results suggest that the two mRNA species observed in retina are produced by utilizing differential polyA addition sites.

Genomic organization of *XLRS1*

To perform mutational analyses in RS patient DNAs, we determined the exon–intron organization of the *XLRS1* gene. Using BLAST search facilities at the Sanger Centre, the assembled cDNA

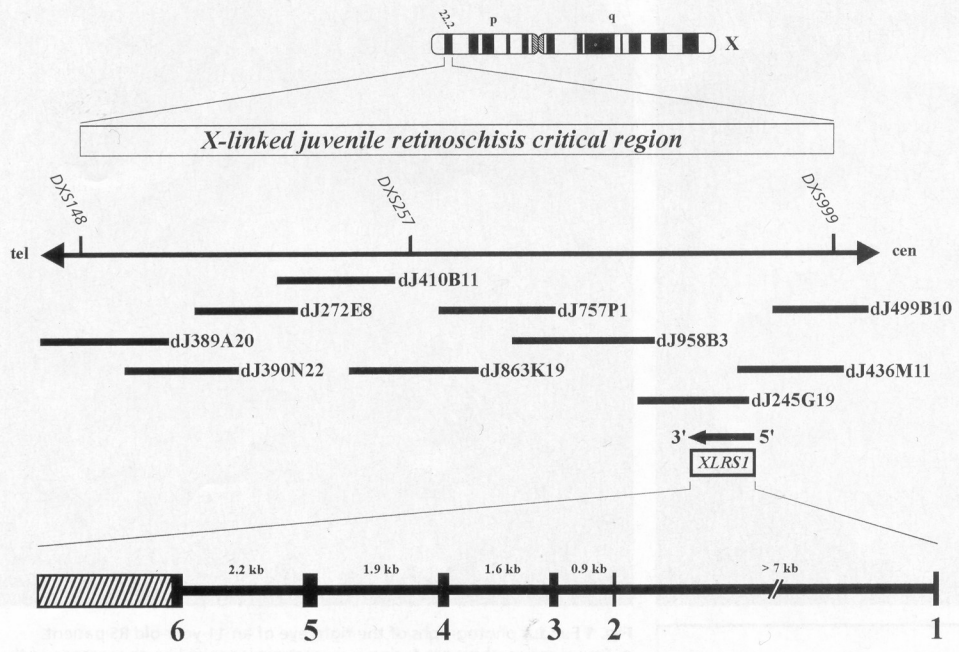

Fig. 2 Physical mapping and genomic organization of the *XLRS1* gene. The RS critical region has previously been mapped between *DXS418* and *DXS999/DXS7161* (ref. 17). Overlapping PAC clones are respresented by horizontal bars. The orientation of transcription of the *XLRS1* gene is indicated by an arrow. The exon–intron organization of the gene is shown in relative spacing. The estimated sizes of introns are given in kilobase pairs (kb). The 3′ untranslated region is represented by a hatched box.

sequence identified five exon–intron boundaries in PAC clone dJ245G19 (Fig. 2). Exon 1 is also present in PAC clone dJ436M11, suggesting the orientation of transcription to be from centromere to telomere (Fig. 2). Alignment of the most 5′ cDNA sequences to the genomic DNA reveals a 5′ donor splice but no 3′ acceptor splice consensus for exon 1 (Table 1). As we have not yet identified the cDNA sequence corresponding to nucleotide position –360 to –15, exon 1 may further be interrupted by intervening sequences upstream of nucleotide position –15.

The genomic equivalent of the cDNA sequence from nucleotide +185 to +326 (corresponding to *XLRS1* exon 4) was missing in the unfinished PAC sequences at the Sanger Centre. To determine the remaining exonic structure, a 3.4-kb *Pst*I genomic clone was derived from PAC dJ245G19 and was partly sequenced. Together, the present analysis has established that *XLRS1* is composed of six coding exons (Table 1) spanning approximately 15 kb of genomic DNA (Fig. 2).

Homology to the discoidin motif

The nucleotide sequence GGGGAAGATGT surrounding the first in-frame ATG starting at nt 16 of the *XLRS1* cDNA is in good agreement with the Kozak consensus for efficient initiation of translation[23]. Based on the genomic sequence, an in-frame stop codon is present 33 bp upstream of the potential translation initiation start site. Hydropathicity plots revealed the first 23 amino acids to be a putative secretory leader peptide sequence for export of the protein[24]. The signal sequence contains a highly hydrophobic domain consisting of Gly-Phe-Leu-Leu-Leu-Leu-Leu-Phe-Gly-Tyr-Glu, which is the most hydrophobic region in the entire peptide sequence. In addition, two positively charged residues, Arg and Lys, are predicted to precede the hydrophobic domain. Finally, there is a putative peptidase cleavage site with Gly21-Xaa-Ser23, satisfying the '-1, -3 rule' for signal peptidase recognition sequences (Fig. 3; ref. 24). Therefore, the mature protein predicted from the ORF of the *XLRS1* cDNA consists of 201 amino-acid residues resulting in a calculated molecular mass of 23 kD. One N-linked myristylation site is predicted at Gly44-Gly45-Pro46-Asn47-Ala48-Leu49. No potential N-linked glycosylation sites were found in the mature protein. An even number of ten cysteine residues are present in the protein and may participate in intra- or interchain disulphide bonding.

Protein database comparison of the predicted amino-acid

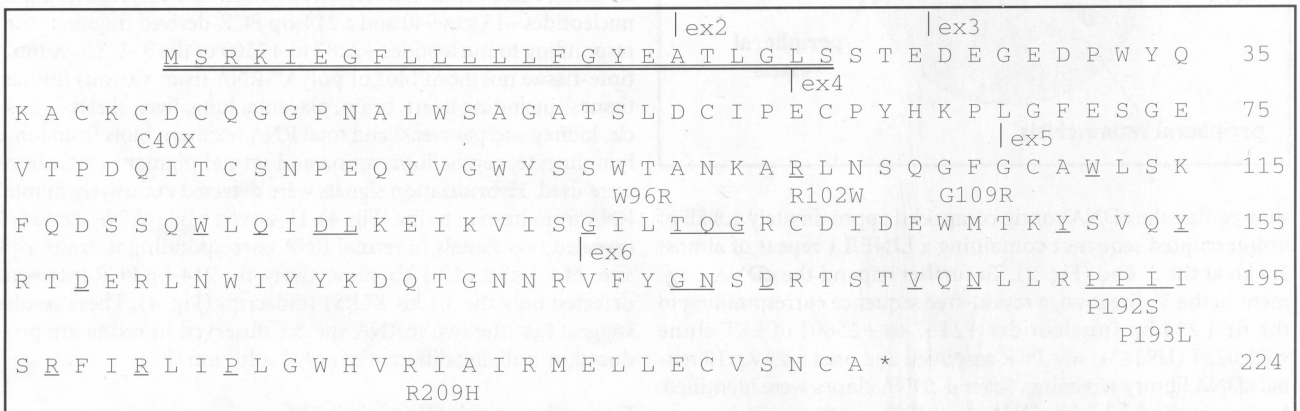

Fig. 3 Amino-acid sequence of the XLRS1 protein. The deduced one-letter amino-acid code is shown. The amino-acid positions are given on the right. The locations of the exon–intron boundaries are indicated by vertical bars. Missense and nonsense mutations identified in RS patients are shown below. Amino-acid residues matching the consensus sequence of the discoidin motif are underlined. The putative 23-amino acid leader sequence is double-underlined.

Table 1 • Exon–intron boundaries of *XLRS1*

Exon no.	Size[a] (bp)	3′ acceptor splice site[b]	5′ donor splice site[b]	Intron size (kb)
1	52		...TATGAAG gtatgtg...	> 7
2	26	...gctttag CCACATT...	...TACCGAG gtatgta...	0.9
3	106	...gntgcag GATGAAG...	...ATACCAG gtgagta...	1.6
4	142	...ttcccag AATGCCC...	...GCTTTGG gtaagca...	1.9
5	196	...tcggcag GTGTGCC...	...CAACCGG gtaagtt...	2.2
6	153	...tctctag GTCTTCT...		

[a]Sizes given refer to the coding portions of the respective exons.
[b]The exonic and intronic sequences are in upper and lower case, respectively.

Table 2 • Exon/intron oligonucleotide primers for *XLRS1*

Exon	Primer[a]	Sequence	T_A
1	rstu12–1f	5′–CTCAGCCAAAGACCTAAGAAC–3′	58 °C
	rstu12–1r	5′–GTATGCAATGAATGTCAATGG–3′	
2	rstu12–2f	5′–GTGATGCTGTTGGATTTCTC–3′	56 °C
	rstu12–2r	5′–CAAAGTGATAGTCCTCTATG–3′	
3	rstu12–3f	5′–CTGCCCTGCCTCTCTGGTTG–3′	60 °C
	rstu12–3r	5′–GGTGTTCCCAATGACTGTTCC–3′	
4	rstu12–f	5′–GGTGCTTGTTGAGTATTGAG–3′	56 °C
	tu12ex4–rev	5′–AAAATCCCCGGGCCCTGC–3′	
5	245638–f	5′–GAGAGCCAGCACCTGCGG–3′	65 °C
	245638–r	5′–GGGTGCGAGCTGAAGTTGG–3′	
6	245263–f	5′–CCCGATGTGATGGTGACAGG–3′	62 °C
	245263–r	5′–CTTTGTTCTGACTTTCTCTGGC–3′	

[a]PCR conditions were 94 °C, 5 min; 30 cycles of 94 °C, 30 s, T_A, 30 s, 72 °C, 30 s; 72 °C, 5 min.

sequence revealed a region of high homology (codons 101–203) to discoidin-1, a lectin first identified in the cellular slime mold *Dictyostelium discoideum* (Fig. 5; ref. 25). The evolutionarily highly conserved discoidin domain is shared by several other proteins, including hemocytin, an insect humoral lectin[26], neuropilin, a neuronal cell surface protein identified in *Xenopus laevis*[27], chick[28] and mouse[29], the milk-fat globule membrane protein from mouse[30] and human[31], the human coagulation factor V[32], the human[33] and mouse[34] coagulation factor VIII and, finally, a cell adhesion receptor tyrosine kinase (Fig. 5; ref. 35). The discoidin domain has been implicated in phospholipid binding and cell–cell interactions on membrane surfaces, suggesting a similar functional property for XLRS1.

Mutational analysis in RS patients

DNA samples from affected individuals in nine RS families unrelated by genealogy were available. Together, almost 100 affected members in a total of seven families had been given a diagnosis of RS. By genetic linkage analysis, the disease gene in these families was shown to be significantly linked to the RS locus on Xp22.2 (ref. 15 and unpublished results). The number of available affected and unaffected individuals in the remaining two pedigrees (families 10 and 26) was too small for genetic linkage analysis to be performed.

The lymphocyte DNAs of one RS patient per family were screened for mutations by single-stranded conformational analysis (SSCA) and direct cycle sequencing of individual PCR amplified exons of *XLRS1* (Table 2). This strategy led to the identification of mutational changes in all nine individuals, including one nonsense, one frameshift, one splice acceptor and six missense mutations (Figs 3,6, Table 3). The nonsense mutation introduces a premature termination signal at codon 40, which should result in a severely truncated polypeptide. Similarly, an insertion of an adenine residue at nt position +316 causes a premature termination, resulting in a 119-amino-acid polypeptide with a modified thirteen C-terminal amino-acid sequence (Fig. 6*c*). Unfortunately, the lack of RNA from affected individuals in family F has made it impossible to assess the effect of the A to G transition at position –2 of the splice acceptor site in intron 2. However, available data from comparisons of 764 splice acceptor sites[36] strongly suggest that this alteration should be expected to lead to a splice variant downstream of exon 2.

Six missense mutations were identified: W96R, R102W, G109R, P192S, P193L and R209H (Fig. 3, Table 3). Four of the six mutations are within the phylogenetically conserved discoidin motif encompassing codons 101 to 203 (Figs 3,5). Moreover, three amino-acid changes (R102W, P192S and P193L) directly affect highly conserved positions in the consensus sequence. The final two missense mutations, W96R and R209H, closely flank the discoidin motif. While the T-to-C transition changes the specificity of the non-polar tryptophan to a positively charged arginine at codon 96 (Fig. 6*b*), the G-to-A transition at codon 209 causes a positively charged arginine to be replaced by a positively charged histidine.

All mutations were shown to segregate with the disease (Fig. 6*a* and data not shown) except R209H and P192S, in which the family structure did not permit a segregation analysis. In addition, as all missense mutations were identified in exons 4 and 6, SSCA was performed on 90 control chromosomes using the conditions in which all six missense

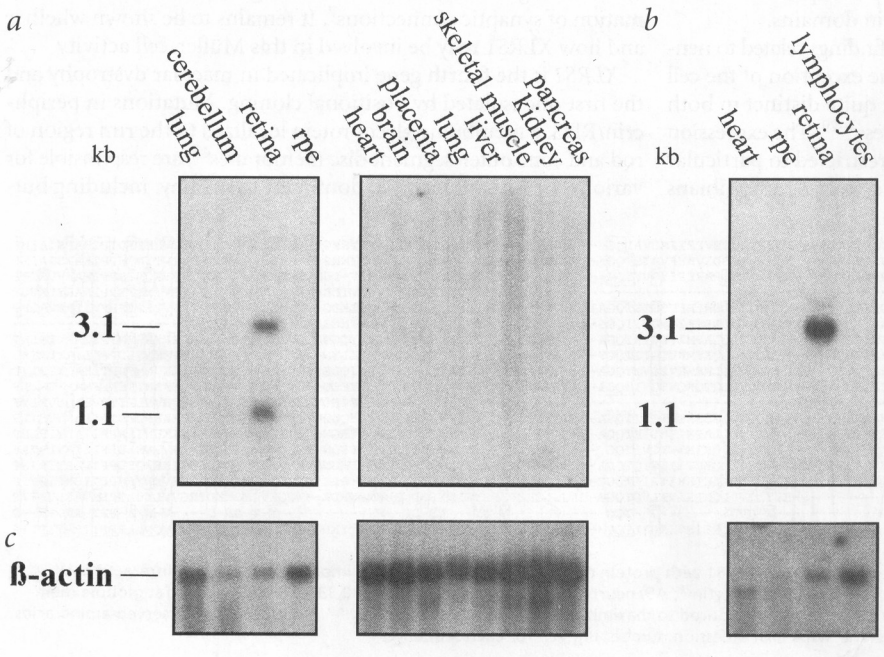

Fig. 4 Northern-blot analysis of *XLRS1*. ***a***, Two abundant transcripts of 1.1 kb and 3.1 kb are detected in total RNA from retina with probe 6/4, containing the entire coding sequence of *XLRS1* and 265 bp of the 3′–UTR. ***b***, In contrast, the 214-bp PCR fragment derived from the 3′–UTR (corresponding to nucleotides +2287 to +2500) reveals only the 3.1-kb transcript. No hybridization signals were detected in the other tissues tested, suggesting retina-specific expression of the *XLRS1* gene. ***c***, To test for equal loading and RNA integrity, the northern blots were subsequently hybridized with a human β-actin probe. rpe, retinal pigment epithelium.

mutations were readily detectable. No mobility shifts resembling those underlying the missense mutations were detected in the control chromosomes (data not shown).

Discussion

By positional cloning, we have identified a new gene, *XLRS1*, that lies within the RS candidate region in Xp22.2, approximately 130 kb from the proximal boundary defined by *DXS999/DXS7161*. The *XLRS1* transcript is highly abundant in retina but appears absent in other tissues tested, suggesting cell-specific expression of the gene in the sensory neuroretina. We show that *XLRS1* is mutated in patients with X-linked juvenile retinoschisis. Understanding the functional properties of *XLRS1* will be an important next step in shedding light on the molecular and cellular basis of this vitreo-retinal disorder.

Structural analysis of the predicted protein sequence has identified a conserved motif within the C-terminus of XLRS1 that is shared with proteins characterized in a variety of species spanning a phylogenetic distance from *Dictyostelium discoideum* to *Homo sapiens*. Although the precise mechanism of action and the key components of the discoidin domain remain to be established, it is thought to be implicated in the promotion of molecular interactions that take place on the membrane surfaces of cells, possibly by anionic phospholipid binding as demonstrated for mammalian coagulation factors V and VIII (ref. 37).

The conserved domains C1 and C2 of human factors V and VIII were shown to bind to negatively charged phospholipids on the surfaces of platelets and endothelial cells, facilitating interactions with other components of the blood coagulation cascade[37]. Consequently, this protein–phospholipid interaction was blocked by antibodies raised against the C domains[38]. Similarly, the conserved domain in discoidin I, a secreted tetrameric lectin, has been proposed to be essential for ordered cell migration and cell-substratum attachment in *D. discoideum*[25,39]. Also, haemocytin, an insect lectin that shares the discoidin motif, is an adhesive protein relating to humoural haemostasis[26]. The attachment of the milk-fat globule membrane protein (MFGM) to the membrane of the mammary epithelial cells is also thought to involve the conserved C-terminal domain[31]. Finally, two cell-surface proteins with discoidin motifs, neuropilin (formerly A5 antigen; refs 27–29) and cell adhesion kinase (Cak; ref. 35), are firmly anchored in the plasma membrane and are likewise believed to participate in cell–cell interactions through their conserved protein domains.

In light of the known RS pathology, some findings related to neuropilin may be of interest, although with the exception of the cell adhesion motif, neuropilin and XLRS1 are quite distinct in both their molecular masses and peptide sequences[27–29]. The expression of neuropilin appears neuron specific and restricted to particular neuronal circuits. Expression in the visual system of amphibians was specifically found in the optic tectum, where the optic nerve fibre terminals form synapses[27]. Moreover, in the tadpole retina neuropilin expression was detected only in the retinal ganglion cell layer, where the optic nerve fibres originate. The retinal expression profile is particularly intriguing in that the ganglion cell layer is intimately involved in RS pathology. Histopathologically, the characteristic feature of RS is a superficial splitting in the retina between the nerve fibre and ganglion cell layer[40–42]. Consequently, immunohistochemical localization of XLRS1 will be a first step in establishing the cellular distribution of the mature protein and identifying the cell type(s) primarily involved in RS pathology.

Cystic maculopathy presenting as a cartwheel-like formation of radial microcysts develops early in RS and may even be congenital[9,42]. This may suggest a role of the XLRS1 in early developmental stages of retinal cell layer formation. Like neuropilin, which has been shown to be expressed in pre- and postsynaptic sites in developing neurons[27], XLRS1 could be active in establishing cell-specific synaptic contacts. Conversely, an absent or defective XLRS1 protein may interfere with the formation of interneuronal connections during embryonic development. Results of electrophysiological tests measuring suppressive rod–cone interactions[9] in RS patients and carriers support this hypothesis. The interactions are thought to be the result of post-synaptic feedback mechanisms and are absent in patients with X-linked retinoschisis, suggesting a defect in the neuronal circuitry during retinal development[9]. The intimate developmental relationship between glial Müller cells and several types of neurons is well established and is thought to mediate neurite outgrowth as well as the formation of synaptic connections[7]. It remains to be shown whether and how XLRS1 may be involved in this Müller-cell activity.

XLRS1 is the fourth gene implicated in macular dystrophy and the first one isolated by positional cloning. Mutations in peripherin/RDS, a membrane glycoprotein localized to the rim region of rod and cone outer-segment disc membranes[43], are responsible for various forms of autosomal dominant dystrophy, including but-

Table 3 • *XLRS1* mutation in families

Mutation[a]	Family	Nucleotide change	Exon/IVS
IVS2-2 A→G	F	splice acceptor site	IVS 2
C40X	E	C120T	ex 3
W96R	A	T286C	ex 4
R102W	D	C304T	ex 4
316insA	B	frameshift	ex 4
G109R	G	G325C	ex 4
P192S	26	C574T	ex 6
P193L	Gr	C578T	ex 6
R209H	10	G626A	ex 6

[a]Mutations are named according to standard nomenclature.

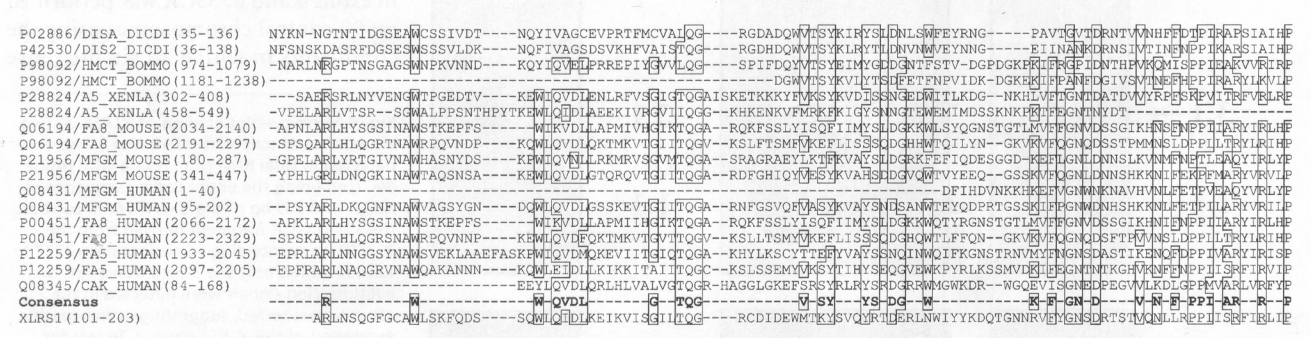

Fig. 5 Amino-acid alignment of the predicted protein sequence of XLRS1 with protein domains from various species implicated in cell–cell interaction. DISA, form A of discoidin I (ref. 25); DIS2, discoidin II (ref. 52); HMCT, haemocytin[26]; A5, neuropilin[27]; FA8, factor VIII (refs 30,33,34); MFGM, milk-fat globule membrane[31]; FA5, factor V (ref. 32); CAK, cell adhesion kinase[35]. Gaps introduced to maximize alignment are indicated by '–'. Evolutionarily conserved amino acids are boxed and the motif consensus is shown in bold. The Swiss-Prot accession number is given for each sequence.

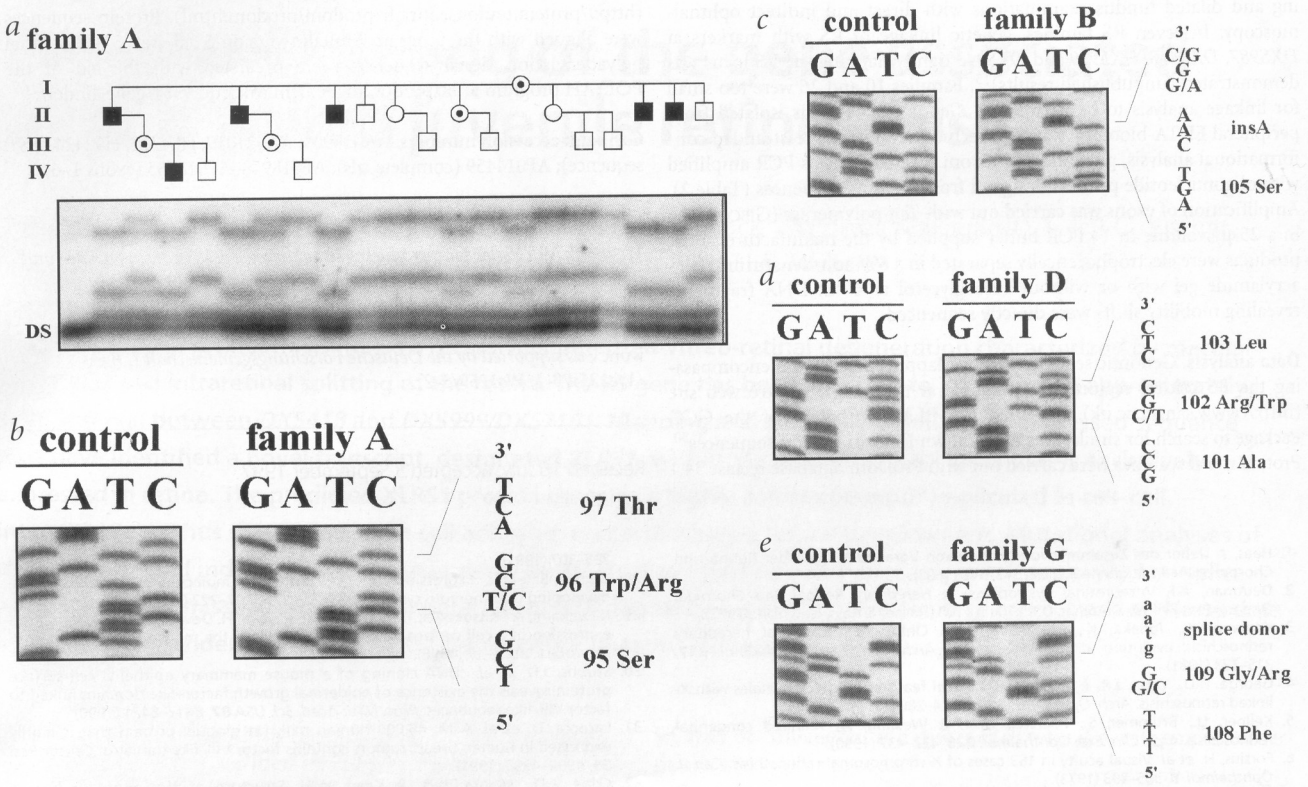

Fig. 6 Mutational analysis in patients diagnosed with RS. ***a***, Co-segregation of RS with a T-to-C transition in codon 96 of the *XLRS1* gene in a branch of family A. The double strand (DS) is indicated. Affected individuals and female carriers are represented by standard symbols. ***b***, Identification of the T-to-C transition in codon 96 (family A). ***c***, Identification of an insertion A at nucleotide 316 in family B leading to a frameshift and a stop 14 amino acids downstream. ***d***, In family D, a C-to-T transition in codon 102 changes an evolutionarily conserved arginine to tryptophan. ***e***, Missense mutation at codon 109 in family G.

terfly dystrophy, central areolar choroidal dystrophy, adult vitelliform macular dystrophy and fundus flavimaculatus[44]. The cloning of the gene was facilitated by the availability of a naturally occurring animal model, the retinal degeneration slow (*rds*) mouse. By the positional candidate approach, the gene encoding the tissue inhibitor of metalloproteinases–3 (*TIMP3*) was shown to be implicated in autosomal dominant Sorsby's fundus dystrophy[45]. By a similar strategy, a new member of the ABC transporter gene family was identified and shown to be associated with autosomal recessive Stargardt's disease[46]. The identification of these and other, unknown genes involved in the pathogenesis of the retinal dystrophies has great implications, as it will provide new and exciting insights into function and dysfunction of the human retina.

Methods

cDNA cloning. A human retinal cDNA library (constructed by J. Nathans, Johns Hopkins University) was initially screened with a radiolabelled PCR fragment corresponding to the first 214 bp of EST clone ys86e07.r1 (H92424) using primers ys86-f (5′–TTGGATAGAAATGCCTGAAC–3′) and ys86-r (5′–TGACAAAAGTTTCCAACATG–3′). To obtain the full-length transcript, we performed subsequent screenings of the cDNA library with additional fragments corresponding to the 5′ ends of the retrieved cDNA fragments, respectively. Hybridizations were performed overnight at 65 °C in Church buffer[47]. The filters were washed at 65 °C in 2×SSPE, 0.1% SDS and 1×SSPE, 0.1% SDS. Primary positives were subjected to secondary screens. The inserts of the resulting positive phage clones were isolated, *Eco*RI digested, subcloned into the pBluescript II-KS(+) vector (Stratagene) and sequenced using vector primers KS (5′–CGAGGTCGACGGTATCG–3′), SK (5′–TCTAGAACTAGTGGATC–3′) and the Thermo Sequenase terminator cycle sequencing kit (Amersham, Life Science). 5′–RACE was carried out with the 5′–RACE system, version 2 (GIBCO BRL) according to the manufacturer's recommendations. For first-strand cDNA synthesis, primer 9orf1-rev (5′–GAAGAATACCAGCCCACATAC–3′) corresponding to nucleotides +264 to +284 was used.

Genomic organization. The cDNA sequence was aligned to partial PAC clone sequences dJ245G19 and dJ436M11 (Sanger Centre, Cambridge, UK). Genomic sequence corresponding to exon 4 was obtained by isolating and partly sequencing a genomic 3.4-kb *Pst*I fragment derived from PAC dJ245G19. Alignment of genomic and cDNA sequences allowed the assignment of donor and acceptor splice recognition sequences (Table 1).

Northern-blot hybridizations. Total RNA was isolated from various human tissues, including lung, cerebellum, retina, retinal pigment epithelium, heart and peripheral blood lymphocytes, using the guanidinium-thiocyanate method[48]. In each lane, 12 µg of total RNA was electrophoretically separated in a 1.2% agarose gel in the presence of formaldehyde and blotted onto a nylon membrane. The multiple-tissue northern (MTN) blot (Clontech Laboratories) was prepared from polyA$^+$ RNA isolated from human heart, brain, placenta, lung, liver, skeletal muscle, kidney and pancreas. cDNA clone 6/4 (corresponding to nucleotides –15 to +940) and a 214-bp PCR fragment amplified from EST clone ys86e07 using primer pair ys86-f/ys86-r were used for filter hybridizations in Church buffer at 65 °C. To test for equal loading and the integrity of the RNA, the northern blots were hybridized with a human β-actin cDNA probe provided with the MTN blot.

Patients and mutational analysis. Detailed clinical descriptions of families A and B have been published elsewhere[49]. In brief, ocular examination included best-corrected Snellen visual acuity, motility, biomicroscopy and dilated ophthalmoscopy. In some cases ancillary tests were performed, including fluorescein angiography, visual field and colour vision. Affected members in family D (5 individuals), family E (5 individuals), family F (3 individuals), family G (9 individuals), family Gr (3 individuals), family 10 (1 individual) and family 26 (1 individual) underwent visual-acuity test-

ing and dilated fundus examinations with direct and indirect ophthalmoscopy. In seven RS families, genetic linkage of RS with markers at *DXS987*, *DXS418*, *DXS999* and *DXS443* tightly flanking the RS locus was demonstrated (unpublished results)[15]. Families 10 and 26 were too small for linkage analysis to be performed. Genomic DNA was isolated from peripheral EDTA-blood by standard techniques. For single-stranded conformational analysis, genomic DNA from RS patients was PCR amplified with oligonucleotide primers designed from intronic sequences (Table 2). Amplification of exons was carried out with *Taq*-polymerase (GIBCO BRL) in a 25-µl volume in 1×PCR buffer supplied by the manufacturer. PCR products were electrophoretically separated in a 6% non-denaturing polyacrylamide gel with or without 10% glycerol at 4 °C. DNA fragments revealing mobility shifts were directly sequenced.

Data analysis. Genomic sequences of overlapping PAC clones encompassing the RS critical region were available at the Sanger Centre web site (http://www.sanger.ac.uk). We used the BLAST program of the GCG Package to search for similarities with known DNA or protein sequences[50]. Protein motif searches were carried out with ProDom database release 34.1 (http://protein.toulouse.inra.fr/prodom/prodom.html). Protein sequences were aligned with the program Multalin version 5.3.3 (ref. 51). Potential polyadenylation signal sequences were predicted with the aid of the POLYAH program at http://dot.imgen.bcm.tmc.edu:9331/gene-finder/.

GenBank accession numbers. AA015909, AA021019, H84712, H92424 (EST sequence); AF014459 (complete cds); AF018958–AF018963 (exons 1–6).

Acknowledgements

We thank M. Gessler for introducing us to the GCG9 Wisconsin package and its endless applications, P. Cooper for PAC screenings and J. Boulter for providing the retinal cDNA library. C.G.S. is supported by a doctoral fellowship of the Deutsche Retinitis Pigmentosa Vereinigung (DRPV). This work was supported by the Deutsche Forschungsgemeinschaft (DFG) (We1259/5-1; We1259/5-2).

Received 16 July; accepted 3 September 1997.

1. Haas, J. Ueber das Zusammenvorkommen von Veraenderungen der Retina und Choroidea. *Arch. Augenheilkd.* **37**, 343–348 (1898).
2. Deutman, A.F. Vitreoretinal dystrophies. In *Hereditary Retinal and Choroidal Diseases* (eds Krill, A. & Archer, D.B.) 1043–1108 (Harper & Row, New York, 1977).
3. Kawano, K., Tanaka, K., Murakami, F. & Ohba, N. Congenital hereditary retinoschisis: evolution at the initial stage. *Arch. Clin. Exp. Ophthalmol.* **217**, 315–323 (1981).
4. George, N.D., Yates, J.R. & Moore, A.T. Clinical features in affected males with X-linked retinoschisis. *Arch. Ophthalmol.* **114**, 274–280 (1996).
5. Kellner, U., Brummer, S., Foerster, M.H. & Wessing, A. X-linked congenital retinoschisis. *Arch. Clin. Exp. Ophthalmol.* **228**, 432–437 (1990).
6. Forsius, H. *et al.* Visual acuity in 183 cases of X-chromosomal retinoschisis. *Can. J. Ophthalmol.* **8**, 385–393 (1973).
7. Reichenbach, A. & Robinson, S.R. The involvement of Müller cells in the outer retina. in *Neurobiology and Clinical Aspects of the Outer Retina* (eds Djamgoz, M.B.A., Archer, S.N. & Vallerga, S.) 395–415 (Chapman and Hall, London, 1995).
8. Miller, R.F. & Dowling, J.E. Intracellular responses of the Müller (glial) cells of mudpuppy retina: their relation to b-wave of the electroretinogram. *J. Neurophysiol.* **33**, 323–341 (1970).
9. Arden, G.B., Gorin, M.B., Polkinghorne, P.J., Jay, M. & Bird, A.C. Detection of the carrier state of X-linked retinoschisis. *Am. J. Ophthalmol.* **105**, 590–595 (1988).
10. Sheffield, J.B. & Li, H.P. Interactions among cells of the developing neural retina in vitro. *Am. Zool.* **27**, 145–159 (1987).
11. Kljavin, I.J. & Reh, T.A. Muller cells are a preferred substrate for *in vitro* neurite extension by rod photoreceptor cells. *J. Neurosci.* **11**, 2985–2994 (1991).
12. Ives, E.J., Ewing, C.C. & Innes, R. X-linked juvenile retinoschisis and Xg linkage in five families. *Am. J. Hum. Genet.* **22**, A17–A18 (1970).
13. Wieacker, P. et al. Linkage relationships between retinoschisis, Xg, and a cloned DNA sequence from the distal short arm of the X chromosome. *Hum. Genet.* **64**, 143–145 (1983).
14. Alitalo, T., Karna, J., Forsius, H. & de la Chapelle, A.E. X-linked retinoschisis is closely linked to *DXS41* and *DXS16* but not *DXS85*. *Clin. Genet.* **32**, 192–195 (1987).
15. Weber, B.H.F. *et al.* X-linked juvenile retinoschisis (RS) maps between *DXS987* and *DXS443*. *Cytogenet. Cell. Genet.* **69**, 35–37 (1995).
16. van de Vosse, E. *et al.* An Xp22.1–p22.2 YAC contig encompassing the disease loci for *RS*, *KFSD*, *CLS*, *HYP* and *RP15*: refined localization of RS. *Eur. J. Hum. Genet.* **4**, 101–104 (1996).
17. Huopaniemi, L., Rantala, A., Tahvanainen, E., de la Chapelle, A. & Alitalo, T. Linkage disequilibrium and physical mapping of X-linked juvenile retinoschisis. *Am. J. Hum. Genet.* **60**, 1139–1149 (1997).
18. Alitalo, T. *et al.* A 6-Mb YAC contig in Xp22.1–p22.2 spanning the DXS69E, XE59, GLRA2, PIGA, GRPR, CALB3, and PHKA2 genes. *Genomics* **25**, 691–700 (1995).
19. Ferrero, G.B. *et al.* An integrated physical and genetic map of a 35 Mb region on chromosome Xp22.3–Xp21.3. *Hum. Mol. Genet.* **4**, 1821–1827 (1995).
20. Nehls, M., Pfeifer, D. & Boehm, T. Exon amplification from complete libraries of genomic DNA using a novel phage vector with automatic plasmid excision facility: application to the mouse neurofibromatosis-1 locus. *Oncogene* **9**, 2169–2175 (1994).
21. Rommens, J.M. *et al.* A transcription map of the region containing the Huntington disease gene. *Hum. Mol. Genet.* **2**, 901–907 (1993).
22. Uberbacher, E.C. & Mural, R.J. Locating protein-coding regions in human DNA sequences by a multiple sensor-neural network approach. *Proc. Natl. Acad. Sci. USA* **88**, 11261–11265 (1991).
23. Kozak, M. Interpreting cDNA sequences: some insights from studies on translation. *Mamm. Genome* **7**, 563–574 (1996).
24. Gierasch, L.M. Signal sequences. *Biochemistry* **28**, 923–930 (1989).
25. Springer, W.R., Cooper, D.N. & Barondes, S.H. Discoidin I is implicated in cell-substratum attachment and ordered cell migration of *Dictyostelium discoideum* and resembles fibronectin. *Cell* **39**, 557–564 (1984).
26. Kotani, E. *et al.* Cloning and expression of the gene of hemocytin, an insect humoral lectin which is homologous with the mammalian von Willebrand factor. *Biochim. Biophys. Acta* **1260**, 245–258 (1995).
27. Takagi, S. *et al.* The A5 antigen, a candidate for the neuronal recognition molecule, has homologies to complement components and coagulation factors. *Neuron* **7**, 295–307 (1991).
28. Takagi, S. *et al.* Expression of a cell adhesion molecule, neuropilin, in the developing chick nervous system. *Dev. Biol.* **170**, 207–222 (1995).
29. Kawakami, A., Kitsukawa, T., Takagi, S. & Fujisawa, H. Developmentally regulated expression of a cell surface protein, neuropilin, in the mouse nervous system. *J. Neurobiol.* **29**, 1–17 (1996).
30. Stubbs, J.D. *et al.* cDNA cloning of a mouse mammary epithelial cell surface protein reveals the existence of epidermal growth factor–like domains linked to factor VIII–like sequences. *Proc. Natl. Acad. Sci. USA* **87**, 8417–8421 (1990).
31. Larocca, D. *et al.* A M_r 46,000 human milk fat globule protein that is highly expressed in human breast tumors contains factor VIII–like domains. *Cancer Res.* **51**, 4994–4998 (1991).
32. Cripe, L.D., Moore, K.D. & Kane, W.H. Structure of the gene for human coagulation factor V. *Biochemistry* **31**, 3777–3785 (1992).
33. Truett, M.A. *et al.* Characterization of the polypeptide composition of human factor VIII:C and the nucleotide sequence and expression of the human kidney cDNA. *DNA* **4**, 333–349 (1985).
34. Elder, B., Lakich, D. & Gitschier, J. Sequence of the murine factor VIII cDNA. *Genomics* **16**, 374–379 (1993).
35. Perez, J.L. *et al.* Identification and chromosomal mapping of a receptor tyrosine kinase with a putative phospholipid binding sequence in its ectodomain. *Oncogene* **9**, 211–219 (1994).
36. Penotti, F.E. Human pre-mRNA splicing signals. *J. Theor. Biol.* **150**, 385–420 (1991).
37. Kane, W.H & Davie, E.W. Blood coagulation factors V and VIII: structural and functional similarities and their relationsship to hemorrhage and thrombic disorders. *Blood* **71**, 539–555 (1988).
38. Arai, M., Scandella, D. & Hoyer, L.W. Molecular basis of factor VIII inhibition by human antibodies: antibodies that bind to the factor VIII light chain prevent the interaction of factor VIII with phospholipid. *J. Clin. Invest.* **83**, 1978–1984 (1989).
39. Rosen, S.D., Kafka, J.A., Simpson, D.L. & Barondes, S.H. Developmentally regulated, carbohydrate-binding protein in *Dictyostelium discoideum*. *Proc. Natl. Acad. Sci. USA* **70**, 2554–2557 (1973).
40. Manschot, W.A. Pathology of hereditary juvenile retinoschisis. *Arch. Ophthalmol.* **88**, 131–138 (1972).
41. Yanoff, M., Kertesz-Rahn, E. & Zimmerman, L.E. Histopathology of juvenile retinoschisis. *Arch. Ophthalmol.* **79**, 49–53 (1968).
42. Condon, G.P., Brownstein, S., Wang, N.S., Kearns, J.A. & Ewing, C.C. Congenital hereditary (juvenile X-linked) retinoschisis: histopathologic and ultrastructural findings in three eyes. *Arch. Ophthalmol.* **104**, 576–583 (1986).
43. Molday, R.S., Hicks, D. & Molday, L. Peripherin: a rim-specific membrane protein of rod outer segment discs. *Invest. Ophthalmol. Vis. Sci.* **28**, 50–61 (1987).
44. Felbor, U., Schilling, H. & Weber, B.H.F. Adult vitelliform macular dystrophy is frequently associated with mutations in the peripherin/RDS gene. *Hum. Mutat.* (in the press).
45. Weber, B.H.F., Vogt, G., Pruett, R.C., Stöhr, H. & Felbor, U. Mutations in the tissue inhibitor of metalloproteinases-3 (TIMP3) in patients with Sorsby's fundus dystrophy. *Nature Genet.* **8**, 352–356 (1994).
46. Allikmets, R. *et al.* A photoreceptor cell-specific ATP-binding transporter gene (ABCR) is mutated in recessive Stargardt macular dystrophy. *Nature Genet.* **15**, 236–246 (1997).
47. Church, C.M. & Gilbert, W. Genomic sequencing. *Proc. Natl. Acad. Sci. USA* **81**, 1991–1995 (1984).
48. Chomczynski, P. & Sacchi, N. Single-step method of RNA isolation by acid guanidinium-thiocyanate-phenol-chloroform extraction. *Anal. Biochem.* **162**, 156–159 (1987).
49. Ewing, C.C. & Ives, E.J. Juvenile hereditary retinoschisis. *Trans. Ophthalmol. Soc. UK* **89**, 29–39 (1970).
50. Genetics Computer Group. Program Manual for Wisconsin Package, Version 9, Madison, Wisconsin, 1996.
51. Corpet, F. Multiple sequence alignment with hierarchical clustering. *Nucleic Acids Res.* **16**, 10881–10890 (1988).
52. Fukuzawa, M. & Ochiai, H. Molecular cloning and characterization of the cDNA for discoidin II of *Dictyostelium discoideum*. *Plant Cell Physiol.* **37**, 505–514 (1996).

6. Anlage 6

First molecular evidence
for a de novo mutation in RS1 (XLRS)
associated with X-linked juvenile retinoschisis

J. Med. Genet. 36: 932-934

First molecular evidence for a de novo mutation in *RS1* (*XLRS1*) associated with X linked juvenile retinoschisis

EDITOR—Juvenile retinoschisis (RS, OMIM 312700) is an X linked recessive vitreoretinal disorder that variably affects visual acuity because of microcystic degeneration of the central retina.[1 2] In approximately 50% of affected males, peripheral schisis may also occur. Major sight threatening complications include vitreal haemorrhages, retinal detachment, and neovascular glaucoma.[3]

Recently, the gene underlying RS, designated *RS1* (also called *XLRS1*), was positionally cloned[4] and more than 80 different mutations covering a wide mutational spectrum, including intragenic deletions, splice site, frameshift, nonsense, and missense mutations, were identified.[4–7] Interestingly, missense mutations mainly cluster in exons 4 to 6 of the *RS1* gene known to encode a highly conserved discoidin domain thought to be involved in cell-cell interactions on membrane surfaces.[8]

The high recurrence rate of some of the *RS1* mutations (for example, Glu72Lys in more than 34 patients from different ethnic backgrounds) suggests a significant de novo mutation rate in RS.[8] In this report, we provide the first molecular evidence of a de novo *RS1* mutation (Pro203Leu) in a Greek family. The Pro203Leu mutation is present in two brothers diagnosed with severe features of RS at the ages of 9 and 5 years, respectively. We show that the mother is a heterozygous carrier while neither of the maternal grandparents carry the Pro203Leu mutation. Haplotyping data from several polymorphic DNA loci flanking the *RS1* gene confirm paternity and strongly suggest that the Pro203Leu mutation originated on the X chromosome of the maternal grandfather.

Two brothers were referred to one of the authors (BL) presenting with unclassified vitreoretinal degeneration in both eyes. By history, retinal detachment had been diagnosed in the right eye in the older (III.1) at the age of 9 months. At the age of 9 years, best corrected visual acuity was 20/200 in the right eye (RE) and 20/40 in the left eye (LE). Fundoscopy showed a bullous peripheral schisis and a flat schisis at the entire posterior pole with inner leaf hole formation in the RE. In the LE, a macular schisis with marked vitreous veils could be seen. Electroretinogram (ERG) recordings corresponding to the ISCEV Standard were consistent with the diagnosis of RS, that is, rod response was unrecordable in the RE and residual in the LE, there was a negative maximal response, and an unrecordable cone response in both eyes.

In the younger brother (III.2), bullous cyst-like retinal changes in both eyes had been diagnosed at the age of 1 year. Four years later fundoscopy showed a bullous retinal detachment in the inferotemporal retina of the RE including the macula with some cystic changes in the area of the inferior temporal vascular arcade. In the LE, only pigmentary abnormalities and whitish subretinal deposits consistent with a collapsed schisis could be seen. Best corrected visual acuity was light perception RE and 2/100 LE. Because of severe nystagmus and reduced compliance, the ERG was not recorded.

Fundus examination and ERG were normal in the mother (II.1) and maternal grandfather (I.2).

Genomic DNA from the members of the Greek family was extracted using standard techniques. Haplotyping was done using microsatellite markers 207F/R (DXS207), 389gt, 418F/R (DXS418), and RX324 (DXS443) closely flanking the RS locus (table 1).[9–11] Microsatellite marker 389gt was identified in PAC clone dJ389A20 as a $(CA)_{30}$ dinucleotide repeat located 50 kb distal to DXS418 (genomic sequence available at http://www.sanger.ac.uk/). The repeat sequences were PCR amplified in the presence of ^{32}P-dCTP (3000 Ci/mmol) using flanking oligonucleotide primers and conditions as given in the references (table 1). To confirm paternity, an additional two highly polymorphic microsatellite markers at the *ATM* locus on 11q23 and the *BRCA1* locus on 17q21 (D17S855) were used (table 1).

For mutational analysis, the six exons of the *RS1* gene were PCR amplified from genomic DNA of patients III.1 and III.2 with intronic oligonucleotide primers flanking the respective coding exons and amplification conditions as described previously.[4] Mutation detection was done by single stranded conformational analysis (SSCA). Amplification of the coding exons was carried out with *Taq* polymerase (Gibco BRL) in a 25 µl volume in 1 × PCR buffer supplied by the manufacturer. PCR products were electrophoretically separated on a 6% non-denaturing polyacrylamide gel with or without 5% glycerol at 4°C. DNA fragments showing aberrant mobility shifts as well as the corresponding maternal and grandparental PCR products were directly sequenced using the Thermo Sequenase radiolabelled terminator cycle sequencing kit (Amersham, Life Science).

Prescreening by SSCA of the six coding exons of the *RS1* gene showed a similar aberrant band shift in exon 6 in the two brothers III.1 and III.2 (fig 1 and data not shown). Direct sequencing of PCR products identified a C to T transition at nucleotide position 608 of the cDNA. This is predicted to result in a proline to leucine substitution at codon 203 (fig 1). Subsequently, sequencing of *RS1* exon 6 was performed in the mother, II.1, as well as in both mater-

Table 1 Polymorphic microsatellite markers used in the study

Name	*Locus*	*Primer sequence 1 (5'—3')*	*Primer sequence 2 (5'—3')*	*Reference*
207	DXS207	TCACTCCACATTCTGCCATC	AATTGACAGCCCTTGAGGAG	12
389gt*	RS	AGTGTCTTAGTCCCTGGCTC	TATGGAATTGAGCCAGATCC	This study
418	DXS418	TGTGAGGTTTTGTTCCCTCC	CTGTTGAGTTTCCTCACAGC	13
RX324	DXS443	TTGTTCAAGGGTCAACTG	TTAGTACCTATCAGTCACTA	14
ATMin45†	ATM	TCCTCATTCTAAACAACAACTG	TTACTGAAGGATTTAGGGCT	This study
AFM248YG9	D17S855/BRCA1	ACACAGACTTGTCCTACTGCC	GGATGGCCTTTTAGAAAGTGG	15

*$(CA)_{30}$ dinucleotide repeat derived from PAC clone dJ389A20 (http://www.sanger.ac.uk)
†GenBank Acc No U82828

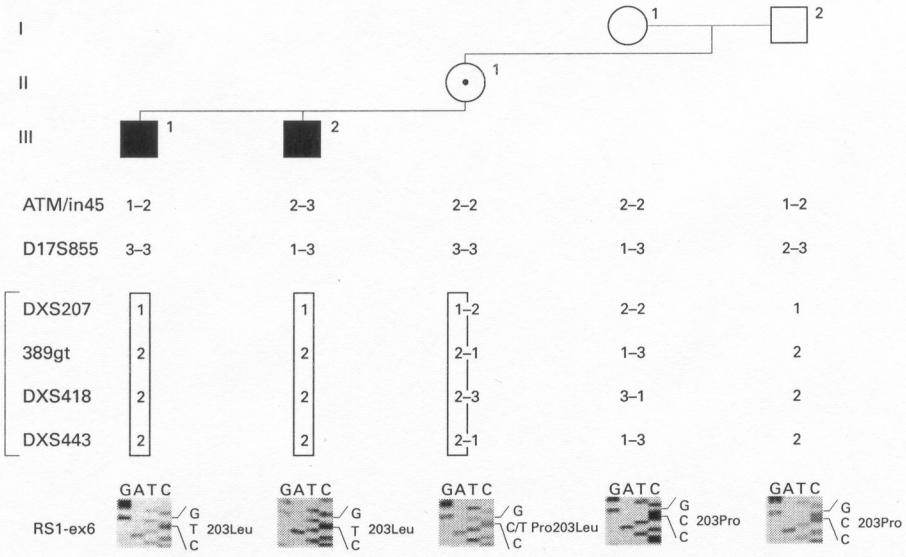

Figure 1 Analysis of a three generation Greek family with two cases of X linked juvenile retinoschisis (III.1 and III.2). Polymorphic markers at the ATM and the BRCA1 locus (D17S855) were used to confirm paternity. Haplotype analysis was performed using microsatellite markers DXS207, 389gt, DXS418, and DXS443 that closely flank the RS1 gene on Xp22.2. The order of markers is from telomere to centromere. Haplotypes associated with the Pro203Leu mutation in exon 6 of the RS1 gene are boxed. Note that the grandfather, I.2, shares the disease associated haplotype with his two grandsons III.1 and III.2 but does not carry the Pro203Leu mutation.

nal grandparents, I.1 and I.2. The mother was heterozygous for the Pro203Leu mutation while neither of the maternal grandparents showed a mutational change (fig 1).

To confirm paternity, genotyping with polymorphic markers ATM/in45 and D17S855 localised within the *ATM* and the *BRCA1* gene, respectively, were performed. Segregation of allelic markers is consistent with the grandfather, I.2, being the father of II.1 (fig 1). In addition, haplotype analysis was done with markers closely flanking the *RS1* locus. A haplotype could be constructed (DXS207-389gt-DXS418-DXS443: 1-2-2-2) which is shared by the carrier mother, II.1, and her two sons, III.1 and III.2, and therefore should be associated with the Pro203Leu mutation (fig 1). The grandfather also carried the 1-2-2-2 haplotype indicating that the Pro203Leu mutation occurred on this haplotype.

Here, we describe a de novo missense mutation in the RS1 gene, Pro203Leu, that is associated with severe features of X linked juvenile retinoschisis (RS) in two Greek brothers. Although the mother is a heterozygous carrier neither of the maternal grandparents have the Pro203Leu mutation. Haplotype analysis with polymorphic markers closely flanking the *RS1* locus provides strong evidence that the Pro203Leu mutation occurred de novo on the X chromosome of the maternal grandfather.

The proline residue at codon 203 of the RS1 protein is part of the evolutionarily highly conserved discoidin domain that is thought to be involved in cell-cell interaction on membrane surfaces.[8] Without exception, the proline residue is retained at this particular position throughout evolution in all proteins containing the discoidin motif.[4 7] In addition, Pro203Leu mutations have independently been identified in affected subjects of three familial RS cases of French and Dutch origin but were not found on 100 additional normal X chromosomes.[7] Together, this strongly suggests that, rather than a polymorphism, the Pro203Leu mutation represents an amino acid change that should severely affect protein function and therefore should be responsible for the RS phenotype in the two Greek brothers.

Haplotype analysis has shown that the maternal grandfather of the two Greek RS patients carries the haplotype that becomes disease associated in his daughter and his two grandsons. This provides strong evidence that the Pro203Leu mutation is in fact a de novo event. It should be pointed out that the Pro203Leu mutation occurred at a CpG dinucleotide (codon 203: CCG to CTG) which, if methylated at the genomic level, is known to be frequently involved in C→T transitions.[16] We cannot exclude that the unaffected grandfather is a mosaic for the Pro203Leu mutation with the mutant genotype being present in one or more tissues, excluding the ocular tissues but including a precursor of the germ cells. Assuming such a situation in the grandfather, the mutation could be transferred to his daughter and would then be perceived as a de novo germinal mutation.

Besides the Greek family, we were able to analyse the segregation of *RS1* mutations in another four pedigrees where RS occurred in a single generation of large families. There was no further evidence of de novo events in the extended families. However, considering the small number of families tested, the present study supports an earlier notion that the new mutation rate in RS may be significant.[7] Further segregation analyses in multigeneration families with "sporadic" or only a few cases of RS will be required to estimate more accurately the frequency of de novo mutations in X linked juvenile retinoschisis.

We thank the patients and their family for their kind cooperation. This work was supported by the Deutsche Forschungsgemeinschaft (We 1259/5-3 and Lo 457/3-1).

ANDREA GEHRIG
BERNHARD H F WEBER
Institut für Humangenetik, Biozentrum, Universität Würzburg, Am Hubland, 97074 Würzburg, Germany

BIRGIT LORENZ
MONIKA ANDRASSI
Abteilung für Kinderophthalmologie, Strabismologie und Ophthalmogenetik, Klinikum der Universität, 93042 Regensburg, Germany

Correspondence to: Dr Weber

1 Condon GP, Brownstein S, Wang N, Kearns AF, Ewing CC. Congenital hereditary (juvenile X-linked) retinoschisis: histological and ultrastructural findings in three eyes. *Arch Ophthalmol* 1986;**104**:576-83.
2 George NDL, Yates JRW, Moore AT. X-linked retinoschisis. *Br J Ophthalmol* 1995;**79**:697-702.
3 Deutman AF. Vitreoretinal dystrophies. In: Krill A, Archer D, eds. *Hereditary retinal and choroidal diseases*. New York: Harper and Row, 1977: 1043-108.
4 Sauer GS, Gehrig A, Warneke-Wittstock R, *et al*. Positional cloning of the gene associated with X-linked juvenile retinoschisis. *Nat Genet* 1997;**17**: 164-70.
5 Hotta Y, Fujiki K, Hayakawa M, *et al*. Japanese juvenile retinoschisis is caused by mutations of the XLRS1 gene. *Hum Genet* 1998;**103**:142-4.
6 Rodriguez IR, Mazuruk K, Jaworski C, Iwata F, Moreira EF, Kaiser-Kupfer MI. Novel mutations in the XLRS1 gene may be caused by early Okazaki fragment sequence replacement. *Invest Ophthalmol Vis Sci* 1998;**39**:1736-9.
7 The Retinoschisis Consortium. Functional implications of the spectrum of mutations found in 234 cases with X-linked juvenile retinoschisis (XLRS). *Hum Mol Genet* 1998;7:1185-92.
8 Baumgartner S, Hofmann K, Chiquet-Ehrismann R, Bucher P. The discoidin domain family revisited: new members from prokaryotes and a homology-based fold prediction. *Protein Sci* 1998;7:1626-31.
9 Pawar H, Bingham EL, Hiriyanna K, Segal M, Richards JE, Sieving PA. X-linked juvenile retinoschisis: localization between (DXS1195, DXS418) and AFM291wf5 on a single YAC. *Hum Hered* 1996;**46**:329-35.
10 Van de Vosse E, Bergen AAB, Meershoek EJ, *et al*. An Xp22.1-p22.2 YAC contig encompassing the disease loci for RS, KFSD, CLS, HYP and RP15: refined localization of RS. *Eur J Hum Genet* 1996;4:101-4.
11 Huopaniemi L, Rantala A, Tahvanainen E, de la Chapelle A, Alitalo T. Linkage disequilibrium and physical mapping of X linked juvenile retinoschisis. *Am J Hum Genet* 1997;**60**:1139-49.
12 Oudet C, Weber C, Kaplan J, *et al*. Characterization of a highly polymorphic microsatellite at the DXS207 locus: confirmation of very close linkage to the retinoschisis disease gene. *J Med Genet* 1993;**30**:300-3.
13 Van de Vosse E, Booms PFM, Vossen RHAM, Wapenaar MC, Van Ommen GJ, Den Dunnen JT. A CA-repeat polymorphism near DXS418 (P122). *Hum Mol Genet* 1993;2:2202.
14 Browne D, Barker D, Litt M. Dinucleotide repeat polymorphisms at the DXS365, DXS443 and DXS451 loci. *Hum Mol Genet* 1992;**1**:213.
15 Dib C, Fauré S, Fizames C, *et al*. A comprehensive genetic map of the human genome based on 5,264 microsatellites. *Nature* 1996;**380**:152-4.
16 Duncan B, Miller J. Mutagenic deamination of cytosine residues in DNA. *Nature* 1980;**287**:560-1.

7. Anlage 7

Assessment of RS1
in X-linked juvenile retinoschisis
and sporadic senile retinoschisis

Clin. Genet. 55: 461-465

Clin Genet 1999: 55: 461–465
Printed in Ireland. All rights reserved

CLINICAL GENETICS
ISSN 0009-9163

Short Report

Assessment of *RS1* in X-linked juvenile retinoschisis and sporadic senile retinoschisis

Gehrig A, White K, Lorenz B, Andrassi M, Clemens S, Weber BHF. Assessment of *RS1* in X-linked juvenile retinoschisis and sporadic senile retinoschisis.
Clin Genet 1999: 55: 461–465. © Munksgaard, 1999

The *RS1* gene is the causative gene in X-linked juvenile retinoschisis (RS). We have screened this gene for mutations in 13 patients with RS and in 7 probands with senile retinoschisis, a sporadic, later-onset form of retinoschisis. Mutations were detected in all RS patients. Of the 11 different mutations identified, six have been reported previously and five are novel. We did not find mutations in any of the senile retinoschisis patients and conclude that senile retinoschisis is not the result of germline mutations in the *RS1* gene.

Andrea Gehrig[a], Karen White[a], Birgit Lorenz[b], Monika Andrassi[b], Stefan Clemens[c] and Bernhard HF Weber[a]

[a] Institut für Humangenetik, Biozentrum, Universität Würzburg, 97074 Würzburg, [b] Abteilung für Kinderophthalmologie, Strabismologie und Ophthalmogenetik, Klinikum der Universität, 93042 Regensburg, [c] Klinik und Poliklinik für Augenheilkunde, Universität Greifswald, 17489 Greifswald, Germany

Key words: mutation analysis – *RS1* – senile retinoschisis – X-linked juvenile retinoschisis

Corresponding author: Bernhard HF Weber, Institut für Humangenetik, Biozentrum, Am Hubland, D-97074 Würzburg, Germany. Fax: + 49 931 8884069; e-mail: bweb@biozentrum.uni-wuerzburg.de

Received 29 December 1998, revised and accepted for publication 10 February 1999

X-linked juvenile retinoschisis (RS; OMIM # 312700) is a rare, early-onset disorder causing progressive visual loss in males. The disease is characterized by schisis, or splitting, of the nerve fiber and ganglion cell layers of the retina (1). Lesions are typically foveal, but 50% of patients also develop a peripheral schisis (2). RS is clinically variable, with symptoms ranging from slightly reduced visual acuity to more significant complications, such as retinal detachment or vitreous hemorrhage. Although the pathogenesis of RS is not well understood, the specific b-wave abnormalities on electroretinogram (ERG) suggest that the disease is due to a defect in the Müller cells, the primary glial cells of the retina that support retinal structure and metabolism (3, 4).

RS1, a retina-specific gene underlying RS pathology, was identified recently using positional cloning methods (5), and 86 different mutations have been described (5–8). A majority of the reported mutations are missense mutations and are located within an evolutionarily conserved discoidin domain that is thought to be involved in cell–cell interaction (9).

Retinoschisis also occurs sporadically in a 'senile' form and is suggested to be a common condition based on findings in one series demonstrating senile retinoschisis in approximately 4% of unselected ophthalmologic patients (10). Clinically, senile retinoschisis is differentiated from RS by an adult onset of symptoms, no specific changes in the macula, an equal sex ratio of affected individuals, a generally good prognosis for visual acuity, and a negative family history (10, 11). Senile retinoschisis is divided into two types, one more benign 'peripheral' form and another more rapidly progressive 'reticular' or 'bullous' form (12). Histologically, the bullous form is similar to RS, whereas the peripheral form is distinct in that the schisis occurs in the outer plexiform layer (12, 13).

An increasing number of genes are being identified in which different mutations in the same gene lead to clinically distinct phenotypes. One example in the group of retinal dystrophies is the ABC transporter (*ABCR*) gene, which is involved in autosomal recessive Stargardt's disease (14), autosomal recessive retinitis pigmentosa (15), cone–rod dystrophy (16), and possibly age-related macular degeneration (17). Similarly, the peripherin/RDS gene is involved in autosomal dominant retinitis pigmentosa (18) and macular dystrophy (19). With this in mind and noticing the similarity in pathology between RS and the bullous senile retinoschisis, we addressed the question of whether the two forms of retinoschisis could be caused by mutations in the same gene.

Our goal is to further understand the role of *RS1* in retinal disease. As mutation analyses have proved important in understanding gene structure and function, we have continued studying the *RS1* gene in an additional 13 RS cases. Simultaneously, we investigated *RS1* in 7 individuals with senile retinoschisis.

Materials and methods

Patients

Peripheral blood was obtained from 13 apparently unrelated males with RS. Diagnostic evaluation included clinical examination, fundoscopy, and ERG recorded corresponding to the ISCEV standards. We have family history information for 11 of the families (Fig. 1). In 7 cases, family history was positive for RS and in the remaining cases there were no other affected family members reported. Additional samples were available in seven families from other affected males, obligate carriers, and unaffected individuals. The families are from Austria (family 11), Germany (families 3, 4, 5, 6, 8, 10, 12, and 13), Great Britain (families 7 and 9), Switzerland (family 2), and the United States (family 1).

Blood was also obtained from 7 individuals with senile retinoschisis. The sample includes both males and females ranging in age from 34 to 72 years. All patients have bullous senile retinoschisis in one or both eyes, and some also show peripheral retinoschisis. Three patients have some degree of retinal detachment and in 1 case this involves the macula. No individual reported a family history of the disease.

Mutation analysis

Genomic DNA was extracted using standard techniques. The six exons of the *RS1* gene and their

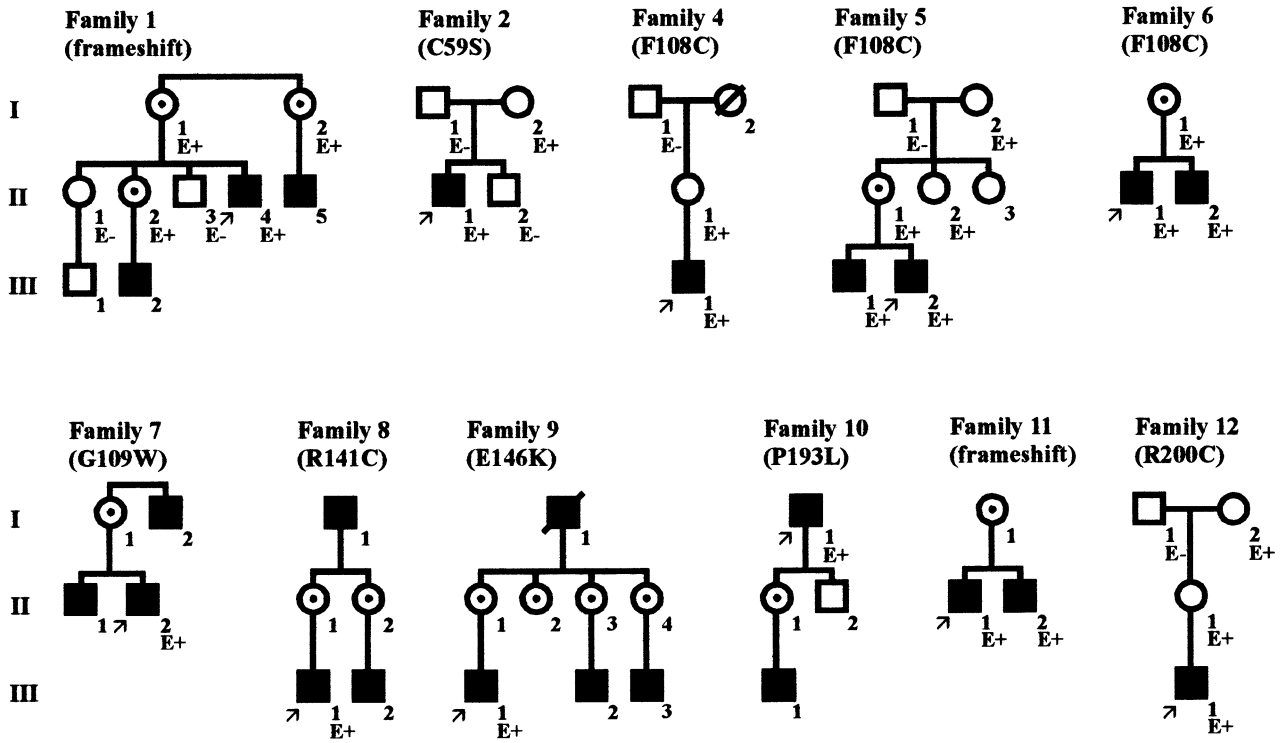

Fig. 1. Partial pedigrees of the RS families studied. Pedigrees are drawn according to standard nomenclature ((23)). Females drawn as carriers are obligate carriers based on family history. E refers to genetic evaluation of the *RS1* gene (+ and − indicate presence versus absence of a mutation). Note that some females drawn as non-carriers (e.g. family 2 I-2) are in fact carriers based on DNA analysis. Mutations are given in parentheses after the family number.

Table 1. Mutations in the *RS1* gene

Family/patient	Family history	Mutation	Amino acid	Exon	Reference
1	Yes	163delA	Frameshift	3	This paper
2	No	T175A	C59S	3	(6)
3	Unknown	C293A	A98E	4	This paper
4	No	T323G	F108C	4	This paper
5	Yes	T323G	F108C	4	This paper
6	Yes	T323G	F108C	4	This paper
7	Yes	G325T	G109W	4	This paper
8	Yes	C421T	R141C	5	(6)
9	Yes	G436A	E146K	5	(6)
10	Yes	C578T	P193L	6	(5)
11	Yes	579insC	Frameshift	6	(6)
12	No	C598T	R200C	6	(6)
13	Unknown	G643A	E215K	6	This paper

flanking sequences were polymerase chain reaction (PCR) amplified using primers and conditions as described previously (5). Single stranded conformational analysis (SSCA) was used to screen for mutations by electrophoretically separating radioactively labeled PCR products on a 6% non-denaturating polyacrylamide gel with or without 5% glycerol at 4°C. DNA fragments with mobility shifts were directly sequenced using the Thermo Sequenase radiolabeled terminator cycle sequencing kit (Amersham, Life Science). For cases in which no mobility shifts were detected by SSCA, all six coding exons were directly sequenced. Additionally, to confirm that all novel missense mutations found in this study are disease associated rather than polymorphisms, the corresponding exons in 72 male controls and 44 female controls were screened by SSCA.

Haplotype analysis

To investigate common ancestry, RS individuals with identical mutations were genotyped with polymorphic markers closely flanking the *RS1* locus. Oligonucleotide primers, PCR conditions, and order of loci DXS418, DXS999, and DXS365 have been reported previously (20). Microsatellite marker 389gt was identified in PAC clone dJ389A20 as a $(CA)_{30}$-dinucleotide repeat located 50 kb distal to DXS418 (genomic sequence available at http://www.sanger.ac.uk/).

Results

Using SSCA and direct DNA sequencing, we detected mutations in all 13 affected RS individuals. There were 11 different mutations identified: nine missense mutations, one deletion, and one insertion (Table 1). Six of the mutations have been described previously (5, 6), and five have not been reported before. Of the five novel mutations, two (F108C and G109W) are located within the discoidin domain, two (A98E and E215K) closely flank the domain, and one is an upstream deletion at nucleotide position 163 (Fig. 2). In the seven families where samples were available from other family members, we were able to confirm segregation of the mutation with the disease (Fig. 1). SSCA of exons 4 and 6 confirmed that none of the four novel missense mutations were present in a total of 160 control X chromosomes.

One mutation, F108C, was found in three German families. Further analysis utilizing the highly polymorphic microsatellite markers, 389gt, DXS418, DXS999, and DXS365, demonstrates segregation of the disease with an identical haplotype (3-2-1-3) in each family (data not shown). This strongly indicates a common founder for the F108C allele.

Simultaneously with the RS patients, all seven senile retinoschisis samples were screened using SSCA. No fragments showed mobility shifts. Subsequent forward and reverse DNA sequencing of all 6 exons of the 7 patients did not detect any alterations.

Discussion

We have identified mutations in all 13 RS families and have described five previously unreported mutations. In agreement with previous studies (5–8), the mutations are located in exons 3–6 and are generally within or closely flanking the conserved discoidin domain (Fig. 3). In our present study, one upstream mutation is a deletion causing an abnormal C-terminus of 70 amino acid residues

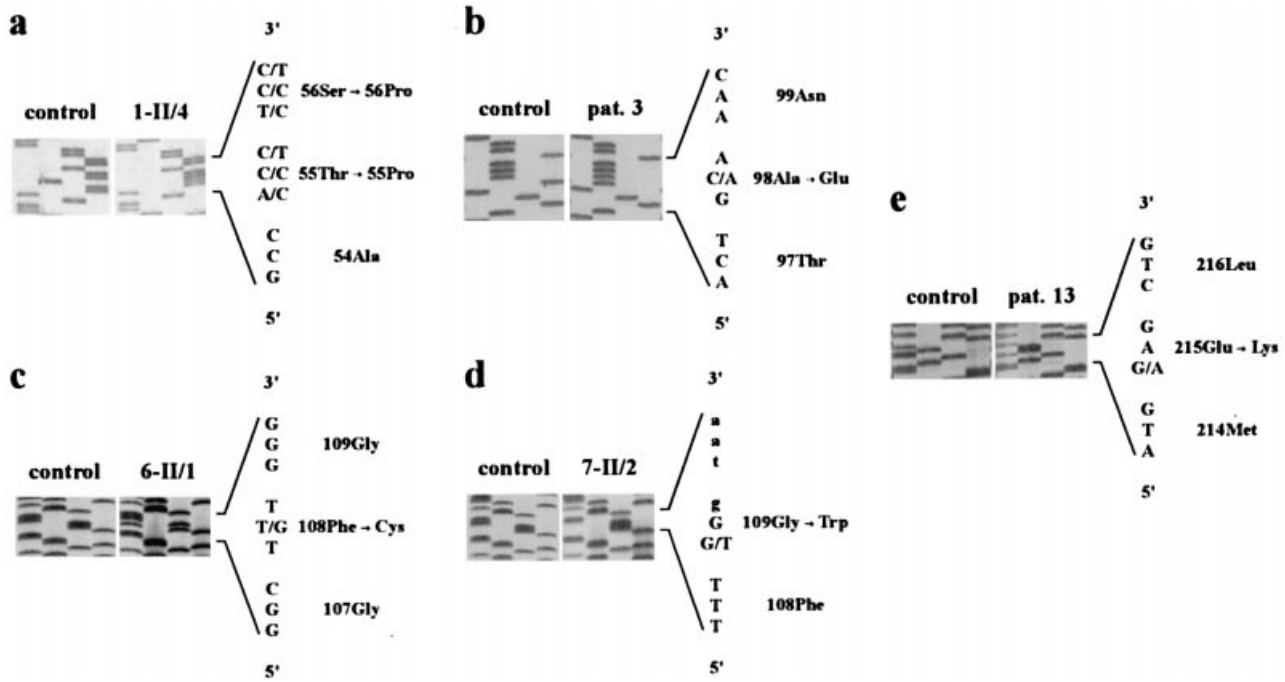

Fig. 2. Mutation analysis showing the five novel sequence alterations found in family 1 (a), patient 3 (b), family 6 (c), family 7 (d), and patient 13 (e). Patient identifications in (a); (c); and (d) refer to pedigree numbering in Fig. 1, whereas patients 3 and 13 represent simplex RS cases.

with a stop at position 125. Another upstream mutation, C59S, destroys a cysteine residue and has been reported previously (6). In total, four mutations involve cysteines, providing further evidence for the importance of these residues for protein structure.

Where possible, we have confirmed the segregation of the mutations with the disease. Looking at the small number of affected males and absence of disease in the more extended family (Fig. 1 and data not shown), we had initially suspected that RS may have arisen in some of the probands by a *de novo* event. Contrary to this, our family studies have demonstrated that for most families these mutations are familial and not *de novo*. In the present study, we have demonstrated that seven out of 11 families for which we have family history information have the mutation in three or more generations (Fig. 1). So far, from all RS cases analyzed in our laboratory, only a single *de novo* mutation in a family of Greek descent has been identified (21).

We were unable to detect any mutations in the 7 RS patients analyzed. However, we cannot entirely exclude an involvement of *RS1* in the pathogenesis of senile retinoschisis for two reasons. One, our analysis was limited to the exons and flanking regions and would not detect large rearrangements or mutations in the introns or promoter regions. Generally, these types of mutations would be expected to result in a truncated or absent protein product and a more severe clinical phenotype rather than a later-onset form. Second, we have not investigated the possibility that *RS1* may be somatically altered in the developing retina. However a mosaic expression of the defect should mimic the situation of a RS carrier female and thus should not lead to a disease phenotype (22). In light of this, we conclude that the *RS1* gene is not directly involved in senile retinoschisis.

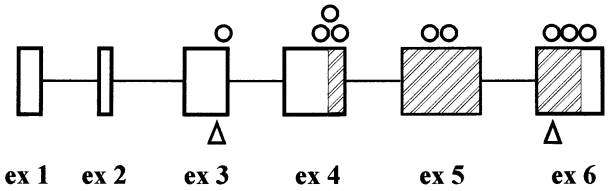

Fig. 3. Schematic representation of the *RS1* gene showing the locations of mutations identified in the present study. Circles represent missense mutations and triangles represent frameshifts. The hatched area indicates the discoidin domain.

Acknowledgements

We would like to thank the families that participated in this study, as well as their referring physicians, including Drs Gyr (Will, Switzerland), Besch (Tübingen, Germany), Rudolph (Munich, Germany), Clarke (Newcastle, UK), Kellner (Berlin, Germany) and Plöchl (Salzburg, Austria). This work was supported by the Deutsche Forschungsgemeinschaft (We 1259/5-3 and Lo 457/3-1).

References

1. Condon GP, Brownstein S, Wang N, Kearns AF, Ewing CC. Congenital hereditary (juvenile X-linked) retinoschisis: Histological and ultrastructural findings in three eyes. Arch Ophthalmol 1986: 104: 576–583.
2. Roesch MT, Ewing CC, Gibson AE, Weber BH. The natural history of X-linked retinoschisis. Can J Ophthalmol 1998: 33: 149–158.
3. Deutman AF. Vitreoretinal dystrophies. In: Krill A, Archer D, eds. Hereditary Retinal and Choroidal Diseases. New York: Harper and Row, 1977: 1043–1108.
4. Reichenbach A, Robinson SR. The involvement of Müller cells in the outer retina. In: Djamgoz MBA, Archer SN, Vallegra S, eds. Neurobiology and Clinical Aspects of the Outer Retina. London: Chapman and Hall, 1995: 395–415.
5. Sauer CS, Gehrig A, Warneke-Wittstock R, Marquardt A, Ewing CC, Gibson A, Lorenz B, Jurklies B, Weber BHF. Positional cloning of the gene associated with X-linked juvenile retinoschisis. Nat Genet 1997: 17: 164–170.
6. Retinoschisis Consortium. Functional implications of the spectrum of mutations found in 234 cases with X-linked juvenile retinoschisis (XLRS). Hum Mol Genet 1998: 7: 1185–92.
7. Hotta Y, Fujiki K, Hayakawa M, Ohta T, Fujimaki T, Tamaki K, Yokoyama T, Kanai A, Hirakata A, Hida T, Nishina S, Azuma N. Japanese juvenile retinoschisis is caused by mutations of the *XLRS1* gene. Hum Genet 1998: 103: 142–144.
8. Rodriguez IR, Mazuruk K, Jaworski C, Iwata F, Moreira EF, Kaiser-Kupfer MI. Novel mutations in the *XLRS1* gene may be caused by early Okazaki fragment sequence replacement. Invest Ophthalmol Vis Sci 1998: 39: 1736–1739.
9. Baumgartner S, Hofmann K, Chiquet-Ehrismann R, Bucher P. The discoidin domain family revisited: new members from prokaryotes and a homology-based fold prediction. Protein Sci 1998: 7: 1626–1631.
10. Byer NE. Clinical study of senile retinoschisis. Arch Ophthalmol 1968: 79: 36–44.
11. Byer NE. Long-term natural history study of senile retinoschisis with implications for management. Ophthalmology 1986: 93: 1127–1137.
12. Foos RY. Senile retinoschisis. Relationship to cystoid degeneration. Trans Am Acad Ophthalmol Otolaryngol 1970: 74: 33–51.
13. Straatsma BR, Foos RY. Typical and reticular degenerative retinoschisis. Am J Ophthalmol 1973: 75: 551–575.
14. Allikmets R, Singh N, Sun H, Shroyer NE, Hutchinson A, Chidambaram A, Gerrard B, Baird L, Stauffer D, Peiffer A, Rattner A, Smallwood P, Li YX, Anderson KL, Lewis RA, Nathans J, Leppert M, Dean M, Lupski JR. A photoreceptor cell-specific ATP-binding transporter gene (*ABCR*) is mutated in recessive Stargardt macular dystrophy. Nat Genet 1997: 15: 236–246.
15. Martinez-Mir A, Paloma E, Allikmets R, Ayuso C, del Rio T, Dean M, Vilageliu L, Gonzalez-Duarte R, Balcells S. Retinitis pigmentosa caused by a homozygous mutation in the Stargardt disease gene *ABCR*. Nat Genet 1998: 18: 11–12.
16. Cremers FP, van de Pol DJ, van Driel M, den Hollander AI, van Haren FJ, Knoers NV, Tijmes N, Bergen AA, Rohrschneider K, Blankenagel A, Pinckers AJ, Deutman AF, Hoyng CB. Autosomal recessive retinitis pigmentosa and cone–rod dystrophy caused by splice site mutations in the Stargardt's disease gene *ABCR*. Hum Mol Genet 1998: 7: 355–362.
17. Allikmets R, Shroyer NF, Singh N, Seddon JM, Lewis RA, Bernstein PS, Peiffer A, Zabriskie NA, Li Y, Hutchinson A, Dean M, Lupski JR, Leppert M. Mutation of the Stargardt disease gene (*ABCR*) in age-related macular degeneration. Science 1997: 277: 1805–1807.
18. Farrar GJ, Kenna P, Jordan SA, Kumar-Singh R, Humphries MM, Sharp EM, Sheils DM, Humphries P. A three-base-pair deletion in the peripherin-RDS gene in one form of retinitis pigmentosa. Nature 1991: 354: 478–480.
19. Wells J, Wroblewski J, Keen J, Inglehearn C, Jubb C, Eckstein A, Jay M, Arden G, Bhattacharya S, Fitzke F, Bird A. Mutations in the human retinal degeneration slow (RDS) gene can cause either retinitis pigmentosa or macular dystrophy. Nat Genet 1993: 3: 213–218.
20. Weber BHF, Janocha S, Vogt G, Sander S, Gibson A, Roesch M, Ewing CC. X-linked juvenile retinoschisis maps between DXS987 and DXS443. Cytogenet Cell Genet 1995: 69: 35–37.
21. Gehrig AE, Lorenz B, Andrassi M, Weber BHF. First molecular evidence for a *de novo* mutation in *RS1* (*XLRS1*) associated with X-linked juvenile retinoschisis. J Med Genet 1999 (in press).
22. George ND, Yates JR, Moore AT. X linked retinoschisis. Br J Ophthalmol 1995: 79: 697–702.
23. Bennett RL, Steinhaus KA, Uhrich SB, O'Sullivan CK, Resta RG, Lochner-Doyle D, Markel DS, Vincent V, Hamanishi J. Recommendations for standardized human pedigree nomenclature. Pedigree Standardization Task Force of the National Society of Genetic Counselors. Am J Hum Genet 1995: 56: 745–752.

8. Anlage 8

Isolation and characterization

of the murine

X-linked juvenile retinoschisis (*Rs1h*) gene

Mamm. Genome 10: 303-307

Mammalian Genome 10, 303–307 (1999).

Mammalian Genome
Incorporating Mouse Genome

Isolation and characterization of the murine X-linked juvenile retinoschisis (*Rs1h*) gene

Andrea E. Gehrig, Regina Warneke-Wittstock, Christian G. Sauer, Bernhard H.F. Weber

Institut für Humangenetik, Biozentrum, Am Hubland, Universität Würzburg, 97074 Würzburg, Germany

Received: 9 September 1998 / Accepted: 17 November 1998

Abstract. X-linked juvenile retinoschisis (RS) is a vitreoretinal degeneration affecting only males. Recently, the RS1 gene underlying this common cause of early vision loss was identified and shown to encode a 224-amino acid precursor protein including a 23-residue leader sequence as well as a highly conserved discoidin motif at the C-terminus. Functional studies in other proteins with discoidin motifs have implicated this domain in phospholipid binding and cell-cell interactions on membrane surfaces. Thus, similar functional properties may exist for RS1 and may be related to the histopathological findings in RS. In order to further pursue the pathophysiology of RS and to understand RS1 function in early eye development, we now report the identification and characterization of the complete murine *Rs1h* gene. The full-length *Rs1h* cDNA was isolated by RT-PCR with degenerate oligonucleotide primers designed from human RS1 cDNA sequences. Subsequently, the exon/intron structure was determined in genomic DNA from mouse strain 129/SvJ. We show that human and murine RS1 coding sequences, exon/intron boundaries, as well as retina-specific expression, are highly conserved between the two species. The conceptual human and murine protein sequences reveal 96% amino acid identity with no amino acid changes within the discoidin domain. In addition, alignment of 5′-flanking sequences upstream of the human and mouse RS1 translation initiation sites identified putative binding sites for several transcription factors including CRX, a homeodomain transcription factor known to activate the transcription of several photoreceptor-specific genes.

Introduction

X-linked juvenile retinoschisis (RS) is a vitreoretinal degeneration characterized by macular pathology and intra-retinal splitting between the nerve-fiber and ganglion cell layer (Yanoff et al. 1968; Manschot 1972; Condon et al. 1986). Generally, loss of visual acuity begins early in life and ranges from mild to severe, with only rare cases approaching legal blindness later in life. The major sight-threatening complications include vitreal hemorrhages, retinal detachments, and neovascular glaucoma (George et al. 1996; Roesch et al. 1998).

In pursuit of the concept of positional cloning (Collins 1995), the RS gene locus was first mapped to distal Xp (Ives et al. 1970) and later refined to an approximately 1-cM region on Xp22.2 between DNA loci DXS418 and DXS999 (Pawar et al. 1996; Van de Vosse et al. 1996; Huopaniemi et al. 1997). By mapping and detailed analysis of expressed sequence tags (ESTs), a retina-specific gene, termed RS1 (alias XLRS1), was identified within the candidate region and shown to be mutated in RS patients (Sauer et al. 1997). Subsequently, a large number of additional RS1 mutations were reported in affected individuals, thus confirming RS1 as the gene underlying X-linked juvenile retinoschisis (Retinoschisis Consortium 1998). The human RS1 gene has an open reading frame of 672 nucleotides and encodes a predicted precursor protein of 224 amino acids, including a 23-residue leader sequence (Sauer et al. 1997). At the C terminus, a discoidin motif that is highly conserved throughout evolution (Kane and Davie 1988; Arai et al. 1989) implicates RS1 in cell-cell interactions such as cell adhesion or cell signalling processes (Sauer et al. 1997).

To further analyze RS1 function and dysfunction in the retina, our current efforts are directed towards the creation of a knock-out model of the corresponding *Rs1h* (retinoschisis 1 homolog) mouse gene. As an initial step, we now report on the isolation and characterization of the *Rs1h* cDNA as well as the genomic structure of the murine gene. Inspection of human and murine putative promoter regions revealed several conserved regulatory sequence elements including a motif known for binding of CRX, a photoreceptor-specific homeodomain transcription factor that regulates the expression of several photoreceptor outer segment proteins such as rhodopsin (Furukawa et al. 1997).

Materials and methods

cDNA cloning. To isolate the coding sequence of the murine *Rs1h* transcript, RT-PCR was performed on total mRNA from mouse eye with Superscript II Reverse Transcriptase (Gibco BRL, Karlsnihe) and degenerate oligonucleotide primers 9orf1 (5′-GTC ACG CAA GAT AGA AGG C-3′) and RSC6R (5′-GAC GCA CTC CAG YTC CAT-3′) designed according to the human RS1 cDNA sequence (Sauer et al. 1997). The resulting 658-bp cDNA fragment was directly cloned into the pCRII cloning vector following the manufacturer's instructions (Invitrogen, Groningen).

Isolation of genomic clones and sequencing. A mouse 129/SvJ genomic phage library (λFIX II-Stratagene, Heidelberg) was screened with the 658-bp cDNA fragment as described (Sambrook et al. 1989). Briefly, the cDNA probe was labeled with [α-^{32}P]dCTP (3000Ci/mmol) following the random hexamer priming method (Feinberg and Vogelstein 1983). After two rounds of purification, four single phage clones were isolated (λ5/1.1, λ5/1.2, λ5′, λ3′), and DNA was extracted by the plate lysate method (Sambrook et al. 1989). Insert sizes were determined by restriction enzyme digestion of phage DNA with *Eco*RI. Partial exon-flanking sequences were obtained with several forward and reverse primers designed from the *Rs1h* cDNA using the Thermo Sequenase radiolabeled terminator cycle sequencing kit (Amersham, Life Science, Freiburg). To estimate sizes of intervening sequences, the Expand™Long Template PCR System (Boehringer, Mannheim) and flanking exonic primers in varying combinations were used for PCR amplification on phage clone DNA.

Determination of the RS1 transcription start sites in human and mouse. The transcription start site in the human RS1 transcript was determined by 5′-RACE with total retinal mRNA (the retinal tissue was

Correspondence to: B.H.F. Weber.

The nucleotide sequence data reported in this paper have been submitted to GenBank and have been assigned the accession numbers AF084561 (complete cDNA sequence), AF084562–AF084567 (exons 1 to 6).

kindly provided by A. Eckstein, University Eye Clinic, Essen), while the murine *Rs1h* transcriptional start was identified by two independent methods including primer extension and 5′-RACE with mRNA from mouse eye. The 5′-RACE System Version 2 (Gibco BRL, Karlstuhe) was used in combination with the following oligonucleotide primers: first-strand primers RSC6R (human) or rs6R (mouse) (5′-GAT GAA GCG GGA AAT GAT GG-3′); first nested primers RSC5R (human) (5′-CTG GTC CTT GTA RTA DAT CCA-3′) or rs5R (mouse) (5′-GCT GCT GTC CTG ATA CTT GG-3); and second nested primers rshm4R (for both human and mouse) (5′-GCG TCG ACT AGT ACC TCC CCT GAC TCG AAA CC-3′). The resulting PCR products were cloned into the pCRII vector (Invitrogen, Groningen) and four to eight individual clones were sequenced.

Following the primer extension method, murine antisense oligonucleotide primer rsm2R (5′-CGA TGA CAA TCC CAA TGT G-3′), which is localized within exon 2 of the *Rs1h* gene, was endlabeled with [γ-^{32}P]ATP (3000 Ci/mmol) and annealed to 1 μg of total mRNA from mouse eye. Reverse transcription was carried out with Superscript II (Gibco BRL, Karlstuhe) at 42°C for 50 min. The resulting products were size fractionated on a 6% polyacrylamide gel next to a [α-^{35}S]ATP-labeled (>1000 Ci/mmol) M13 sequencing ladder to determine the size of the respective extension products.

Computational analysis. Genomic sequences of the 5′ flanking region of the human RS1 gene were available from PAC clone dJ436M11 at the Sanger Centre (http://www.sanger.ac.uk). Repetitive elements were detected by the RepeatMasker program (http://ftp.genome.washington.edu/cgi-bin/RepeatMasker). The BESTFIT program of the Wisconsin GCG9 package was used for optimal sequence alignment of putative human and mouse promoter regions. Putative transcription factor binding sites were identified by the program MatInspector (Quandt et al. 1995) in the TRANSFAC Database (http://transfac.gbf-braunschweig.de/welcome.html; Heinemeyer et al. 1998). Program criteria for database searches were matches to a core sequence of at least 80% and to the entire consensus sequence of at least 85%.

Northern-blot analysis. Total mRNA was isolated from various mouse tissues including skeletal muscle, liver, kidney, spleen, brain, eye, heart, and lung by the guanidinium-thiocyanate method (Chomczynski and Sacchi 1987). In each lane, 12 μg of total RNA was electrophoretically separated in a 1.2% agarose gel in the presence of formaldehyde and blotted onto a nylon membrane. The filter was hybridized with a 436-bp cDNA fragment which was obtained by PCR with *Rs1h*-specific primers rsm3F (5′-TAC CTC CTT AGA CTG TAT TCC-3′) and rs6R. Hybridizations were carried out in 0.5 M sodium phosphate buffer, pH 7.2, 7% sodium dodecyl sulfate (SDS) at 65°C (Church and Gilbert 1984). To test for equal loading and the integrity of the RNA, the Northern blot was hybridized with a 290-bp fragment of the murine β-actin gene.

Results

cDNA cloning and genomic organization of Rs1h. In order to isolate the murine *Rs1h* cDNA, we performed PCR amplification with first-strand cDNAs from reverse-transcribed mouse eye mRNA and degenerate oligonucleotide primers 9orf1/RSC6R designed from the most 5′ and 3′ coding sequences of the human RS1 gene, respectively (Sauer et al. 1997). This resulted in a single PCR fragment 658 bp in size. Sequence analysis and alignment to the human RS1 cDNA revealed a high degree of identity (89%) between the human and mouse cDNA nucleotide sequences. The conceptual *Rs1h* translation product shows 96% sequence identity to the human RS1 protein, differing in only 9 amino acid residues (Fig. 1). In both species, the discoidin motif is present, and there is complete conservation of all amino acid positions within the consensus sequence. Three amino acid changes were identified within the putative secretory leader peptide sequence (amino acid residues 2, 3, and 9) (Fig. 1).

To establish the genomic organization of the *Rs1h* gene, we screened a mouse genomic phage library (constructed from mouse strain 129/SvJ) with a 658-bp *Rs1h* cDNA fragment as probe. Four strongly hybridizing phage clones were isolated, namely, λ5/1.1, λ5/1.2, λ5′, and λ3′. Restriction enzyme mapping demonstrated

```
mouse MPHKIEGFFLLLLFGYEATLGLSSTEDEGEDPWYQKACKCDCQVGANALWSAGATS
      |  ||||| |||||||||||||||||||||||||||||||||.| ||||||||||
human MSRKIEGFLLLLLFGYEATLGLSSTEDEGEDPWYQKACKCDCQGGPNALWSAGATS

mouse LDCIPECPYHKPLGFESGEVTPDQITCSNPEQYVGWYSSWTANKARLNSQGFGCAW
      ||||||||||||||||||||||||||||||||||||||||||||||||||||||||
human LDCIPECPYHKPLGFESGEVTPDQITCSNPEQYVGWYSSWTANKARLNSQGFGCAW

mouse LSKYQDSSQWLQIDLKEIKVISGILTQGRCDIDEWVTKYSVQYRTDERLNWIYYKD
      |||:|||||||||||||||||||||||||||| ||||||||||||||||||||
human LSKFQDSSQWLQIDLKEIKVISGILTQGRCDIDEWMTKYSVQYRTDERLNWIYYKD

mouse QTGNNRVFYGNSDRSSTVQNLLRPPIISRFIRLIPLGWHVRIAIRMELLECASKCA
      ||||||||||||||:|||||||||||||||||||||||||||||||||.||||
human QTGNNRVFYGNSDRTSTVQNLLRPPIISRFIRLIPLGWHVRIAIRMELLECVSKCA
```

Fig. 1. Alignment of the predicted mouse and human RS1 amino acid sequences. Identities (lines), conservative substitutions (colons), and amino acids with similar properties (dots) are indicated.

Table 1. Exon-intron boundaries of Rs1

Exon	Size[a] (bp)	3′ acceptor splice site[b,c]	5′ donor splice site[b,c]	Intron size (kb)
1	52		...AAG gtatgt...	>5
2	26	...tgttcttttgctcag CCA...	...GAG gtatgt...	2.7
3	106	...tctggatgcttgcag GAT...	...CAG gtgagt...	2.2
4	142	...gtttttcctccccag AAT...	...TGG gtaagt...	0.6
5	196	...gtgtgttcctggcag GTC...	...CGG gtaagt...	3.0
6	153	...cctctttctctttag GTC...		

[a] Sizes given refer to the coding portions of the respective exons.
[b] The exonic and intronic sequence are in upper and lower case, respectively.
[c] More detailed intron sequence may be obtained from GenBank submissions (AF084562-AF084567).

that the four clones were overlapping, containing 13, 11, 17, and 16 kb of genomic DNA, respectively (data not shown). Southern blot hybridizations on restriction enzyme-digested phage clone filters with end-labeled primers 9orf1, rsm3F, and rs6R demonstrated that the overlapping clones λ5/1.1, λ5′, and λ3′ contain the entire coding sequences of *Rs1h* (data not shown). Using forward and reverse primers designed from the murine *Rs1h* cDNA, approximately 150 bp of intervening sequences flanking the exons of *Rs1h* as well as 800 bp of the 5′- and 400 bp of 3′-untranslated region were obtained. The overall organization of the murine *Rs1h* gene is highly conserved between mouse and human in that in both species the coding sequences are interrupted by five intervening sequences at identical nucleotide positions within the respective triplet codons. The sizes of the intervening sequences were determined by PCR, with forward and reverse primers flanking the respective introns. Compared with the intron sizes in human (Sauer et al. 1997), the intervening sequences of the mouse *Rs1h* gene have similar but different sizes. In both species, exon 1 is noticeably separated from the rest of the coding exons by more than 5–7 kb of intervening DNA (Table 1).

Analysis of the 5′-regulatory region in human and mouse. The transcription start site of the RS1 transcript was determined for both human and mouse. The analysis of 5′-RACE products indicated at least four different transcriptional start sites for the human RS1 gene at positions −34, −40, −43, and −61 (Fig. 2a). For the murine *Rs1h* transcript, only a single 5′-RACE product was identified mapping the transcriptional start at position −44 (Fig. 2a). With mouse antisense primer rsm2R, extension products were observed at position −27 and −32 (Fig. 2a, Fig. 3). Together, these results suggest multiple transcriptional start sites for both the human and mouse RS1 transcript.

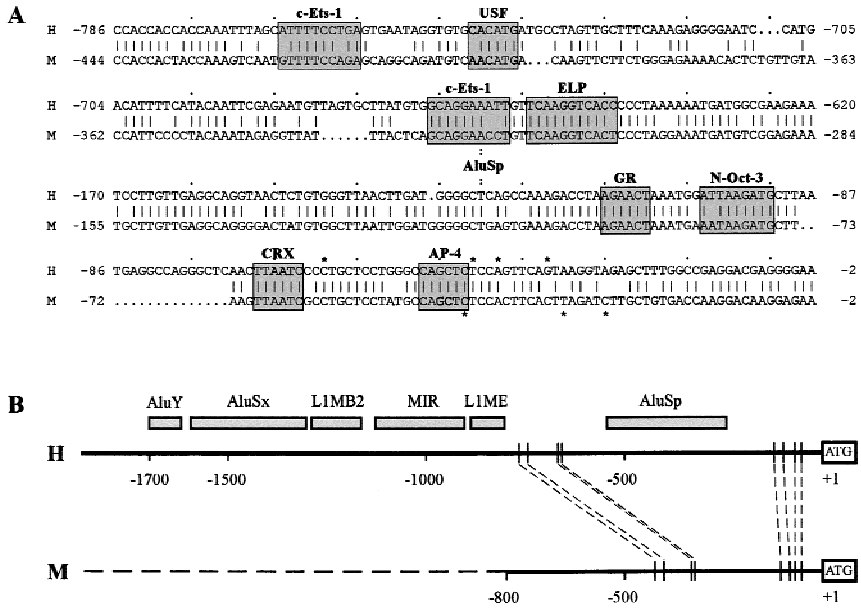

Fig. 2. Comparison between the 5′-flanking regions of the human (H) and murine (M) RS1 gene. **A.** BESTFIT alignment of the nucleotide sequences of the putative promoter regions. Sequence data for the putative human RS1 promoter were taken from the Sanger Centre (http://www.sanger.ac.uk). The asterisks above the human and below the murine sequence denote the transcription start sites as determined by 5′-RACE and primer extension. Putative transcription factor binding sites (boxed) were identified by searching the TRANSFAC Database (http://transfac.gbf-braunschweig.de/welcome.html). **B.** Schematic representation of repeat elements in human (H) and conserved transcription factor binding sites between human and mouse (M) (dotted lines) in their relative position to the ATG start codon of the RS1 gene. Solid lines correspond to known DNA sequences. The murine sequence upstream of nucleotide position −800 (dashed line) was not determined. Shaded boxes indicate the relative extent of the respective repeat elements in the human sequence. Additional information on the nature of the repeats is available at http://ftp.genome.washington.edu/cgi-bin/RepeatMasker.

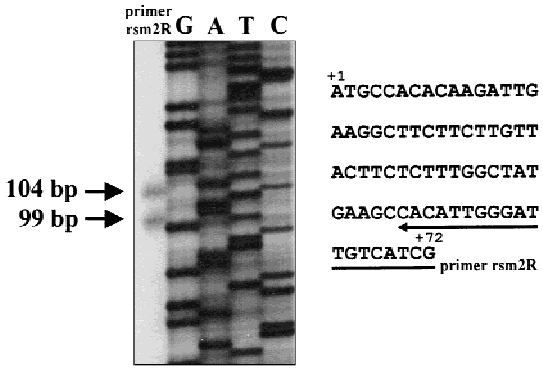

Fig. 3. Determination of the transcriptional start site of the *Rs1h* transcript. Primer extension of end-labeled antisense oligonucleotide primer rsm2R in 1 μg mouse eye total mRNA revealed two products of 104 bp and 99 bp positioning the transcriptional start sites at nucleotide positions −27 and −32. A ^{35}S-labeled M13 sequencing ladder served as size marker.

Regarding the high degree of identity between the human and mouse protein, the regulation of expression should similarly be subjected to strong evolutionary constraints. To search for putative promoter elements, BESTFIT alignment of human and mouse 5′-untranslated sequences upstream the respective translation initiation codon ATG (1.9 kb and 0.8 kb, respectively) was performed. Two regions of interest were found. The more distant region between nucleotide position −444 and −284 of the mouse sequence showed 68.3% identity, whereas the proximal region from mouse nucleotide position −155 to −2 revealed 81.7% identity to the human sequence (Fig. 2a). In human, the two blocks of significant homology to the mouse are interrupted by an insertion of an AluSp repeat element (Fig. 2b). In human, numerous additional repetitive elements are located further upstream of the distal region of sequence conservation (Fig. 2b). Beyond human nucleotide position −1700, we could not identify any further significant sequence similarities with sequences from the mouse 5′-untranslated region (data not shown). The putative promoter region of the human and mouse RS1 transcript does not contain an increased amount of C and G nucleotides. Also, no CpG islands were detected.

Searching the TRANSFAC Database, several possible transcription factor binding sites were identified within the conserved sequences of the putative human and mouse promoter regions (Fig. 2a). Among these were a glucocorticoid response (GR) element, a DNA binding site for the AP4 transcription factor of the basic-helix-loop-helix-zipper family, one N-Oct-3 binding site with tissue specificity in the adult nervous system (Hara et al. 1992; Schreiber et al. 1993), two putative binding sites for c-Ets-1, a transcription factor involved in mesodermal development (Kola et al. 1993), a binding site for the ubiquitously expressed upstream stimulatory factor (USF), and one binding consensus sequence for a transcriptional repressor termed embryonal long terminal repeat-binding protein (ELP). Additionally, a site for a photoreceptor-specific transcription factor, CRX (Chen et al. 1997; Furukawa et al. 1997), was detected at mouse position −69 to −64 (Fig. 2a).

Expression analysis. Northern blot analysis was carried out to determine the expression profile of *Rs1h.* Similar to human (Sauer et al. 1997), mouse *Rs1h* transcription appears restricted to the ocular tissues. Two transcripts, 5.6 kb and 4.9 kb in size were present in mouse eye total mRNA only, but not in the other tissues tested including skeletal muscle, liver, kidney, spleen, brain, heart, and lung (Fig. 4). In analogy to human (Sauer et al. 1997) the two mouse mRNA transcripts may be the result of differential usage of poly A addition sites.

Discussion

Here, we report the identification and characterization of the complete sequence of the murine *Rs1h* gene including the putative promoter region. Several findings strongly suggest that *Rs1h* indeed is the mouse ortholog of the recently identified human RS1 gene (Sauer et al. 1997). First, nucleotide sequence analysis revealed a high degree of identity of almost 90% within the coding sequences of the two genes. Second, the exon/intron organization is strictly conserved in both species with triplet codons interrupted by intervening sequences at identical nucleotide positions. Third, the putative promoter regions of the two genes are highly conserved with sequence identities of up to 82%. Interestingly, an Alu insertion into the human promoter must have occurred during evolution, thus splitting the region of human/mouse homologies in a more proximal and more distal part in the human promoter. Finally, the expression profile in mouse and human is very similar in that transcription of both genes appears to be restricted to the ocular tissues. Together, these results suggest that the murine *Rs1h* gene has been highly conserved structurally as well as functionally

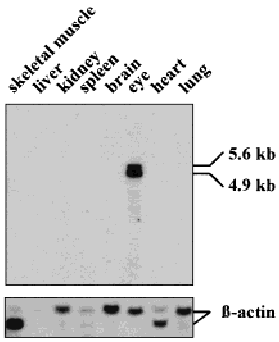

Fig. 4. Northern blot analysis of the murine *Rs1h*. Two abundant transcripts of 5.6 kb and 4.9 kb were detected in total mRNA from mouse eye with a 436-bp cDNA fragment representing exons 3 to 6 of *Rs1h*. To test for equal loading and RNA integrity, the Northern blots were subsequently hybridized with a mouse β-actin probe.

throughout evolution. Therefore, the mouse appears to represent an excellent model system to further study RS1 function.

As in human, mouse *Rs1h* transcripts are present in two different-sized mRNA species. Overall, the murine transcripts are larger (4.9 kb and 5.6 kb) than their human counterparts (1.1 kb and 3.1 kb; Sauer et al. 1997). Since 5′-RACE and primer extension experiments have limited the transcriptional start for the murine *Rs1h* transcript to a narrow region between nucleotide position −44 and −27, the two mRNA species in the mouse probably arise owing to the usage of different poly A addition signals in the 3′-untranslated region. A similar mechanism has already been demonstrated to give rise to two human RS1 transcripts, 1.1 kb and 3.1 kb in size (Sauer et al. 1997).

Alignment of the putative human and mouse RS1 promoter regions revealed several putative transcription factor binding sites, of which the consensus binding element GATTAA of the photoreceptor-specific trans-acting factor CRX, encoded by the cone-rod homeobox-containing gene (Chen et al. 1997; Furukawa et al. 1997), might be most interesting in light of RS1 transcriptional activity in human and mouse retinal tissues. CRX has been shown to transactivate the expression of many, if not all, rod and cone outer segment proteins (for example, rhodopsin, interphotoreceptor retinoid binding protein [IRBP], cone opsin, arrestin; for references see Furukawa et al. 1997). In the case of IRBP, a combination of the CRX-binding element and the retina-specific AATTAG element (Ret-1/PCE-I) is thought to confer partial tissue specificity of IRBP gene expression (Boatright et al. 1997). Within the putative promoter region of the human and mouse RS1 gene, the CRX-binding element is present in reverse and complementary orientation, but does not appear to be in combination with a Ret-1/PCE-I element. Further promoter studies are required to demonstrate possible CRX function in tissue-specific regulation of RS1 expression. However, if confirmed, it would point to the possibility that RS1 may be expressed as early as mouse embryonal day E12.5 when CRX transcription is first detected in the retina (Furukawa et al. 1997). In this context, it is interesting to note that we have also identified two conserved binding sites for c-Ets-1 in the putative RS1 promoter. In adults, Ets-1 expression is restricted to lymphoid cells, whereas this factor is widely expressed during embryonal development (Kola et al. 1993). In neonatal development, expression is reduced to lymphoid organs and brain. Thus, it is suggested that Ets-1 plays an important role in morphogenetic development (Kola et al. 1993). Taken together, our preliminary data on the conserved transcription factor binding sites in the human and mouse RS1 promoter are consistent with a role of RS1 in early retinal morphogenesis (Sauer et al. 1997).

The characterization of the complete *Rs1h* gene from mouse strain 129/CvJ will greatly facilitate future studies of RS1 regulation and function and should further contribute to the understanding of the mechanism(s) underlying X-linked juvenile retinoschisis.

Acknowledgments. We thank H. Schrewe for kindly providing genomic phage library from mouse strain 129/CvJ and M. Gessler for critical comments and suggestions to the manuscript. This work was supported by the Deutsche Forschungsgemeinschaft (DFG) (We1259/5-3). C.G. Sauer is a doctoral fellow supported by a studentship from the Pro Retina Deutschland e.V.

References

Arai M, Scandella D, Hoyer LW (1989) Molecular basis of factor VIII inhibition by human antibodies. Antibodies that bind to the factor VIII light chain prevent the interaction of factor VIII with phospholipid. J Clin Invest 83, 1978–1984

Boatright JH, Borst DE, Peoples JW, Bruno J, Edwards CL et al. (1997) A major cis activator of the IRBP gene contains CRX-binding and Ret-1/PCE-I elements. Mol Vis 3, 15 (http://www.emory.edu/molvis/v3/boatright)

Chen SM, Wang QL, Nie ZQ, Sun H, Lennon G et al. (1997) Crx, a novel Otx-like paired-homeodomain protein, binds to and transactivates photoreceptor cell-specific genes. Neuron 19, 1017–1030

Chomczynski P, Sacchi N (1987) Single-step method of RNA isolation by acid guanidinium thiocyanate-phenol-chloroform extraction. Anal Biochem 162, 156–159

Church CM, Gilbert W (1984) Genomic sequencing. Proc Natl Acad Sci USA 81, 1991–1995

Collins FS (1995) Positional cloning moves from perditional to traditional. Nat Genet 9, 347–350

Condon GP, Brownstein S, Wang NS, Kearns JA, Ewing CC (1986) Congenital hereditary (juvenile X-linked) retinoschisis: histopathologic and ultrastructural findings in three eyes. Arch Ophthalmol 104, 576–583

Feinberg AP, Vogelstein B (1983) A technique for radiolabeling DNA restriction fragments to high specificity. Anal Biochem 132, 6–13

Furukawa T, Morrow EM, Cepko CL (1997) *Crx*, a novel *otx*-like homeobox gene, shows photoreceptor-specific expression and regulates photoreceptor differentiation. Cell 91, 531–541

George ND, Yates JR, Moor AT (1996) Clinical features in affected males with X-linked retinoschisis. Arch Ophthalmol 114, 274–280

Hara Y, Rovescalli AC, Kim Y, Nirenberg M (1992) Structure and evolution of four POU domain genes expressed in mouse brain. Proc Natl Acad Sci USA 89, 3280–3284

Heinemeyer T, Wingender E, Reuter I, Hermjakob H, Kel AE et al. (1998) Databases on transcriptional regulation: TRANSFAC, TRRD, and COMPEL. Nucleic Acids Res 26, 362–367

Huopaniemi L, Rantala A, Tahvanainen E, De la Chapelle A, Alitalo T (1997) Linkage disequilibrium and physical mapping of X linked juvenile retinoschisis. Am J Hum Genet 60, 1139–1149

Ives EJ, Ewing CC, Innes R (1970) X-linked juvenile retinoschisis and Xg linkage in five families. Am J Hum Genet 22, A17–A18

Kane WH, Davie EW (1988) Blood coagulation factors V and VIII: structural and functional similarities and their relationship to hemorrhage and thrombic disorders. Blood 71, 539–555

Kola I, Brookes S, Green AR, Garber R, Tymms M et al. (1993) The Ets1 transcription factor is widely expressed during murine embryo development and is associated with mesodermal cells involved in morphogenetic processes such as organ formation. Proc Natl Acad Sci USA 90, 7588–7592

Manschot WA (1972) Pathology of hereditary juvenile retinoschisis. Arch Ophthalmol 88, 131–138

Pawar H, Bingham EL, Hiriyanna K, Segal M, Richards JE et al. (1996) X-linked juvenile retinoschisis: localization between (DXS1195, DXS418) and AFM291wf5 on a single YAC. Hum Hered 46, 329–335

Quandt K, Frech K, Karas H, Wingender E, Werner T (1995) MatInd and MatInspector—new fast and versatile tools for detection of consensus matches in nucleotide sequence data. Nucleic Acids Res 23, 4878–4884

Retinoschisis Consortium (1998) Functional implications of the spectrum of mutations found in 234 cases with X-linked juvenile retinoschisis (XLRS). Hum Mol Genet 7, 1185–1192

Roesch MT, Ewing CC, Gibson AE, Weber BHF (1998) The natural history of X-linked retinoschisis. Can J Ophthalmol 33, 149–158

Sambrook J, Fritsch EF, Maniatis T (1989) *Molecular Cloning: A Laboratory Manual* (Cold Spring Harbor, N.Y.: Cold Spring Harbor Laboratory Press)

Sauer CG, Gehrig A, Warneke-Wittstock R, Marquardt A, Ewing CC et al. (1997) Positional cloning of the gene associated with X-linked juvenile retinoschisis. Nat Genet 17, 164–170

Schreiber E, Tobler A, Malipiero U, Schaffner W, Fontana A (1993) cDNA cloning of human N-Oct3, a nervous-system specific POU domain transcription factor binding to the octamer DNA motif. Nucleic Acids Res 21, 253–258

Van de Vosse E, Bergen AAB, Meershoek EJ Oosterwijk JC, Gregory S et al. (1996) An Xp22.1-p22.2 YAC contig encompassing the disease loci for RS, KFSD, CLS, HYP and RP15: refined localization of RS. Eur J Hum Genet 4, 101–104

Yanoff M, Kertesz-Rahn E, Zimmermann LE (1968) Histopathology of juvenile retinoschisis. Arch Ophthalmol 79, 49–53

9. Anlage 9

Inactivation of the murine X-linked juvenile retinoschisis gene, *Rs1h*, suggests a role of retinoschisin in retinal cell layer organization and synaptic structure

Proc. Nat. Acad. Sci. 99: 6222-6227

Inactivation of the murine X-linked juvenile retinoschisis gene, Rs1h, suggests a role of retinoschisin in retinal cell layer organization and synaptic structure

Bernhard H. F. Weber*†, Heinrich Schrewe‡§, Laurie L. Molday¶, Andrea Gehrig*, Karen L. White*, Mathias W. Seeliger‖, Gesine B. Jaissle‖, Christoph Friedburg‖, Ernst Tamm, and Robert S. Molday¶**

*Institute of Human Genetics, Biocenter, University of Würzburg, D-97074 Würzburg, Germany; ‡School of Biosciences, University of Birmingham, Edgbaston, Birmingham B15 2TT, United Kingdom; §Department of Developmental Biology, Max-Planck Institute of Immunobiology, D-79108 Freiburg, Germany; ¶Department of Biochemistry and Molecular Biology and Department of Ophthalmology, University of British Columbia, Vancouver, British Columbia, Canada V6T 1Z4; ‖Retinal Electrodiagnostics Research Group, Department of Pathophysiology of Vision and Neuro-ophthalmology, University of Tübingen, D-72076 Tübingen, Germany; and **Department of Anatomy, University of Erlangen, 91058 Erlangen, Germany

Edited by Jeremy Nathans, Johns Hopkins University School of Medicine, Baltimore, MD, and approved March 12, 2002 (received for review October 5, 2001)

Deleterious mutations in *RS1* encoding retinoschisin are associated with X-linked juvenile retinoschisis (RS), a common form of macular degeneration in males. The disorder is characterized by a negative electroretinogram pattern and by a splitting of the inner retina. To gain further insight into the function of the retinoschisin protein and its role in the cellular pathology of RS, we have generated knockout mice deficient in *Rs1h*, the murine ortholog of the human *RS1* gene. We show that pathologic changes in hemizygous *Rs1h*$^{-/Y}$ male mice are evenly distributed across the retina, apparently contrasting with the macula-dominated features in human. Similar functional anomalies in human and *Rs1h*$^{-/Y}$ mice, however, suggest that both conditions are a disease of the entire retina affecting the organization of the retinal cell layers as well as structural properties of the retinal synapse.

X-linked juvenile retinoschisis (RS) is a common form of macular degeneration in males (1–3). It is characterized by a splitting within the retina at the level of the nerve fiber and ganglion cell layers, resulting in cystic degeneration of the central retina but also may involve the periphery, predominantly the inferotemporal quadrant of the fundus (4–7). Severely affected persons may be blind at birth, although generally the clinical course is more benign, with only a moderate decrease in visual acuity (1). In advanced stages, complications may occur and include vitreal hemorrhages, retinal detachment, and neovascular glaucoma (8). The brief-flash electroretinogram (ERG) of affected males exhibit normal or near normal a-wave amplitudes suggestive of preserved rod and cone photoreceptor systems but substantially reduced b-waves, indicating loss of bipolar cell activity (9).

The gene causing RS was identified by positional cloning (10) and encodes a retina-specific polypeptide of 24 kDa, termed retinoschisin, that is secreted as a disulfide-linked oligomeric protein complex from both the rod and cone photoreceptors and the bipolar cells (11, 12). The protein consists almost exclusively of a discoidin-like domain first characterized in the *Dictyostelium discoideum* protein discoidin I (ref. 13). Discoidin domains are found in a large family of secreted or membrane-bound proteins and have been implicated in cell adhesion and cell–cell interaction (14, 15).

To gain further insight into the function of retinoschisin and its role in the cellular pathology of RS, we have generated knockout mice deficient in *Rs1h*, the murine ortholog of *RS1* (ref. 16). Histologically, we found a marked splitting of the inner nuclear layer, overall disorganization of the retinal cell layers with irregular displacement of cells, and later degeneration of the photoreceptors that appears more pronounced in cones. These findings are supported by *in vivo* imaging, electrodiagnostic data, immunolabeling studies, and transmission electron microscopy. In the *Rs1h*$^{-/Y}$ retina, we observed disturbed vectorial transport of MAGUK protein PSD-95 to the outer and inner plexiform layers, where the X-linked juvenile retinoschisis-1 (Rs1h) protein is ordinarily present in high amounts. Our findings suggest that, via its discoidin domain, retinoschisin may directly or indirectly be involved in retinal cell-layer architecture and synaptic structure.

Methods

Construction of the Rs1h Gene-Targeting Vector. Parts of the 5′ (intron 2 to exon 3) and 3′ (exon 4 to intron 5) genomic regions of the murine *Rs1h* gene were amplified from CJ7 embryonic stem (ES) cell DNA (17) with PCR primers rsmint2FGGG (5′-GGG AGT CGA CTG AGT GGA AAG GCA GGT CT-3′)/rsm3R (5′-TGG AAT ACA GTC TAA GGA GG-3′) and rsm4F (5′-CCA ACC CAG AGC AGT ATG TG-3′)/rsm6R (5′-GAT GAA GCG GGA AAT GAT GG-3′), respectively. The *lacZ* gene was cloned in-frame into exon 3 as part of a bpA-*PGK-neo*^{r}-bpA cassette, resulting in a final targeting construct in which the cassette is flanked by the 5′ (2.4 kb) and 3′ (3.5 kb) sequences homologous to the wild-type (wt) allele (Fig. 1*a*). Thereby, parts of exons 3 and 4, as well as the entire intron 3, were deleted in the targeting construct. Before electroporation, the resulting plasmid was linearized with *Sma*I.

Generation of Rs1h-Deficient Mice. CJ7 ES cells were electroporated and selected as described (17). DNA was isolated from 300 colonies according to published methods (18). Positive homologous recombination was identified by Southern blot analysis by using 5′ and 3′ probes external to the targeting construct generated with primer pairs rsm2F (5′-CAC ATT GGG ATT GTC ATC G-3′)/rsmint2R (5′-GGC TTC AGG AGT AGG GTA TC-3′) and rsm3′pF (5′-TGT AGC AAC CAT CCA ATA GG-3′)/rsm3′pR (5′-ATG TCC TCG TAT GTG CTA AG-3′), respectively, as well as by PCR with primer pairs rsm2F/lacZR2

Abbreviations: RS, X-linked juvenile retinoschisis; ERG, electroretinography; ES, embryonic stem; wt, wild type; POS, photoreceptor outer segments; Rs1h, X-linked juvenile retinoschisis-1, homologue; SLO, scanning-laser ophthalmoscopy; INL, inner nuclear layer; IPL, inner plexiform layer; OPL, outer plexiform layer.

†To whom reprint requests should be addressed at: Institute of Human Genetics, Biocenter, Am Hubland, D-97074 Würzburg, Germany. E-mail: bweb@biozentrum.uni-wuerzburg.de.

The publication costs of this article were defrayed in part by page charge payment. This article must therefore be hereby marked "*advertisement*" in accordance with 18 U.S.C. §1734 solely to indicate this fact.

 www.pnas.org/cgi/doi/10.1073/pnas.092528599

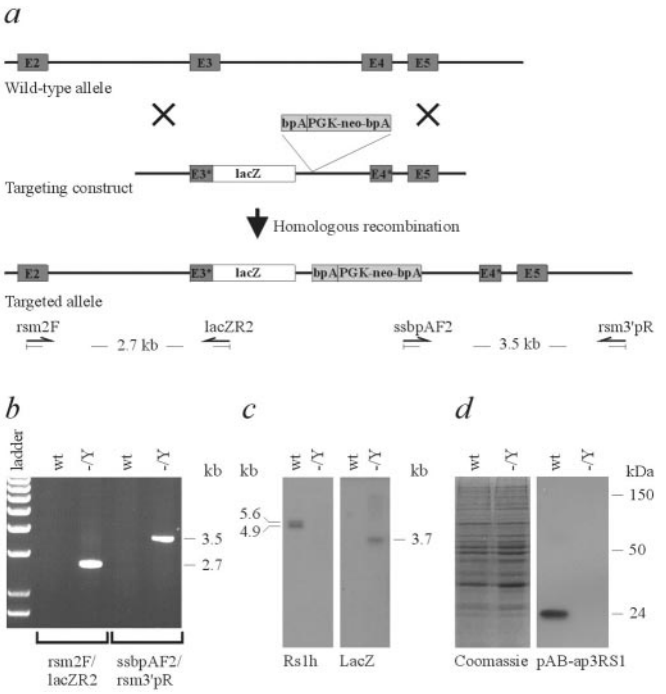

Fig. 1. Targeted disruption of exon 3 of the *Rs1h* gene. (*a*) In the targeting construct, 1 bp of exon 3 (E3*), all of intron 3, and 66 bp of exon 4 (E4*) are deleted and replaced with a *lacZ-neo*^{r} cassette. (*b*) PCR amplification demonstrates the correct targeting of *Rs1h*. The relative positions of oligonucleotide primers and expected product sizes are given in *a*. (*c*) By using a probe spanning exons 4 to 6 of *Rs1h*, Northern blot analyses reveal the expected 5.6- and 4.9-kb transcripts in eye total RNA from the wt (wt) but not from the *Rs1h* knockout (−/Y) male mouse. Subsequent hybridization with a *lacZ* probe exhibits a fusion transcript of 3.7 kb only in the Rs1h-deficient animal. (*d*) Western blot analysis using eye cup protein extracts. Polyclonal antibody pAB-ap3RS1 labels the 24-kDa RS1 protein in WT mice. With the same antibody, the expected fusion protein of 120 kDa is not observed in mutant males, although it contains the antibody epitope, thus indicating that the targeted allele represents a true null allele. Equal loading of protein extracts is demonstrated by Coomassie staining.

(5′-CAA GGC GAT TAA GTT GGG TAA C-3′) and ssbpAF2 (5′-AGA GCT CCG CGG CTC GAC TGT GCC TTC TAG TT-3′)/rsm3′pR (Fig. 1 *a* and *b*). The injection of mutant ES cells into C57BL/6 blastocysts (19) resulted in five high-percentage coat-color chimeras, two of which exhibited germline transmission when bred to C57BL/6 females. Female F1 animals heterozygous for the *Rs1h* mutation were intercrossed with C57BL/6 mice to generate hemizygous male offspring.

Northern Blot Analysis. Total RNA from murine eye cups was prepared by using standard techniques. Hybridization probes were generated by RT-PCR, with primers rsm4F/rsm6R encompassing exons 4 to 6 of the *Rs1h* gene and by excision of the recombinant *lacZ* gene. The fragments were randomly labeled in the presence of ^{32}PdCTP (3,000 Ci/mmol; 1 Ci = 37 GBq).

Western Blot Analysis. Polyclonal peptide antibody pAB-ap3RS1 (ref. 12) was affinity purified from rabbit antiserum. Peroxidase-conjugated anti-rabbit IgG was used as a secondary antibody and visualized by using the enhanced chemiluminescence detection system (Amersham Pharmacia).

Scanning-Laser Ophthalmoscopy. Fundus imaging was performed with an HRA scanning-laser ophthalmoscope (SLO) with an infrared wavelength of 835 nm (Heidelberg Instruments, Heidelberg, Germany). The confocal diaphragm of the SLO allows imaging of different planes of the posterior pole, ranging from the surface of the retina down to the retinal pigment epithelium (RPE) and the choroid. Different planes can be viewed sequentially by varying the focus by about ±20 diopters.

Electroretinogram. ERGs were obtained according to reported procedures (20). Briefly, before anesthesia with ketamine (66.7 mg/kg), xylazine (11.7 mg/kg), and atropine (1 mg/kg), the pupils of dark-adapted mice were dilated. The ERG equipment consisted of a Ganzfeld bowl, a DC amplifier, and a PC-based control and recording unit (Toennies Multiliner Vision, Hoechberg, Germany). Band-pass filter cut-off frequencies were 0.1 and 3,000 Hz. Single flash recordings were obtained both under dark-adapted (scotopic) and light-adapted (photopic) conditions. Light adaptation before the photopic session was performed with a background illumination of 30 cd/m^2 for 10 min. Single flash stimulus intensities were increased from 10^{-4} cd·s/m^2 to 25 cd·s/m^2 and divided into 10 steps of 0.5 and 1 log cd·s/m^2. Ten responses were averaged, with an inter-stimulus interval of either 5 s or 17 s (for 1, 3, 10, 25 cd·s/m^2).

Histology and Electron Microscopy. Two-month-old mutant mice and wt littermates were perfusion-fixed via the heart with Ito's fixative (21). After enucleation, the eyes were bisected equatorially and immersed in the same fixative for 24 h. After fixation, the samples were washed overnight in cacodylate buffer, post-fixed with OsO_4, dehydrated, and embedded in Epon (Fa. Roth, Karlsruhe, Germany). Semithin sections (1 μm) were stained with toluidine blue for serial histological analysis. Ultrathin sections were stained with uranyl acetate and lead citrate and viewed with an EM 902 electron microscope (Zeiss).

Immunofluorescence Labeling. For immunofluorescence studies, retina dissected from two-month-old mutant and wt mice were paraformaldehyde-fixed for 1–2 h and subsequently rinsed in PBS containing 10% (wt/vol) sucrose. Cryosections were blocked with PBS containing 0.2% Triton X-100 (PBS-T) and 10% (vol/vol) goat serum for 20 min and labeled overnight with the primary antibody. The samples then were rinsed in PBS and labeled for 1 h with the secondary antibody conjugated to Cy3 (red) or Alexi 488 (green) (Jackson ImmunoResearch). The Rs1 3R10 monoclonal antibody was produced from a mouse immunized with a glutathione *S*-transferase fusion protein containing the LSSTEDEGEDPWYQKAC peptide, corresponding to amino acids 22–39 of the human RS1 precursor protein (10). Cell-specific antibodies used were Rho 1D4 monoclonal antibody to rhodopsin (22), Mab 115A10 monoclonal antibody to rat olfactory bulb (a generous gift of Shinobu C. Fujita, Mitsubishi Kasei Institute of Life Sciences, Tokyo; ref. 23); JH 492 polyclonal antibody to red/green (middle wavelength) cone opsin and JH 455 blue (short wavelength) cone opsin (a generous gift of J. Nathans, Johns Hopkins University, Baltimore), PAN-SAP polyclonal antibody (a generous gift of Craig C. Garner, Department of Neurobiology, Univ. of Alabama, Birmingham) and 7E3–1B8 monoclonal antibody (Affinity BioReagents, Golden, CO) to the postsynaptic density protein 95 (PSD95), and CRALBP polyclonal antibody to cellular retinal binding protein (a generous gift of Jack Saari, Department of Ophthalmology, Univ. of Washington, Seattle; ref. 24). The PAN-SAP and 7E3–1B8 antibodies showed the same labeling pattern, although the PAN-SAP stained mouse retina more intensely.

Cone Photoreceptor Count. The relative number of cone photoreceptor cells was estimated from counts of total cone opsin-labeled cells (JH492 and JH455) in a series of retinal sections through the eyes of three wt and *Rs1h*$^{-/Y}$ mice, respectively.

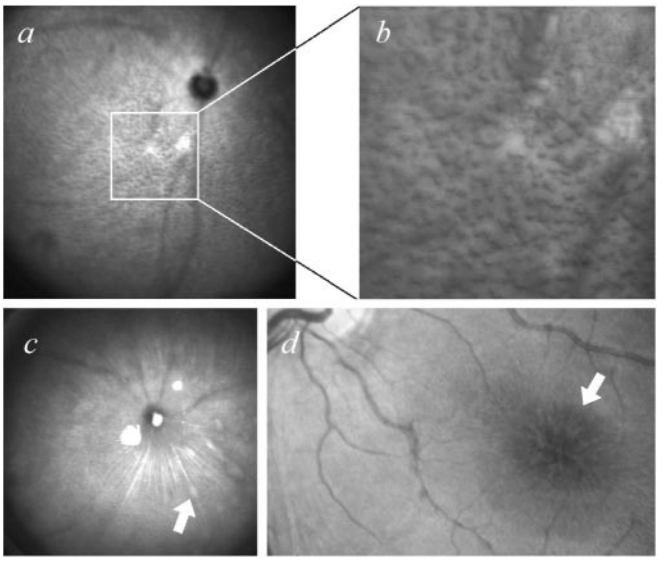

Fig. 2. Macromorphological evaluation of the *Rs1h*$^{-/Y}$ retina with scanning laser ophthalmoscopy. (*a*) Survey of the fundus, demonstrating a layer of cyst-like elevations in the inner retina. (*b*) Optical magnification reveals that the densely packed structures are clearly demarcated from the surrounding normal-appearing regions. (*c*) Focus on the retinal surface shows superficial vessels and the nerve fiber layer. Visible in the lower right quadrant are several larger cysts, one displacing a retinal vessel (arrow). (*d*) Fundus photograph of a patient with RS, featuring typical small macular cysts arranged in a stellate pattern (arrow) and radial striae centered on the fovea. There is an obvious similarity to the appearance of the mouse retina as shown in *b*.

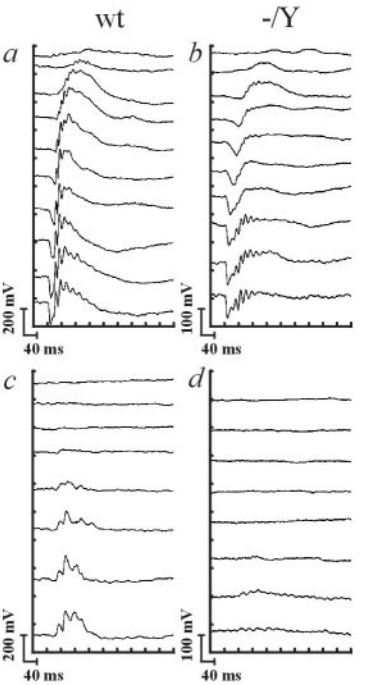

Fig. 3. Electrophysiology of Rs1h$^{-/Y}$ and wt mice. Scotopic intensity series of a wt (*a*) and an Rs1h mutant mouse (*b*). Log light intensities (from top to bottom) were −4, −3, −2, −1.5, −1, −0.5, 0, 0.5, 1, 1.5 log cd·s/m^2. The overall loss of amplitude and the additional selective reduction of the b-wave are clearly visible. Photopic intensity series of a wt control (*c*) and an Rs1h-deficient mouse (*d*). Log light intensities (from top to bottom) were −2, −1.5, −1, −0.5, 0, 0.5, 1, 1.5 log cd·s/m^2. The photopic ERG of the Rs1h$^{-/Y}$ mice is strongly reduced, indicating a much more severe cone than rod dysfunction.

Results

Disruption of the *Rs1h* gene was obtained by introducing a *lacZ* reporter gene in-frame into exon 3 of the *Rs1h* gene together with a neomycin-resistance gene (*neo*) expression cassette under the separate control of the mouse phosphoglycerate kinase gene (*Pgk*) promoter (Fig. 1*a*). Successful germline transmission of the correctly targeted allele was confirmed in the F1 generation by PCR analysis of tail DNA with primers rsm2F/lacZR2 and ssbpAF2/rsm3′pR (Fig. 1 *a* and *b*). Carrier female offspring (*Rs1h*$^{-/+}$) were mated with C57BL/6 male mice to obtain hemizygous *Rs1h*$^{-/Y}$ males whose general appearance was indistinguishable from their wt litter mates. Northern blot analysis of eye cup RNA from 6-week-old mice with an *Rs1h*3′-UTR probe detects 5.6- and 4.9-kb transcripts in wt but not in *Rs1h*$^{-/Y}$ mice, whereas a *lacZ* probe reveals the expected 3.7-kb fusion transcript in the mutant animals (Fig. 1*c*). However, the translation product of the fusion transcript was not detected by Western blot analysis with the pAB-ap3RS1 antibody directed against the N terminus of human retinoschisin (12), indicating that the disrupted *Rs1h* locus represents a true null allele (Fig. 1*d*).

In vivo imaging of 3-month-old *Rs1h*$^{-/Y}$ mice with an SLO revealed a densely packed layer of small cyst-like structures in the inner retina, sometimes extending to the nerve fiber layer (Fig. 2 *a* and *b*). In contrast to the human condition where the cyst formation is largely restricted to the macular area (Fig. 2*d*), their distribution was homogenous across the entire retina (Fig. 2 *a* and *b*). Similar to human, larger cysts were observed in the retinal periphery of *Rs1h*$^{-/Y}$, which, in some instances, displaced superficial retinal vessels (Fig. 2*c*).

Analogous to the "negative ERG" typically observed in human RS (1, 25), dark-adapted (scotopic) ERGs in the *Rs1h*$^{-/Y}$ mice showed a dramatic loss of the positive b-wave, which is mostly shaped by the neurons of the inner retina. Although amplitudes were less than one-half of normal, the negative a-wave representing both inner and outer retinal components was relatively preserved (Fig. 3 *a* and *b*). Under light-adapted (photopic) conditions, ERG responses were virtually absent, suggesting a profound dysfunction of the cone system (Fig. 3 *c* and *d*). A more specific analysis of rod photoreceptor responses using the double flash method (26) did not show detectable abnormalities beyond amplitude reduction (data not shown), indicating that *Rs1h* deficiency does not specifically impair rod function. Taken together, the ERG findings suggest a decrease in the number of functional photoreceptors with the remaining cells responding normally to light stimuli. The additional selective attenuation of the b-wave, in conjunction with the retinal depth estimate of the cyst layer by SLO and previous evidence that retinoschisin is associated with photoreceptors and bipolar cells (12), point to the bipolar cell layer or the bipolar cell/photoreceptor connection as likely sites of pathology in *Rs1h*$^{-/Y}$ mice.

Histologic examination of retina sections from two-month-old wt and *Rs1h*$^{-/Y}$ mice showed striking changes in the inner and outer nuclear layers (INL and ONL) of the mutant animals. Essentially, a pronounced disorganization of the retinal layers was observed, accompanied by a significant reduction in the number of photoreceptor nuclei (Fig. 4 *a–c*). In two Rs1h$^{-/Y}$ eyes, areas with preserved photoreceptor outer segments (POS) were still present at this age (Fig. 4*b*), whereas one mutant animal revealed an almost complete absence of POS over the entire retinal sections (Fig. 4*c*), suggesting a certain degree of heterogeneity in disease phenotype. Mainly in those areas where photoreceptor outer segments were still present, large schisis-like gaps were observed between the cells of the inner nuclear layer (Fig. 4*b*). In areas of Rs1h$^{-/Y}$ retinae where complete loss

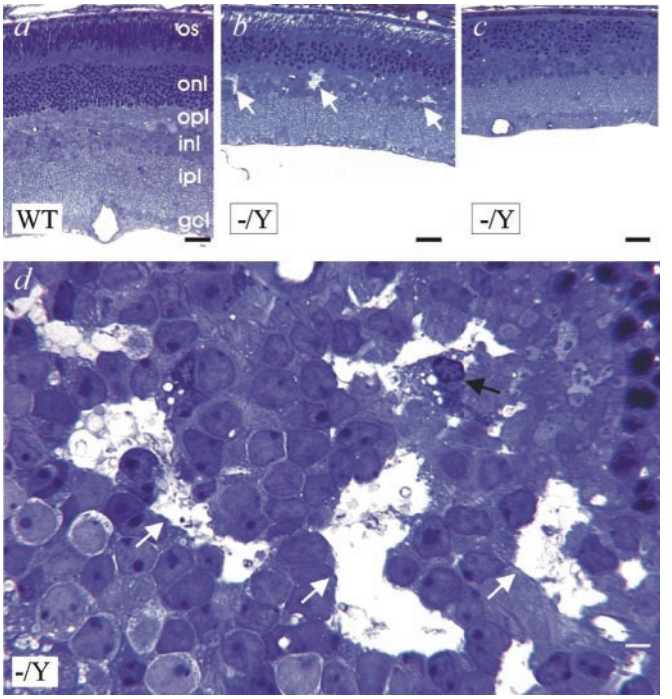

Fig. 4. (*a–d*) Semithin retinal sections of wt (WT) and Rs1h$^{-/Y}$ (−/Y) mice at 2 months of age. In meridional sections, the thickness of the central retina is markedly reduced in Rs1h$^{-/Y}$ mice (*b* and *c*) as compared with wt mice (*a*). In some Rs1h$^{-/Y}$ eyes, photoreceptor outer segments (POS) are present (*b*), whereas others show partial or complete absence of the POS (*c*). In Rs1h$^{-/Y}$ eyes with areas of preserved POS, large gaps are present between the cells of the INL (arrows in *b*). Such gaps are absent in areas with complete degeneration of POS (*c*). (*d*) Oblique tangential section through the INL of an Rs1h$^{-/Y}$ retina reveals large extracellular gaps (white arrows). In some of the gaps, cell bodies of microglia are observed (black arrow). os, photoreceptor outer segments; onl, outer nuclear layer; opl, outer plexiform layer, inl, inner nuclear layer; ipl, inner plexiform layer; gcl, ganglion cell layer. [Bars = 25 μm (*a–c*) and 2.8 μm (*d*).]

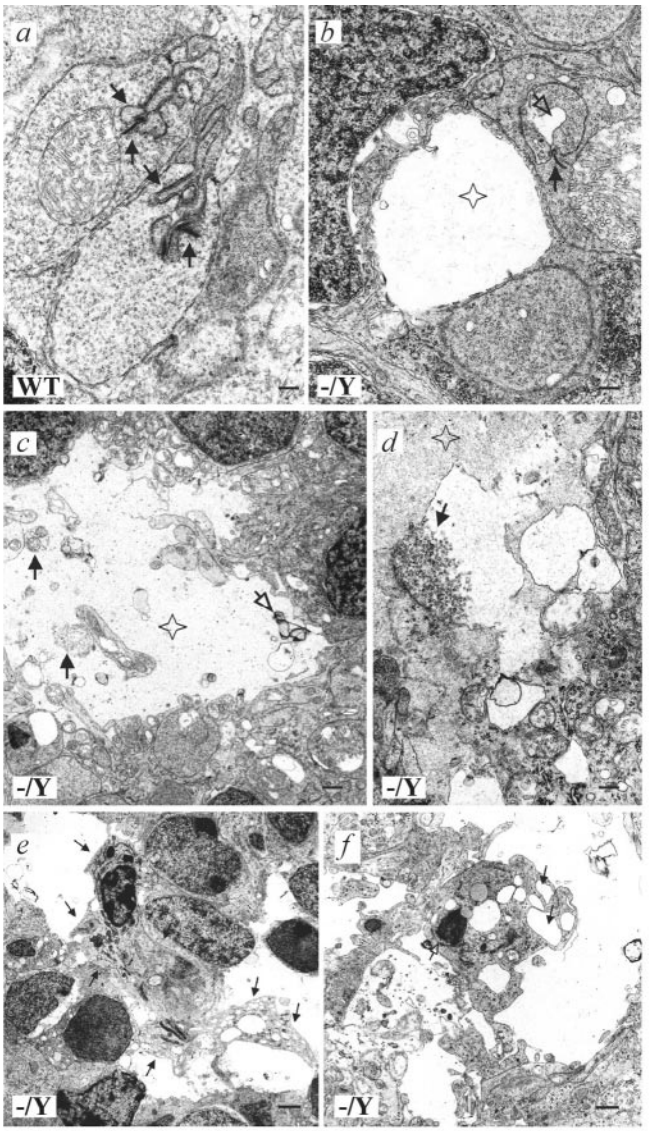

Fig. 5. (*a–f*) Electron microscopy of the retina of wt (WT) and Rs1h$^{-/Y}$ (−/Y) mice at 2 months of age. (*a*) In the retina of wt mice, typical ribbon synapses are present at the photoreceptor terminals (black arrows). (*b*) In the retina of Rs1h$^{-/Y}$ mice, increased extracellular spaces (open arrow) are observed in regions of ribbon synapses (solid arrow). Larger extracellular gaps are present between individual photoreceptor terminals (asterisk). (*c*) The extracellular gaps (asterisk) in the INL of Rs1h$^{-/Y}$ mice are filled with cellular debris (solid arrows) and membranous whorls (open arrow). (*d*) Part of the extracellular debris in the INL gaps (asterisk) of Rs1h$^{-/Y}$ mice consists of fragmented nerve cell terminals (solid arrow) containing synaptic vesicles. (*e*) Cells with ultrastructural characteristics of microglia in the retina of Rs1h$^{-/Y}$ mice. In the increased extracellular spaces, cells with long cytoplasmic processes (arrows) are observed. (*f*) Upon higher magnification, multiple clear vesicles (solid arrow) and electron-dense phagolysosomes (open arrow) are observed in the cytoplasm of the cells. [Bars = 0.53 μm (*a*, *b*, *d*, and *f*) and 1.4 μm (*c* and *e*).]

of photoreceptor outer segments was obvious, schisis formation was not evident histologically (Fig. 4*c*).

Normal ribbon synapses were found by electron microscopy at the photoreceptor terminals of a two-month-old wt mouse (Fig. 5*a*). In contrast, the retina of an Rs1h$^{-/Y}$ littermate revealed increased extracellular spaces in the region of photoreceptor ribbon synapses. In addition, larger extracellular gaps were present between individual photoreceptor terminals (Fig. 5*b*) and the perikarya of the inner nuclear layer (Fig. 5*c*). The extracellular gaps (asterisk in Fig. 5*c*) in the inner nuclear layer of the Rs1h$^{-/Y}$ retina were filled with membranous whorls and cellular debris containing fragmented mitochondria and nerve-cell terminals (Fig. 5 *c* and *d*). In addition, cells with ultrastructural characteristics of microglia, which expressed long cytoplasmic processes, multiple clear vesicles, and electron-dense phagolysosomes were present in the spaces (Fig. 5 *e* and *f*).

To delineate further the consequences of Rs1h deficiency for specific retinal cell types, cryosections from wt and *Rs1h*$^{-/Y}$ retinas were labeled with cell-specific antibodies for analysis by immunofluorescence microscopy (Fig. 6 *a–l*). Supporting our Western blot results (Fig. 1*d*), Rs1 3R10 antibody labeling was absent from the mutant retina (Fig. 6*a*). DAPI staining identifies some nuclei (cells) past the outer limiting membrane and in the inner and outer segment layers as well as displacement of nuclei into the inner plexiform layer (IPL; Fig. 6*a*). The wt retina shows a typical distribution of Rs1h with the protein localizing throughout much of the inner and outer retina with intense staining of the photoreceptor inner segments and bipolar cells (Fig. 6*b*; ref. 12). In addition, significant amounts of Rs1h are present in the IPL and outer plexiform layer (OPL). Immunolabeling of rhodopsin shows that it is translocated to the outer segments in the *Rs1h*$^{-/Y}$ mouse, although the outer segments appear disorganized compared with those in wt retina (Fig. 6 *c* and *d*). Analysis of short and medium cone opsin-immunolabeled cells indicated that there were three times fewer cones in the retina of *Rs1h*$^{-/Y}$ mice than in wt mice. A marked delocalization of opsin to the

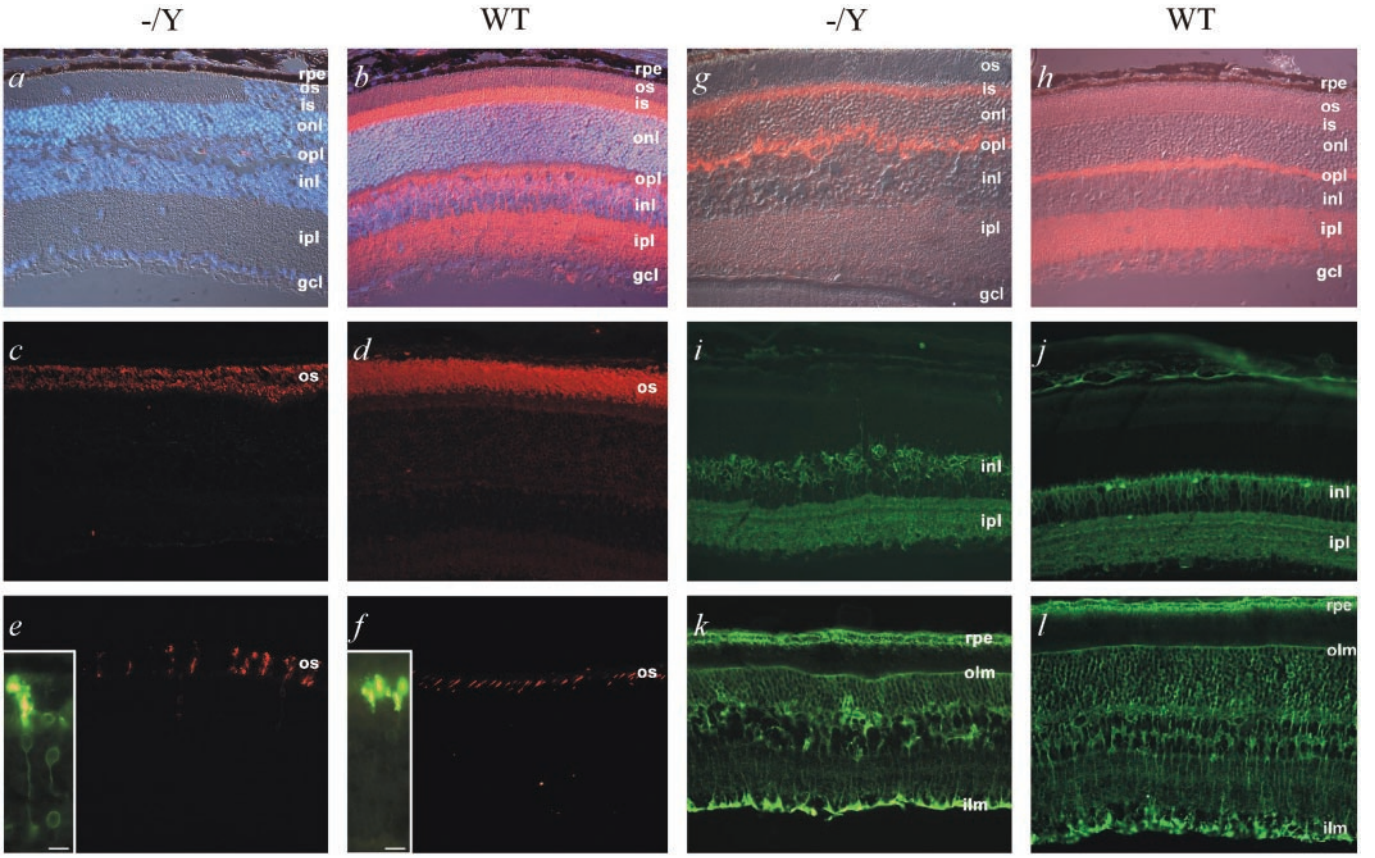

Fig. 6. Immunofluorescence microscopy of retinal cryosections from 2-month-old *Rs1h*$^{-/Y}$ and wt mice. (*a* and *b*) Rs1 labeling with the Rs1 3R10 monoclonal antibody (red). Image is merged with DAPI nuclear staining (blue) and differential interference contrast (DIC) microscopy. (*c* and *d*) Rhodopsin staining with the Rho 1D4 monoclonal antibody. (*e* and *f*) Cone opsin labeling with a mixture of polyclonal antibody JH 455 and JH 492. (*Insets*) Bar = 10 μm. (*g* and *h*) PAN-SAP antibody labeling of PSD-95 in the OPL and IPL in the wt mouse compared with the IS and OPL in the *Rs1h*$^{-/Y}$ mouse. Image is merged with DIC image showing the retinal layers. (*i* and *j*) Labeling of bipolar cells with the monoclonal antibody Mab 115A10. (*k* and *l*) Labeling of Mueller cells and retinal pigment epithelial (RPE) cells with an anti-CRALBP antibody. Abbreviations used are as in Fig. 4, plus (is), inner segment.

inner segment, cell body, and synaptic region was evident in many cone photoreceptors of the Rs1h$^{-/Y}$ knockout, but not wt, mice (Fig. 6 *e*, *f*, and *Insets*). Labeling of the postsynaptic density (PSD)-95 MAGUK protein with the PAN-SAP or 7E3–1B8 antibody produces immunoreactivity in the OPL and IPL of the retina of the wt mouse (Fig. 6*h*), similar to that described for rat retina (27). In the *Rs1h*$^{-/Y}$ retina, the staining pattern reveals significant disorganization of the OPL and an accumulation of PSD-95 in the photoreceptor inner segment (Fig. 6*g*). In addition, there is a significant decrease in PSD-95 in the IPL (Fig. 6*g*). By using monoclonal antibody Mab 115A10, substantial disorganization also is evident that involves the INL bipolar cells of the mutant retina (Fig. 6 *i* and *j*). Staining of the Mueller cells with an anti-CRALBP antibody shows a similar pattern in both knockout and wt mice; however, in the mutant retina, areas devoid of staining within the INL and more intense staining of the inner limiting membrane were observed (Fig. 6 *k* and *l*).

Discussion

In this report, we present the generation and characterization of an *Rs1h*$^{-/Y}$ knockout mouse. It establishes this mouse line as a valuable model for RS with a retinal phenotype closely paralleling that of the human condition. Although the murine retina lacks a macular organization, our findings in the *Rs1h*$^{-/Y}$ mutant animals demonstrate that mice can still be useful for modeling human diseases that display a primary macular phenotype such as RS.

The major pathology in the retina of the retinoschisin-deficient mouse seems to be a generalized disruption of cell layer architecture, most evident in the loss of integrity of the OPL/INL and an irregular displacement of cells in various retinal layers. Functionally, ERG recordings point to severe impairment of bipolar cell-associated pathways and a loss of photoreceptors that is more pronounced in cone than in rod pathways. This finding also is supported by immunofluorescence labeling studies. Rod staining indicates a generalized decrease in cell number, whereas cone labeling demonstrates a more striking cell loss as well as a defect in the targeting of cone opsin to the outer segments. Similarly, in the organization of the bipolar cell layer, there are clear abnormalities, which may be instrumental to the relative b-wave attenuation demonstrated by ERG recordings in human (28, 29) and the *Rs1h*$^{-/Y}$ mouse.

The observed distortion of retinal layers in the *Rs1h*$^{-/Y}$ mouse could be explained by the loss of cell–cell and/or cell–matrix interactions, both of which are thought to be mediated by the discoidin domain of retinoschisin (14, 15). The functional importance of this domain also is reflected by the mutational profile determined in more than 320 RS patients worldwide (http://www.dmd.nl/rs/rshome.html). Of the 125 distinct sequence changes identified so far, 101 (81%) occur in exons 4 to 6 that encode the discoidin motif and likely impair defined functional aspects of this domain. Two types of discoidin-mediated binding can be envisioned. A collagen–discoidin interaction (30, 31) could anchor cells into an extracellular matrix

scaffold or mediate transmembrane-signaling processes. For example, in a direct ligand-binding assay, the introduction of amino acid mutations in the discoidin domain of the discoidin domain receptor 1 (DDR1) at positions homologous to several retinoschisin mutations affects collagen binding and/or receptor phosphorylation of DDR1 (ref. 32). These experiments suggest that binding of discoidin domains to (collagenous) components of the extracellular matrix could be a more general property of these modules. Binding to membrane-anchored carbohydrate residues could represent an alternative mode of discoidin-mediated function. Such interactions would facilitate cell-to-cell contacts and are thought to play a critical role in the activation of the blood clotting cascade on platelet membrane surfaces (33, 34).

One of the most important cellular contacts in the retina occurs at the synapse, where retinoschisin is ordinarily present in high amounts (Fig. 6*b* and ref. 12). Our finding of loss of the synaptic MAGUK protein PSD-95 in the IPL of the *Rs1h* deficient mouse and defects in its translocation to the OPL points to a direct or indirect role of retinoschisin in the proper assembly and stabilization of this region of the cell. This finding also is supported by transmission electron microscopy revealing atypical ribbon synapse formation at the photoreceptor terminals of $Rs1h^{-/Y}$ mice. Failure to establish or maintain the proper synaptic connections could lead to subsequent photoreceptor cell death, a phenomenon that also has been reported in an animal model transgenic for P347L rhodopsin (35).

Earlier studies have suggested that the Müller cells are primarily involved in RS1 pathology (6, 7), a view that has recently been challenged by the fact that retinoschisin was not detected on Müller glial cells (12). In agreement with the latter findings, the Müller cells seem to be relatively unaffected in the $Rs1h^{-/Y}$ retina, arguing for a secondary rather than a primary role of these glial cells in the disease process. A more detailed analysis of cytoplasmic and membranous Müller cell proteins will be required to address the extent of involvement of this particular cell type in disease evolution.

The $Rs1h^{-/Y}$ mouse shares several diagnostic features with human RS, including the typical ''negative ERG'' response and the development of cystic structures within the inner retina, followed by a dramatic loss of photoreceptor cells. Therefore, we conclude that the $Rs1h^{-/Y}$ mouse represents an important model system for further investigations into the molecular mechanisms underlying the cellular disorganization of the retinal structure. This model may be particularly useful to evaluate the role of retinoschisin in the assembly and stabilization of synaptic contacts and will provide a suitable experimental system for novel therapeutic approaches in X-linked juvenile retinoschisis.

We thank Benoît Kanzler for ES cell injection, Vladimir Milenkovic for assistance with the Western blot experiment, and Andrea Rivera for help with mouse breeding. This work was supported by Deutsche Forschungsgemeinschaft Grants We1259/12-2, Se837/1-1, and SFB 430 C2 and National Eye Institute Grant EY 2422.

1. Kellner, U., Brummer, S., Foerster, M. H. & Wessing, A. (1990) *Arch. Clin. Exp. Ophthalmol.* **228,** 432–437.
2. George, N. D., Yates, J. R. & Moore, A. T. (1995) *Br. J. Ophthalmol.* **79,** 697–702.
3. Puech, B., Kostrubiec, B., Hache, J. C. & Francois, P. (1991) *J. Fr. Ophtalmol.* **4,** 153–164.
4. Yanoff, M., Kertesz-Rahn, E. & Zimmerman, L. E. (1968) *Arch. Ophthalmol.* **79,** 49–53.
5. Manschot, W. A. (1972) *Arch. Ophthalmol.* **88,** 131–138.
6. Condon, G. P., Brownstein, S., Wang, N. S., Kearns, J. A. & Ewing, C. C. (1986) *Arch. Ophthalmol.* **104,** 576–583.
7. Kirsch, L. S., Brownstein, S. & de Wolff-Rouendaal, D. (1996) *Can. J. Ophthalmol.* **31,** 301–310.
8. Roesch, M. T., Ewing, C. C., Gibson, A. E. & Weber, B. H. F. (1998) *Can. J. Ophthalmol.* **33,** 149–158.
9. Robson, J. G. & Frishman, L. J. (1998) *Doc. Ophthalmol.* **95,** 187–215.
10. Sauer, C. G., Gehrig, A., Warneke-Wittstock, R., Marquardt, A., Ewing, C. C., Gibson, A., Lorenz, B., Jurklies, B. & Weber, B. H. F. (1997) *Nat. Genet.* **17,** 164–170.
11. Reid, S. N., Akhmedov, N. B., Piriev, N. I., Kozak, C. A., Danciger, M. & Farber, D. B. (1999) *Gene* **227,** 257–266.
12. Molday, L. L., Hicks, D., Sauer, C. G., Weber, B. H. F. & Molday, R. S. (2001) *Invest. Ophthalmol. Visual Sci.* **42,** 816–825.
13. Simpson, D. L., Rosen, S. D. & Barondes, S. H. (1974) *Biochemistry* **13,** 3487–3493.
14. Baumgartner, S., Hofmann, K., Chiquet-Ehrismann, R. & Bucher, P. (1998) *Protein Sci.* **7,** 1626–1631.
15. Vogel, W. (1999) *FASEB J.* **13,** S77–S82.
16. Gehrig, A. E., Warneke-Wittstock, R., Sauer, C. G. & Weber, B. H. F. (1999) *Mamm. Genome* **10,** 303–307.
17. Swiatek, P. J. & Gridley, T. (1993) *Genes Dev.* **7,** 2071–2084.
18. Ramirez-Solis, R., Davis, A. C. & Bradley, A. (1993) *Methods Enzymol.* **225,** 855–878.
19. Schrewe, H., Gendron-Maguire, M., Harbison, M. L. & Gridley, T. (1994) *Mech. Dev.* **47,** 43–51.
20. Seeliger, M. W., Grimm, C., Stahlberg, F., Friedburg, C., Jaissle, G., Zrenner, E., Guo, H., Reme, C. E., Humphries, P., Hofmann, F., *et al.* (2001) *Nat. Genet.* **29,** 70–74.
21. Ito, S. & Karnovsky, M. J. (1968) *J. Cell Biol.* **39,** 168A–169A.
22. MacKenzie, D. & Molday, R. S. (1982) *J. Biol. Chem.* **157,** 7100–7105.
23. Onoda, N. & Fujita, S. C. (1987) *Brain Res.* **416,** 359–363.
24. Bunt-Milam, A. H. & Saari, J. C. (1983) *J. Cell Biol.* **97,** 703–712.
25. Hirose, T., Wolf, E. & Hara, A. (1977) *Doc. Ophthalmol. Proc. Ser.* **13,** 173–184.
26. Hetling, J. R. & Pepperberg, D. R. (1999) *J. Physiol.* **516,** 593–609.
27. Koulen, P., Fletcher, E. L., Craven, S. E., Bredt, D. S. & Wässle, H. (1998) *J. Neurosci.* **18,** 10136–10149.
28. Green, D. G. & Kapousta-Bruneau, N. V. (1999) *Visual Neurosci.* **16,** 727–741.
29. Lei, B. & Perlman, I. (1999) *Visual Neurosci.* **16,** 743–754.
30. Shrivastava, A., Radziejewski, C., Campbell, E., Kovac, L., McGlynn, M., Ryan, T. E., Davis, S., Goldfarb, M. P., Glass, D. J., Lemke, G. & Yancopoulos, G. D. (1997) *Mol. Cell* **1,** 25–34.
31. Vogel, W., Gish, G. D., Alves, F. & Pawson, T. (1997) *Mol. Cell* **1,** 13–23.
32. Curat, C. A., Eck, M., Dervillez, X. & Vogel, W. F. (2001) *J. Biol. Chem.* **276,** 45952–45958.
33. Kim, S. W. Quinn-Allen, M. A., Camp, J. T., Macedo-Ribeiro, S., Fuentes-Prior, P., Bode, W. & Kane, W. H. (2000) *Biochemistry* **39,** 1951–1958.
34. Knight, C. G., Morton, L. F., Onley, D. J., Peachey, A. R., Ichinohe, T., Okuma, M., Farndale, R. W. & Barnes, M. J. (1999) *Cardiovasc. Res.* **41,** 450–457.
35. Blackmon, S. M., Peng, Y. W., Hao, Y., Moon, S. J., Oliveira, L. B., Tatebayashi, M., Petters, R. M. & Wong, F. (2000) *Brain Res.* **885,** 53–61.

IX. Publikationen

1. Veröffentlichungen

Gehrig, A.; Schmidt, S.R.; Müller, C.R.; Srsen, S.; Srsnova, K.; Kress, W.; (1997) Molecular defects in alkaptonuria. *Cytogenet. Cell Genet.* 76: 14-16.

Sauer, C.G.; Gehrig, A.; Warneke-Wittstock, R.; Marquardt, A.; Ewing, C.C.; Gibson, A.; Lorenz, B.; Jurklies, B.; Weber, B.H.F.; (1997) Positional cloning of the gene associated with X-linked juvenile retinoschisis. *Nature Genet.* 17: 164-170.

Felbor, U.; Gehrig, A.; Sauer, C.G.; Marquardt, A.; Köhler, M.; Schmid, M.; Weber, B.H.F.; (1998) Genomic organization and chromosomal localization of the interphotoreceptor matrix proteoglycan-1 (IMPG1) gene: a candidate for 6q-linked retinopathies. *Cytogenet. Cell. Genet.* 81: 12-17.

Gehrig, A.; Felbor, U.; Kelsell, R.E.; Hunt, D.M.; Maumenee, I.H.; Weber, B.H.F.; (1998) Assessment of the interphotoreceptor matrix proteoglycan-1 (IMPG-1) gene localised to 6q13-q15 in autosomal dominant Stargardt-like disease (ADSTGD), progressive bifocal chorioretinal atrophy (PBCRA), and North Carolina macular dystrophy (MCDR1). *J. Med. Genet.* 35: 641-645.

Warneke-Wittstock, R.; Marquardt, A.; Gehrig, A.; Sauer, C.G.; Gessler, M.; Weber, B.H.F.; (1998) Transcript Map of a 900-kb Genomic Region in Xp22.1-p22.2: Identification of 12 Novel Genes. *Genomics* 51: 59-67.

Stöhr, H.; Klein, J.; Gehrig, A.; Koehler, M.R.; Jurklies, B.; Kellner, U.; Leo-Kottler, B.; Schmid, M.; Weber, B.H.F.; (1999) Mapping and genomic charac-terization of the gene encoding diacylglycerol kinase γ (DAGK3): assessment of its role in dominant optic atrophy (OPA1). *Hum. Genet.* 104: 99-105.

Gehrig, A.; Lorenz, B.; Andrassi, M.; Weber, B.H.F.; (1999) First molecular evidence for a de novo mutation in RS1 (XLRS) associated with X linked juvenile retinoschisis. *J. Med. Genet.* 36: 932-934.

Gehrig, A.; White, K.; Lorenz, B.; Andrassi, M.; Clemens, S.; Weber, B.H.F.; (1999) Assessment of RS1 in X-linked juvenile retinoschisis and sporadic senile retinoschisis. *Clin. Genet.* 55: 461-465.

Gehrig, A.; Warneke-Wittstock, R.; Sauer, C.G.; Weber, B.H.F.; (1999) Isolation and characterization of the murine X-linked juvenile retinoschisis (*Rs1h*) gene. *Mamm. Genome* 10: 303-307.

Stöhr, H.; Mah, N.; Schulz, H.L.; Gehrig, A.; Fröhlich, S.; Weber, B.H.F.; (2000) EST mining of the Unigene dataset to identify retina-specific genes. *Cytogenet. Cell Genet.* 91: 267-277.

Krämer, F.; White, K.; Pauleikhoff, D.; Gehrig, A.; Passmore, L.; Rivera, A.; Rudolph, G.; Kellner, U.; Andrassi, M.; Lorenz, B.; Rohrschneider, K.; Blankenagel, A.; Jurklies,

B.; Schilling, H.; Schütt, F.; Holz, F.G.; Weber, B.H.F. (2000) Mutations in the VMD2 gene are associated with juvenile-onset vitelliform macular dystrophy (Best disease) and adult vitelliform macular dystrophy but not age-related macular degeneration. *Europ. J. Hum. Genet.* 8: 286-292.

Weber, B.H.F.; Schrewe, H.; Molday, L.L.; Gehrig, A.; White, K.L.; Seeliger, M.W.; Jaissle, G.B.; Friedburg, C.; Tamm, E.; Molday, R.S.; (2002) Inactivation of the murine X-linked juvenile retinoschisis gene, *Rs1h*, suggests a role of retinoschisin in retinal cell layer organization and synaptic structure. *Proc. Nat. Acad. Sci.* 99: 6222-6227.

2. Kongreßbeiträge

Schmidt, S.R.; Gehrig, A.; Werner, E.; Srsen, S.; Srsnova, K.; Müller, C.R.; Kress, W.; (1997) Cloning of HGO, the key enzyme of Alkaptonuria and defining the molecular defects in mouse and man. *47. Annual Meeting of The American Society of Human Genetics in Baltimore.*

Felbor, U.; Gehrig, A.; Koehler, M.; Schmid, M.; Kelsell, R.; Hunt, D.M.; Kuehn, M.; Hageman, G.S.; Maumenee, H.; Weber, B.H.F.; (1997) Mapping, genomic organization and mutational analysis of a novel interphotoreceptor matrix gene (IPM 150): A candidate for 6q-linked retinopathies? *47. Annual Meeting of The American Society of Human Genetics in Baltimore.*

Weber, B.H.F.; Gehrig, A.; Warneke-Wittstock, R.; Sauer, C.G.; Ewing, C.C.; Jurklies, B.; Lorenz, B.; Gibson, A.; (1997) Towards cloning the gene causing X-linked juvenile retinoschisis (RS): Generation of a transcript map of the RS locus in Xp22.2 and analysis of candidate genes. *47. Annual Meeting of The American Society of Human Genetics in Baltimore.*

Gehrig, A.; Warneke-Wittstock, R.; Sauer, C.G.; Schrewe, H.; Molday, R.S.; Weber, B.H.F.; (1998) Towards understanding the function of the XLRS1 gene associated with X-linked juvenile retinoschisis. *48. Annual Meeting of The American Society of Human Genetics in Denver.*

Gehrig, A.; Schrewe, H.; Weber, B.H.F.; (1998) Towards understanding the function of the XLRS1 gene associated with X-linked juvenile retinoschisis. *10. Jahrestagung der Deutschen Gesellschaft für Humangenetik in Jena.*

Sauer, C.G.; Gehrig, A.; Stuhrmann, M.; Bhattacharya, S.S.; Weber, B.H.F.; (1998) Cloning and characterization of a retina-specific gene from 2p16: A candidate gene for Doyne honeycomb retinal dystrophy and Malattia leventenese. *10. Jahrestagung der Deutschen Gesellschaft für Humangenetik in Jena. Posterpräsentation.*

Warneke-Wittstock, R.; Marquardt, A.; Sauer, C.; Gehrig, A.; Weber, B.H.F.; (1998) Transcription map of a 900 kb region around the X-linked juvenile retinoschisis gene locus. *10. Jahrestagung der Deutschen Gesellschaft für Humangenetik in Jena. Posterpräsentation.*

Kellner, U., Krämer, F.; Gehrig, A.; Kraus, H.; Foerster, M.H.; Weber, B.H.F.; (1999) Clinical Variability in Patients with Mutations in the *VMD2*-Gene. *Annual meeting of the Association for Research in Vision and Ophthalmology in Fort Lauderdale (USA).*

Warneke-Wittstock, R.; Herterich, S.; Gehrig, A.; Weber, B.H.F.; (1999) Analysis of the 5' region of the X-linked juvenile retinoschisis gene. *31. Annual meeting of The European Society of Human Genetics in Geneva.*

Krämer, F.; Gehrig, A.; Marquardt, A.; Rivera, A.; Weber, B.H.F.; (1999) The cloning of the VMD2 gene: Mutation analysis in Best disease and adult vitelliform macular dystrophy. *11. Jahrestagung der Deutschen Gesellschaft für Humangenetik in Nürnberg.*

Warneke-Wittstock, R.; Herterich, S.; Gehrig, A.; Weber, B.H.F.; (1999) Analysis of the 5'region of the X-linked juvenile retinoschisis gene. *11. Jahrestagung der Deutschen Gesellschaft für Humangenetik in Nürnberg. Posterpräsentation.*

Gehrig, A.; Hemmrich, N.; Molday, R.S.; Schrewe, H.; Weber, B.H.F.; (2001) Generation of a mouse model for X-linked juvenile retinoschisis. *10th International Congress of Human Genetics in Vienna. Posterpräsentation.*

Gehrig, A.; Schrewe, H.; Weber B.H.F.; (2002) Investigations into the mechanisms of retinal degeneration in a mouse model for X-linked juvenile retinoschisis. *13. Jahrestagung der Deutschen Gesellschaft für Humangenetik in Leipzig. Posterpräsentation.*

Milenkovic, V.; Krämer, F.; Gehrig, A.; Weber, B.H.F.; (2002) The search for proteins interacting with bestrophin. *13. Jahrestagung der Deutschen Gesellschaft für Humangenetik in Leipzig. Posterpräsentation.*

Moula, F.M.; Rahman, F.M.;Gehrig, A.; Keilhauer, C.; Weber, B.H.F.; (2002) Construction of a Relational Database Management System (RDBMS) for the analysis of PRE-enriched expressed sequence tags. *13. Jahrestagung der Deutschen Gesellschaft für Humangenetik in Leipzig. Posterpräsentation.*

Rahman, F.M.; Moula, F.M.; Gehrig, A.; Keilhauer C.; Weber, B.H.F.; (2002) Identification and characterization of genes from the retinal pigment epithelium (RPE) as candidate for age related macular degeneration (AMD). *13. Jahrestagung der Deutschen Gesellschaft für Humangenetik in Leipzig.*

Stojic, J.; Gehrig, A.; Schulz, H.L.; Wagner, M.; Weber, B.H.F.; (2002) Identifying novel retina-specific genes by characterising a suppression subtracted cDNA library highly enriched for retinal genes. *13. Jahrestagung der Deutschen Gesellschaft für Humangenetik in Leipzig. Posterpräsentation.*

Weber, B.H.F.; Schrewe, H.; Molday, L.L.; Gehrig, A.; Seeliger, M.W.; Friedburg, C.; Tamm, E.; Molday, R.S.; (2002) Inactivation of the Murine X-linked Juvenile Retinoschisis gene, Rs1h, Suggests a Role of Retinoschisin in Retinal Cell Layer Organization and Synaptic Structure. *Annual meeting of the Association for Research in Vision and Ophthalmology in Fort Lauderdale (USA). Posterpräsentation.*

Stöhr, H.B.; Molday, L.L.; Molday, R.S.; Weber, B.H.F.; Gehrig, A.; (2003) Cellular and Subcellular Localization of the Retina-specific MPP4 Protein. *Annual meeting of the Association for Research in Vision and Ophthalmology in Fort Lauderdale (USA). Posterpräsentation.*

Weber, B.H.F.; Gehrig, A.; Schrewe, H.; (2003) Investigation into the Final Pathway of Photoreceptor Degeneration in a Mouse Model of X-linked Juvenile Retinoschisis. *Annual meeting of the Association for Research in Vision and Ophthalmology in Fort Lauderdale (USA). Posterpräsentation.*

X. CURRICULUM VITAE

Persönliche Daten

Name	Andrea Elisabeth Gehrig
Geburtsdatum	12.09.1970
Geburtsort	Miltenberg
Familienstand	ledig
Staatsangehörigkeit	deutsch

Schulbildung

1977-1981	Grundschule, Gissigheim
1981-1990	Matthias-Grünewald-Gymnasium, Tauberbischofsheim
Mai 1990	Abitur

Studium

1990-1996	Studium der Biologie (Diplom) an der Julius-Maximilians-Universität Würzburg
Dezember 1996	Diplom Thema der Diplomarbeit: „Molekulare Ursache der Alkaptonurie“

Promotion

Januar-April 1997	Werkvertrag am Institut für Humangenetik
Mai 1997-August 2003	Wissenschaftliche Mitarbeiterin am Institut für Humangenetik in der Arbeitsgruppe Molekulare Ophthalmologie und Onkologie unter der Leitung von Prof. Dr. Bernhard Weber